The Astrophysical Journal Supplement Series, 242:18 (138pp), 2019 June https://doi.org/10.3847/1538-4365/ab1b43

A Light-curve Analysis of 32 Recent Galactic Novae: Distances and White Dwarf Masses

Izumi Hachisu[1] and Mariko Kato[2]
[1] Department of Earth Science and Astronomy, College of Arts and Sciences, The University of Tokyo, 3-8-1 Komaba, Meguro-ku, Tokyo 153-8902, Japan
hachisu@ea.c.u-tokyo.ac.jp
[2] Department of Astronomy, Keio University, Hiyoshi, Kouhoku-ku, Yokohama 223-8521, Japan
Received 2018 October 18; revised 2019 April 17; accepted 2019 April 21; published 2019 May 31

Abstract

We obtained the absolute magnitudes, distances, and white dwarf (WD) masses of 32 recent galactic novae based on the time-stretching method for nova light curves. A large part of the light/color curves of two classical novae often overlap each other if we properly squeeze/stretch their timescales. Then, a target nova brightness is related to the other template nova brightness by $(M_V[t])_{\rm template} = (M_V[t/f_{\rm s}] - 2.5\log f_{\rm s})_{\rm target}$, where t is the time, $M_V[t]$ is the absolute V magnitude, and $f_{\rm s}$ is their timescaling ratio. Moreover, when these two time-stretched light curves, $(t/f_{\rm s})$–$(M_V - 2.5\log f_{\rm s})$, overlap each other, $(t/f_{\rm s})$–$(B-V)_0$ do too, where $(B-V)_0$ is the intrinsic $B-V$ color. Thus, the two nova tracks overlap each other in the $(B-V)_0$–$(M_V - 2.5\log f_{\rm s})$ diagram. Inversely, using these properties, we obtain/confirm the distance and reddening by comparing each nova light/color curves with well-calibrated template novae. We classify the 32 novae into two types, LV Vul and V1500 Cyg, in the time-stretched $(B-V)_0$–$(M_V - 2.5\log f_{\rm s})$ color–magnitude diagram. The WD mass is obtained by direct comparison of the model V light curves with the observation. Thus, we obtain a uniform set of 32 galactic classical novae that provides the distances and WD masses from a single method. Many novae broadly follow the universal decline law and the present method can be applied to them, while some novae largely deviate from the universal decline law and so the method cannot be directly applied to them. We discuss such examples.

Key words: novae, cataclysmic variables – stars: individual (V1535 Sco, V2944 Oph, V5667 Sgr, V5668 Sgr)

1. Introduction

A nova is a thermonuclear explosion event on a mass-accreting white dwarf (WD) in a close binary. A hydrogen-rich envelope accumulates on the WD. When the envelope mass increases and reaches a critical value, hydrogen ignites to trigger a nova explosion. The envelope expands to giant size and blows strong winds. The nova peak brightness depends on the radius of the photosphere and the wind mass-loss rate (e.g., Hachisu & Kato 2015). After the maximum expansion of the photosphere or the maximum wind mass-loss rate is attained, the nova brightness begins to decline (e.g., Hachisu & Kato 2017). A large part of the hydrogen-rich envelope is blown in the wind. After the winds stop, the envelope mass decreases further by nuclear burning. When it decreases below a critical mass (minimum mass for steady hydrogen-shell burning), nuclear burning extinguishes (e.g., Kato et al. 2014). The WD cools down, and the nova ends.

After the optical peak, optical/IR fluxes are dominated by free–free emission. Hachisu & Kato (2006) calculated many free–free emission model light curves based on the optically thick wind model calculated by Kato & Hachisu (1994), in which the wind is accelerated deep inside the photosphere (owing to the iron peak of opacity at $\log T$ (K) ~ 5.2). Their theoretical light curves show a homologous shape. If we properly normalize the timescales, all light curves overlap each other, independently of the WD mass and chemical composition (see, e.g., Figure 8 of Hachisu & Kato 2006). They called this property of nova model light curves the universal decline law.

Hachisu & Kato (2014) clarified that many classical novae also show a similarity even in their color evolutions. Physically, these properties mean that two novae with different speed classes experience a similar temporal change relative to the total duration. The timescaling law is very useful for analyzing a (target) nova light curve because the distance modulus, extinction, and other various quantities can be derived from a well-calibrated (template) nova by comparing/overlapping the light/color curves. Hachisu & Kato (2010, 2015, 2016a) formulated the method and called it the time-stretching method.

Hachisu & Kato (2010, 2015, 2016a, 2018b) showed that if a substantial part of two light curves overlap each other by stretching the timescale of the template nova, the absolute magnitude $(M_V[t])_{\rm target}$ of the target nova is related to the $(M_V[t])_{\rm template}$ of the template nova by $(M_V[t])_{\rm target} = (M_V[f_{\rm s}\times t] + 2.5\log f_{\rm s})_{\rm template}$ or $(M_V[t])_{\rm template} = (M_V[t/f_{\rm s}] - 2.5\log f_{\rm s})_{\rm target}$, where t is the time since the outburst and $f_{\rm s}$ is the timescaling factor of the target against the template nova. Note that they required the overlap of a large (substantial) part of the light curves, including the nebular phase (and supersoft X-ray source phase, if available), to accurately determine the time-scaling factor. This means that these two time-stretched absolute light curves overlap each other in the $(t/f_{\rm s})$–$(M_V - 2.5\log f_{\rm s})$ plane, and the two time-stretched color curves also overlap in the $(t/f_{\rm s})$–$(B-V)_0$ plane. Here, M_V is the absolute V magnitude and $(B-V)_0$ is the intrinsic $B-V$ color. (See, e.g., Figure 1 for such an example.) Then, a large part of the two nova tracks overlap each other in the time-stretched $(B-V)_0$–$(M_V - 2.5\log f_{\rm s})$ color–magnitude diagram. We applied these properties to 32 recent novae and analyzed their distances and reddenings by comparing each nova light/color curve and time-stretched color–magnitude track with those of well-calibrated (known distance and reddening) template novae (see Appendix A for the 32 recent novae and Hachisu & Kato 2019 for the other 20 novae).

The color–magnitude diagram of stars plays an important role in the study of stellar evolution and is also used to estimate the absolute magnitude of a star. The color–magnitude diagram

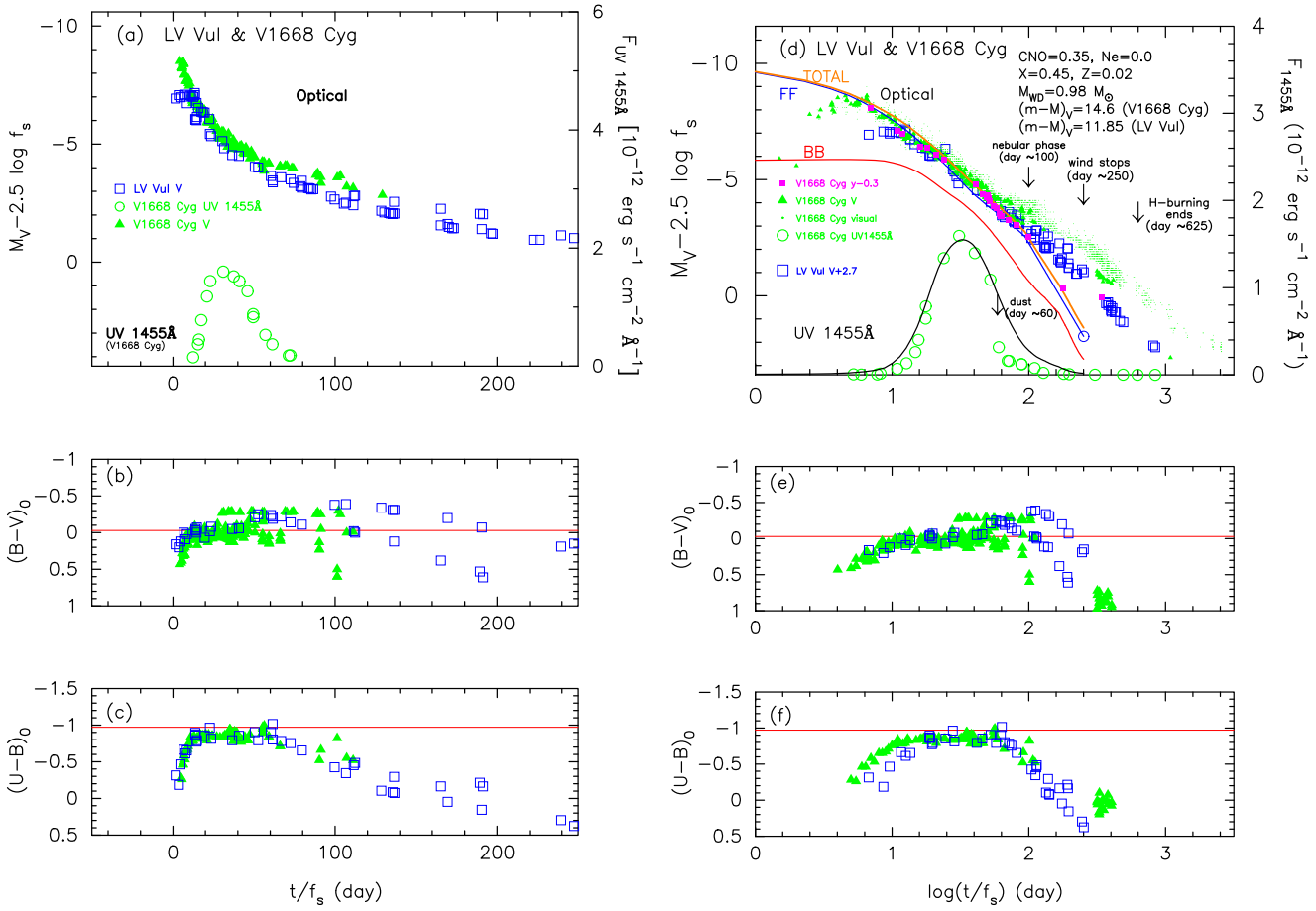

Figure 1. The light/color curves of LV Vul and V1668 Cyg on a linear (left column) and logarithmic (right column) timescale. Here, t is the time since the outburst, M_V is the absolute V magnitude, and f_s is the stretching factor of a target nova. Here, we adopt $f_s = 1.0$ for both LV Vul and V1668 Cyg. (a) and (d) The V light curves of LV Vul and V1668 Cyg. We added the UV 1455 Å light curve of V1668 Cyg. The data of V1668 Cyg and LV Vul are the same as those in Figures 1 and 4 of Hachisu & Kato (2016b). We adopt $(m-M)_V = 11.85$ for LV Vul and $(m-M)_V = 14.6$ for V1668 Cyg (Hachisu & Kato 2019). In panel (d), we plot the model light curves of a 0.98 $M_\odot$ WD (CO3, Hachisu & Kato 2016a). The orange line labeled "TOTAL" denotes the total V flux of photospheric (red line labeled "BB") plus free–free (blue line labeled "FF") emissions. The blue unfilled circle at the right end of the blue line corresponds to the end of the optically thick wind phase. The black solid line represents the UV 1455 Å flux. (b) and (e) The $(B-V)_0$ color curves of V1668 Cyg and LV Vul are dereddened with $E(B-V) = 0.30$ and $E(B-V) = 0.60$, respectively. The horizontal red lines show $(B-V)_0 = -0.03$, which are the intrinsic colors of optically thick free–free emission (Hachisu & Kato 2014). (c) and (f) The $(U-B)_0$ color curve of LV Vul and V1668 Cyg. The horizontal red lines show $(U-B)_0 = -0.97$, the intrinsic color of optically thick free–free emission (Hachisu & Kato 2014).

of classical novae in outburst was extensively studied by Hachisu & Kato (2016b). They proposed several "template tracks" of novae in outburst (see Figure 12 of Hachisu & Kato 2016b), where the template tracks are taken from novae that have a well-defined distance modulus in the V band, $(m-M)_V$; color excess, $E(B-V)$; and shape of the track. Using these template tracks, they obtained the $(m-M)_V$ and $E(B-V)$ of a target nova by directly comparing the target nova track with one of these template tracks. However, they were not fully successful because the absolute V magnitude of each track has very different brightnesses and never overlap each other. They found six different types of tracks in the $(B-V)_0$–M_V diagram, but they could not determine the reason for the differences or similarities.

Hachisu & Kato (2019) revised Hachisu & Kato's (2016b) method. Hachisu & Kato (2019) used the $(B-V)_0$–$(M_V - 2.5\log f_s)$ diagram instead of the $(B-V)_0$–M_V diagram. This is because the (t/f_s)–$(M_V - 2.5\log f_s)$ light curves overlap each other, and therefore, the time-stretched absolute magnitude, $M_V - 2.5\log f_s$, guarantees the same brightness in the time-stretched $(B-V)_0$–$(M_V - 2.5\log f_s)$ diagram.

Hachisu & Kato (2006) showed that nova light curves follow the universal decline law when free–free emission dominates the nova spectra. Hachisu & Kato (2010) further showed that the time-stretched absolute V brightnesses, $M_V - 2.5\log f_s$, overlap each other in the (t/f_s)–$(M_V - 2.5\log f_s)$ light curve (see, e.g., Figures 48 and 49 of Hachisu & Kato 2018b). We show this property in more detail in Appendix B. If we are able to overlap the light curve of the template nova to the target nova by stretching/squeezing its timescale as $t' = t/f_s$, we have the relation

$$\begin{aligned}(M_V[t])_{\rm template} &= (M'_V[t'])_{\rm target} \\ &= (M_V[t/f_s] - 2.5\log f_s)_{\rm target} \end{aligned} \quad (1)$$

between the (t', M'_V) and (t, M_V) coordinate systems (see Appendix A of Hachisu & Kato 2018b), where $M_V[t]$ is the original brightness and $M'_V[t']$ is the time-stretched brightness after time stretching by $t' = t/f_s$.

The color $(B-V)_0$ is not changed by this time stretch because the both M_B and M_V are shifted by $-2.5\log f_s$ after time stretching (e.g., Hachisu & Kato 2018a). Hachisu & Kato (2019) called this $(B-V)_0$–$(M_V-2.5\log f_s)$ diagram the time-stretched color–magnitude diagram. They applied this method to 20 well-observed novae and confirmed that each nova track follows a template track in the time-stretched $(B-V)_0$–$(M_V-2.5\log f_s)$ diagram. If a target nova track overlaps the template nova track in the $(B-V)_0$–$(M_V-2.5\log f_s)$ diagram, we can confirm that (1) our method gives the correct value of the absolute V magnitude, $M_V-2.5\log f_s$, from the vertical fit, and, at the same time, (2) the correct value of the color excess from the horizontal fit. Thus, we can check the distance to the target nova because the $M_V-2.5\log f_s$ and $E(B-V)$ of the template nova are known. In the present paper, we apply this method to 32 recent novae and obtain their distances and reddenings.

We also obtain the $(m-M)_V$ and the WD mass, $M_{\rm WD}$, from our model light-curve fitting. Hachisu & Kato (2015) calculated many $M_V[t]$ model light curves for various WD masses and envelope chemical compositions based on Kato & Hachisu's (1994) results. Their model M_V light curve is composed of photospheric emission and free–free emission. The photospheric emission is approximated by blackbody emission at the photosphere while the free–free emission originates from optically thin plasma outside the photosphere. Fitting an M_V model light curve with the observed apparent m_V, we specify the $(m-M)_V$ and $M_{\rm WD}$ for a nova.

Our paper is organized as follows. First we describe our method based on the time-stretched $(B-V)_0$–$(M_V-2.5\log f_s)$ diagram in Section 2. We apply this method to 32 recent novae, and determine their distances and WD masses in Section 3. A discussion and conclusions follow in Sections 4 and 5, respectively. The model light-curve fitting and time-stretching method for each of the 32 novae are summarized in Appendix A. In Appendix B, we explain a timescaling law of novae based on optically thick wind solutions. In Appendix C, we discuss exceptional novae that deviate largely from the universal decline law. We show that the present method applies to them if we adopt a different template nova depending on the reason for deviation.

2. Method and Examples

We briefly summarize the time-stretching method of nova light curves and how to determine the distance and WD mass.

2.1. Model Light Curves of Novae

We determine the WD mass of a target nova by directly fitting the model light curve with the observation. Figure 1 shows the light/color curves of V1668 Cyg and LV Vul on linear (left side column) and logarithmic (right side column) timescales. We explain our method based on these figures.

Kato & Hachisu (1994) calculated evolutions of nova outbursts based on the optically thick wind theory. Hachisu & Kato (2015) obtained the M_V light curves based on Kato & Hachisu's (1994) envelope models. Their M_V flux is composed of photospheric emission and free–free emission. The photospheric emission is approximately calculated from blackbody emission at the photosphere (red line labeled "BB" in Figure 1(d)) while the free–free emission is estimated from plasma outside the photosphere (blue line labeled "FF"). The observed flux (orange line labeled "TOTAL") is the sum of the free–free and photospheric emissions.

The flux of free–free emission can easily exceed the Eddington limit (which is as close as the flat part of the red line (BB) in Figure 1(d)), if the wind mass-loss rate is large enough (see also, e.g., Hachisu & Kato 2017). Fitting an M_V model light curve with the observed m_V, we specify the $(m-M)_V$ and $M_{\rm WD}$ for a nova (e.g., Hachisu & Kato 2015, 2016a, 2017, 2018a, 2018b, 2019, for such examples).

We can determine the WD mass more accurately if the UV 1455 Å band and/or supersoft X-ray fluxes are available. The UV 1455 Å band is a narrowband (1445–1465 Å) flux that represents well the UV continuum fluxes of novae (Cassatella et al. 2002). The UV 1455 Å flux is calculated from the photospheric emission assumed to be blackbody. The soft X-ray band (0.3–1.5 keV) flux is also calculated from the photospheric emission (blackbody assumption).

Figure 1(d) shows such an example of model light-curve fitting. In the case of V1668 Cyg, we adopt $(m-M)_V=14.6$ and $M_{\rm WD}=0.98\,M_\odot$ with the chemical composition of CO nova 3 (CO3; Hachisu & Kato 2016a). We estimate the fitting error to be $\epsilon((m-M)_V)=\pm0.2$ mag and $\epsilon(M_{\rm WD})=\pm0.02\,M_\odot$. The simultaneous fitting of the V and UV 1455 Å light curves gives a relatively more accurate mass of the WD compared to the fitting only of a V light curve.

2.2. Deviation from a Model V Light Curve

Our model V light curve is composed of free–free emission and blackbody emission. Therefore, the model light curves deviate from observation when the effect of strong emission lines or dust absorption is important.

Nova ejecta become optically thin when the nebular phase starts. In Figure 1(d), we denote the start of the nebular phase of V1668 Cyg by the arrow labeled "nebular phase" about 100 days after the outburst. Our M_V light curve (orange line) begins to deviate from the V observation (filled green triangles) about 80–100 days after the outburst.

In the nebular phase, strong [O III] lines start to contribute to the V band. This makes $B-V$ color redder. The $(B-V)_0$ color turns to the red in Figures 1(b) and (e). The response function of each V filter sometimes shows a slight difference in its blue edge. Such a small difference in the V filter makes a large difference in the V magnitude because [O III] contribute to the blue edge of the V filter (see, e.g., Figure 1 of Munari et al. 2013). We observe a large scatter or multiple branches of $(B-V)_0$ color evolution, which start at the nebular phase (Figures 1(b) and (e)). Therefore, we do not expect a unique path of nova evolution in the $(B-V)_0$ color curve especially in the nebular phase.

The intermediate-width band, y, is designed to avoid strong [O III] lines (see, e.g., Figure 1 of Munari et al. 2013). So, the y magnitude can follow the continuum well. We add the y observations (filled magenta square) of V1668 Cyg to Figure 1(d). Our model V light curve shows a good agreement with the y observation even after the nebular phase started, except for the last data point. This confirms that our model V light curve follows well the continuum flux of a nova.

Dust formation usually occurs far outside the photosphere whereas continuum free–free emission comes mainly from near outside the photosphere. Therefore, dust absorbs optical and UV photons and re-emit IR photons. For example, V1668 Cyg

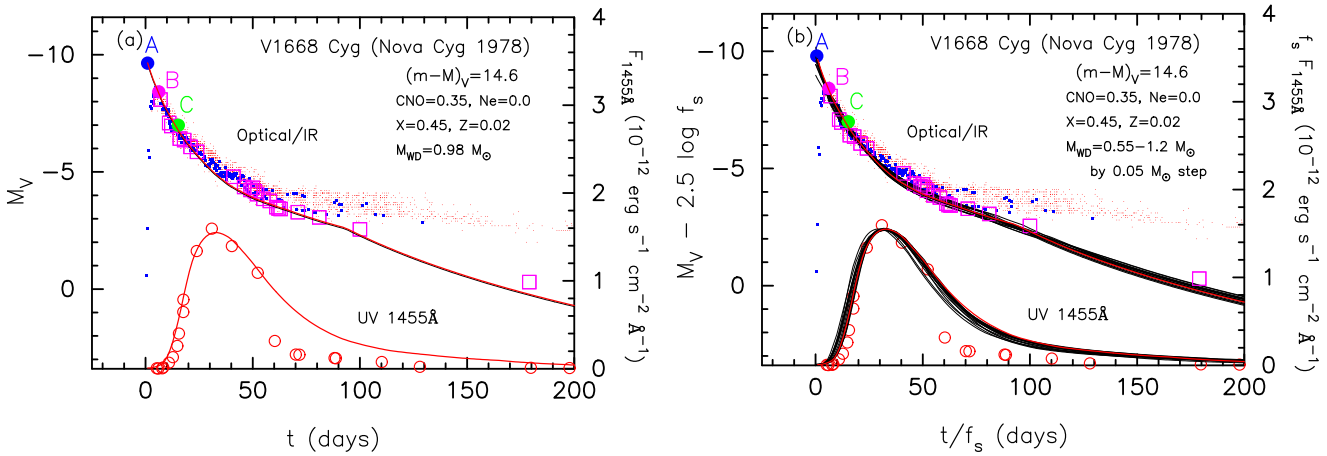

Figure 2. (a) A slight close-up view of the V1668 Cyg light curves in Figure 1(a). The 0.98 $M_\odot$ WD (CO3) model reasonably reproduces the V1668 Cyg optical *y* (unfilled magenta squares), *V* (filled blue squares), and UV 1455 Å (large unfilled red circles) light curves. We add the visual magnitudes (red dots). These data are all the same as Figure 46 of Hachisu & Kato (2018b). We place three points, A, B, and C, on the model *V* light curve, corresponding to three different initial envelope masses, $M_{\rm env,0} = 2.0 \times 10^{-5}\,M_\odot$, $1.4 \times 10^{-5}\,M_\odot$, and $0.93 \times 10^{-5}\,M_\odot$, respectively. Point B is the optical peak of V1668 Cyg, $m_V = 6.2$ ($M_V = 6.2–14.6 = -8.4$). (b) Free–free emission model *V* and UV 1455 Å model light curves for 0.55, 0.60, 0.65, 0.70, 0.75, 0.80, 0.85, 0.90, 0.95, 1.0, 1.05, 1.1, 1.15, and 1.20 $M_\odot$ WDs (solid black lines), but in the (t/f_s)–$(M_V - 2.5\log f_s)$ coordinates for the *V* and the (t/f_s)–$(f_s F_{1455\,\text{Å}})$ coordinates for the UV 1455 Å. The timescaling factor f_s of each model, tabulated in Table 3 of Hachisu & Kato (2016a), is measured against that of the V1668 Cyg light curves.

showed an optically thin dust blackout on day 60. Hachisu & Kato (2006) discussed such optical and near-infrared (NIR) light curves of V1668 Cyg. The UV 1455 Å light curve shows a small drop around day 60 as plotted in Figure 1(d). A much thicker dust formation is shown, e.g., in Figure 51(a), in which the optical flux suddenly drops due to dust shell formation. Our model *V* light curve does not include the effect of dust shell formation far outside the photosphere. Therefore, we do not follow well the dust blackout phase.

To summarize, we basically exclude the nebular phase and dust blackout phase, but we include the nebular phase when their light/color curves overlap in the nebular phase (e.g., V1663 Aql, V2575 Oph, V5117 Sgr, V2576 Oph, V390 Nor, V459 Vul, V2670 Oph, QY Mus, NR TrA, V5585 Sgr, PR Lup, V834 Car, V2677 Oph, V5592 Sgr, V962 Cep, V2659 Cyg, V5667 Sgr, V5668 Sgr, V2944 Oph).

2.3. Peak Brightness versus Timescaling Factor

Figure 2(a) shows that the peak *V* brightness of our model light curve depends on the initial envelope mass. In general, the initial envelope mass ($M_{\rm env,0}$) is close to the ignition mass ($M_{\rm ig}$), which is the hydrogen-rich envelope mass at the start of hydrogen burning. The ignition mass depends mainly on the mass accretion rate ($\dot{M}_{\rm acc}$) and WD mass (see, e.g., Kato et al. 2014 for a recent calculation). The larger the mass-accretion rate is, the smaller the ignition mass . (The smaller the WD mass is, the larger the ignition mass.)

Points A, B, and C in Figure 2(a) correspond to the different initial envelope mass, i.e., $M_{\rm env,0} = 2.0 \times 10^{-5}\,M_\odot$, $1.4 \times 10^{-5}\,M_\odot$, and $0.93 \times 10^{-5}\,M_\odot$, respectively. When the ignition mass is $M_{\rm env,0} = 2.0 \times 10^{-5}\,M_\odot$, the peak brightness reaches $M_{V,\rm max} = -9.7$ (point A), which is very bright compared with the ignition mass of $1.4 \times 10^{-5}\,M_\odot$, for which the peak brightness reaches $M_{V,\rm max} = -8.4$ (point B), which is moderately bright.

The peak brightness of LV Vul is about $M_{V,\rm max} = -7.15$ (point C). This means that, if both WD masses are the same, the mass-accretion rate to the WD is smaller in V1668 Cyg than in LV Vul. This also shows that, even if the timescaling factors are the same between V1668 Cyg and LV Vul, the peak *V* brightnesses are very different from each other.

2.4. MMRD Relations

We explain the theory behind the maximum magnitude versus rate of decline (MMRD) relations based on the universal decline law. The MMRD methods require the decline rates in the very early phase of a nova outburst, usually t_2 or t_3, which are the times during which the *V* brightness decays by 2 or 3 mag from the peak, respectively. Many empirical MMRD relations between the peak *V* brightness, $M_{V,\rm max}$, and the decline timescale, t_2 or t_3, have been proposed (e.g., Schmidt 1957; de Vaucouleurs 1978; Cohen 1988; della Valle & Livio 1995; Downes & Duerbeck 2000). Hachisu & Kato (2010, 2015, 2016a, 2018b) formulated a theory of MMRD relations. Here, we summarize their main points.

It should be noted that the timescales t_2 and t_3 are local timescales just after the *V* peak but not global timescales like f_s. For example, LV Vul and V1668 Cyg have the same global timescale of $f_s = 1$ (Figure 2), but their t_3 times are different from each other, that is, $t_3 = 43$ days (point C in Figure 4) for LV Vul (Downes & Duerbeck 2000) and $t_3 = 26$ days (point B in Figure 4) for V1668 Cyg (Hachisu & Kato 2010). Thus, the MMRD methods are theoretically not the same as the time-stretching method.

First, we explain the main trend of the MMRD relations, which is derived from the universal decline law. The brightness of the free–free emission declines along the universal decline law, as shown in Figures 2(b) and 3(a). This is the sequence of decreasing envelope mass, $M_{\rm env}$, and thus, the peak *V* brightness is closely related to the initial envelope mass, $M_{\rm env,0}$, which is almost equal to the envelope mass at maximum. We can determine the peak brightness on the *V* light curve if we specify the WD mass and initial envelope mass.

Point B is the peak *V* brightness of V1668 Cyg as shown in Figure 2(a). We assume that the brightness at point B is typical of the 0.98 $M_\odot$ WD. We further assume that point B is also a typical brightness for each WD mass in the (t/f_s)–$(M_V - 2.5\log f_s)$ plane

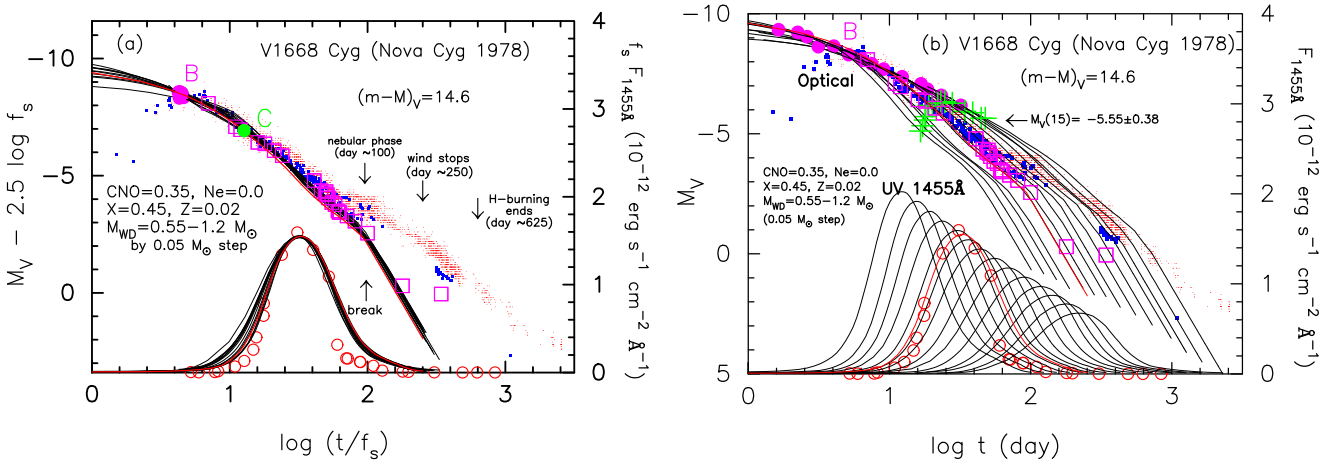

Figure 3. (a) Same as Figure 2(b), but on logarithmic timescales. (b) Same model light curves as those in panel (a), but for real timescale and absolute V magnitude. The magenta filled circles are point B on each V light curve in panel (a). The green pluses represent $M_V(15)$, the absolute V magnitude 15 days after the V maximum at each point B. We also recover the real flux of the UV 1455 Å band.

in Figure 2(b). For the other speed classes (other WD masses, $M_{\rm WD}$) of novae, we have the typical peak V brightness at point B, that is, $M_V({\rm B}, M_{\rm WD}) - 2.5\log f_{\rm s} = M_V({\rm B}, 0.98\,M_\odot)$, in Figure 2(b). A more massive WD ($M_{\rm WD} > 0.98\,M_\odot$) with a smaller $f_{\rm s} < 1$ than that of V1668 Cyg has a brighter maximum magnitude of $M_{V,\rm max}({\rm B}, M_{\rm WD}) = M_V({\rm B}, 0.98\,M_\odot) + 2.5\log f_{\rm s}$ over that of V1668 Cyg and vice versa (see Figure 3(b)).

Figure 3(a) shows the same model light curves of Figure 2(b), but on a logarithmic timescale. Figure 3(b) shows the real M_V magnitudes and real timescales of each model light curves. We plot point B on each nova model light curve by the filled magenta circles. We read the value of $M_{V,\rm max}$ at point B (filled magenta circle) on each model light curve (different WD mass) and obtain its t_3 time on the log t–M_V light curve. Thus, we plot the MMRD relations for point B on each WD mass. Such MMRD points are shown in Figure 4, that is, the unfilled blue circles on the log t_3 versus $M_{V,\rm max}$ plot, which show the main (central) trend of the MMRD distribution. Thus, we can explain the main trend of MMRD relations by typical brightness (point B) for different WD masses. We approximate this trend as $M_{V,\rm max} = 2.5\log t_3 - 11.9$, the line of which (thick solid black line) has the slope of 2.5 and is passing through point B (filled green square with black outline) in Figure 4.

Second, we explain the large scatter of individual novae from the main trend of the MMRD relation. The ignition mass depends on the mass accretion rate if we fix the WD mass (for example, $M_{\rm WD} = 0.98\,M_\odot$ in Figure 2(a)). When the mass accretion rate is smaller than that of point B, the initial envelope mass, $M_{\rm env,0}$, is larger than that at point B. Then, the peak V brightness reaches, for example, point A, which is much brighter than that for point B. This clearly shows a different peak V brightness (and initial envelope mass) for a different mass-accretion rate even if the WD mass is the same as $0.98\,M_\odot$ and the chemical composition is also the same as CO3. Plotting this brighter MMRD relation of point A for the other speed classes of novae (different WD masses), we have a brighter end for the (t_3, $M_{V,\rm max}$) distribution, that is, $M_{V,\rm max}({\rm A}, M_{\rm WD}) = M_V({\rm A}, 0.98\,M_\odot) + 2.5\log f_{\rm s}$, which is depicted by the upper thin solid black line passing through point A in Figure 4. If we plot a fainter MMRD relation for point C for the other speed classes of novae (different WD masses), we have a fainter end for the (t_3, $M_{V,\rm max}$) distribution, that is, $M_{V,\rm max}({\rm C}, M_{\rm WD}) = M_V({\rm C}, 0.98\,M_\odot) + 2.5\log f_{\rm s}$, which is represented by the lower solid black line passing through point C in Figure 4.

The three black lines passing through points A, B, and C indicate a degree of scatter, originating from the difference in the mass-accretion rate, that is, the difference in the initial envelope mass at ignition. These upper and lower black lines broadly envelop the MMRD points of galactic novae (filled red circles in Figure 4), which were studied by Downes & Duerbeck (2000). Very fast and very faint novae detected in M31 (Kasliwal et al. 2011; Darnley et al. 2016) can be also explained in the same context. We plot the MMRD point of the one-year recurrence period nova M31N 2008-12a (unfilled red diamond in Figure 4) for such an example. Hachisu & Kato (2018b) examined such very fast and faint novae in our Galaxy and nearby galaxies, i.e., YY Dor, LMC N2009a, LMC N 2012a, LMC N 2013, in LMC, SMC N 2016 in SMC, and M31N 2008-12a in M31. They applied the time-stretching method to these novae and concluded that their time-stretched light curves show good agreement with the known distance to each nearby galaxy except for SMC 2016 (e.g., Orio et al. 2019). These very fast and faint novae should have extremely large mass-accretion rates onto very massive WDs (e.g., Kato et al. 2015, 2017a, 2017b).

To summarize the theory of MMRD relations, the main trend of MMRD relations is closely related to the WD mass, which is represented by the timescaling factor $f_{\rm s}$. The large scatter from the main trend originates from the different mass accretion rates and, as a result, different initial envelope masses at ignition. This second parameter of the mass accretion rate can reasonably explain the degree of scatter of individual novae from the proposed empirical MMRD relations (see Figure 4).

2.5. Properties of Universal Decline Law

Hachisu & Kato (2006) found that, when free–free emission dominates the spectrum, there is a universal decline law of novae. Figures 2(b) and 3(a) demonstrate that 14 free–free emission model light curves (solid black lines) for different WD masses overlap each other if they are properly stretched in the time direction, $t/f_{\rm s}$, and shifted by $-2.5\log f_{\rm s}$ (see Appendix B for the derivation). Hachisu & Kato (2006) called this property of the model light curves the universal decline

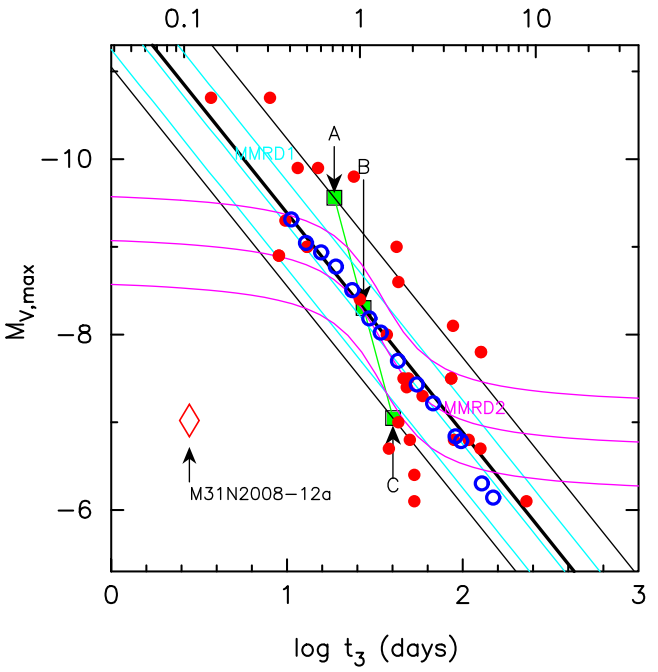

Figure 4. Maximum magnitude vs. rate of decline (MMRD) relation for classical novae. The ordinate is the V peak $M_{V,\max}$ and the bottom abscissa is the t_3 time, during which the nova brightness decays by 3 mag from the peak. Point B (filled green square with black outline) is the MMRD point of V1668 Cyg on the $0.98M_\odot$ WD (CO3) model light curve. We assume that point B on each WD mass model in Figure 3 is a typical initial envelope mass for each WD mass. Therefore, the thick black line passing through point B is an MMRD relation for a typical nova with different WD masses. The top abscissa is the timescaling factor of a different WD mass model on this line, in which f_s is measured against the $0.98M_\odot$ WD model. The upper solid black line passing through point A is an MMRD relation for a much brighter nova than that for point B, which corresponds to a much lower mass accretion rate and, as a result, a much larger initial envelope mass, than that for point B. The lower solid black line passing through point C is an MMRD relation for a much fainter nova than that for point B, which corresponds to a higher mass accretion rate and, as a result, a much smaller initial envelope mass, than that for point B. The unfilled blue circles are the MMRD points for different WD masses calculated from each point B in Figure 3(b). We plot MMRD points (filled red circles) for individual galactic novae, which are taken from Table 5 of Downes & Duerbeck (2000). We also add the MMRD point for M31N 2008-12a (unfilled red diamond; Darnley et al. 2016). We further add the two well-known empirical MMRD relations: one is Kaler-Schmidt's law (solid cyan lines labeled "MMRD1"; Schmidt 1957), and the other is della Valle & Livio's law (solid magenta lines labeled "MMRD2"; della Valle & Livio 1995). We plot ±0.5 mag upper/lower bounds for each of these two relations.

law. They determined the f_s of the 14 theoretical light curves against the optical/UV light curves of V1668 Cyg. The $0.98\ M_\odot$ WD (CO3) model reasonably reproduces the observed optical/UV light curves of V1668 Cyg, that is, $f_s = 1.0$. The other f_s of each WD mass is tabulated in Table 3 of Hachisu & Kato (2016a).

Figures 2(b) and 3(a) also show UV 1455 Å model light curves. Assuming blackbody emission at the photosphere, Hachisu & Kato (2006) calculated the model UV 1455 Å light curves. We stretch them with the same factor f_s as those of the optical/NIR light curves (see Appendix B for details). Strictly speaking, we obtain each UV 1455 Å flux with the reddening of $E(B-V) = 0.30$ and the distance of $d = 5.4$ kpc. These two parameters are the same as those of V1668 Cyg.

Because we already know the absolute V magnitude of the template nova, we obtain the absolute V magnitude of the target nova from Equation (1). If we convert the (t, M_V) of the target nova to (t', M_V') by a time stretch of $t' = t/f_s$, we obtain $M_V'[t'] = M_V[t/f_s] - 2.5\log f_s$. This relation is derived in Appendix B. Equation (1) is equivalent to

$$(M_V[t \times f_s])_{\rm template} = (M_V'[t])_{\rm target} = (M_V[t])_{\rm target} - 2.5\log f_s. \quad (2)$$

Using the time stretch of $t' = t \times f_s$, we obtain $M_V'[t'] = M_V[t \times f_s] + 2.5\log f_s$ for the template, and we can rewrite Equation (1) as

$$(M_V[t])_{\rm target} = (M_V'[t'])_{\rm template} = (M_V[t \times f_s])_{\rm template} + 2.5\log f_s. \quad (3)$$

The observed V light curves of the novae are given in the apparent V magnitude of m_V. If we can overlap the two novae after horizontally shifting by $\log f_s$ and vertically shifting by ΔV the template nova light curve in the $(\log t,\ m_V)$ plane, we have the relation

$$(m_V[t])_{\rm target} = (m_V[t \times f_s] + \Delta V)_{\rm template}. \quad (4)$$

Subtracting Equation (3) from Equation (4), we obtain

$$(m[t] - M[t])_{V,\rm target} = ((m[t \times f_s] - M[t \times f_s])_V + \Delta V)_{\rm template} - 2.5\log f_s. \quad (5)$$

It should be noted that the absolute V light curve of $M_V[t]$ has the same shape as the apparent V light curve of $m_V[t]$, both for the target and template novae. Therefore, we can suppose that $(m[t] - \mathrm{M}[t])_V =$ constant in time. Finally, we obtain

$$(m - M)_{V,\rm target} = ((m - M)_V + \Delta V - 2.5\log f_s)_{\rm template}, \quad (6)$$

where $(m - M)_{V,\rm template}$ is the distance modulus of the template nova and is already known. Equation (5) is a function of time but Equation (6) is just a constant value. Thus, we can derive the distance modulus of a target nova from the template nova. Hachisu & Kato (2010) called this method (Equation (6)) the time-stretching method.

It should be noted that individual novae more or less deviate from the universal decline law. We suppose that the overall trends of these novae broadly follow the universal decline law and Equation (6) approximately applies to such novae. We will really see it in the rest of this paper.

2.6. Distance from the Time-stretched Color–Magnitude Diagram Method

We analyze the light/color curves of novae in the following procedure.

1. We plot the V light curve and dereddened $(B-V)_0$ and $(U-B)_0$ color curves of a target nova on a logarithmic timescale (for example, Figure 1). The color excess $E(B-V)$ of the target nova is taken from the literature or our time-stretching method mentioned below. We obtain the dereddened colors of $(B-V)_0$ and $(U-B)_0$ via

$$(B-V)_0 = (B-V) - E(B-V) \quad (7)$$

and

$$(U-B)_0 = (U-B) - 0.64E(B-V), \quad (8)$$

where the factor of 0.64 is taken from Rieke & Lebofsky (1985).

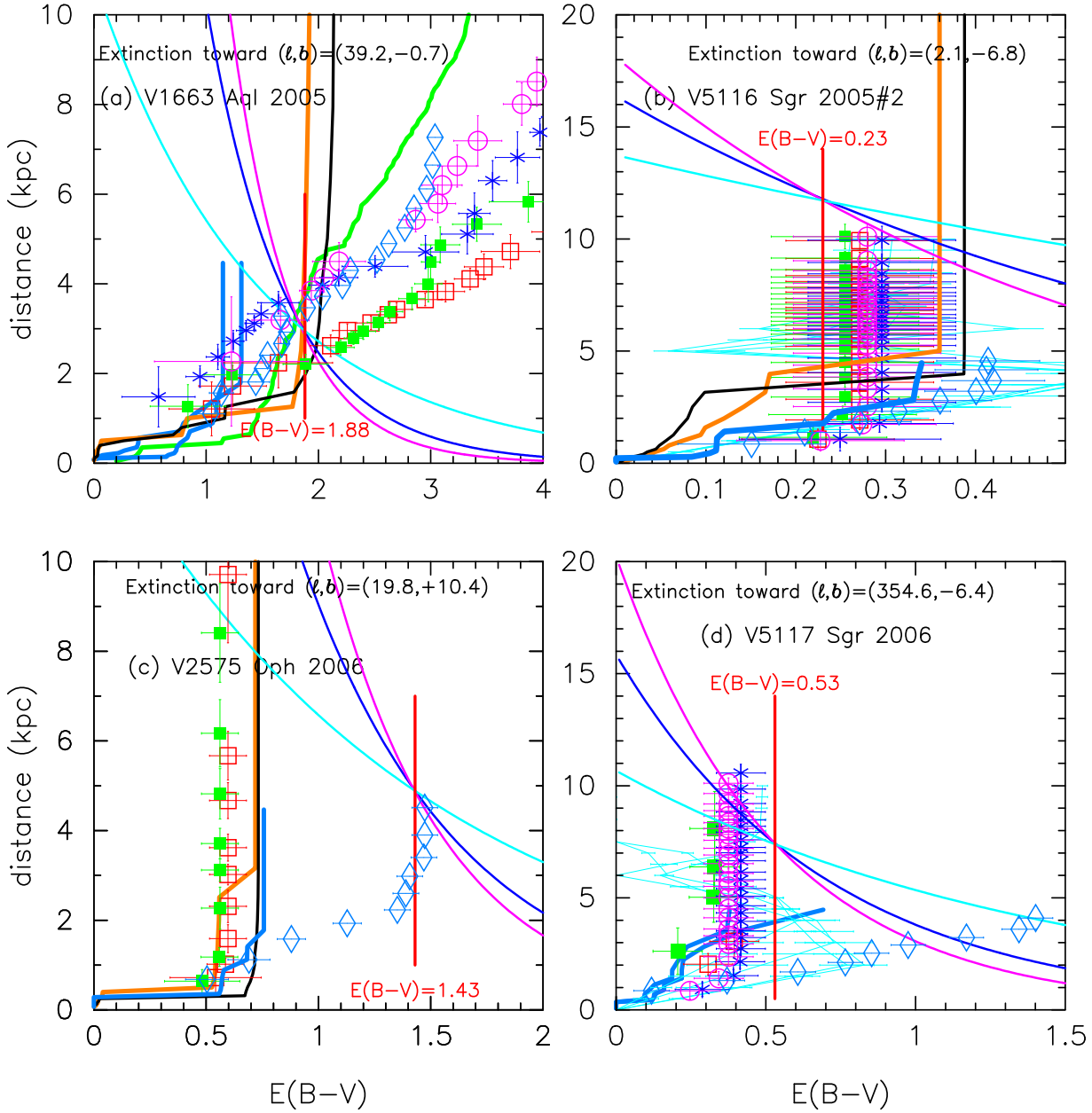

Figure 5. Distance–reddening relations toward (a) V1663 Aql, (b) V5116 Sgr, (c) V2575 Oph, and (d) V5117 Sgr. In panel (a), we plot $(m-M)_B = 19.98$ and Equation (12), $(m-M)_V = 18.16$ and Equation (11), and $(m-M)_I = 15.17$ and Equation (13) with the thin magenta, blue, and cyan lines, respectively. The three lines cross at $d = 2.9$ kpc and $E(B-V) = 1.88$. The vertical solid red line indicates the reddening of $E(B-V) = 1.88$. The four relations toward (l, b) = (39.°0, −0.°50), (39.°25, −0.°50), (39.°0, −0.°75), and (39.°25, −0.°75) are taken from Marshall et al. (2006) and depicted by unfilled red squares, filled green squares, blue asterisks, and unfilled magenta circles, respectively, each with error bars. Among the four nearby directions, the direction closest to V1663 Aql is that of the unfilled magenta circles. The thick solid green line denotes the relation of Sale et al. (2014). The thick solid black line indicates the relation of Green et al. (2015) and the orange one is their revised version (Green et al. 2018). The unfilled cyan-blue diamonds represent the relation of Özdörmez et al. (2018). We also plot the two thick solid cyan-blue lines of Chen et al. (2018) for (l, b) = (39.°15, −0.°65) and (l, b) = (39.°15, −0.°75). In panels (b) and (d), we add the relations of Schultheis et al. (2014) with the very thin cyan lines.

2. We use a well-calibrated nova as a template nova, for which the distance modulus, $\mu_V \equiv (m-M)_V$, and color excess, $E(B-V)$, are well defined. We add the light/color curves of the template novae and overlap them with the target nova as much as possible by shifting them back and forth ($\log f_s$) and up and down (ΔV). Then, we estimate the distance modulus of the target nova, $(m-M)_{V,\rm target}$, from Equation (6). We shift the light/color curves in steps of $\delta \log f_s = 0.01$ and $\delta(\Delta V) = 0.1$ mag and find the best match by eye. In our previous paper (Hachisu & Kato 2018a), we estimated the error for V959 Mon. Its typical allowance is about $\log f_s = 0.14 \pm 0.05$ and $\Delta V = +1.6 \pm 0.2$ from a least-squares fit. Therefore, we usually obtain typical errors of $\epsilon(\log f_s) = 0.05$ and $\epsilon(\Delta V) = 0.2$ even when fitting by eye unless otherwise mentioned. We adopt LV Vul (or V1500 Cyg, V1668 Cyg, and V1974 Cyg) as a template nova, unless otherwise specified. Theoretically, the spectrum of free–free emission is almost independent of frequency, i.e., $F_\nu \propto \nu^0$. This means that the other broadband light curves follow the same universal decline law as the V band. We apply the same relation to the

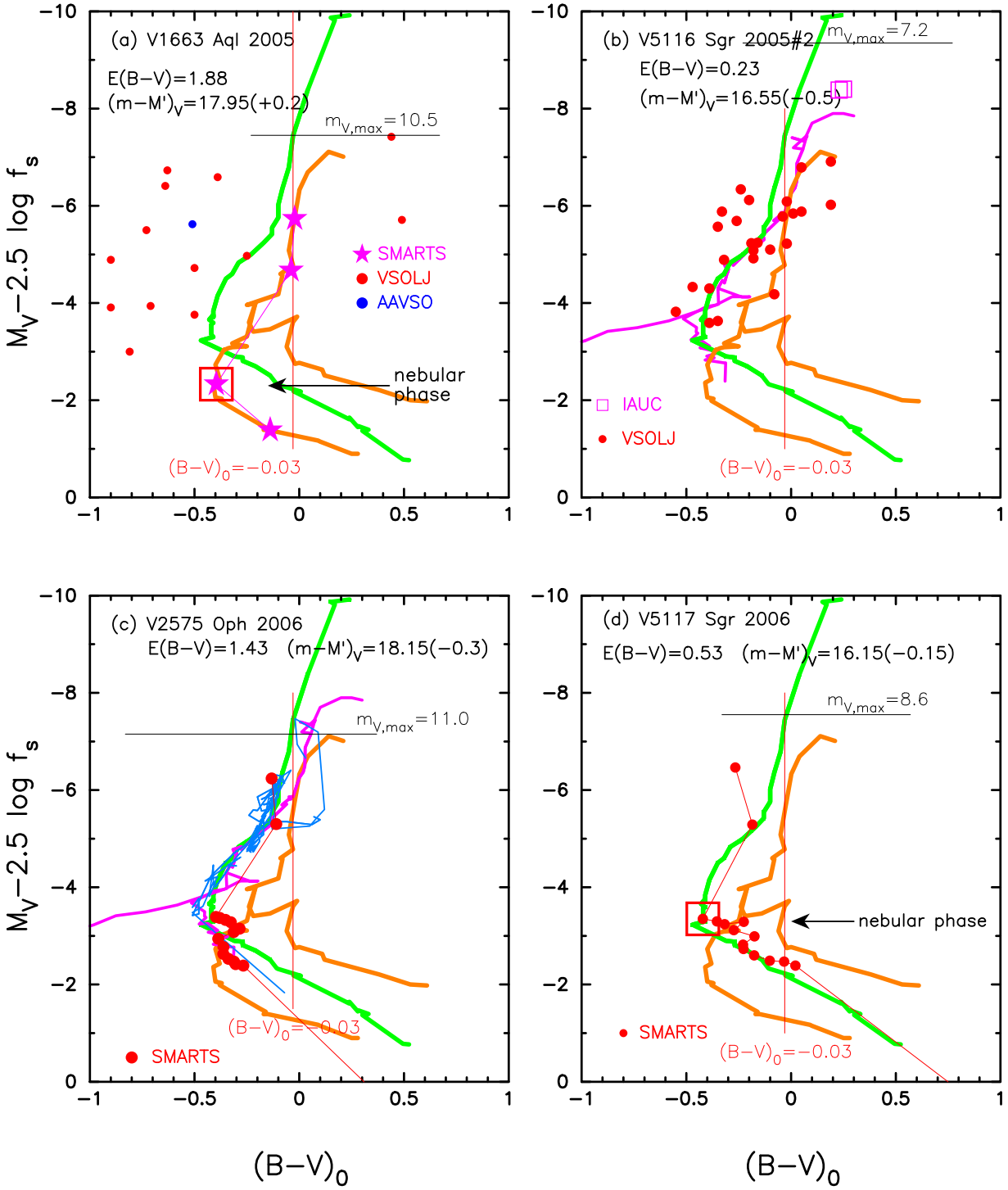

Figure 6. Time-stretched color–magnitude diagram for (a) V1663 Aql, (b) V5116 Sgr, (c) V2575 Oph, and (d) V5117 Sgr. The timescaling factor of f_s is measured against LV Vul. The thick solid orange lines represent the template track of LV Vul while the thick solid green lines denote that of V1500 Cyg. In panels (b) and (c), we add the track of V1974 Cyg (solid magenta lines). In panel (c), we add the track of PW Vul (solid cyan-blue lines).

B and I_C bands, that is,

$$(m-M)_{B,\rm target} = ((m-M)_B + \Delta B - 2.5\log f_s)_{\rm template}, \quad (9)$$

$$(m-M)_{I,\rm target} = ((m-M)_I + \Delta I_C - 2.5\log f_s)_{\rm template}, \quad (10)$$

where the timescaling factor f_s is the same as that in Equation (6). Thus, we obtain the three distance moduli in the B, V, and I_C bands (for example, Figure 25).

3. We adopt the relations between the distance d and color excess $E(B-V)$ to the target nova, i.e.,

$$(m-M)_V = 3.1E(B-V) + 5\log(d/10\,{\rm pc}), \quad (11)$$

where the factor $R_V = A_V/E(B-V) = 3.1$ is the ratio of total to selective extinction (e.g., Rieke & Lebofsky 1985),

$$(m - M)_B = 4.1E(B - V) + 5\log(d/10\ \mathrm{pc}), \quad (12)$$

where $A_B/E(B-V) = 4.1$ (Rieke & Lebofsky 1985), and

$$(m - M)_I = 1.5E(B - V) + 5\log(d/10\ \mathrm{pc}), \quad (13)$$

where $A_I/E(B-V) = 1.5$ from Rieke & Lebofsky (1985).

4. Using the $(m-M)_V$, $(m-M)_B$, and $(m-M)_I$ obtained in step 2, we plot the three relations of Equations (11), (12), and (13) in the reddening–distance plane, respectively. If the three lines cross at the same point, this point gives the correct values of reddening $E(B-V)$ and distance d (for example, Figure 5).
5. Using $E(B-V)$, $(m-M)_V$, and f_s obtained above in steps 1–4, we plot the $(B-V)_0$–$(M_V - 2.5\log f_s)$ diagram of the target nova (for example, Figure 6).
6. If the track of the target nova overlaps one of the template novae (LV Vul or V1500 Cyg) in the $(B-V)_0$–$(M_V - 2.5\log f_s)$ diagram, we regard our adopted values of f_s, $E(B-V)$, $(m-M)_V$, and d to be reasonable. When the target nova overlaps the track of LV Vul, we classify it as LV Vul type.

Many novae, including the present 32 novae, approximately follow the universal decline law, and we apply our method to them. However, it should be noted that some exceptional novae deviate greatly from the universal decline law, and the present method cannot be directly applied to them. We discuss such examples in more detail in Appendix C.

2.7. Comparison with Galactic Reddening–Distance Relations

We compare the obtained $E(B-V)$ and d of a nova with several galactic reddening–distance relations toward (l, b), where (l, b) is the galactic coordinates of the nova. We use six results:

(1) Marshall et al. (2006) published a three-dimensional (3D) extinction map of the Galaxy in the direction of $-100.^\circ0 \leqslant l \leqslant 100.^\circ0$ and $-10.^\circ0 \leqslant b \leqslant +10.^\circ0$ with grids of $\Delta l = 0.^\circ25$ and $\Delta b = 0.^\circ25$. We convert their A_{K_s} to our $E(B-V)$ with the relation of $A_{K_s} = A_K/0.95 = 0.112A_V/0.95 = (0.112 \times 3.1/0.95)E(B-V) = 0.365E(B-V)$.

(2) Sale et al. (2014) calculated a 3D reddening map for a region toward $30^\circ \leqslant l < 215^\circ$ and $|b| < 5^\circ$ based on the INT Photometric H-Alpha Survey photometry. We convert their A_0 to our $E(B-V)$ using the relation $A_0 = A_V = 3.1E(B-V)$.

(3) Schultheis et al. (2014) presented a 3D dust extinction map toward the galactic bulge covering $-10.^\circ0 < l < 10.^\circ0$ and $-10.^\circ0 < b < 5.^\circ0$, using data of the VISTA Variables in the Via Lactea (VVV) survey together with the Besançon stellar population synthesis model of the Galaxy. The resolution is $0.^\circ1 \times 0.^\circ1$, and the distance is extended up to 10 kpc in 0.5 kpc steps. We convert their $E(J-K_s)$ to our $E(B-V)$ using the relations $A_{K_s} = 0.364\,E(B-V)$ (Saito et al. 2013) and $A_{K_s} = 0.528\,E(J-K_s)$ (Nishiyama et al. 2009).

(4) Green et al. (2015) presented a 3D extinction map, which covers three quarters of the sky with grids $(\Delta l, \Delta b)$ of $3.'4$–$13.'7$. The data were recently revised (Green et al. 2018).

(5) Özdörmez et al. (2016) provided distance–reddening relations toward 46 novae. They used the unique position of the red clump giants in the color–magnitude diagram. The data have been revised and extended (Özdörmez et al. 2018). We convert their $E(J-K_s)$ to our $E(B-V)$ using the relation $A_{K_s} = 0.346E(B-V)$ and $A_{K_s} = 0.657E(J-K_s)$ (Rieke & Lebofsky 1985).

(6) Chen et al. (2018) obtained 3D reddening maps in the three colors of $E(G-K_s)$, $E(G_{BP}-G_{RP})$, and $E(H-K_s)$. We convert their $E(G_{BP}-G_{RP})$ to our $E(B-V)$ using the relation $E(B-V) = 0.75E(G_{BP}-G_{RP})$ (Chen et al. 2018). The maps have a spatial angular resolution of $6'$ and covers $0^\circ < l < 360^\circ$ and $|b| < 10^\circ$. The maps are based on the distances from *Gaia* Data Release 2 (*Gaia* DR2) and the photometry of the 2MASS, *WISE*, and *Gaia* DR2 surveys.

We regard our set of reddening and distance to be reasonable when the result $(E(B-V), d)$ for the target nova is consistent with one of the above six distance–reddening relations.

3. Time-stretched Color–Magnitude Diagram of 32 Novae

We select 32 novae that have enough BVI_C data and analyze their light and color curves in the order of discovery date. To avoid repetitive descriptions, we put all routines of the time-stretching method into Appendix A. The results of our light/color curve fittings are summarized in Table 1 for distance moduli and in Table 2 for WD masses. The WD mass is estimated from the model (free–free plus blackbody) light-curve fitting. The data on a total of 73 novae including previous data (Hachisu & Kato 2018b, 2019) provide a uniform quality data set obtained with a single method, that is, the time-stretching method of nova light curves.

3.1. V1663 Aql 2005

V1663 Aql reached $m_V = 10.5$ at V maximum on UT 2005 July 10.226 (Pojmanski & Oksanen 2005). Based on the O I lines of their 0.47–2.5 μm spectroscopy, Puetter et al. (2005) suggested a large reddening of $E(B-V) \sim 2$. Boyd & Poyner (2006) reported that the nova reached its maximum light on HJD 2,453,531.2 $\pm$ 0.2, when the apparent V magnitude was 10.7 ± 0.1. They estimated the decline times to be $t_{2,V} = 17$ days and $t_{3,V} = 32$ days, and derived a maximum absolute V magnitude of $M_{V,\max} = -7.8 \pm 0.2$ (from the MMRD and $M_{V,15}$ relations), color excess of $E(B-V) = 2$, and distance of $d = 2.9 \pm 0.4$ kpc. Here, $t_{2,V}$ and $t_{3,V}$ are the times during which the V magnitude decays by 2 and 3 mag from maximum, respectively. Poggiani (2006) obtained $t_2 = 10.9 \pm 2.0$ days and $t_3 = 22.0 \pm 3.5$ days, and derived a maximum V magnitude of $M_{V,\max} = -8.4$ (based on the MMRD and $M_{V,15}$ relations), color excess of $E(B-V) = 1.22$, and distance of $d = 7.3$–11.3 kpc. Lane et al. (2007) resolved sizes of the nova 5–18 days after the outburst, using NIR interferometry, and derived the distance of 8.9 ± 3.6 kpc. Hachisu & Kato (2007) analyzed the light curve of V1663 Aql based on their free–free emission model light curves and concluded that the V and I_C light curves are consistent with those of a 0.95 $M_\odot$ WD (CO2).

We obtain three distance moduli, $(m-M)_B = 19.98$, $(m-M)_V = 18.16$, and $(m-M)_I = 15.17$, in Appendix A.1 and plot them in Figure 5(a) with the magenta, blue, and cyan lines,

Table 1
Extinctions, Distance Moduli, and Distances for Selected Novae

Object	Outburst (year)	$E(B-V)$	$(m-M)_V$	d (kpc)	$\log f_s$[a]	$(m-M')_V$	References[b]
OS And	1986	0.15	14.8	7.3	−0.15	14.4	2
CI Aql	2000	1.0	15.7	3.3	−0.22	15.15	4
V1370 Aql	1982	0.35	16.3	11	0.05	16.4	6
V1419 Aql	1993	0.52	15.0	4.7	0.15	15.4	5
V1663 Aql	2005	1.88	18.15	2.9	−0.08	17.95	6
V679 Car	2008	0.69	16.1	6.2	0.0	16.1	5
V834 Car	2012	0.50	17.25	14	−0.19	16.75	6
V705 Cas	1993	0.45	13.45	2.6	0.45	14.55	5
V1065 Cen	2007	0.45	15.0	5.3	0.0	15.0	4
V1213 Cen	2009	0.78	16.95	8.1	0.05	17.05	6
V1368 Cen	2012	0.93	17.6	8.8	0.10	17.85	6
V1369 Cen	2013	0.11	10.25	0.96	0.17	10.65	5
IV Cep	1971	0.65	14.5	3.1	0.0	14.5	3
V962 Cep	2014	1.10	18.45	10.2	0.12	18.75	6
T CrB	1946	0.056	10.1	0.96	−1.32	13.4	4
V407 Cyg	2010	1.0	16.1	3.9	−0.37	15.2	4
V1500 Cyg	1975	0.45	12.3	1.5	−0.22	11.75	2
V1668 Cyg	1978	0.30	14.6	5.4	0.0	14.6	2
V1974 Cyg	1992	0.30	12.2	1.8	0.03	12.3	2
V2362 Cyg	2006	0.60	15.4	5.1	0.25	16.0	5
V2468 Cyg	2008	0.65	16.2	6.9	0.38	17.15	5
V2491 Cyg	2008	0.45	17.4	15.9	−0.34	16.55	5
V2659 Cyg	2014	0.80	15.7	4.4	0.52	17.0	6
YY Dor	2010	0.12	18.9	50	−0.72	17.1	4
V446 Her	1960	0.40	11.95	1.38	0.0	11.95	5
V533 Her	1963	0.038	10.65	1.28	0.08	10.85	5
V838 Her	1991	0.53	13.7	2.6	−1.22	10.65	4
PR Lup	2011	0.74	16.1	5.8	0.23	16.65	6
V959 Mon	2012	0.38	13.15	2.5	0.14	13.5	3
QY Mus	2008	0.58	14.65	3.7	0.35	15.55	6
V390 Nor	2007	0.89	16.6	5.8	0.45	17.75	6
RS Oph	2006	0.65	12.8	1.4	−1.02	10.25	4
V2575 Oph	2006#1	1.43	17.85	4.9	0.11	18.15	6
V2576 Oph	2006#2	0.62	16.65	8.8	−0.15	16.25	6
V2615 Oph	2007	0.90	15.95	4.3	0.20	16.45	5
V2670 Oph	2008#1	1.05	17.6	7.4	0.33	18.45	6
V2676 Oph	2012#1	0.90	17.3	8.0	0.53	18.65	6
V2677 Oph	2012#2	1.30	19.2	10.7	−0.17	18.75	6
V2944 Oph	2015	0.62	16.5	8.2	0.25	17.15	6
V574 Pup	2004	0.45	15.0	5.3	0.10	15.25	5
V597 Pup	2007	0.24	16.4	13.5	−0.18	15.95	6
U Sco	2010	0.26	16.3	12.6	−1.32	13.0	4
V745 Sco	2014	0.70	16.6	7.8	−1.32	13.3	4
V1281 Sco	2007#2	0.82	17.4	9.4	−0.07	17.25	6
V1313 Sco	2011#2	1.30	19.0	9.9	−0.22	18.45	6
V1324 Sco	2012	1.32	16.95	3.7	0.28	17.75	6
V1534 Sco	2014	0.93	17.6	8.8	−1.22	14.55	4
V1535 Sco	2015	0.78	18.3	15	0.38	19.25	6
V475 Sct	2003	0.55	15.4	5.5	0.36	16.3	2
V496 Sct	2009	0.45	13.7	2.9	0.30	14.45	5
V5114 Sgr	2004	0.47	16.65	10.9	−0.12	16.35	5
V5116 Sgr	2005#2	0.23	16.05	12	0.20	16.55	6
V5117 Sgr	2006	0.53	16.0	7.5	0.05	16.15	6
V5579 Sgr	2008	0.82	15.95	4.8	0.28	16.65	6
V5583 Sgr	2009#3	0.30	16.3	12	−0.29	15.55	6
V5584 Sgr	2009#4	0.70	16.7	8.0	0.13	17.05	6
V5585 Sgr	2010	0.47	16.7	11	0.10	16.95	6
V5589 Sgr	2012#1	0.84	17.6	10	−0.67	15.95	6
V5592 Sgr	2012#4	0.33	16.05	10	0.13	16.35	6
V5666 Sgr	2014	0.50	15.4	5.8	0.25	16.0	5
V5667 Sgr	2015#1	0.63	15.4	4.9	0.57	16.85	6
V5668 Sgr	2015#2	0.20	11.0	1.2	0.27	11.65	6
NR TrA	2008	0.24	15.35	8.3	0.43	16.45	6

Table 1
(Continued)

Object	Outburst (year)	$E(B-V)$	$(m-M)_V$	d (kpc)	$\log f_s$[a]	$(m-M')_V$	References[b]
V382 Vel	1999	0.25	11.5	1.4	−0.29	10.75	5
LV Vul	1968#1	0.60	11.85	1.0	0.0	11.85	2, 3, 5
PW Vul	1984#1	0.57	13.0	1.8	0.35	13.85	5
QU Vul	1984#2	0.55	13.6	2.4	0.33	14.45	1
V459 Vul	2007#2	0.90	15.45	3.4	−0.15	15.05	6
LMC N 2009a	2014	0.12	18.9	50	−0.52	17.6	4
LMC N 2012a	2012	0.12	18.9	50	−1.22	15.85	4
LMC N 2013	2013	0.12	18.9	50	−0.42	17.85	4
SMC N 2016	2016	0.08	16.8	20.4	−0.72	15.0	4
M31 N 2008−12a	2015	0.30	24.8	780	−1.32	21.5	4

Notes.
[a] f_s is the timescale against that of LV Vul.
[b] (1) Hachisu & Kato (2016a), (2) Hachisu & Kato (2016b), (3) Hachisu & Kato (2018a), (4) Hachisu & Kato (2018b), (5) Hachisu & Kato (2019), (6) present paper.

respectively, which cross at $d = 2.9$ kpc and $E(B-V) = 1.88$. Taking into account our fitting accuracy, we obtain $E(B-V) = 1.88 \pm 0.05$ and $d = 2.9 \pm 0.3$ kpc. The distance modulus in the V band is $(m-M)_V = 18.15 \pm 0.2$, and the timescaling factor is $f_s = 0.83$ against that of LV Vul. These values are listed in Table 1.

Our distance estimate of $d = 2.9 \pm 0.3$ kpc is largely different from that of Lane et al. (2007), i.e., 8.9 ± 3.6 kpc, based on the expansion parallax method. In general, the result of the expansion parallax method depends on the assumed expansion velocity and asphericity of ejecta. Lane et al. (2007) adopted $v_{\rm exp} = 1375 \pm 500$ km s^{-1}. If we adopt the $v_{\rm exp} \sim 700$ km s^{-1} given by Dennefeld et al. (2005) from the P-Cygni profiles at Hα and O I (777 nm), the distance becomes 4.5 ± 1.8 kpc, which is reasonably consistent with our results.

For the reddening toward V1663 Aql, Poggiani (2006) obtained $E(B-V) = 1.22$ from the intrinsic color at t_2, i.e., $(B-V)_{0,\ t2} = -0.02 \pm 0.04$ (van den Bergh & Younger 1987). However, the $B-V$ data of the Variable Star Observers League of Japan (VSOLJ) and the American Association of Variable Star Observers (AAVSO) are rather scattered and about 0.7 mag bluer than those of the Small and Medium Aperture Telescope System (SMARTS; Walter et al. 2012) as shown in Figures 6(a) and 23(b). If we use only the SMARTS data, we obtain $E(B-V) = 1.88 \pm 0.1$. Then, the $(B-V)_0$ colors of LV Vul and V1668 Cyg are similar to that of V1663 Aql during $\log t$ (day) $= 1$–2 as shown in Figure 24(b). Our reddening value of V1663 Aql is consistent with the estimates of $E(B-V) \sim 2$ given by Puetter et al. (2005) and Boyd & Poyner (2006). The $(B-V)_0$ color curve is located on the line of $B-V = -0.03$ (denoted by the thin red line in Figures 6(a) and 23(b)), which is the color of optically thick free–free emission (Hachisu & Kato 2014).

We further check our results by comparing with the galactic distance–reddening relations toward V1663 Aql, $(l,\ b) = (39^\circ.1610, -0^\circ.6648)$, in Figure 5(a). The four relations toward $(l,\ b) = (39^\circ.0, -0^\circ.50)$, $(39^\circ.25, -0^\circ.50)$, $(39^\circ.0, -0^\circ.75)$, and $(39^\circ.25, -0^\circ.75)$ are taken from Marshall et al. (2006) and depicted by unfilled red squares, filled green squares, blue asterisks, and unfilled magenta circles, respectively, each with error bars. The closest direction toward V1663 Aql in the galactic coordinates is that of the unfilled magenta circles. The thick solid green line denotes the relation of Sale et al. (2014). The thick solid black line indicates the relation of Green et al. (2015), and the orange one is their revised version (Green et al. 2018). The unfilled cyan-blue diamonds represent the relation of Özdörmez et al. (2018). We plot two thick solid cyan-blue lines of Chen et al. (2018) for $(l,\ b) = (39^\circ.15, -0^\circ.65)$ and $(l,\ b) = (39^\circ.15, -0^\circ.75)$. Our crossing point of $d = 2.9$ kpc and $E(B-V) = 1.88$ is consistent with Green et al.'s relation (orange line).

Using $E(B-V) = 1.88$ and $(m-M')_V = 17.95$ from Equation (16), we plot the time-stretched color–magnitude diagram of V1663 Aql in Figure 6(a). The text "$(m-M')_V = 17.95(+0.2)$" in the figure means $(m-M')_V = 17.95$ and $(m-M)_V = 17.95 + 0.2 = 18.15$. The data from SMARTS (Walter et al. 2012; filled magenta stars) are just on the track of LV Vul. Therefore, we regard V1663 Aql to belongs to the LV Vul type in the $(B-V)_0$–$(M_V - 2.5 \log f_s)$ diagram. Puetter et al. (2005) showed that the nova had already entered the nebular phase on UT 2005 November 14.16 (JD 2,453,688.66), 164 days after the outburst (the outburst day, $t_{\rm OB} =$ 2,453,525.0, is taken from Hachisu & Kato 2007). The SMARTS spectra also showed that the nebular phase had already started at least on UT 2005 September 2 (JD 2,453,615.5). We regard the nova to have entered the nebular phase about 80–100 days after the outburst. The start of the nebular phase is close to the third data point of SMARTS, so we plot a large unfilled red square in Figure 6(a). This overlap of the SMARTS data with the track of LV Vul suggests that our adopted values of $E(B-V) = 1.88$ and $(m-M')_V = 17.95$ are reasonable, that is, $E(B-V) = 1.88 \pm 0.05$, $f_s = 0.83$, $(m-M)_V = 18.15 \pm 0.2$, and $d = 2.9 \pm 0.3$ kpc.

We check the value of $(m-M)_V = 18.15$ by comparing our model V light curve with the observation. Figure 24(a) shows the model V and UV 1455 Å light curves (thin solid black lines) of a 1.0 $M_\odot$ WD (CO3). We add another model V light curve (green lines) of a 0.98 $M_\odot$ WD (CO3). This is a model for V1668 Cyg, which is time-stretched by $\Delta \log t = \log f_s = \log 0.83 = -0.08$. The V light curve of V1668 Cyg follows the model V light curve until day ∼100. V1668 Cyg entered the nebular phase on day ∼100. Strong [O III] lines make a significant contribution to the V band and, as a result, the observed V light curve keeps a similar decay trend of $F_\nu \propto t^{-1.75}$ in the nebular phase. Because our model light curve does not include the effect of emission lines, it

Table 2
White Dwarf Masses of Selected Novae

Object	$\log f_s$	M_{WD} f_s[a] ($M_\odot$)	M_{WD} UV 1455 Å[b] ($M_\odot$)	M_{WD} $t_{SSS\text{-}on}$[c] ($M_\odot$)	M_{WD} $t_{SSS\text{-}off}$[d] ($M_\odot$)	Chem. Comp.
OS And	−0.15	1.05	⋯	⋯	⋯	CO3
CI Aql	−0.22	1.18	⋯	⋯	⋯	interp.[e]
V1419 Aql	+0.15	0.90	⋯	⋯	⋯	CO3
V1663 Aql	−0.08	0.95	⋯	⋯	⋯	CO2
V1663 Aql	−0.08	1.0	⋯	⋯	⋯	CO3
V679 Car	+0.0	0.98	⋯	⋯	⋯	CO3
V834 Car	−0.19	1.20	⋯	⋯	⋯	Ne3
V705 Cas	+0.45	0.78	0.78	⋯	⋯	CO4
V1065 Cen	+0.0	0.98	⋯	⋯	⋯	CO3
V1368 Cen	+0.10	0.95	⋯	⋯	⋯	CO3
V1369 Cen	+0.17	0.90	⋯	⋯	⋯	CO3
IV Cep	+0.0	0.98	⋯	⋯	⋯	CO3
V962 Cep	+0.12	0.95	⋯	⋯	⋯	CO3
T CrB	−1.32	1.38	⋯	⋯	⋯	interp.
V407 Cyg	−0.37	1.22	⋯	⋯	⋯	interp.
V1500 Cyg	−0.22	1.20	⋯	⋯	⋯	Ne2
V1668 Cyg	+0.0	0.98	0.98	⋯	⋯	CO3
V1974 Cyg	+0.03	0.98	0.98	0.98	0.98	CO3
V2362 Cyg	+0.25	0.85	⋯	⋯	⋯	interp.
V2468 Cyg	+0.38	0.85	⋯	⋯	⋯	CO4
V2491 Cyg	−0.34	1.35	⋯	1.35	1.35	Ne2
V2659 Cyg	+0.52	0.75	⋯	⋯	⋯	CO4
YY Dor	−0.72	1.29	⋯	⋯	⋯	interp.
V446 Her	+0.0	0.98	⋯	⋯	⋯	CO3
V533 Her	+0.08	1.03	⋯	⋯	⋯	Ne2
V838 Her	−1.22	1.35	1.35	⋯	⋯	Ne2
V838 Her	−1.22	1.37	1.37	⋯	⋯	Ne3
PR Lup	+0.23	0.90	⋯	⋯	⋯	CO3
V959 Mon	+0.14	0.95	⋯	0.95	⋯	CO3
V959 Mon	+0.14	1.05	⋯	1.05	⋯	Ne2
V959 Mon	+0.14	1.1	⋯	1.10	⋯	Ne3
QY Mus	+0.35	0.75	⋯	⋯	⋯	CO2
QY Mus	+0.35	0.80	⋯	⋯	⋯	CO3
QY Mus	+0.35	0.85	⋯	⋯	⋯	CO4
V390 Nor	+0.45	0.75	⋯	⋯	⋯	CO3
RS Oph	−1.02	1.35	1.35	1.35	1.35	evol.[f]
V2575 Oph	+0.11	0.90	⋯	⋯	⋯	CO3
V2576 Oph	−0.15	1.15	⋯	⋯	⋯	Ne2
V2615 Oph	+0.20	0.90	⋯	⋯	⋯	CO3
V2670 Oph	+0.33	0.80	⋯	⋯	⋯	CO3
V2676 Oph	+0.53	0.70	⋯	⋯	⋯	CO2
V2677 Oph	−0.17	1.15	⋯	⋯	⋯	Ne2
V2944 Oph	+0.25	0.85	⋯	⋯	⋯	CO3
V574 Pup	+0.10	1.05	⋯	1.05	1.05	Ne2
V597 Pup	−0.18	1.2	⋯	1.2	1.2	Ne3
U Sco	−1.32	1.37	⋯	1.37	1.37	evol.
V745 Sco	−1.32	1.38	⋯	1.385	1.385	evol.
V1281 Sco	−0.07	1.13	⋯	⋯	⋯	Ne2
V1313 Sco	−0.22	1.20	⋯	⋯	⋯	Ne2
V1324 Sco	+0.28	0.80	⋯	⋯	⋯	CO2
V1534 Sco	−1.22	1.37	⋯	⋯	⋯	interp.
V1535 Sco	+0.38	0.85	⋯	⋯	⋯	CO4
V475 Sct	+0.36	0.80	⋯	⋯	⋯	CO3
V496 Sct	+0.30	0.85	⋯	⋯	⋯	CO3
V5114 Sgr	−0.12	1.15	⋯	⋯	⋯	Ne2
V5116 Sgr	+0.20	0.90	⋯	⋯	⋯	CO2
V5116 Sgr	+0.20	1.07	⋯	⋯	⋯	Ne3
V5117 Sgr	+0.05	0.95	⋯	⋯	⋯	CO3
V5579 Sgr	+0.28	0.85	⋯	⋯	⋯	CO3
V5583 Sgr	−0.29	1.23	⋯	1.23	1.23	Ne2
V5584 Sgr	+0.13	0.90	⋯	⋯	⋯	CO3
V5585 Sgr	+0.10	0.95	⋯	⋯	⋯	CO3

Table 2
(Continued)

Object	$\log f_s$	M_{WD} f_s[a] ($M_\odot$)	M_{WD} UV 1455 Å[b] ($M_\odot$)	M_{WD} $t_{SSS\text{-}on}$[c] ($M_\odot$)	M_{WD} $t_{SSS\text{-}off}$[d] ($M_\odot$)	Chem. Comp.
V5589 Sgr	−0.67	1.33	⋯	⋯	⋯	Ne2
V5592 Sgr	+0.13	0.93	⋯	⋯	⋯	CO4
V5666 Sgr	+0.25	0.85	⋯	⋯	⋯	CO3
V5667 Sgr	+0.57	0.78	⋯	⋯	⋯	CO4
V5668 Sgr	+0.27	0.85	⋯	⋯	⋯	CO3
NR TrA	+0.43	0.75	⋯	⋯	⋯	CO3
V382 Vel	−0.29	1.23	⋯	⋯	1.23	Ne2
LV Vul	+0.0	0.98	⋯	⋯	⋯	CO3
PW Vul	+0.35	0.83	0.83	⋯	⋯	CO4
QU Vul	+0.33	0.96	⋯	⋯	⋯	Ne3
QU Vul	+0.33	0.90	⋯	⋯	⋯	Ne2
QU Vul	+0.33	0.86	⋯	⋯	⋯	CO4
QU Vul	+0.33	0.82	⋯	⋯	⋯	CO2
V459 Vul	−0.15	1.15	⋯	⋯	⋯	Ne2
LMC N 2009a	−0.52	1.25	⋯	1.25	1.25	Ne3
LMC N 2012a	−1.22	1.37	⋯	⋯	⋯	interp.
LMC N 2013	−0.42	1.23	⋯	⋯	⋯	interp.
SMC N 2016	−0.72	1.29	⋯	⋯	1.3	Ne3
SMC N 2016	−0.72	1.29	⋯	⋯	1.25	Ne2
M31N 2008-12a	−1.32	1.38	⋯	1.38	1.38	evol.

Notes.
[a] WD mass estimated from the f_s timescale.
[b] WD mass estimated from the UV 1455 Å fit.
[c] WD mass estimated from the t_{SSS-on} fit.
[d] WD mass estimated from the $t_{SSS-off}$ fit.
[e] WD mass estimated from the linear interpolation of the $\log f_s$ versus WD mass relation (see Hachisu & Kato 2018b).
[f] WD mass estimated from the time-evolution calculation with a Henyey type code (see, e.g., Hachisu & Kato 2018b).

begins to deviate from the observed V light curve (see Figure 24(a)).

The optically thick winds eventually stop. The end of the optically thick winds is denoted by the unfilled circle at the right end of the model V light curve (day ∼230) in Figure 24(a). After the optically thick winds stop, the V light curve follows the trend of $F_\nu \propto t^{-3}$ (solid blue line) in Figure 24(a). This line indicates the decay of homologously expanding ejecta, i.e., the total mass of the ejecta is kept constant in time (see, e.g., Woodward et al. 1997; Hachisu & Kato 2006). The V light curve of V1663 Aql decays along t^{-3} after day ∼230. Thus, the end of the model V light curve corresponds reasonably well to the change of slope at the epoch of "wind stops" (day ∼230). Thus, we confirm that the values of $(m-M)_V = 18.15$ and $M_{WD} = 1.0\,M_\odot$ (CO3) are reasonable.

As already discussed in Hachisu & Kato (2016a), if we fix the chemical composition of the hydrogen-rich envelope, the mass determination has an accuracy of $\pm 0.01\,M_\odot$ for the case of V1668 Cyg because we simultaneously fit the V and UV 1455 Å light curves with the observation. On the other hand, Hachisu & Kato (2010) obtained a $0.95\,M_\odot$ WD as a best fit for V1663 Aql assuming the other chemical composition of CO2. To summarize, the WD mass determination depends on the chemical composition of the hydrogen-rich envelope, especially on the hydrogen content of X and the carbon–nitrogen–oxygen abundance (X_{CNO}) by weight, as discussed by Hachisu & Kato (2007). We again discuss the accuracy of WD mass determination for more detail in Section 4.2.

3.2. V5116 Sgr 2005#2

The nova reached 7.2 mag at maximum on UT 2005 July 5.085 (Liller 2005). Hachisu & Kato (2007) analyzed the light curve of V5116 Sgr based on their free–free emission model light curves and concluded that the V light curve is consistent with that of a $0.90 \pm 0.1\,M_\odot$ WD (CO2). The nova became a supersoft X-ray source (Sala et al. 2008) at least 674 days after the outburst (the outburst day of t_{OB} = JD 2,453,552.0, i.e., UT 2005 July 1.5, taken from Hachisu & Kato 2007). Sala et al. (2008) reported that the X-ray light curve shows abrupt decreases and increases of the flux by a factor of ∼8. This periodicity is consistent with a 2.97 hr orbital period suggested by Dobrotka et al. (2008). These authors speculated that the X-ray light curve may result from a partial coverage by an asymmetric accretion disk in a high-inclination system (see also Sala et al. 2017). Ness et al. (2007) also reported the supersoft X-ray detection with *Swift* 768 days after the outburst (UT 2007 August 7.742).

Sala et al. (2008) estimated the absorption of $A_V = 3.1E(B-V) = 0.8 \pm 0.2$ from the color at maximum, $(B-V)_{0,max} = 0.23 \pm 0.06$ (van den Bergh & Younger 1987), and the distance of $d = 11 \pm 3$ kpc from $t_2 = 6.5 \pm 1.0$ days (Dobrotka et al. 2008) together with the MMRD relation

proposed by della Valle & Livio (1995). Sala et al. (2008) concluded that O/Ne-rich WD atmosphere models provide a better fit than C/O-rich WD atmosphere models. Hachisu & Kato (2010) adopted the chemical composition of Ne nova 3 (Ne3) and obtained a new best-fitting model of a 1.07 $M_\odot$ WD (see Figure 24 of Hachisu & Kato 2010) based on their free–free emission model light curves. They also obtained the distance modulus of $(m-M)_V = 16.2 \pm 0.2$ and the distance of $d = 12 \pm 1$ kpc based on their light-curve fitting with their model light curve. Özdörmez et al. (2016) obtained the very different distance of $d = 1.55 \pm 0.70$ kpc from their distance–reddening relation together with $E(B-V) = 0.23 \pm 0.06$.

We obtain $(m-M)_B = 16.28$, $(m-M)_V = 16.07$, and $(m-M)_I = 15.68$, which cross at $d = 11.7$ kpc and $E(B-V) = 0.23$, in Appendix A.2 and plot them in Figure 5(b). Taking into account our fitting accuracy, we obtain $E(B-V) = 0.23 \pm 0.05$ and $d = 12 \pm 2$ kpc. The distance modulus in the V band is $(m-M)_V = 16.05 \pm 0.1$, and the timescaling factor is $f_s = 1.58$ against LV Vul.

For the reddening toward V5116 Sgr, $(l,\ b) = (2.^\circ1363, -6.^\circ8326)$, the VVV survey catalog (Saito et al. 2013) gives $E(B-V) = A_{K_s}/0.36 = 0.084/0.36 = 0.23$. Also Sala et al. (2008) adopted $E(B-V) = A_V/3.1 = 0.8/3.1 = 0.25$. The NASA/IPAC Infrared Science Archive,[3] which is calculated using the data from Schlafly & Finkbeiner (2011), gives $E(B-V) = 0.224 \pm 0.003$ toward V5116 Sgr. All of these reddening values are consistent with our crossing point.

We further examine our result in Figure 5(b). The vertical solid red line represents $E(B-V) = 0.23$, and the thick solid blue line denotes the relation of Equation (11) together with $(m-M)_V = 16.05$. These two lines cross each other at $d = 12$ kpc. The four relations toward $(l,\ b) = (2.^\circ00, -6.^\circ75)$, $(2.^\circ25, -6.^\circ75)$, $(2.^\circ00, -7.^\circ00)$, and $(2.^\circ25, -7.^\circ00)$ are taken from Marshall et al. (2006). The closest direction is that of the filled green squares. We denote four of Schultheis et al.'s (2014) distance–reddening relations toward $(l,\ b) = (2.^\circ1, -6.^\circ8)$, $(2.^\circ1, -6.^\circ9)$, $(2.^\circ2, -6.^\circ8)$, and $(2.^\circ2, -6.^\circ9)$ with very thin solid cyan lines in Figure 5(b). These four lines show zigzag patterns, although the reddening should increase monotonically with the distance. In this sense, Schultheis et al.'s relation may not be appropriate in the middle distance. The other symbols/lines have the same meanings as those in Figure 5(a).

The reddening toward V5116 Sgr seems to saturate at $d > 5$ kpc as shown in Figure 5(b). Our crossing point, $d = 12$ kpc and $E(B-V) = 0.23$, is consistent with Marshall et al.'s relations considering their error bars, although it ends at $d = 10$ kpc. On the other hand, Green et al.'s black/orange lines and Chen et al.'s cyan-blue line deviate slightly from Marshall et al.'s relation. Özdörmez et al. (2016) obtained $d = 1.55 \pm 0.70$ kpc as mentioned earlier, assuming $E(B-V) = 0.23 \pm 0.06$ and using their distance–reddening relation. We think that this distance is too small. Their results come from their distance–reddening relation, which is similar to the distance–reddening relations of Schultheis et al. (2014). This distance–reddening relation is rather different from the distance–reddening relations of Marshall et al. (2006). We confirmed that the adopted set of $E(B-V) = 0.23$ and $d = 12$ kpc is consistent with Marshall et al.'s relation.

We plot the track of V5116 Sgr in Figure 6(b), using $E(B-V) = 0.23$ and $(m-M')_V = 16.55$ $(f_s = 1.58)$ in Equation (21). The track of V5116 Sgr almost follows that of V1974 Cyg, although the data points of VSOLJ are rather scattered around the track of V1974 Cyg (solid magenta lines) and V1500 Cyg (solid green line). In general, the VSOLJ data were obtained by many amateur astronomers, and their typical errors were not reported. Therefore, we do not examine the typical deviation of their data. However, the mean trend of the V light and $(B-V)_0$ color curves in Figures 27(a) and (b) broadly follow the trends of V1974 Cyg. This suggests that the mean trend of the track in Figure 6(b) broadly overlaps the track of V1974 Cyg.

Basically, we overlap the track of a target nova to that of the template nova, LV Vul, and measure the timescaling factor against LV Vul. The V1500 Cyg and V1974 Cyg tracks have been calibrated in our previous paper (Hachisu & Kato 2019) and their timescaling factors were measured against LV Vul. Therefore, their time-stretched color–magnitude tracks are also well calibrated. This means that we can use either V1500 Cyg or V1974 Cyg as another template nova. However, it should be noted that the timescaling factor of f_s is measured against LV Vul even if we use the V1500 Cyg track as a template nova, because we have to use common timescales for various novae that belong to one of the LV Vul and V1500 Cyg types.

We regard V5116 Sgr to belong to the V1500 Cyg type. This rough overlapping with the V1974 Cyg track may support our adopted values of $E(B-V) = 0.23$ and $(m-M')_V = 16.55$, that is, $E(B-V) = 0.23 \pm 0.05$, $(m-M)_V = 16.05 \pm 0.1$, $d = 12 \pm 2$ kpc, $f_s = 1.58$.

We further check our value of $(m-M)_V = 16.05$ by fitting our model V light curve with the observation as shown in Figure 27(a). Assuming $(m-M)_V = 16.05$, our model V light curve (black line) and the soft X-ray light curve (red line) of a 1.07 $M_\odot$ WD (Ne3, Hachisu & Kato 2016a) fit reasonably well with the observed V and X-ray light curves. This confirms that our result of $(m-M)_V = 16.05$ is reasonable. We also add a 0.98 $M_\odot$ WD (CO3) model for V1974 Cyg (see also Hachisu & Kato 2016a). If we adopt Özdörmez et al.'s results of $d = 1.55$ kpc and $E(B-V) = 0.23$, then the distance modulus in the V band should be $(m-M)_V = 11.7$, being much smaller than $(m-M)_V = 16.05$ and not consistent with our model light curve. This means that, if we plot our model light curve of 1.07 $M_\odot$ WD assuming $(m-M)_V = 11.7$, its V model light curve is located −4.35 mag far above the observed V light curve.

3.3. V2575 Oph 2006

The nova reached $m_{V,\max} = 10.96$ on JD 2,453,779.0 (taken from the AAVSO data). Russell et al. (2006) reported that V2575 Oph is an Fe II type nova and the reddening is $E(B-V) = 1.42$ from their 0.8–5.4 μm spectroscopy. Rudy et al. (2006) obtained $E(B-V) = 1.5$ from the O I lines.

We obtain $(m-M)_B = 19.3$, $(m-M)_V = 17.88$, and $(m-M)_I = 15.59$, which cross at $d = 4.9$ kpc and $E(B-V) = 1.43$, in Appendix A.3 and plot them in Figure 5(c). Thus, we obtain $E(B-V) = 1.43 \pm 0.05$ and $d = 4.9 \pm 0.5$ kpc. Our value of $E(B-V) = 1.43 \pm 0.05$ is consistent with and close to the values obtained by Rudy et al. (2006) and Russell et al. (2006).

Figure 6(c) shows the $(B-V)_0$–$(M_V - 2.5\log f_s)$ diagram of V2575 Oph for $E(B-V) = 1.43$ and $(m-M')_V = 18.15$ in Equation (26). The data taken from SMARTS (filled red circles) follow well the track of V1974 Cyg (solid magenta lines) and PW Vul (solid cyan-blue lines). We regard V2575 Oph to belong to the V1500 Cyg type, because both

[3] http://irsa.ipac.caltech.edu/applications/DUST/

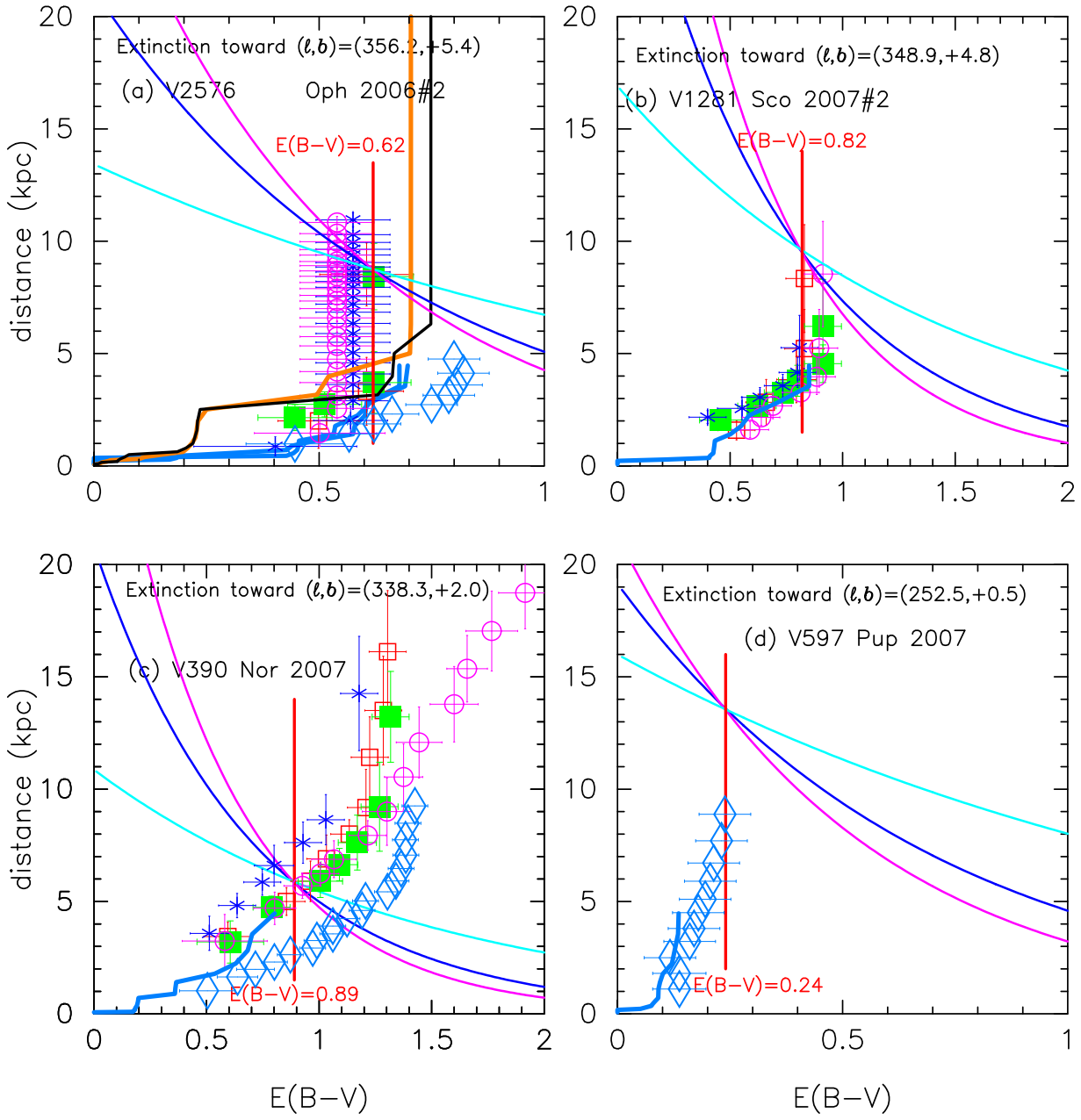

Figure 7. Same as Figure 5, but for (a) V2576 Oph, (b) V1281 Sco, (c) V390 Nor, and (d) V597 Pup.

V1974 Cyg and PW Vul belong to the V1500 Cyg type (see Hachisu & Kato 2019). This overlapping with the PW Vul track may support the fact that our adopted values of $E(B-V) = 1.43$ and $(m-M')_V = 18.15$ are reasonable, that is, $E(B-V) = 1.43 \pm 0.05$, $(m-M)_V = 17.85 \pm 0.1$, $f_s = 1.29$, and $d = 4.9 \pm 0.5$ kpc.

We examine the distance and reddening toward V2575 Oph, $(l,\ b) = (19.^{\circ}7995,\ +10.^{\circ}3721)$, in Figure 5(c). Two relations toward $(l,\ b) = (19.^{\circ}75,\ +10.^{\circ}00)$ and $(20.^{\circ}00,\ +10.^{\circ}00)$ are taken from Marshall et al. (2006) and depicted by the unfilled red squares and filled green squares, respectively, each with error bars. The closer direction in galactic coordinates is that of the unfilled red squares. The solid black/orange lines are taken from the relations given by Green et al. (2015, 2018), respectively, which deviate slightly from Marshall et al.'s relations. The unfilled cyan-blue diamonds are the relation of Özdörmez et al. (2016). The solid cyan-blue line corresponds to the relation of Chen et al. (2018). Our crossing point, $d = 4.9$ kpc and $E(B-V) = 1.43$, is rather far from Marshall et al.'s, Green et al.'s, and Chen et al.'s relations. The NASA/IPAC absorption map gives $E(B-V) = 0.64 \pm 0.03$ toward V2575 Oph, which is consistent with Marshall et al.'s, Green et al.'s, and Chen et al.'s relations. On the other hand, the VVV catalog (Saito et al. 2013) gives $E(B-V) = A_{K_s}/0.36 = 0.488/0.36 = 1.35$, which is close to our value of $E(B-V)$ =1.43. Özdörmez et al.'s relation is also consistent with our crossing point.

We further check our value of $(m-M)_V = 17.85$ by fitting our model V light curve with the observation as shown in Figure 30(a). Assuming $(m-M)_V = 17.85$, our model light curve of a 0.90 $M_{\odot}$ WD (CO3; Hachisu & Kato 2016a) fits reasonably well with the observed V light curve. This confirms that our result of $(m-M)_V = 17.85$ is reasonable.

3.4. V5117 Sgr 2006#2

The nova reached $m_{V,\max} = 8.6$ on JD 2,453,785.0 ± 1.0 (UT 2006 February 18.5 ± 1.0, IAU Circular 8673, 1). Lynch et al. (2006b) reported that V5117 Sgr is an Fe II type nova and the reddening is $E(B-V) = 0.50 \pm 0.15$ from their 0.8–5.5 μm spectroscopy on UT 2006 May 1.

We obtain $(m-M)_B = 16.53$, $(m-M)_V = 16.01$, and $(m-M)_I = 15.12$, which cross at $d = 7.5$ kpc and $E(B-V) = 0.53$, in Appendix A.4 and plot them in Figure 5(d). Thus, we obtain $d = 7.5 \pm 0.8$ kpc and $E(B-V) = 0.53 \pm 0.05$.

For the reddening toward V5117 Sgr, $(l, b) = (354.^\circ6241, -6.^\circ3774)$, our obtained value of $E(B-V) = 0.53$ is consistent with Lynch et al.'s result as mentioned above. On the other hand, the NASA/IPAC absorption map gives $E(B-V) = 0.37 \pm 0.02$. The VVV catalog (Saito et al. 2013) gives $E(B-V) = A_{K_s}/0.36 = 0.098/0.36 = 0.27$. We further check our result toward V5117 Sgr in Figure 5(d). We plot Marshall et al.'s (2006) relations toward $(l, b) = (354.^\circ50, -6.^\circ50)$, $(354.^\circ75, -6.^\circ50)$, $(354.^\circ50, -6.^\circ25)$, and $(354.^\circ75, -6.^\circ25)$. Green et al.'s (2015, 2018) relations are not available for this direction. We also add the 3D reddening map obtained by Schultheis et al. (2014) with the very thin solid cyan lines (four close directions toward V5117 Sgr). The two thick solid cyan-blue lines correspond to the relations of Chen et al. (2018), toward $(l, b) = (354.^\circ65, -6.^\circ35)$ and $(l, b) = (354.^\circ65, -6.^\circ45)$. The other symbols/lines have the same meanings as those in Figure 5(a). These 3D maps are largely different from each other, but Marshall et al.'s relations with error bars are roughly close to our crossing point.

Using $E(B-V) = 0.53$ and $(m-M')_V = 16.15$ in Equation (31), we plot the $(B-V)_0$–$(M_V - 2.5\log f_s)$ diagram of V5117 Sgr in Figure 6(d). The track of V5117 Sgr almost follows that of V1500 Cyg, so we regard V5117 Sgr to belong to the V1500 Cyg type. The nova had already entered the nebular phase on UT 2006 September 6 from the SMARTS spectra, corresponding to $m_V = 13.6$ ($M_V = -2.4$). We consider that V5117 Sgr entered the nebular phase at the turning point from blue toward red (Hachisu & Kato 2016b) as shown by the large unfilled red square in Figure 6(d). This overlapping with the V1500 Cyg track supports $E(B-V) = 0.53$ and $(m-M')_V = 16.15$, that is, $E(B-V) = 0.53 \pm 0.05$, $(m-M)_V = 16.0 \pm 0.1$, $f_s = 1.12$, and $d = 7.5 \pm 0.8$ kpc. If the distance of 7.5 kpc is correct, V5117 Sgr belongs to the galactic bulge.

We further check the distance modulus of $(m-M)_V = 16.0$ by comparing our model V light curve with the observation in Figure 33(a). Assuming that $(m-M)_V = 16.0$, we plot a model V light curve (solid black lines) of a 0.95 $M_\odot$ WD (CO3; Hachisu & Kato 2016a). The model light curve reproduces well the observation, supporting our value of $(m-M)_V = 16.0$. We also plot a model V light curve (solid green lines) of a 0.98 $M_\odot$ WD (CO3), assuming that $(m-M)_V = 14.6$ for V1668 Cyg.

3.5. V2576 Oph 2006#2

Russell et al. (2006) reported that the nova showed an Fe II type spectrum from their 0.8–5.4 μm spectroscopy on UT 2006 April 30. They obtained $E(B-V) = 0.62$. Lynch et al. (2006a) reported a much smaller value of $E(B-V) = 0.25$ and no evidence of dust in the nova ejecta based on their 0.47–2.5 μm spectroscopy on UT 2006 June 14.4.

We obtain $(m-M)_B = 17.25$, $(m-M)_V = 16.63$, and $(m-M)_I = 15.64$ (see Appendix A.5), which cross at $d = 8.8$ kpc and $E(B-V) = 0.62$, and plot them in Figure 7(a). Thus, we have $E(B-V) = 0.62 \pm 0.05$ and $d = 8.8 \pm 1$ kpc.

For the reddening toward V2576 Oph, $(l, b) = (356.^\circ2004, +5.^\circ3694)$, the NASA/IPAC absorption map gives $E(B-V) = 0.62 \pm 0.01$, which is consistent with our result and the value obtained by Russell et al. (2006). We further check our result in Figure 7(a). We plot four relations of Marshall et al. (2006) toward $(l, b) = (356.^\circ00, +5.^\circ25)$, $(356.^\circ25, +5.^\circ25)$, $(356.^\circ00, +5.^\circ50)$, and $(356.^\circ25, +5.^\circ50)$. The closest direction is that of the filled green squares. We add the 3D reddening maps calculated by Özdörmez et al. (2016; unfilled cyan-blue diamonds with error bars) and by Chen et al. (2018; thick solid cyan-blue lines toward $(l, b) = (356.^\circ15, +5.^\circ35)$ and $(l, b) = (356.^\circ25, +5.^\circ35)$). The other symbols/lines have the same meanings as those in Figure 5(a). These 3D maps are largely different from each other. Only Marshall et al.'s relation, shown by the filled green squares with error bars, is consistent with our crossing point.

Figure 8(a) shows the $(B-V)_0$–$(M_V - 2.5\log f_s)$ diagram of V2576 Oph for $E(B-V) = 0.62$ and $(m-M')_V = 16.25$ in Equation (36). The track of V2576 Oph almost follows that of LV Vul in the middle phase of nova evolution, so we regard V2576 Oph to belong to the LV Vul type. From the SMARTS spectra, the nova had already entered the nebular phase on UT 2006 August 9 (JD 2,453,956.5), corresponding to $m_V = 15.0$ ($M_V = -1.65$). We consider that V2576 Oph entered the nebular phase at the point denoted by the large unfilled red square in Figure 8(a), i.e., $M_V = -2.5$ and $(B-V)_0 = -0.31$. This overlapping with the LV Vul track suggests that $E(B-V) = 0.62$ and $(m-M')_V = 16.25$ are reasonable. Thus, we confirm $E(B-V) = 0.62 \pm 0.05$, $(m-M)_V = 16.65 \pm 0.1$, $f_s = 0.71$, and $d = 8.8 \pm 1$ kpc. If the distance is correct, V2576 Oph belongs to the galactic bulge.

We finally check the distance modulus of $(m-M)_V = 16.65$ by comparing our model V light curve with the observation. Assuming that $(m-M)_V = 16.65$, we plot a model light curve of a 1.15 $M_\odot$ WD (Ne2; solid black line, Hachisu & Kato 2010) for V2576 Oph as shown in Figure 36(a). Our model light curve reasonably follows the V light curve of V2576 Oph. This again confirms that the distance modulus of $(m-M)_V = 16.65$ is reasonable. For comparison, we add the model light curve of a 0.98 $M_\odot$ WD (CO3; solid green lines, Hachisu & Kato 2016a) and show that it follows well the light curve of V1668 Cyg, assuming that $(m-M)_V = 14.6$ for V1668 Cyg.

3.6. V1281 Sco 2007#2

The nova was as bright as 9.3 mag when Y. Nakamura discovered the nova (Yamaoka et al. 2007). Henden & Munari (2007) estimated a maximum around UT 2007 February 20.5 at $m_{V,\max} = 8.5$ from their extrapolation of the available data. The nova had declined to 8.8 mag by UT 2007 February 20.85 (Yamaoka et al. 2007). Russell et al. (2007) reported the reddening of $E(B-V) = 0.7$ derived from the O I lines based on their 0.8–5.5 μm spectroscopy on UT 2007 May 6. Hachisu & Kato (2010) obtained a best-fitting model of 1.13 $M_\odot$ WD (Ne2) based on their free–free emission model light curves, $(m-M)_V = 17.8 \pm 0.2$, and $d = 13 \pm 1$ kpc for $E(B-V) = 0.7$. The nova was detected with *Swift* as a supersoft X-ray source on UT 2008 January 24.18 (Schwarz et al. 2011).

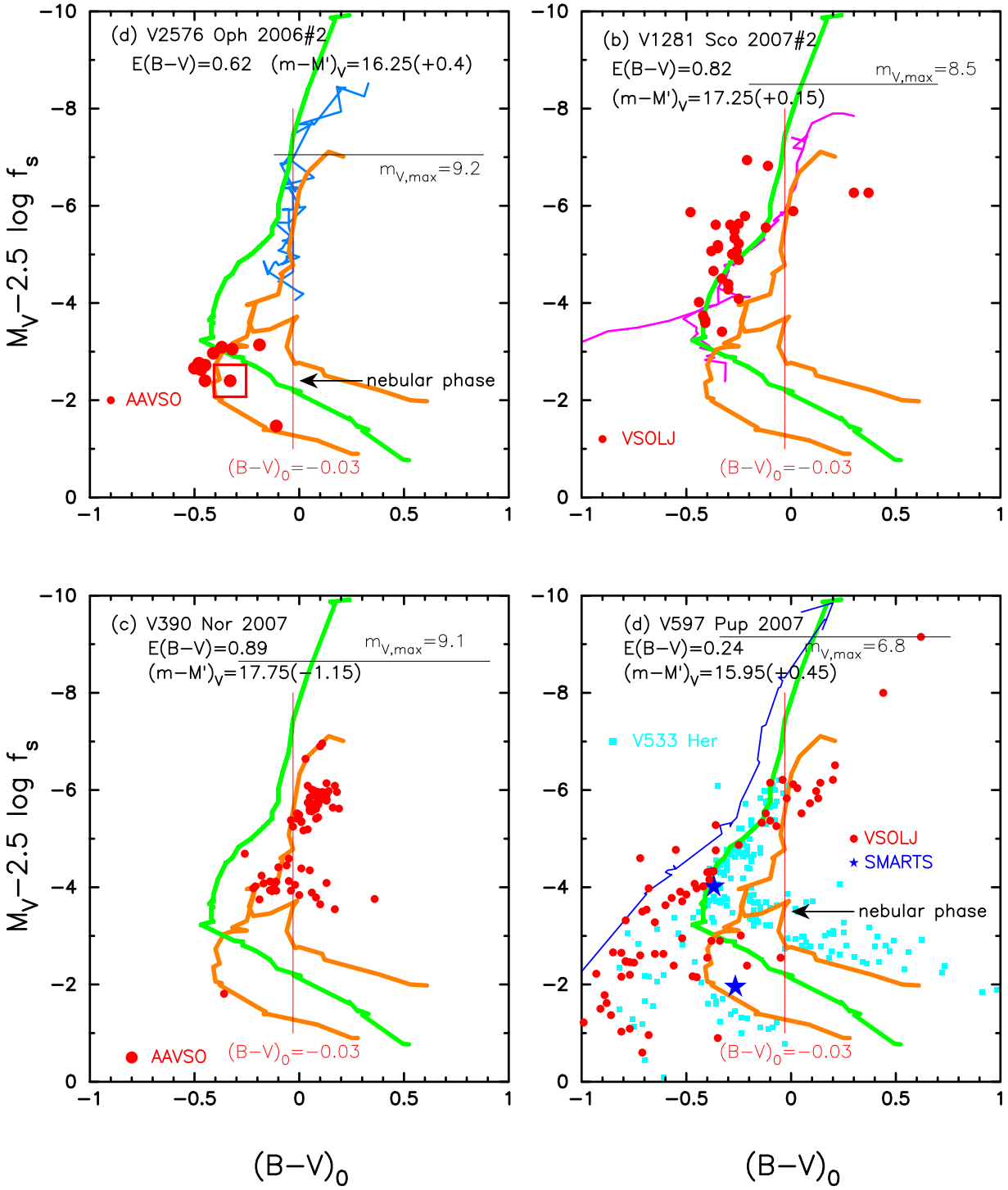

Figure 8. Same as Figure 6, but for (a) V2576 Oph, (b) V1281 Sco, (c) V390 Nor, and (d) V597 Pup. The solid green lines show the template track of V1500 Cyg. The solid orange lines represent that of LV Vul. In panel (a), we add the track of V1668 Cyg (thin solid cyan-blue lines). In panel (b), we add the track of V1974 Cyg (thin solid magenta lines). In panel (d), we add the track of V1500 Cyg (thin solid blue lines) obtained by Pfau (1976) and the track of V533 Her (filled cyan squares), which are taken from Figure 25(b) of Hachisu & Kato (2019).

We obtain $(m-M)_B = 18.25$, $(m-M)_V = 17.43$, and $(m-M)_I = 16.14$, which cross at $d = 9.4$ kpc and $E(B-V) = 0.82$, in Appendix A.6 and plot them in Figure 7(b). Thus, we have $E(B-V) = 0.82 \pm 0.05$ and $d = 9.4 \pm 1$ kpc.

For the reddening toward V1281 Sco, $(l,\ b) = (348.^{\circ}8564, +4.^{\circ}7984)$, the NASA/IPAC absorption map gives $E(B-V) = 0.77 \pm 0.02$, consistent with our value of $E(B-V) = 0.82 \pm 0.05$. Our result is slightly larger than the $E(B-V) = 0.7$ obtained by Russell et al. (2007). We further check our result toward V1281 Sco in Figure 7(b). We plot Marshall et al.'s (2006) relations toward $(l,\ b) = (348.^{\circ}75, +5.^{\circ}00)$, $(349.^{\circ}00, +5.^{\circ}00)$, $(348.^{\circ}75, +4.^{\circ}75)$, and $(349.^{\circ}00, +4.^{\circ}75)$. The closest direction is that of the blue asterisks. The solid cyan-blue line corresponds to the relation of Chen et al. (2018). Our crossing point of $d = 9.4$ kpc and $E(B-V) = 0.82$ is consistent with Marshall et al.'s relation (blue asterisks). This again supports our result that $E(B-V) = 0.82$ is reasonable.

We plot the $(B-V)_0$–$(M_V-2.5\log f_s)$ diagram of V1281 Sco in Figure 8(b) for $E(B-V)=0.82$ and $(m-M')_V=17.25$ in Equation (41). Unfortunately, we only have the VSOLJ data. The typical errors of the VSOLJ data were not reported, so we do not have a way to evaluate the typical deviation of their data. The V light and $(B-V)_0$ color evolutions of V1281 Sco in Figures 39(a) and (b) are also scattered, but they broadly follow the trend of V1500 Cyg. We may conclude that the mean trend in the time-stretched color–magnitude diagram in Figure 8(b) broadly follows the track of V1500 Cyg, so we regard V1281 Sco to belong to the V1500 Cyg type. This rough overlapping supports our adopted values of $E(B-V)=0.82$ and $(m-M')_V=17.25$. Thus, we obtain $E(B-V)=0.82\pm0.05$, $(m-M)_V=17.4\pm0.1$, $f_s=0.80$, and $d=9.4\pm1$ kpc. If this distance is correct, V1281 Sco belongs to the galactic bulge.

We check the distance modulus of $(m-M)_V=17.4$ by comparing our model V light curve with the observation. Assuming that $(m-M)_V=17.4$, we plot a model light curve of a 1.13 $M_\odot$ WD (Ne2, solid black line; Hachisu & Kato 2010) as shown in Figure 39(a). Our model light curve reasonably follows the V light curve of V1281 Sco. This again confirms that the distance modulus of $(m-M)_V=17.4$ is reasonable. For comparison, we add the model light curve of a 1.20 $M_\odot$ WD (Ne2, solid blue lines) and show that it follows well the light curve of V1500 Cyg, assuming that $(m-M)_V=12.3$ for V1500 Cyg (Hachisu & Kato 2019).

Hachisu & Kato (2010) obtained $(m-M)_V=17.8$ using the V model light curve fitting of a 1.13 $M_\odot$ WD (Ne2). The VSOLJ data of V magnitude are quite scattered. They fitted the V model light curve with the lower bound of the broad distribution of data points, which resulted in the distance modulus of $(m-M)_V=17.8$. If we adopt the central value of the broad distribution of data points, we obtain $(m-M)_V=17.4$ as shown in Figure 39(a). This is because the scatter of V data points is about ±0.5 mag. Hachisu & Kato (2010) also obtained $(m-M)_V=17.5$ from the light curve fitting between V1281 Sco and V1500 Cyg, which is consistent with the present result.

3.7. V390 Nor 2007

The nova reached 9.1 mag at maximum on UT 2007 June 7.2 (JD 2,454,258.7; Liller et al. 2007). Lynch et al. (2007) reported the reddening of $E(B-V)\sim1.0$ derived from the strong O I lines based on their 0.8–5.5 μm spectroscopy on UT 2007 June 21.

We obtain $(m-M)_B=17.48$, $(m-M)_V=16.59$, and $(m-M)_I=15.19$, which cross at $d=5.8$ kpc and $E(B-V)=0.89$, in Appendix A.7, and plot them in Figure 7(c). Thus, we obtained $E(B-V)=0.89\pm0.05$ and $d=5.8\pm0.6$ kpc toward V390 Nor, whose galactic coordinates are $(l,\ b)=(338\overset{\circ}{.}3371,\ +2\overset{\circ}{.}0061)$.

We check our result in Figure 7(c). We plot four relations of Marshall et al. (2006) toward $(l,\ b)=(338\overset{\circ}{.}25,\ +2\overset{\circ}{.}25)$, $(338\overset{\circ}{.}50,\ +2\overset{\circ}{.}25)$, $(338\overset{\circ}{.}25,\ +2\overset{\circ}{.}00)$, and $(338\overset{\circ}{.}50,\ +2\overset{\circ}{.}00)$. The closest direction is that of the blue asterisks. The other symbols/lines have the same meanings as those in Figure 5(a). Our crossing point of $d=5.8$ kpc and $E(B-V)=0.89$ is consistent with Marshall et al.'s relation (unfilled red squares, filled green squares, and unfilled magenta circles) and a linear extension of Chen et al.'s relation (solid cyan-blue line).

We plot the $(B-V)_0$–$(M_V-2.5\log f_s)$ diagram of V390 Nor in Figure 8(c) for $E(B-V)=0.89$ and $(m-M')_V=17.75$ in Equation (46). The track of V390 Nor almost follows that of LV Vul, although the AAVSO data are rather scattered. Therefore, we regard V390 Nor to belong to the LV Vul type. Thus, we confirmed that $E(B-V)=0.89$ and $(m-M')_V=17.75$ are reasonable, that is, $E(B-V)=0.89\pm0.05$, $(m-M)_V=16.6\pm0.2$, $f_s=2.82$, and $d=5.8\pm0.6$ kpc.

We check the distance modulus of $(m-M)_V=16.6$ by comparing our model V light curve with the observation. Assuming that $(m-M)_V=16.6$, we plot a model light curve of a 0.75 $M_\odot$ WD (CO3, solid red line; Hachisu & Kato 2016a) as shown in Figure 42(a). Our model light curve reasonably follows the V light curve of V390 Nor. This again confirms that the distance modulus of $(m-M)_V=16.6$ is reasonable. For comparison, we add the model light curve of a 0.98 $M_\odot$ WD (CO3, solid green lines) and show that it follows the light curve of V1668 Cyg, assuming that $(m-M)_V=14.6$ for V1668 Cyg.

3.8. V597 Pup 2007

The nova reached $m_{V,\max}=6.8$ on JD 2,454,419.2 from the VSOLJ data. Naito & Tokimasa (2007) reported that the nova belongs to the Fe II type from a spectrum obtained on UT 2007 November 14.77. Rudy et al. obtained a small reddening of $E(B-V)\sim0.3$ from the O I lines based on their 0.8–2.42 μm spectroscopy obtained on UT 2008 January 7.48 (Ness et al. 2008). The nova was observed as a supersoft X-ray source on UT 2008 January 8.02 and 17.18 (Ness et al. 2008; Schwarz et al. 2011). Warner & Woudt (2009) reported that V597 Pup is an intermediate polar with the orbital period of $P_{\rm orb}=2.6687$ hr and the spin period of $P_{\rm spin}=261.9$ s. Naik et al. (2009) obtained NIR spectra in the decline phase and concluded that the nova belongs to the He/N type. Hachisu & Kato (2010) analyzed the optical and supersoft X-ray light curves based on their free–free emission model light curves, and obtained the WD mass of $M_{\rm WD}=1.2$ $M_\odot$ (Ne3) and the distance modulus of $(m-M)_V=17.0\pm0.2$. Hounsell et al. (2016) revealed the rising phase of the nova from the data obtained with the *Solar Mass Ejection Imager* (*SMEI*).

We obtain $(m-M)_B=16.63$, $(m-M)_V=16.41$, and $(m-M)_I=16.02$, which broadly cross at $d=13.5$kpc and $E(B-V)=0.24$, in Appendix A.8 and plot them in Figure 7(d). Thus, we have $E(B-V)=0.24\pm0.05$ and $d=13.5\pm2$ kpc.

For the reddening toward V597 Pup, $(l,\ b)=(252\overset{\circ}{.}5295,\ +0\overset{\circ}{.}5453)$, the NASA/IPAC absorption map gives $E(B-V)=0.381\pm0.003$. This value is slightly larger than our value of $E(B-V)=0.24$ and $E(B-V)\sim0.3$ obtained by Rudy et al. (Ness et al. 2008). We plot two distance–reddening relations in Figure 7(d). The unfilled cyan-blue diamonds are the relation of Özdörmez et al. (2016). The solid cyan-blue line corresponds to the relation of Chen et al. (2018). No data of Marshall et al. (2006) and Green et al. (2015, 2018) are available. It seems that our crossing point of $d=13.5$ kpc and $E(B-V)=0.24$ is consistent with the relation of Özdörmez et al. (2016) if the reddening saturates at the distance of $d>10$ kpc.

We plot the $(B-V)_0$–$(M_V-2.5\log f_s)$ diagram of V597 Pup in Figure 8(d) for $E(B-V)=0.24$ and $(m-M')_V=15.95$ in Equation (51). In this case, the scatter

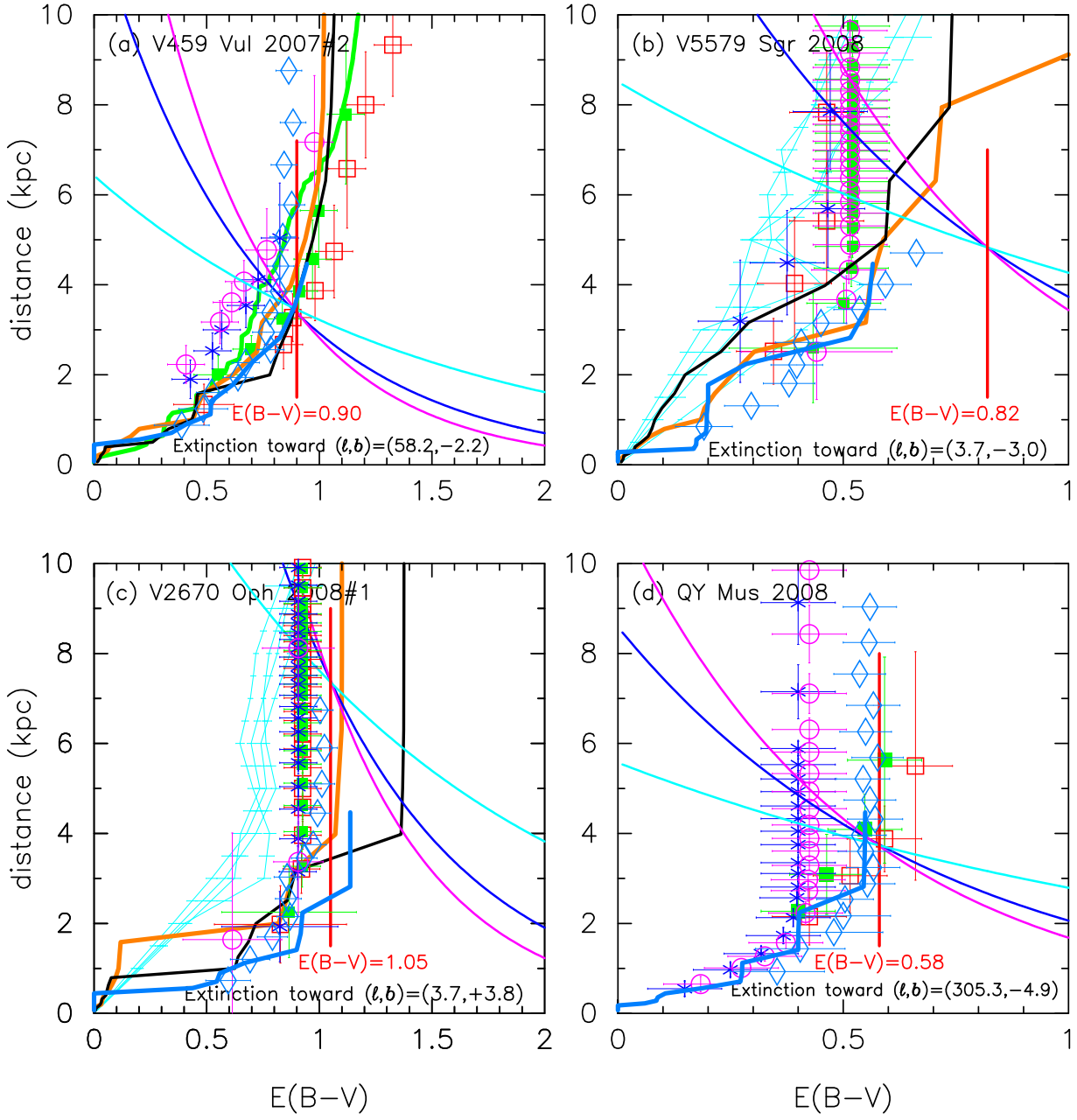

Figure 9. Same as Figure 5, but for (a) V459 Vul, (b) V5579 Sgr, (c) V2670 Oph, and (d) QY Mus.

of the $(B-V)_0$ colors is too large to immediately conclude overlapping. As already mentioned, the VSOLJ data have large errors and their degrees of errors were not reported. The scatter of the $B-V$ color may come from the different responses of each V filter among various observers. We plot another track of V1500 Cyg obtained by Pfau (1976) with the thin solid blue line, which deviates from the solid green line when strong emission lines contribute to the V filter. This is because strong [O III] lines contribute to the blue edge of the V filter and a small difference in the V filter response makes a large difference in the $B-V$ color. To demonstrate such effects, we add the track of V533 Her, which belongs to the V1500 Cyg type (Hachisu & Kato 2019). The V533 Her data bifurcate into three major branches because of different V filter systems after the nebular phase started (see, e.g., Figure 11(b) of Hachisu & Kato 2019). Similarly, the data of V597 Pup seem to bifurcate into two (or three) branches. There are two data points of SMARTS that have very small errors (0.003 mag). The first data point is located on the V1500 Cyg (and V533 Her) track and the second one is near the second (from left to right) branch of V533 Her. Considering such bifurcation in the nebular phase, we may conclude a broad overlapping of the V597 Pup track with that of V1500 Cyg or V533 Her. This may confirm that $E(B-V)=0.24$ and $(m-M')_V=15.95$ are reasonable, that is, $E(B-V)=0.24\pm0.05$, $(m-M)_V=16.4\pm0.1$, $f_s=0.66$, and $d=13.5\pm2$ kpc.

We check the distance modulus of $(m-M)_V=16.4$ by comparing our model V light curve with the observation in Figure 45. Assuming the distance modulus of $(m-M)_V=16.4$, we plot the V light curve of our 1.2 $M_\odot$ WD (Ne3). Our

model light curves simultaneously follows the V and supersoft X-ray fluxes of V597 Pup, confirming that our adopted value of $(m-M)_V = 16.4$ is reasonable.

Our WD model is essentially the same as that obtained by Hachisu & Kato (2010), but the distance modulus in the V band is improved from their $(m-M)_V = 17.0 \pm 0.2$ to our $(m-M)_V = 16.4 \pm 0.1$. This is partly because Hachisu & Kato (2010) assumed $(m-M)_{V,\mathrm{V1500\ Cyg}} = 12.5$ while we adopt $(m-M)_{V,\mathrm{V1500\ Cyg}} = 12.3$ (Hachisu & Kato 2014) and partly because we improve the vertical fit of ΔV including the effect of photospheric emission (Hachisu & Kato 2015).

3.9. V459 Vul 2007#2

The nova reached $m_{V,\max} = 7.4$ on JD 2,454,462.47 from the AAVSO data. The *SMEI* light curve showed several oscillations in the decline with amplitudes on the order of a few tenths of a magnitude (see Figure 8 of Hounsell et al. 2016). The spectra show prominent Balmer lines and Fe II lines with P-Cygni profile (Yamaoka et al. 2007), indicating that the nova is an Fe II type (Hounsell et al. 2016). Munari et al. (2007) reported that strong diffuse interstellar bands and Na I interstellar lines suggest a large reddening, possibly $E(B-V) > 0.7$. Russell et al. (2008a) reported, based on their IR spectroscopy, that the O I lines indicate a reddening of $E(B-V) \sim 1.0$, a part of which is local to the nova because the spectrum shows dust thermal emission beyond 1.5 μm. Poggiani (2010) obtained the reddening of $E(B-V) = (2.75 \pm 0.38)/3.1 = 0.89 \pm 0.12$, $d = 2.3$–5.0 kpc. The spectra at day 114 (UT 2008 April 19) show strong [O III] lines (Poggiani 2010), so the nova had already entered the nebular phase.

We obtain $(m-M)_B = 16.35$, $(m-M)_V = 15.43$, and $(m-M)_I = 14.04$, which broadly cross at $d = 3.4$kpc and $E(B-V) = 0.90$, in Appendix A.9 and plot them in Figure 9(a). Thus, we have $E(B-V) = 0.90 \pm 0.05$ and $d = 3.4 \pm 0.4$ kpc.

For the reddening toward V459 Vul, $(l,\ b) = (58\overset{\circ}{.}2138, -2\overset{\circ}{.}1673)$, Munari et al. (2007) reported $E(B-V) > 0.7$. Russell et al. (2008a) also reported $E(B-V) \sim 1.0$. Poggiani (2010) obtained the reddening of $E(B-V) = 0.89 \pm 0.12$. All of the reported reddenings are consistent with our value of $E(B-V) = 0.90 \pm 0.05$. The distance of $d = 2.3$–5.0 kpc obtained by Poggiani (2010) is also consistent with our value of $d = 3.4 \pm 0.4$ kpc. We further check our result in Figure 9(a). We plot four relations of Marshall et al. (2006) toward $(l,\ b) = (58\overset{\circ}{.}00, -2\overset{\circ}{.}00)$, $(58\overset{\circ}{.}25, -2\overset{\circ}{.}00)$, $(58\overset{\circ}{.}00, -2\overset{\circ}{.}25)$, and $(58\overset{\circ}{.}25, -2\overset{\circ}{.}25)$. The nova direction is almost between that of the unfilled magenta circles and filled green squares in the galactic coordinates. The other symbols/lines have the same meanings as those in Figure 5(a). Our crossing point at $d = 3.4$ kpc and $E(B-V) = 0.90$ is consistent with Green et al.'s, Marshall et al.'s (filled green squares), and Chen et al.'s relations. Thus, we again confirm that our adopted values of $d = 3.4$ kpc and $E(B-V) = 0.90$ are reasonable.

We plot the $(B-V)_0$–$(M_V - 2.5\log f_s)$ diagram of V459 Vul in Figure 10(a) for $E(B-V) = 0.90$ and $(m-M')_V = 15.05$ in Equation (56). Basically, the error of the $B-V$ data was not reported for the VSOLJ and AAVSO data. So, we cannot select $(B-V)_0$ data with high accuracy from them. The CBET data are on the LV Vul track (orange line). The AAVSO data are consistent with the LV Vul track. The redder side of the $(B-V)_0$ data distribution including CBET data almost follows the track of LV Vul. This suggests a rough overlapping of the V459 Vul track with the LV Vul track in the $(B-V)_0$–$(M_V - 2.5\log f_s)$ diagram. This rough agreement of the redder side of the $(B-V)_0$ distribution with the track of LV Vul may support that $E(B-V) = 0.90$ and $(m-M')_V = 15.05$ are reasonable, i.e., $E(B-V) = 0.90 \pm 0.05$, $(m-M)_V = 15.45 \pm 0.1$, $f_s = 0.71$, and $d = 3.4 \pm 0.5$ kpc.

We check the distance modulus of $(m-M)_V = 15.45$ by comparing our model V light curve with the observation. Assuming that $(m-M)_V = 15.45$, we plot the V light curve of our 1.15 $M_\odot$ WD (Ne2; Hachisu & Kato 2010) in Figure 48(a). The model light curve fits well the V magnitude of V459 Vul, suggesting that our adopted value of $(m-M)_V = 15.45$ is reasonable.

3.10. V5579 Sgr 2008

The nova reached $m_{V,\max} = 6.6$ at maximum on JD 2,454,579.9 from the AAVSO data. Russell et al. (2008b) identified the nova as being of Fe II class. They also estimated the reddening of the nova to be $E(B-V) \sim 1.2$ based on the O I lines of their infrared spectrum obtained on UT 2008 May 9 (JD 2,454,595.5), and suggested that a part of the reddening may be local to the nova because the nova already formed dust (denoted by the arrow labeled "dust" in Figure 10(b)). Raj et al. (2011) reported their NIR spectroscopy and photometry. They estimated the reddening to be $E(B-V) = 0.72 \pm 0.06$ from $(B-V)_{0,\max} = 0.23 \pm 0.06$ (van den Bergh & Younger 1987), the maximum brightness to be $M_{V,\max} = -8.8$ from the MMRD relation of della Valle & Livio (1995) together with $t_2 = 8 \pm 0.5$ days, and the distance to be $d = 4.4 \pm 0.2$ kpc. The VVV catalog (Saito et al. 2013) gives $E(B-V) = A_{K_s}/0.36 = 0.237/0.36 = 0.65$ toward V5579 Sgr.

We obtain $(m-M)_B = 16.78$, $(m-M)_V = 15.96$, and $(m-M)_I = 14.67$, which cross at $d = 4.8$ kpc and $E(B-V) = 0.82$, in Appendix A.10 and plot them in Figure 9(b). Thus, we have $E(B-V) = 0.82 \pm 0.05$ and $d = 4.8 \pm 0.5$ kpc.

For the reddening toward V5579 Sgr, $(l,\ b) = (3\overset{\circ}{.}7342, -3\overset{\circ}{.}0225)$, the NASA/IPAC absorption 2D map gives $E(B-V) = 0.86 \pm 0.04$. This value is roughly consistent with our result of $E(B-V) = 0.82 \pm 0.05$. Russell et al. (2008b) obtained $E(B-V) \sim 1.2$ from the O I lines. But, they suggested that a part of the reddening is local to the nova. Raj et al. (2011) estimated the reddening to be $E(B-V) = 0.72 \pm 0.06$ from $(B-V)_{0,\max} = 0.23 \pm 0.06$ (van den Bergh & Younger 1987), which is slightly smaller than our result. However, if we adopt $B-V = 1.21$ on UT 2008 April 23.12 (Munari et al. 2008), we obtain the reddening of $E(B-V) = 0.98 \pm 0.06$. The arithmetic average of these two estimates, $E(B-V) = (0.72 + 0.98)/2 = 0.85$, is roughly consistent with our value of $E(B-V) = 0.82 \pm 0.05$. The VVV catalog (Saito et al. 2013) gives $E(B-V) = A_{K_s}/0.36 = 0.237/0.36 = 0.65$ toward V5579 Sgr, which is slightly smaller than our value.

We further check our result in Figure 9(b). We plot four relations of Marshall et al. (2006) toward $(l,\ b) = (3\overset{\circ}{.}50, -3\overset{\circ}{.}00)$, $(3\overset{\circ}{.}75, -3\overset{\circ}{.}00)$, $(3\overset{\circ}{.}50, -3\overset{\circ}{.}25)$, and $(3\overset{\circ}{.}75, -3\overset{\circ}{.}25)$. The closest direction is that of the filled green squares. The other symbols/lines have the same meanings as those in Figure 5(a). Our crossing point of $d = 4.8$ kpc and $E(B-V) = 0.82$ slightly deviates from Green et al.'s results but is roughly consistent with a linear extension of Özdörmez et al.'s

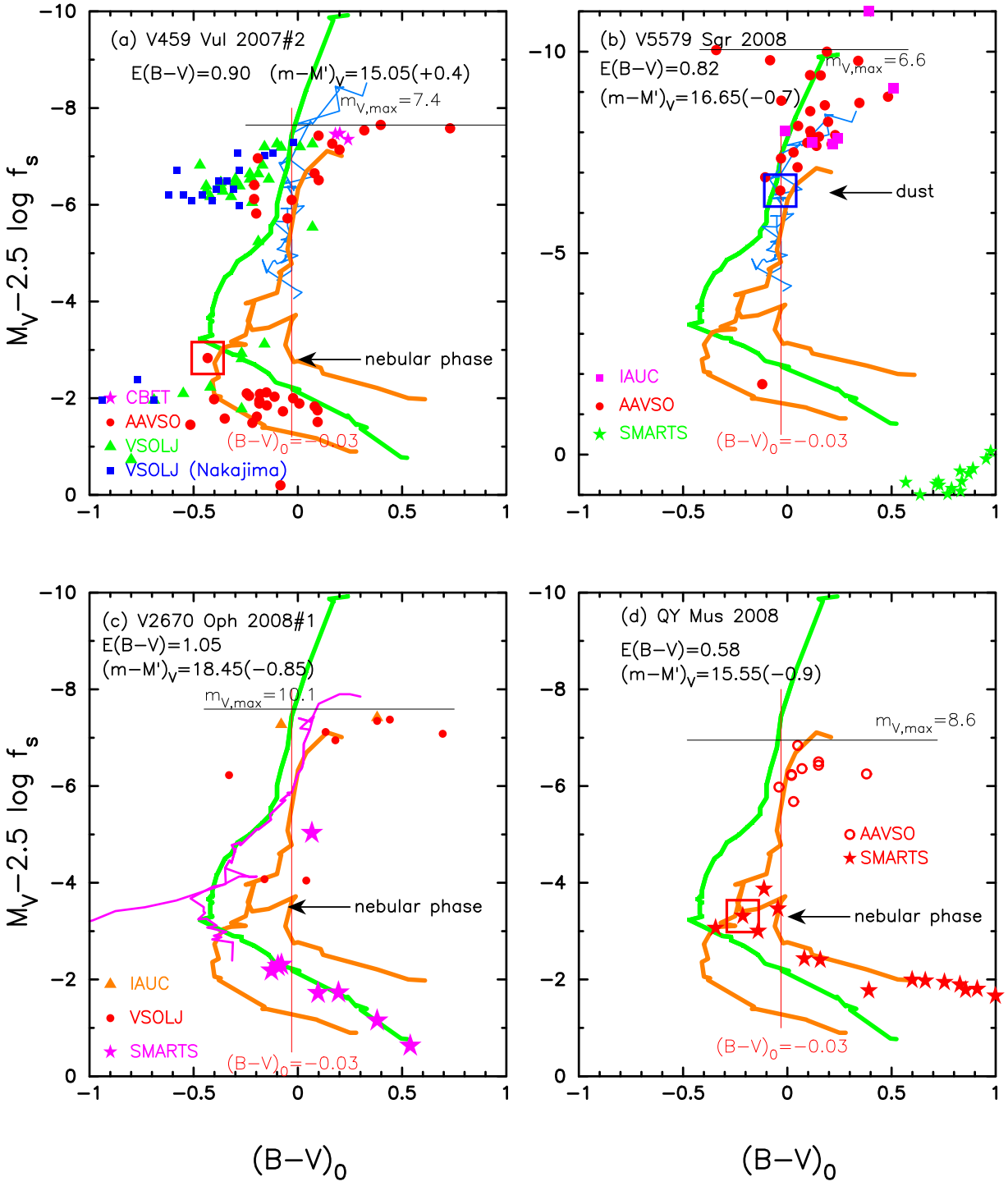

Figure 10. Same as Figure 6, but for (a) V459 Vul, (b) V5579 Sgr, (c) V2670 Oph, and (d) QY Mus. The solid green lines show the template track of V1500 Cyg. The solid orange lines represent that of LV Vul. We add the track of V1668 Cyg (thin solid cyan-blue lines) and V1974 Cyg (thin solid magenta lines).

relation. These 3D dust maps give the average value of a relatively broad region. The pinpoint reddening could be different from it because their resolutions are considerably larger than those of the molecular cloud structures.

We plot the $(B-V)_0$–$(M_V-2.5\log f_s)$ diagram of V5579 Sgr in Figure 10(b) for $E(B-V)=0.82$ and $(m-M')_V=16.65$ in Equation (61). The data are scattered but the redder side distribution almost follows the track of V1668 Cyg before it abruptly goes down due to dust blackout. This overlapping of the distribution of the redder side of V5579 Sgr with the track of V1668 Cyg may support $(B-V)=0.82$ and $(m-M')_V=16.65$, that is, $E(B-V)=0.82\pm0.05$, $(m-M)_V=15.95\pm0.1$, $f_s=1.91$, and $d=4.8\pm0.5$ kpc.

We check our distance modulus of $(m-M)_V=15.95$ by comparing our model light curve with the observation. In Figure 51(a), we plot a 0.85 $M_\odot$ WD (CO3, solid black lines; Hachisu & Kato 2016a), assuming that $(m-M)_V=15.95$. The model V light curve is calculated based on the free–free

emission plus blackbody emission as explained in Sections 1 and 2. Because the model does not include the effects of dust absorption and strong emission lines, it cannot correctly follow the dust blackout and nebular phases in Figure 51. The model light curves fit well the V magnitude of V5579 Sgr in the early phase before the dust blackout started, suggesting that $(m-M)_V = 15.95$ is reasonable. For comparison, we also add 0.85 $M_\odot$ WD (CO4, solid red line) and 0.98 $M_\odot$ WD (CO3, solid green lines), assuming that $(m-M)_V = 18.3$ and $(m-M)_V = 14.6$, respectively, for V1535 Sco and V1668 Cyg.

3.11. V2670 Oph 2008#1

The nova reached $m_{V,\max} = 10.1$ on UT 2008 May 26 (Poggiani 2008). Russell et al. (2008c) identified the nova as probably an Fe II type, which was later confirmed by Helton et al. (2008) and Poggiani (2008). Russell et al. (2008c) and Sitko et al. (2008) reported that there was no evidence for dust formation. Russell et al. (2008c) obtained the reddening of $E(B-V) \sim 1.3$ from O I lines based on their 0.8–5.5 μm spectroscopy on UT 2008 June 14. Poggiani (2008) estimated the absolute magnitude at maximum to be $M_{V,\max} = -7.9$ to -7.4 from the MMRD relation (della Valle & Livio 1995) together with $t_3 = 42 \pm 2$ days and the distance to be $d = 4.7$–5.8 kpc together with $E(B-V) = 1.3$. The VVV catalog gives $E(B-V) = A_{K_s}/0.36 = 0.356/0.36 = 0.98$ toward V2670 Oph (Saito et al. 2013).

We obtain $(m-M)_B = 18.65$, $(m-M)_V = 17.6$, and $(m-M)_I = 15.92$, which cross at $d = 7.4$ kpc and $E(B-V) = 1.05$, in Appendix A.11 and plot them in Figure 9(c). Thus, we have $E(B-V) = 1.05 \pm 0.1$ and $d = 7.4 \pm 0.8$ kpc.

For the reddening toward V2670 Oph, $(l,\ b) = (3\overset{\circ}{.}6656, +3\overset{\circ}{.}7799)$, the NASA/IPAC galactic absorption 2D map gives $E(B-V) = 0.90 \pm 0.01$ and the VVV catalog gives $E(B-V) = 0.98$ (Saito et al. 2013). On the other hand, Russell et al. (2008c) obtained $E(B-V) \sim 1.3$ from the O I lines as mentioned above. The arithmetic average of these three values is $E(B-V) = (0.90 + 0.98 + 1.3)/3 = 1.06$, which is consistent with our value of $E(B-V) = 1.05$ at the crossing point. Figure 9(c) shows various distance–reddening relations. We plot four relations of Marshall et al. (2006) toward $(l,\ b) = (3\overset{\circ}{.}50, 3\overset{\circ}{.}75)$, $(3\overset{\circ}{.}75, 3\overset{\circ}{.}75)$, $(3\overset{\circ}{.}50, 4\overset{\circ}{.}00)$, and $(3\overset{\circ}{.}75, 4\overset{\circ}{.}00)$. The closest direction is that of the filled green squares. The other symbols/lines have the same meanings as those in Figure 5(a). Our crossing point of $d = 7.4 \pm 0.8$ kpc and $E(B-V) = 1.05 \pm 0.1$ is consistent with Green et al.'s (2018) orange line and Özdörmez et al.'s result.

We plot the $(B-V)_0$–$(M_V - 2.5\log f_s)$ diagram of V2670 Oph in Figure 10(c) for $E(B-V) = 1.05$ and $(m-M')_V = 18.45$ in Equation (67). Although the number of data points are few, the track follows that of V1500 Cyg (solid green line) in the later phase. Therefore, we regard V2670 Oph to belong to the V1500 Cyg type because its light curve is similar to that of QU Vul and NR TrA (see Figures 54 and 56) and these two novae also belong to the V1500 Cyg type. The SMARTS spectra (Walter et al. 2012) showed that the nova had already entered the nebular phase on UT 2008 June 20 (JD 2,454,637.5) at $m_V = 17.4$. Therefore, we suppose that the nebular phase began at the turning point denoted by the arrow labeled "nebular phase" in Figure 10(c).

We check our distance modulus of $(m-M)_V = 17.6$ by comparing our model light curve with the observation. Assuming that $(m-M)_V = 17.6$, we plot the V (free–free plus blackbody emission) light curves of a 0.80 $M_\odot$ WD model (CO3, solid green/red lines) in Figures 54(a) and 55(a), respectively. The model light curve follows well the observed V light curve of V2670 Oph, confirming that $(m-M)_V = 17.6$ is reasonable. In Figure 55(a), for comparison, we plot the V and UV 1455 Å light curves of a 0.98 $M_\odot$ WD (CO3, solid green lines), assuming that $(m-M)_V = 14.6$ for V1668 Cyg.

3.12. QY Mus 2008

The nova reached $m_{V,\max} = 8.6$ at maximum on JD 2,454,748.9 from the VSOLJ data. The SMARTS spectra showed that QY Mus is a typical Fe II-type nova (Liller & Walter 2009).

We obtain $(m-M)_B = 15.23$, $(m-M)_V = 14.67$, and $(m-M)_I = 13.74$, which cross at $d = 3.7$ kpc and $E(B-V) = 0.58$ as shown in Figure 9(d), in Appendix A.12 and plot them in Figure 9(d). Thus, we obtain $d = 3.7 \pm 0.4$ kpc, $E(B-V) = 0.58 \pm 0.05$, $(m-M)_V = 14.65 \pm 0.1$, and $f_s = 2.2$ against LV Vul.

For the reddening toward QY Mus, $(l,\ b) = (305\overset{\circ}{.}3330, -4\overset{\circ}{.}8590)$, the 2D NASA/IPAC galactic dust absorption map gives $E(B-V) = 0.58 \pm 0.03$, which is consistent with our result. We further check our result in Figure 9(d). We plot four relations of Marshall et al. (2006) toward $(l,\ b) = (305\overset{\circ}{.}25, -4\overset{\circ}{.}75)$, $(305\overset{\circ}{.}50, -4\overset{\circ}{.}75)$, $(305\overset{\circ}{.}25, -5\overset{\circ}{.}00)$, and $(305\overset{\circ}{.}50, -5\overset{\circ}{.}00)$. The closest direction is that of the unfilled red squares. The other symbols/lines have the same meanings as those in Figure 5(a). Our crossing point of $d = 3.7$ kpc and $E(B-V) = 0.58$ is consistent with Marshall et al.'s, Özdörmez et al.'s, and Chen et al.'s relations.

We plot the $(B-V)_0$–$(M_V - 2.5\log f_s)$ diagram of QY Mus in Figure 10(d) for $E(B-V) = 0.58$ and $(m-M')_V = 15.55$ in Equation (72). The track of QY Mus almost follows that of LV Vul. Therefore, we identify QY Mus as an LV Vul type. This matching with the LV Vul track also supports our results of $E(B-V) = 0.58$ and $(m-M')_V = 15.55$, that is, $E(B-V) = 0.58 \pm 0.05$, $(m-M)_V = 14.65 \pm 0.1$, $f_s = 2.2$, and $d = 3.7 \pm 0.4$ kpc. The SMARTS spectra of QY Mus showed that the nova had entered the nebular phase on UT 2009 May 12 (JD 2,454,963.5) at $m_V = 12.5$. We plot the start of the nebular phase by a large unfilled red square in Figure 10(d).

We check the distance modulus of $(m-M)_V = 14.65$ by comparing our V model light curve with the observation. We also discuss the accuracy of the WD mass determination from the light curve modeling in Section 4.2. Our model light-curve fitting gives the WD mass of $M_{\rm WD} = 0.75$, 0.80, and 0.85 $M_\odot$ for the hydrogen content of $X = 0.35$, 0.45, and 0.55 by weight, respectively. It should also be noted that our model light curves reasonably reproduce the V light curve of QY Mus. This confirms that the distance modulus of $(m-M)_V = 14.65$ is reasonable.

3.13. NR TrA 2008

NR TrA was discovered by N. J. Brown at mag 9.2 on UT 2008 April 1.73 (=JD 2,454,558.23; Brown et al. 2008). It reached $m_{V,\max} = 8.6$ at maximum on JD 2,454,570.15 and showed a 2.5 mag largest secondary peak and then a few smaller secondary peaks with half a magnitude. This feature of multiple secondary peaks is similar to that of V2670 Oph in Section 3.11. The novae is in the nebular phase at least until

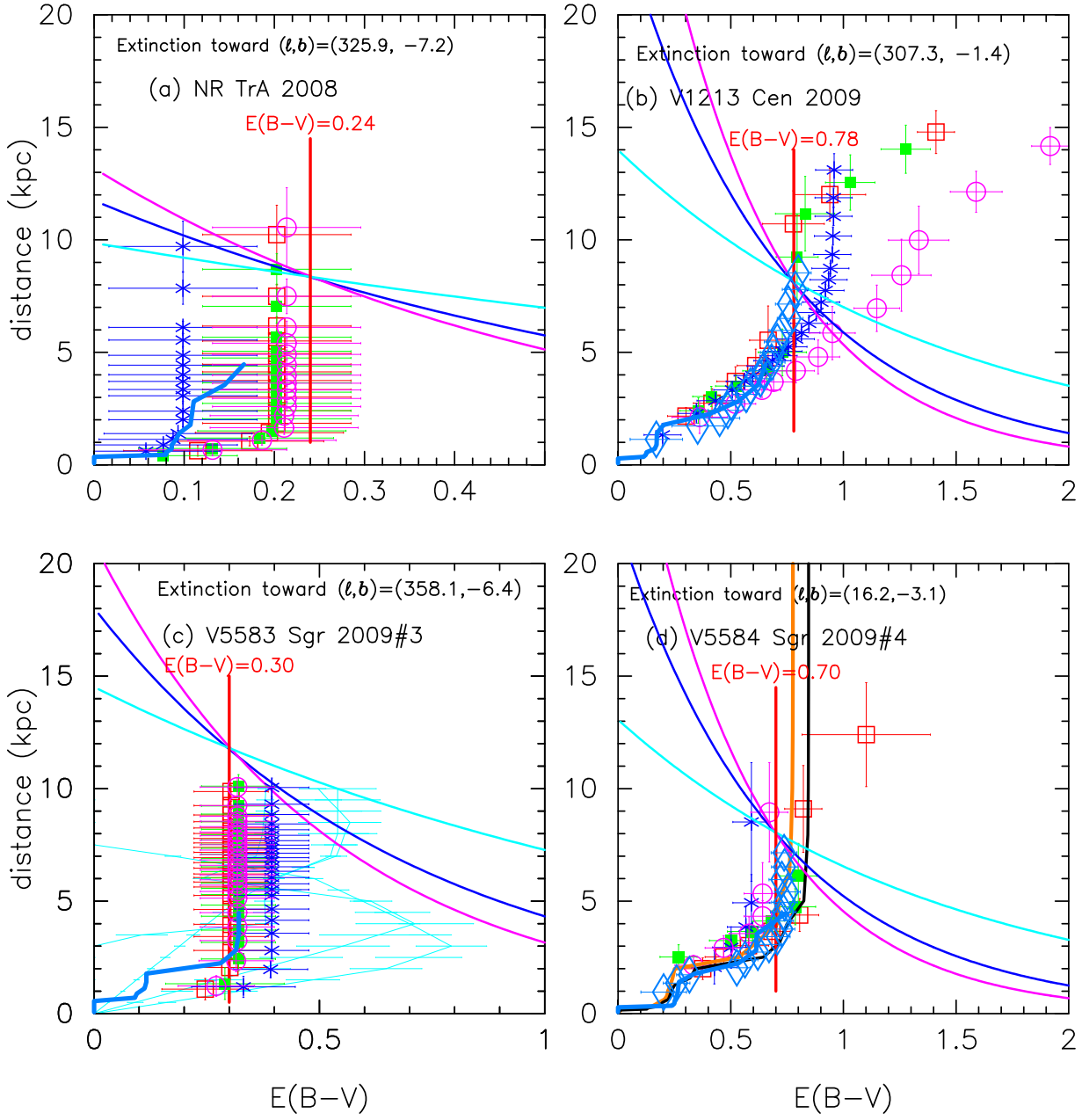

Figure 11. Same as Figure 5, but for (a) NR TrA, (b) V1213 Cen, (c) V5583 Sgr, and (d) V5584 Sgr.

Day 1237 (Walter 2015b). Walter (2015b) also reported that the nova light curve showed an eclipse of 5.25 hr binary period and obtained the mass function of $M_2^3/(M_1+M_2)^2 = 0.024\ M_\odot$.

We obtain $(m-M)_B = 15.6$, $(m-M)_V = 15.35$, and $(m-M)_I = 14.97$, which cross at the distance of $d = 8.3$ kpc and the reddening of $E(B-V) = 0.24$, in Appendix A.13 and plot them in Figure 11(a). Thus, we obtain $d = 8.3 \pm 1.0$ kpc, $E(B-V) = 0.24 \pm 0.05$, $(m-M)_V = 15.35 \pm 0.2$, and f_s =2.7 against LV Vul.

For the reddening toward NR TrA, $(l,\ b) = (325.^\circ9316, -7.^\circ2184)$, the 2D NASA/IPAC galactic dust absorption map gives $E(B-V) = 0.19 \pm 0.01$, which is consistent with our value of $E(B-V) = 0.24 \pm 0.05$ at the crossing point. We check our result in Figure 11(a). We plot four relations of Marshall et al. (2006) toward $(l,\ b) = (325.^\circ75, -7.^\circ00)$, $(326.^\circ00, -7.^\circ00)$, $(325.^\circ75, -7.^\circ25)$, and $(326.^\circ00, -7.^\circ25)$. The closest direction is that of the unfilled magenta circles. The other symbols/lines have the same meanings as those in Figure 5(a). Our crossing point of $d = 8.3$ kpc and $E(B-V) = 0.24$ is consistent with Marshall et al.'s relation (unfilled magenta circles with error bars). Walter (2015b) discussed his spectra and concluded that $E(B-V) < 0.3$ if the blue continuum arose from the accretion disk. Our value of $E(B-V) = 0.24$ is also consistent with his estimate.

We plot the $(B-V)_0$–$(M_V - 2.5\log f_s)$ diagram of NR TrA in Figure 12(a) for $E(B-V) = 0.24$ and $(m-M')_V = 16.45$ in Equation (78). The track is close to that of V1974 Cyg (and V1500 Cyg) until the nebular phase starts. Therefore, we regard NR TrA to belong to the V1500 Cyg type. The broadband filter light curves are contaminated by strong emission lines in the nebular phase. This effect results in a large difference

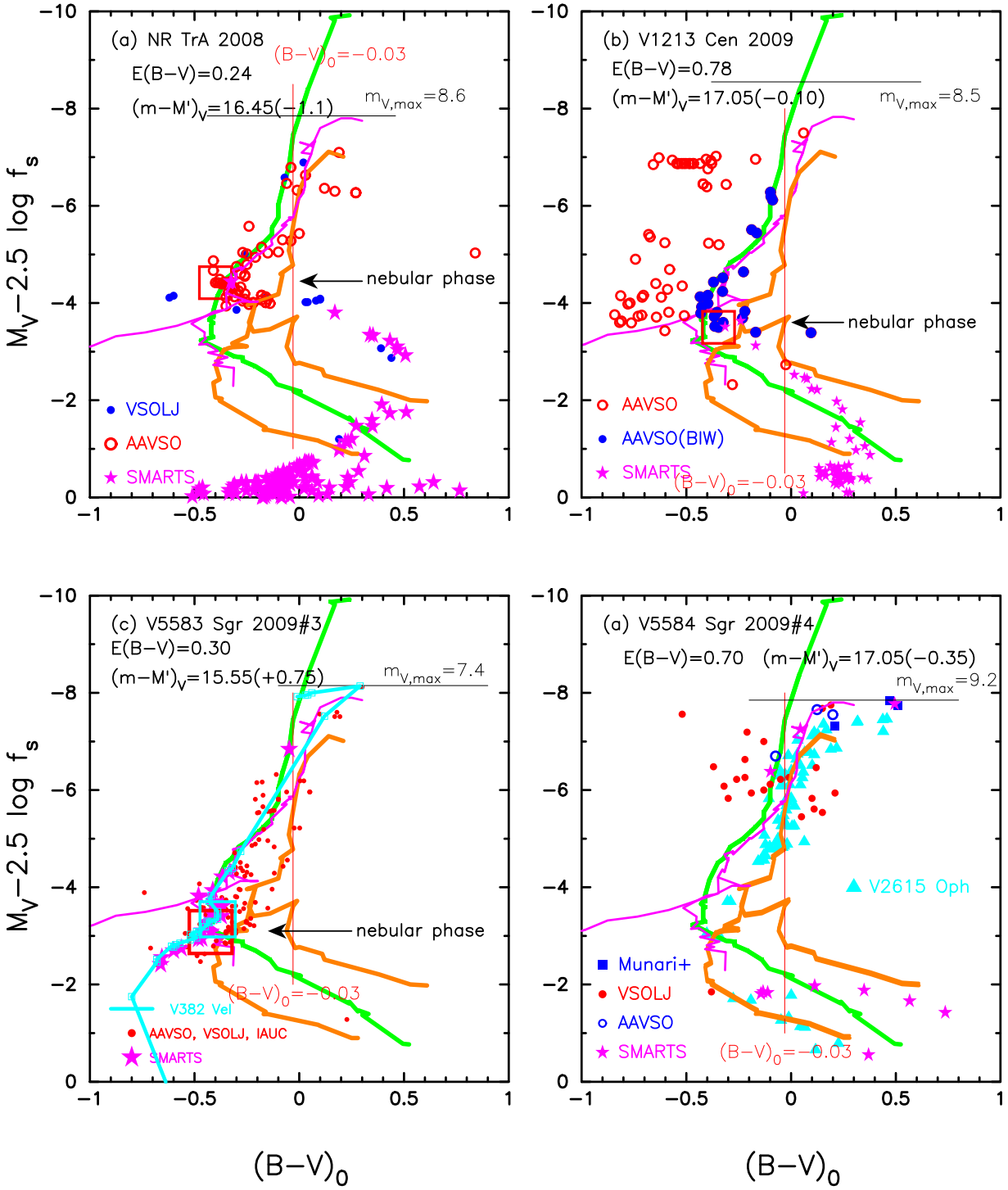

Figure 12. Same as Figure 6, but for (a) NR TrA, (b) V1213 Cen, (c) V5583 Sgr, and (d) V5584 Sgr. The solid green lines show the template track of V1500 Cyg. The solid orange lines represent that of LV Vul. We add the track of V1974 Cyg (solid magenta lines). In panel (c), we add the tracks of V382 Vel (cyan line). In panel (d), we add the track of V2615 Oph (filled cyan triangles).

especially in the $(B-V)_0$ color, because the color is the difference between two magnitudes and a strong line usually contributes to one of the bands. Similarly, a slight difference in the filter response makes a large difference in the $(B-V)_0$ color. We sometimes find large scatters in the $(B-V)_0$ color among various observers. The effect of strong [O III] lines could be slightly different from nova to nova, even if they are globally similar in their light curves. This means that, even if their early color–magnitude tracks overlap the template tracks, the later tracks in the nebular phase separate from the template tracks. The early-phase data of NR TrA follows well the V1974 Cyg track. The SMARTS spectra of NR TrA showed that the nova had entered the nebular phase on UT 2008 August 26 (JD 2,454,704.5) at $m_V = 11.9$. We denote the start of the nebular phase with a large unfilled red square at $M_V = m_V - (m-M)_V = 11.9 - 15.35 = -3.45$ and $(B-V)_0 = (B-V) - E(B-V) = -0.16 - 0.24 = -0.40$. We may conclude that the track of NR TrA overlaps the V1974 Cyg

track except for the nebular phase. The similarity of NR TrA to V1974 Cyg in the $(B-V)_0$–$(M_V-2.5\log f_s)$ diagram may support our obtained values, $E(B-V)=0.24$ and $(m-M')_V=16.45$, that is, $E(B-V)=0.24\pm0.05$, $(m-M)_V=15.35\pm0.2$, $f_s=2.7$, $d=8.3\pm1.0$ kpc.

We check our distance modulus of $(m-M)_V=15.35$ by comparing our model light curve with the observation. Assuming that $(m-M)_V=15.35$, we plot the V light curves of a 0.75 $M_\odot$ WD model (CO3, solid green/red line) in Figures 61(a) and 62(a), respectively. The distance modulus of $(m-M)_V=15.35$ shows good agreement with the observed V light curve of NR TrA, confirming that $(m-M)_V=15.35$ is reasonable. For comparison, assuming that $(m-M)_V=14.6$ for V1668 Cyg, we plot the V and UV 1455 Å light curves of a 0.98 $M_\odot$ WD model (CO3, solid green lines) in Figure 62(a). If we adopt the WD mass of 0.75 $M_\odot$, then the companion mass is about $M_2=0.30\ M_\odot$ from the mass function of $M_2^3/(M_1+M_2)^2=0.024\ M_\odot$ obtained by Walter (2015b). The Roche lobe radius of the donor star is $R_2=0.47\ R_\odot$, slightly evolving from the main sequence.

3.14. V1213 Cen 2009

V1213 Cen was discovered on UT 2009 May 8.235 at $m_V=8.53$ by ASAS-3 (Pojmanski et al. 2009). Then, the nova declined with $t_2=11\pm2$ days and became a supersoft X-ray source on UT 2010 March 29.6 (Schwarz et al. 2010). Schwarz et al. (2010) obtained a blackbody fit with $kT=31\pm4$ eV and $N_{\rm H}=(6.4\pm1.8)\times10^{21}$ cm^{-2}. We assume that $m_{V,\rm max}=8.5$. We estimate the reddening to be $E(B-V)=N_{\rm H}/8.3\times10^{21}=(6.4\pm1.8)\times10^{21}/8.3\times10^{21}=0.77\pm0.22$, based on the relation of Liszt (2014).

We obtain $(m-M)_B=17.74$, $(m-M)_V=16.95$, and $(m-M)_I=15.75$, which cross at $d=8.1$ kpc and $E(B-V)=0.78$, in Appendix A.14 and plot them in Figure 11(b). Thus, we obtain $d=8.1\pm1$ kpc, $E(B-V)=0.78\pm0.05$, $(m-M)_V=15.95\pm0.1$, and $f_s=1.12$ against LV Vul.

For the reddening toward V1213 Cen, $(l,\ b)=(307\overset{\circ}{.}2862, -1\overset{\circ}{.}4263)$, the hydrogen column density obtained by Schwarz et al. (2010) suggests $E(B-V)=0.77\pm0.22$, consistent with our crossing point, but the 2D NASA/IPAC galactic dust absorption map gives $E(B-V)=1.77\pm0.14$, which is much larger than our results. This implies that the reddening does not saturate yet at the distance of $d=8.1$ kpc as shown in Figure 11(b). We further check our result in Figure 11(b). We plot four relations of Marshall et al. (2006) toward $(l,\ b)=(307\overset{\circ}{.}25, -1\overset{\circ}{.}50)$, $(307\overset{\circ}{.}50, -1\overset{\circ}{.}50)$, $(307\overset{\circ}{.}25, -1\overset{\circ}{.}25)$, and $(307\overset{\circ}{.}50, -1\overset{\circ}{.}25)$. The closest direction is that of the unfilled red squares. The other symbols/lines have the same meanings as those in Figure 5(a). Our crossing point of $d=8.1$ kpc and $E(B-V)=0.78$ is consistent with Marshall et al.'s (unfilled red squares with error bars), Özdörmez et al.'s, and Chen et al.'s relations.

We plot the $(B-V)_0$–$(M_V-2.5\log f_s)$ diagram of V1213 Cen in Figure 12(b) for $E(B-V)=0.78$ and $(m-M')_V=17.05$ in Equation (82). We plot the data points of AAVSO and SMARTS, but separately depict BIW's data (filled blue circles) from the other AAVSO data (unfilled red circles), because BIW's data are systematically redder than the others and consistent with the SMARTS data. If we use BIW's data, the track of V1213 Cen is close to that of V1500 Cyg and V1974 Cyg, so we regard V1213 Cen to belong to the V1500 Cyg type. The SMARTS spectra (Walter et al. 2012) of V1213 Cen showed that the nova had already entered the nebular phase on UT 2009 December 20 (JD 2,455,185.5) at $m_V=14.5$. We regard the nova to have entered the nebular phase soon after UT 2009 September 13 (JD 2,455,087.5) at $m_V=13.6$. We denote the start of the nebular phase by a large unfilled red square at $M_V=m_V-(m-M)_V=13.6-16.95=-3.35$ and $(B-V)_0=(B-V)-E(B-V)=0.43-0.78=-0.35$. The overlapping of V1213 Cen with the V1500 Cyg track may support that our adopted values of $E(B-V)=0.78$ and $(m-M')_V=17.05$ are reasonable, that is, $E(B-V)=0.78\pm0.05$, $(m-M)_V=16.95\pm0.2$, $f_s=1.12$, and $d=8.1\pm1$ kpc.

We check the distance modulus of $(m-M)_V=16.95$ by comparing our model V light curve with the observation. Assuming the distance modulus of $(m-M)_V=16.95$, we plot the V light curve of our 1.0 $M_\odot$ WD (Ne2, solid blue lines; Hachisu & Kato 2010) in Figure 65(a). The model light curve fits the V magnitude of V1213 Cen as well as the supersoft X-ray light curve, suggesting that our adopted value of $(m-M)_V=16.95$ and the WD mass of 1.0 $M_\odot$ are reasonable. For comparison, we also plot the V and supersoft X-ray light curves of V4743 Sgr and compare our model light curves of a 1.15 $M_\odot$ WD (Ne2, solid red lines).

3.15. V5583 Sgr 2009#3

The light curve obtained with NASA's *Solar TErrestrial RElations Observatory*/Heliospheric Imager (*STEREO*/HI) instruments constrained the optical peak at JD 2,455,050.54 ± 0.17 (UT 2009 August 7.04; Holdsworth et al. 2014). This time is almost the same as the peak time of JD 2,455,050.6 ± 0.04 (UT 2009 August 7.08) determined from the *SMEI* light curve (Hounsell et al. 2016). Therefore, we regard the V maximum to be $m_{V,\rm max}=7.43$ on JD 2,455,050.635 from the VSOLJ data (observed by H. Maehara). Holdsworth et al. (2014) suggested that the nova is most likely a neon nova, based on their optical spectroscopy and abundance analysis. Hachisu et al. (2009) analyzed the early-phase $BVyR_CI_C$ light curves and estimated the WD mass and supersoft X-ray source phase based on their model light curves. They concluded that the light curves of V5583 Sgr is almost identical with those of V382 Vel.

We obtain $(m-M)_B=16.6$, $(m-M)_V=16.28$, and $(m-M)_I=15.79$, which cross at $d=12$ kpc and $E(B-V)=0.30$, in Appendix A.15 and plot them in Figure 11(c). Thus, we have $E(B-V)=0.30\pm0.05$ and $d=12\pm2$ kpc.

For the reddening toward V5583 Sgr, $(l,\ b)=(358\overset{\circ}{.}1004, -6\overset{\circ}{.}3941)$, the 2D NASA/IPAC galactic dust absorption map gives $E(B-V)=0.337\pm0.005$. The VVV survey catalog (Saito et al. 2013) gives $E(B-V)=A_{K_s}/0.36=0.107/0.36=0.30$ toward V5583 Sgr. Both values of reddening are consistent with our crossing point of $E(B-V)=0.30\pm0.05$ and $d=12\pm2$ kpc. We further check our result in Figure 11(c). We plot four relations of Marshall et al. (2006) toward $(l,\ b)=(358\overset{\circ}{.}00, -6\overset{\circ}{.}50)$, $(358\overset{\circ}{.}25, -6\overset{\circ}{.}50)$, $(358\overset{\circ}{.}00, -6\overset{\circ}{.}25)$, and $(358\overset{\circ}{.}25, -6\overset{\circ}{.}25)$. The closest direction is that of the unfilled red squares. Unfortunately, Green et al.'s (2015, 2018) data are not available for this direction. The other symbols/lines have the same meanings as those in Figure 5(a). Our crossing point of $d=12$ kpc and $E(B-V)=0.30$ is consistent with Marshall et al.'s relation (unfilled red squares) and Chen et al.'s relation.

We plot the $(B-V)_0$–$(M_V-2.5\log f_s)$ diagram of V5583 Sgr in Figure 12(c) for $E(B-V)=0.30$ and $(m-M')_V=15.55$ in Equation (87). We add the track of V382 Vel (solid cyan line), the data of which are the same as

those in Hachisu & Kato (2019). The data of V5583 Sgr are scattered in the early phase but its track is very similar to that of V382 Vel. Therefore, we can conclude that V5583 Sgr belongs to the V1500 Cyg type in the $(B-V)_0$–$(M_V-2.5\log f_s)$ diagram because V382 Vel belongs to the V1500 Cyg type (Hachisu & Kato 2019). This overlapping with the V382 Vel, V1974 Cyg, and V1500 Cyg tracks supports $E(B-V)=0.30$ and $(m-M')_V=15.55$, that is, $E(B-V)=0.30\pm0.05$, $(m-M)_V=16.3\pm0.1$, $f_s=0.51$, and $d=12\pm2$ kpc.

The SMARTS spectra of V5583 Sgr showed that the nova had already entered the nebular phase on UT 2009 October 2 (JD 2,455,106.5) at $m_V=12.5$. We regard the nova to have entered the nebular phase soon after UT 2009 September 13 (JD 2,455,087.5) at $m_V=12.5$. We denote the start of the nebular phase by a large unfilled red square at $M_V=m_V-(m-M)_V=12.5-16.3=-3.8$ and $(B-V)_0=(B-V)-E(B-V)=-0.123-0.30=-0.42$. This phase is also similar to that of V382 Vel (a large unfilled cyan square).

We check the distance modulus of $(m-M)_V=16.3$ by comparing our model V light curve with the observation. Assuming $(m-M)_V=16.3$, we plot a model V light curve of a 1.23 $M_\odot$ WD (Ne2, solid black line; Hachisu & Kato 2010, 2016a) for V5583 Sgr and V382 Vel in Figure 68(a). We also plot the supersoft X-ray flux (solid black line: 0.1–2.4 keV) of the 1.23 $M_\odot$ WD model. Both the V and supersoft X-ray light curve models reasonably reproduce the observation. We show the X-ray flux for V382 Vel in units of erg s^{-1} cm^{-2} but only the count rate in units of cts s^{-1} for V5583 Sgr (scaled from 100 at the upper bound to 10^{-4} at the lower bound). The X-ray flux of V382 Vel is taken from Orio et al. (2002) and Burwitz et al. (2002) while the X-ray data of V5583 Sgr are from the *Swift* website (Evans et al. 2009). This confirms that the distance modulus of $(m-M)_V=16.3$ is reasonable. The WD mass of 1.23 $M_\odot$ is consistent with the neon nova suggestion by Holdsworth et al. (2014). For comparison, we add a light curve of a 0.98 $M_\odot$ WD (CO3, solid green line; Hachisu & Kato 2016a) for LV Vul.

3.16. V5584 Sgr 2009#4

V5584 Sgr reached $m_{V,\max}=9.2$ at V maximum on JD 2,455,134.7 (UT 2009 October 29; Poggiani 2011). Poggiani (2011) estimated $t_2=27\pm2$ days and the distance of 5.1–7.8 kpc based on various MMRD relations. Munari et al. (2009) suggested that V5584 Sgr is an Fe II-type nova based on their spectra obtained on UT October 28 and 29. Russell et al. (2010) reported that V5584 Sgr had already formed dust on UT 2010 February 10.

We obtain $(m-M)_B=17.39$, $(m-M)_V=16.69$, and $(m-M)_I=15.58$, which cross at $d=8.0$ kpc and $E(B-V)=0.70$, in Appendix A.16 and plot them in Figure 11(d). Thus, we have $E(B-V)=0.70\pm0.05$ and $d=8.0\pm1$ kpc. The distance modulus in the V band is $(m-M)_V=16.7\pm0.1$.

For the reddening toward V5584 Sgr, $(l,\ b)=(16\overset{\circ}{.}1682, -3\overset{\circ}{.}1003)$, the 2D NASA/IPAC galactic dust absorption map gives $E(B-V)=0.91\pm0.08$. We further check our result in Figure 11(d). We plot four relations of Marshall et al. (2006) toward $(l,\ b)=(16\overset{\circ}{.}00, -3\overset{\circ}{.}00)$, $(16\overset{\circ}{.}25, -3\overset{\circ}{.}00)$, $(16\overset{\circ}{.}00, -3\overset{\circ}{.}25)$, and $(16\overset{\circ}{.}25, -3\overset{\circ}{.}25)$. The closest direction is that of the filled green squares. The other symbols/lines have the same meanings as those in Figure 5(a). Our crossing point of $d=8.0$ kpc and $E(B-V)=0.70$ is consistent with these relations.

We plot the $(B-V)_0$–$(M_V-2.5\log f_s)$ diagram of V5584 Sgr in Figure 12(d) for $E(B-V)=0.70$ and $(m-M')_V=17.05$ in Equation (92). The track of V5584 Sgr almost follows that of V2615 Oph, so we regard V5584 Sgr to belong to the LV Vul type because V2615 Oph belongs to the LV Vul type (Hachisu & Kato 2019). The broad overlapping of the V5584 Sgr track to the V2615 Oph track may support that our adopted values of $E(B-V)=0.70$ and $(m-M')_V=17.05$, that is, $E(B-V)=0.70\pm0.05$, $(m-M)_V=16.7\pm0.1$, $f_s=1.35$, and $d=8.0\pm1$ kpc.

We check the distance modulus of $(m-M)_V=16.7$ by comparing our model V light curve with the observation. Assuming $(m-M)_V=16.7$, we plot a model V light curve of a 0.90 $M_\odot$ WD (CO3, solid red line; Hachisu & Kato 2016a) in Figure 71(a). The V light-curve model reproduces the observation well. This confirms that distance modulus of $(m-M)_V=16.7$ is reasonable.

3.17. V5585 Sgr 2010

The nova was discovered by Seach (2010) on UT 2010 January 20.72 at mag ~8.5. V5585 Sgr reached its optical maximum sometime between UT 2009 November 15.89 and UT 2010 January 20.72, but the optical peak was missed because of its proximity in the sky to the Sun (e.g., Mróz et al. 2015). The spectrum obtained by Maehara (2009) showed that the nova is of Fe II class. This nova showed sharp-peaked brightenings (flares) in the I-band more than 15 times as shown in Figure 3 of Mróz et al. (2015). Mróz et al. (2015) found that the nova shows eclipses with an orbital period of 3.3 hr. They discussed the resemblance of V5585 Sgr to V4745 Sgr and V5588 Sgr, both of which show similar sharp-peaked brightenings (see also Tanaka et al. 2011; Munari et al. 2015a).

We obtain $(m-M)_B=17.23$, $(m-M)_V=16.72$, and $(m-M)_I=15.93$, which cross at $d=11$ kpc and $E(B-V)=0.47$, in Appendix A.17 and plot them in Figure 13(a). Thus, we have $E(B-V)=0.47\pm0.05$ and $d=11\pm2$ kpc. The distance modulus in the V band is $(m-M)_V=16.7\pm0.2$.

For the reddening toward V5585 Sgr, $(l,\ b)=(2\overset{\circ}{.}3311, -4\overset{\circ}{.}1679)$, the VVV catalog (Saito et al. 2013) gives $E(B-V)=A_{K_s}/0.36=0.170/0.36=0.47$ toward V5585 Sgr. The 2D NASA/IPAC galactic dust absorption map gives $E(B-V)=0.49\pm0.04$ for V5585 Sgr. The both reddening values are consistent with our obtained value of $E(B-V)=0.47\pm0.05$. We further check our result in Figure 13(a). We plot four relations of Marshall et al. (2006) toward $(l,\ b)=(2\overset{\circ}{.}25, -4\overset{\circ}{.}00)$, $(2\overset{\circ}{.}50, -4\overset{\circ}{.}00)$, $(2\overset{\circ}{.}25, -4\overset{\circ}{.}25)$, and $(2\overset{\circ}{.}50, -4\overset{\circ}{.}25)$. The closest direction is that of the blue asterisks. The other symbols/lines have the same meanings as those in Figure 5(a). Our crossing point of $d=11$ kpc and $E(B-V)=0.47$ is consistent with Marshall et al.'s relations.

We plot the $(B-V)_0$–$(M_V-2.5\log f_s)$ diagram of V5585 Sgr in Figure 14(a) for $E(B-V)=0.47$ and $(m-M')_V=16.95$ in Equation (97). The data are taken from VSOLJ. The track of V5585 Sgr is close to that of LV Vul and V1668 Cyg, so we regard V5585 Sgr to belong to the LV Vul type. This overlapping of the V5585 Sgr track with the LV Vul track confirms $E(B-V)=0.47$ and $(m-M')_V=16.95$, that is, $E(B-V)=0.47\pm0.05$, $(m-M)_V=16.7\pm0.2$, $f_s=1.26$, and $d=11\pm2$ kpc.

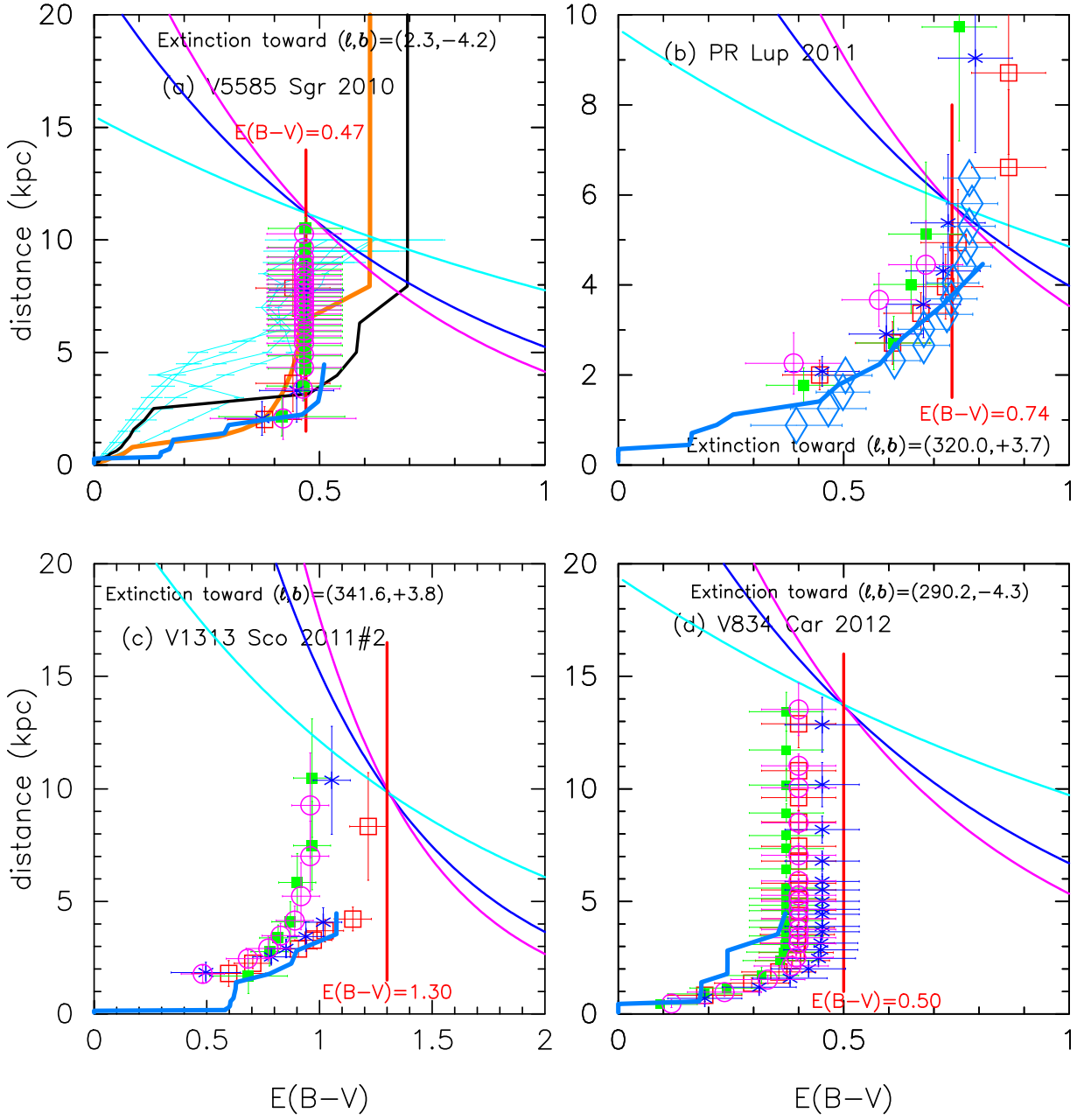

Figure 13. Same as Figure 5, but for (a) V5585 Sgr, (b) PR Lup, (c) V1313 Sco, and (d) V834 Car.

We check the distance modulus of $(m-M)_V = 16.7$ by comparing our model V light curve with the observation. Assuming $(m-M)_V = 16.7$, we plot a model V light curve of a 0.95 $M_\odot$ WD (CO3, solid red line; Hachisu & Kato 2016a) in Figure 74(a). The V light-curve model reasonably reproduces the observation. This confirms again that the distance modulus of $(m-M)_V = 16.7$ is reasonable. For comparison, we add light curves of a 0.98 $M_\odot$ WD (CO3, solid green lines), assuming that $(m-M)_V = 14.6$ for V1668 Cyg.

3.18. PR Lup 2011

PR Lup reached $m_{V,\max} = 8.7$ on UT 2,455,787.867 (UT 2011 August 14.367). The early spectra showed that PR Lup belongs to the Fe II type (Malasan et al. 2011; Walter 2011). The K_s magnitudes of SMARTS showed a rise at JD 2,455,833.5 (UT 2011 September 29.0) about 50 days after the optical maximum. This clearly indicates the formation of a dust shell. The V light curve correspondingly drops at this epoch (see Figure 76).

We obtain $(m-M)_B = 16.84$, $(m-M)_V = 16.1$, and $(m-M)_I = 14.94$, which cross at $d = 5.8$ kpc and $E(B-V) = 0.74$, in Appendix A.18 and plot them in Figure 13(b). Thus, we obtain $d = 5.8 \pm 0.6$ kpc, $E(B-V) = 0.74 \pm 0.05$, $(m-M)_V = 16.1 \pm 0.1$, and $f_s = 1.7$ against LV Vul.

For the reddening toward PR Lup, $(l,\ b) = (319.^\circ9767, +3.^\circ6641)$, the 2D NASA/IPAC galactic dust absorption map gives $E(B-V) = 0.78 \pm 0.02$, being roughly consistent with our obtained value of $E(B-V) = 0.74 \pm 0.05$. Figure 13(b) shows several distance–reddening relations toward PR Lup. We plot Marshall et al.'s (2006) relations toward $(l,\ b) = (319.^\circ75, +3.^\circ75)$, $(320.^\circ00, +3.^\circ75)$, $(319.^\circ75, +3.^\circ50)$, and $(320.^\circ00. + 3.^\circ50)$. The closest direction is that of the filled

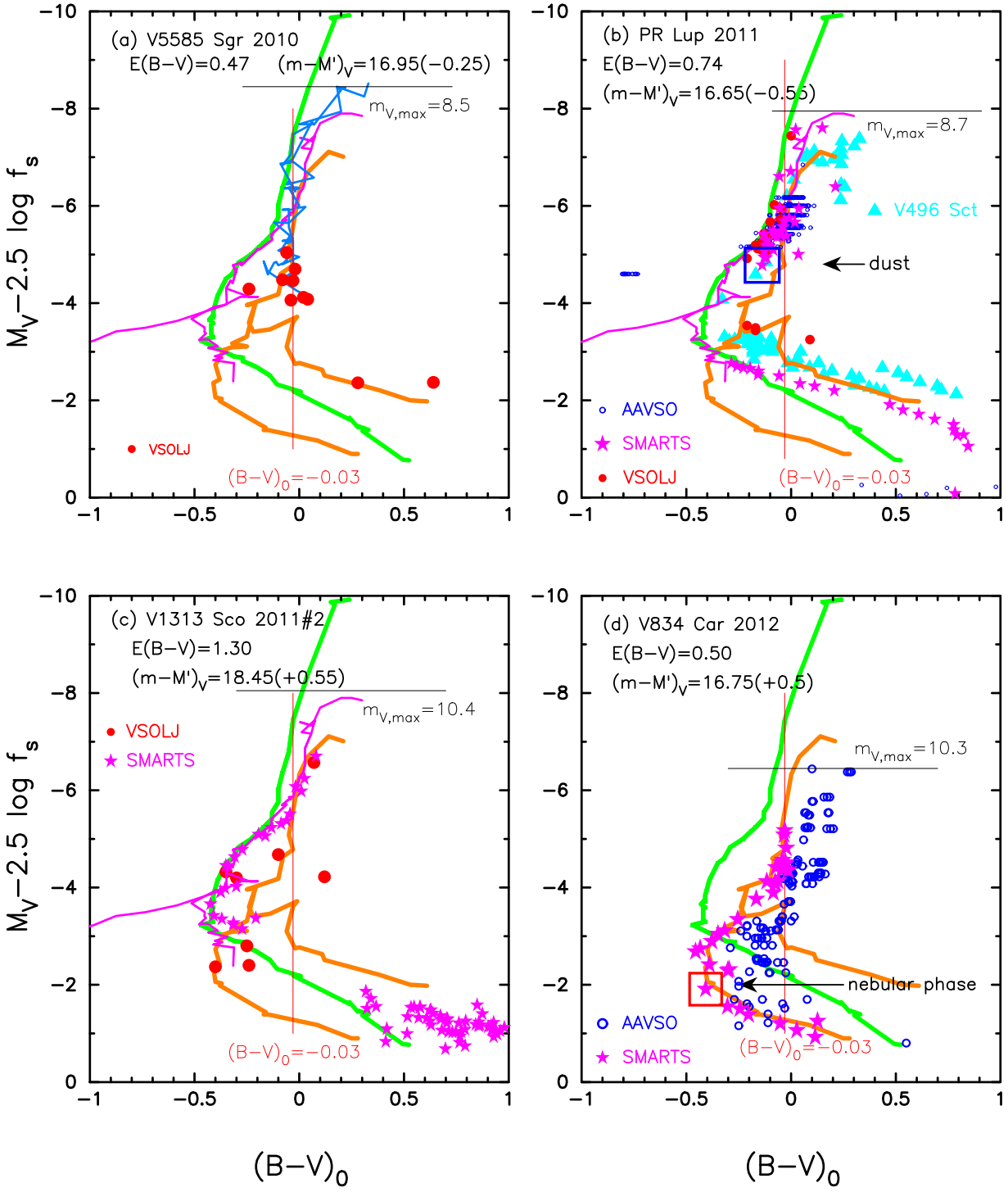

Figure 14. Same as Figure 6, but for (a) V5585 Sgr, (b) PR Lup, (c) V1313 Sco, and (d) V834 Car. The solid green lines show the template track of V1500 Cyg. The solid orange lines represent that of LV Vul. In panels (a), (b), and (c), we add the track of V1974 Cyg (solid magenta lines). In panel (a), we add the track of V1668 Cyg (solid cyan-blue lines). In panel (b), we add the track of V496 Sct (filled cyan triangles).

green squares. The other symbols/lines have the same meanings as those in Figure 5(a). Our crossing point of $d = 5.8 \pm 0.6$ kpc and $E(B-V) = 0.74 \pm 0.05$ is consistent with these relations.

We plot the $(B-V)_0$–$(M_V - 2.5\log f_s)$ diagram of PR Lup in Figure 14(b) for $E(B-V) = 0.74$ and $(m-M')_V = 16.65$ in Equation (102). We also add the data points of V496 Sct (filled cyan triangles) for comparison. The PR Lup track is close to that of V496 Sct and LV Vul. Therefore, we regard PR Lup to belong to the LV Vul type. This similarity of PR Lup to V496 Sct and LV Vul supports the fact that our adopted values of $E(B-V) = 0.74$ and $(m-M')_V = 16.65$, that is, $E(B-V) = 0.74 \pm 0.05$, $(m-M)_V = 16.1 \pm 0.1$, $f_s = 1.70$, and $d = 5.8 \pm 0.6$ kpc are reasonable.

We check the distance modulus of $(m-M)_V = 16.1$ by comparing our model V light curve with the observation. Assuming $(m-M)_V = 16.1$, we plot a model V light curve of a 0.80 $M_\odot$ WD (CO2, solid red line; Hachisu & Kato 2010) in

Figure 77(a). The V light-curve models reproduces the observation well. This confirms that distance modulus of $(m-M)_V = 16.1$ is reasonable.

3.19. V1313 Sco 2011#2

V1313 Sco reached $m_{V,\max} = 10.4$ on JD 2,455,812.0 (UT 2011 September 7.5; Waagen & Noguchi 2011). The nova was identified as an Fe II type (Arai et al. 2011), but later Walter et al. (2012) classified V1313 Sco as a hybrid of the Fe II and He/N types.

We obtain $(m-M)_B = 20.33$, $(m-M)_V = 19.01$, and $(m-M)_I = 16.92$, which cross at $d = 9.9$ kpc and $E(B-V) = 1.30$, in Appendix A.19 and plot them in Figure 13(c). Thus, we have $E(B-V) = 1.30 \pm 0.1$ and $d = 9.9 \pm 2$ kpc.

For the reddening toward V1313 Sco, $(l, b) = (341.^\circ5552, +3.^\circ8397)$, the 2D NASA/IPAC galactic dust absorption map gives $E(B-V) = 1.20 \pm 0.10$, which is consistent with our crossing point of $E(B-V) = 1.30 \pm 0.1$. We further check our result in Figure 13(c). We plot four of Marshall et al.'s (2006) relations toward $(l, b) = (341.^\circ50, +3.^\circ75)$, $(341.^\circ75, +3.^\circ75)$, $(341.^\circ50, +4.^\circ00)$, and $(341.^\circ75, +4.^\circ00)$. The closest direction is that of the unfilled red squares. The other symbols/lines have the same meanings as those in Figure 5(a). Our crossing point is consistent with Marshall et al.'s distance–reddening relation (unfilled red squares with error bars).

We plot the $(B-V)_0$–$(M_V - 2.5\log f_s)$ diagram of V1313 Sco in Figure 14(c) for $E(B-V) = 1.30$ and $(m-M')_V = 18.45$ in Equation (107). The track of V1313 Sco closely follows that of V1974 Cyg and V1500 Cyg. Thus, we regard V1313 Sco to belong to the V1500 Cyg type. This similarity of the V1313 Sco track to the V1974 Cyg and V1500 Cyg tracks supports our adopted values of $E(B-V) = 1.30$ and $(m-M')_V = 18.45$, that is, $E(B-V) = 1.30 \pm 0.1$, $(m-M)_V = 19.0 \pm 0.1$, $f_s = 0.60$, and $d = 9.9 \pm 2$ kpc.

We check the distance modulus of $(m-M)_V = 19.0$ by comparing our model V light curve with the observation. Assuming that $(m-M)_V = 19.0$, we plot a model V light curve of a 1.20 $M_\odot$ WD (Ne2, solid red line; Hachisu & Kato 2010) in Figure 80(a). The V light-curve model reproduces the observation. This confirms that the distance modulus of $(m-M)_V = 19.0$ is reasonable. For comparison, we add light curves of a 0.98 $M_\odot$ WD (CO3, solid green lines), assuming that $(m-M)_V = 14.6$ for V1668 Cyg.

3.20. V834 Car 2012

V834 Car reached $m_{V,\max} = 10.3$ on JD 2,455,987.8 (UT 2012 March 1.3) from the AAVSO data. Walter et al. (2012) identified the nova as an Fe II type and estimated the decline rates of $t_2 = 20 \pm 3$ days and $t_3 = 38 \pm 1$ days.

We obtain $(m-M)_B = 17.75$, $(m-M)_V = 17.23$, and $(m-M)_I = 16.44$ in Appendix A.20 and plot them in Figure 13(d), which broadly cross at $d = 14$ kpc and $E(B-V) = 0.50$. Thus, we have $E(B-V) = 0.50 \pm 0.05$ and $d = 14 \pm 2$ kpc. The distance modulus in the V band is $(m-M)_V = 17.25 \pm 0.1$.

For the reddening toward V834 Car, $(l, b) = (290.^\circ1799, -4.^\circ2820)$, the 2D NASA/IPAC galactic dust absorption map gives $E(B-V) = 0.52 \pm 0.01$, which is consistent with our value of $E(B-V) = 0.50 \pm 0.05$. We further check our result in Figure 13(d). Marshall et al.'s (2006) relations are plotted toward $(l, b) = (290.^\circ00, -4.^\circ25)$, $(290.^\circ25, -4.^\circ25)$, $(290.^\circ00, -4.^\circ50)$, and $(290.^\circ25, -4.^\circ50)$. The closest direction is that of the filled green squares. The other symbols/lines have the same meanings as those in Figure 5(a). Our crossing point is roughly consistent with Marshall et al.'s relation (blue asterisks with error bars).

We plot the $(B-V)_0$–$(M_V - 2.5\log f_s)$ diagram of V834 Car in Figure 14(d) for $E(B-V) = 0.50$ and $(m-M')_V = 16.75$ in Equation (112). The track of V834 Car (SMARTS data; filled magenta stars) follows that of LV Vul. Thus, we regard V834 Car to belong to the LV Vul type. This overlapping with the LV Vul track supports the fact that $E(B-V) = 0.50$ and $(m-M')_V = 16.75$, that is, $E(B-V) = 0.50 \pm 0.05$, $(m-M)_V = 17.25 \pm 0.1$, $f_s = 0.65$, and $d = 14 \pm 2$ kpc.

The nova had already entered the nebular phase on UT 2012 May 27 (JD 2,456,074.5), because [O III] lines developed as shown in the SMARTS spectra (Walter et al. 2012). We identify the start of the nebular phase as $M_V = 14.82 - 17.25 = -2.43$ and $(B-V)_0 = 0.105 - 0.50 = -0.395$ denoted by the large unfilled red square in Figure 14(d).

We check the distance modulus of $(m-M)_V = 17.25$ by comparing our model V light curve with the observation. Assuming that $(m-M)_V = 17.25$, we plot a V model light curve (solid red line) of a 1.20 $M_\odot$ WD (Ne2; Hachisu & Kato 2010) in Figure 83(a). The model V light curve reasonably reproduces the observation. This confirms that the distance modulus of $(m-M)_V = 17.25$ is reasonable. In the same figure, we also plot the model light curves of a 0.98 $M_\odot$ WD (CO3, solid green lines), assuming $(m-M)_V = 14.6$ for V1668 Cyg.

3.21. V1368 Cen 2012

V1368 Cen reached $m_{V,\max} = 9.4$ on JD 2,456,010.6. The K_s magnitudes of SMARTS showed a rise on JD 2,456,042.7 (UT 2012 April 25.2) about 32 days after the optical maximum. This clearly indicates the formation of a dust shell (Walter et al. 2012). The V light curve correspondingly drops at this epoch as shown by the arrow in Figure 85. Walter et al. (2012) identified this nova to be of Fe II type and estimated the decline rates as $t_2 = 16 \pm 1$ days and $t_3 \sim 32$ days.

We obtain $(m-M)_B = 18.53$, $(m-M)_V = 17.6$, and $(m-M)_I = 16.12$, which broadly cross at $d = 8.8$ kpc and $E(B-V) = 0.93$, in Appendix A.21 and plot them in Figure 15(a). Thus, we have $E(B-V) = 0.93 \pm 0.05$ and $d = 8.8 \pm 1$ kpc. The distance modulus in the V band is $(m-M)_V = 17.6 \pm 0.1$.

For the reddening toward V1368 Cen, $(l, b) = (309.^\circ4457, +3.^\circ9788)$, the 2D NASA/IPAC galactic dust absorption map gives $E(B-V) = 0.97 \pm 0.06$, which is consistent with our value of $E(B-V) = 0.93 \pm 0.05$. We further check our result in Figure 15(a). Marshall et al.'s (2006) relations are plotted toward $(l, b) = (309.^\circ25, +3.^\circ75)$, $(309.^\circ50, +3.^\circ75)$, $(309.^\circ25, +4.^\circ00)$, and $(309.^\circ50, +4.^\circ00)$. The closest direction is that of the unfilled magenta circles. The other symbols/lines have the same meanings as those in Figure 5(a). Our crossing point is consistent with Marshall et al.'s distance–reddening relation (unfilled magenta circles with error bars).

We plot the $(B-V)_0$–$(M_V - 2.5\log f_s)$ diagram of V1368 Cen in Figure 16(a) for $E(B-V) = 0.93$ and $(m-M')_V = 17.85$ from Equation (117). The track of V1368 Cen almost follows V1668 Cyg in the early phase. The V1368 Cen track follows the LV Vul track after the dust blackout ended. We plot the start of the dust blackout with the arrow labeled "dust." Therefore, we

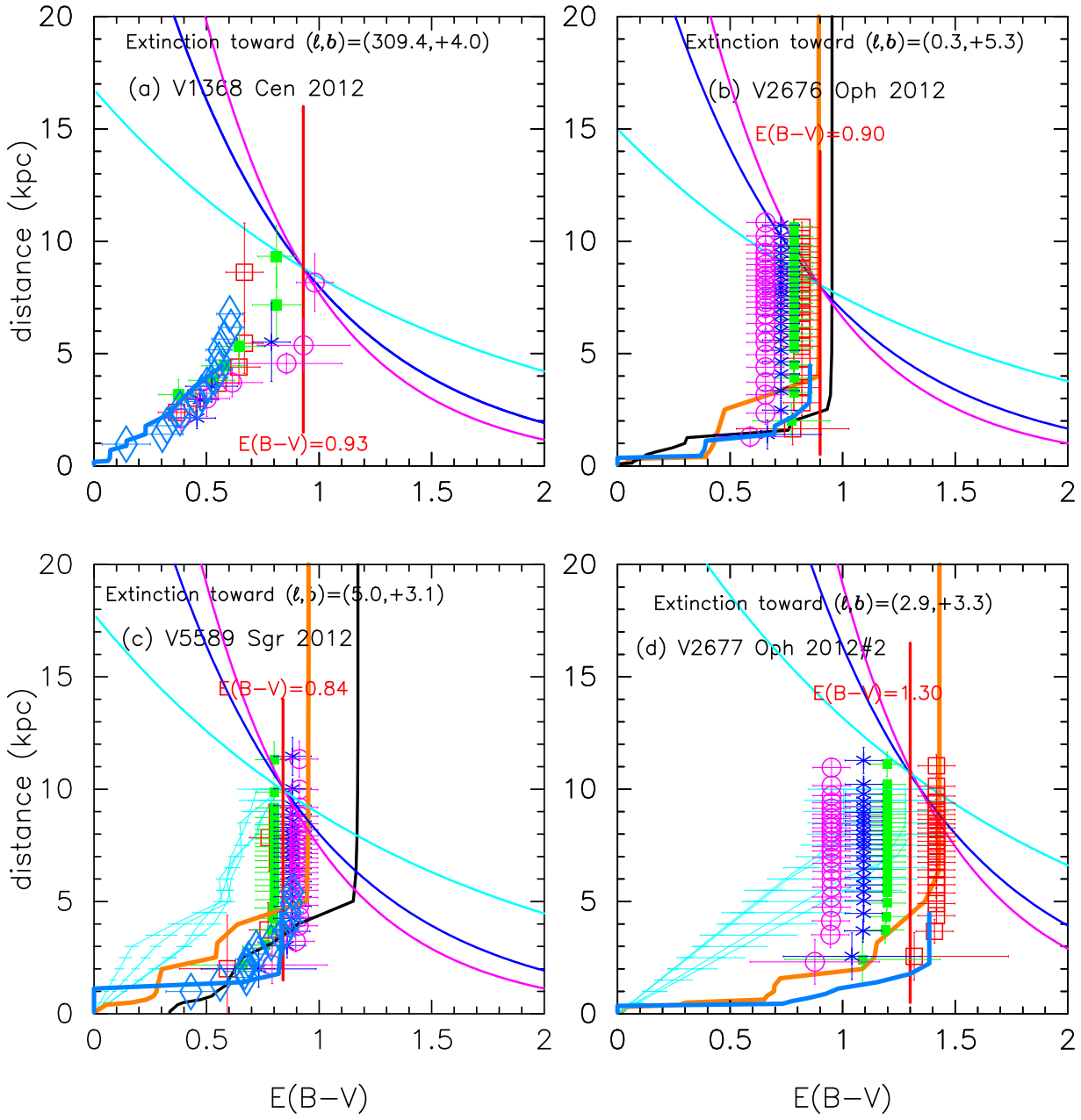

Figure 15. Same as Figure 5, but for (a) V1368 Cen, (b) V2676 Oph, (c) V5589 Sgr, and (d) V2677 Oph.

regard V1368 Cen to belong to the LV Vul type. This overlapping of V1368 Cen with the V1668 Cyg and LV Vul tracks supports $E(B-V) = 0.93$ and $(m-M')_V = 17.85$, that is, $E(B-V) = 0.93 \pm 0.05$, $(m-M)_V = 17.6 \pm 0.1$, $f_s = 1.26$, and $d = 8.8 \pm 1$ kpc. The nova had already entered the nebular phase on UT 2012 May 27 (JD 2,456,074.5), because [O III] lines developed as shown in SMARTS spectra (Walter et al. 2012). We identify the start of the nebular phase as $M_V = 14.23 - 17.6 = -3.37$ and $(B-V)_0 = 0.799 - 0.93 = -0.13$, denoted by a large unfilled red square.

We check the distance modulus of $(m-M)_V = 17.6$ by comparing our model V light curve with the observation. Assuming $(m-M)_V = 17.6$, we plot a V model light curve of a 0.95 $M_\odot$ WD (CO3, solid green line; Hachisu & Kato 2016a) in Figure 86(a). The model V light curve reasonably reproduces the observation. This confirms that the distance modulus of $(m-M)_V = 17.6$ is reasonable. In the same figure, we also plot model light curves of a 0.98 $M_\odot$ WD (CO3, solid blue lines) for V1668 Cyg and a 1.05 $M_\odot$ WD (CO3, solid red lines) for OS And, assuming $(m-M)_V = 14.6$ for V1668 Cyg and $(m-M)_V = 14.8$ for OS And.

3.22. V2676 Oph 2012

V2676 Oph reached $m_{V,\max} = 10.4$ on JD 2,456,038.97 (UT 2012 April 21.47) from the VSOLJ data. Arai & Isogai (2012) identified the nova as an Fe II type. The K_s magnitudes of SMARTS showed a rise on JD 2,456,103.7 (UT 2012 June 25.2), about 95 days after outburst (see Figure 88). This clearly indicates the formation of a dust shell (Walter et al. 2012). The V light curve correspondingly drops at this epoch as shown by the arrow in Figure 88. Rudy et al. (2012) found

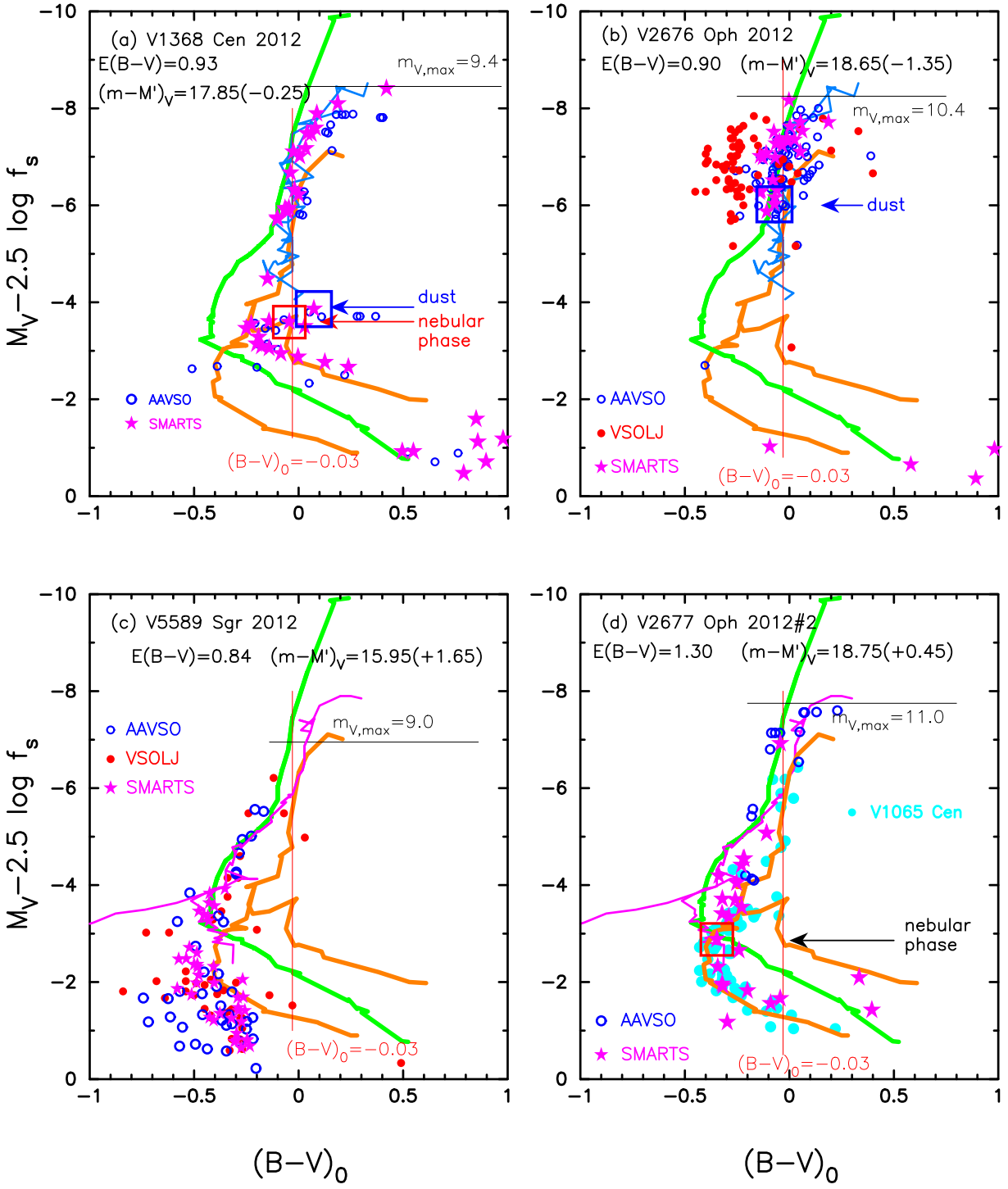

Figure 16. Same as Figure 6, but for (a) V1368 Cen, (b) V2676 Oph, (c) V5589 Sgr, and (d) V2677 Oph. The solid green lines show the template track of V1500 Cyg. The solid orange lines show the template tracks of LV Vul. In panels (a) and (b), we add the track of V1668 Cyg (solid cyan-blue lines). In panels (c) and (d), we add the tracks of V1974 Cyg (solid magenta lines). In panel (d), we add the track of V1065 Cen (filled cyan circles).

carbon-monoxide emission from the fundamental and the first and second overtones on UT 2012 May 1 and 2 before the dust shell formation. Nagashima et al. (2014) and Kawakita et al. (2015) also found strong emission from C_2 and CN molecules. The mid-infrared spectroscopic and photometric observations in 2013 and 2014 (452 and 782 days after its discovery, respectively) showed no significant Ne II emission at 12.8 μm, suggesting evidence for a CO-rich WD (Kawakita et al. 2017).

We obtain $(m-M)_B = 18.2$, $(m-M)_V = 17.3$, and $(m-M)_I = 15.88$, which cross at $d = 8.0$ kpc and $E(B-V) = 0.90$, in Appendix A.22 and plot them in Figure 15(b). Thus, we have $E(B-V) = 0.90 \pm 0.05$ and $d = 8.0 \pm 1$ kpc. The distance modulus in the V band is $(m-M)_V = 17.3 \pm 0.1$.

For the reddening toward V2676 Oph, $(l, b) = (0.^\circ2631, +5.^\circ3013)$, the 2D NASA/IPAC galactic dust absorption map gives $E(B-V) = 0.91 \pm 0.05$, consistent with our value

of $E(B-V) = 0.90 \pm 0.05$. Nagashima et al. (2015) obtained $E(B-V) = 0.71 \pm 0.02$ from the Balmer decrement. Kawakita et al. (2016) obtained $E(B-V) = A_V/3.1 = (2.65 \pm 0.15)/3.1 = 0.85 \pm 0.05$ from the $T_{\rm eff}$ versus $E(V-{\rm I})$ relation. Raj et al. (2017) obtained $E(B-V) = A_V/3.1 = (2.9 \pm 0.1)/3.1 = 0.94 \pm 0.03$ from the Balmer decrement. However, hydrogen recombination lines are usually not described by Case B approximation, and the extinction estimated from this method likely has a large error. Our value of $E(B-V) = 0.90 \pm 0.05$ at the crossing point is roughly consistent with $E(B-V) = 0.85 \pm 0.05$ (Kawakita et al. 2016) and $E(B-V) = 0.94 \pm 0.03$ (Raj et al. 2017).

We further check our result in Figure 15(b). Marshall et al.'s (2006) relations are plotted toward $(l,\ b) = (0.^\circ25,\ +5.^\circ25)$, $(0.^\circ50,\ +5.^\circ25)$, $(0.^\circ25,\ +5.^\circ50)$, and $(0.^\circ50,\ +5.^\circ50)$. The closest direction is that of the unfilled red squares. The other symbols/lines have the same meanings as those in Figure 5(a). Our crossing point is consistent with Marshall et al.'s (unfilled red squares with error bars), Green et al.'s (orange line), and Chen et al.'s (cyan-blue line) distance–reddening relations.

We plot the $(B-V)_0$–$(M_V - 2.5\log f_{\rm s})$ diagram of V2676 Oph in Figure 16(b) for $E(B-V) = 0.90$ and $(m-M')_V = 18.65$ in Equation (122). The track of V2676 Oph (SMARTS data) is close to that of V1668 Cyg and LV Vul until the dust blackout started. Thus, we regard V2676 Oph to belong to the LV Vul type in the $(B-V)_0$–$(M_V - 2.5\log f_{\rm s})$ diagram like V1065 Cen and V1368 Cen. This overlapping with the LV Vul track is consistent with our values of $E(B-V) = 0.90$ and $(m-M')_V = 18.65$, that is, $E(B-V) = 0.90 \pm 0.05$, $(m-M)_V = 17.3 \pm 0.2$, $f_{\rm s} = 3.4$, and $d = 8.0 \pm 1.0$ kpc.

We check the distance modulus of $(m-M)_V = 17.3$ by comparing our model V light curve with the observation in Figure 89(a). Assuming $(m-M)_V = 17.3$, we plot a V model light curve of a 0.70 $M_\odot$ WD (CO2, solid red line; Hachisu & Kato 2010). The model V light curve reasonably reproduces the observation, although the light curve has a wavy structure before the dust blackout. This may confirm that the distance modulus of $(m-M)_V = 17.3$ is reasonable. In the same figure, we also plot model light curves of a 0.80 $M_\odot$ WD (CO3, solid black line), assuming that $(m-M)_V = 14.65$ for QY Mus.

3.23. V5589 Sgr 2012#1

V5589 Sgr reached $m_{V,{\rm max}} \sim 9.0$ on JD 2,456,039.56 (UT 2012 April 22.06; e.g., Mróz et al. 2015). Walter et al. (2012) estimated the decline rates of $t_2 = 4.5 \pm 1.5$ days and $t_3 = 7$ days, while Weston et al. (2016) obtained $t_2 = 6.8 \pm 0.8$ days and $t_3 = 12.8 \pm 1.5$ days. Thompson (2017) analyzed *Solar Terrestrial Relations Observatory* (*STEREO*) data and obtained optical maximum at mag 8.23 ± 0.03 in the Heliospheric Imager (HI)-1 bandpass on JD 2,456,039.3224. They also obtained $t_2 = 5.0 \pm 0.6$ days and $t_3 = 10.9 \pm 0.7$ days. So the nova belongs to the very fast nova speed class defined by Payne-Gaposchkin (1957).

V5589 Sgr was identified as a hybrid nova from Fe II to He/N type (Walter et al. 2012). The nova had entered the coronal phase of [Fe X], [Fe XI], and [Fe XIV] by day 65 (Walter et al. 2012). The detection of the coronal phase sometimes indicates that the nova had already entered the supersoft X-ray source (SSS) phase. The *Swift*/XRT observation showed that the nova increased its soft X-ray flux on day 64.5 (Weston et al. 2016). We may regard the nova to have entered the SSS phase by at least day 64.5. Mróz et al. (2015) obtained the orbital period of this nova as $P_{\rm orb} = 1.5923$ days ($P_{\rm orb} = 38.215$ hr). They suggested that the companion has already evolved off the main sequence and is a subgiant like the recurrent nova U Sco.

We obtain $(m-M)_B = 18.45$, $(m-M)_V = 17.62$, and $(m-M)_I = 16.25$, which cross at $d = 10$ kpc and $E(B-V) = 0.84$, in Appendix A.23 and plot them in Figure 15(c). Thus, we have $E(B-V) = 0.84 \pm 0.05$ and $d = 10 \pm 1$ kpc. The distance modulus in the V band is $(m-M)_V = 17.6 \pm 0.1$.

For the reddening toward V5589 Sgr, $(l,\ b) = (4.^\circ9766,\ +3.^\circ0724)$, the 2D NASA/IPAC galactic dust absorption map gives $E(B-V) = 0.84 \pm 0.04$. The VVV survey catalog gives $E(B-V) = A_{K_{\rm s}}/0.36 = 0.274/0.36 = 0.76$ (Saito et al. 2013). Weston et al. (2016) estimated the reddening of $E(B-V) = 0.8 \pm 0.19$ from four diffuse interstellar band (DIB) features. These reddening values are roughly consistent with our crossing point of $E(B-V) = 0.84 \pm 0.05$.

We further check our result in Figure 15(c). Marshall et al.'s (2006) relations are plotted toward $(l,\ b) = (4.^\circ75,\ +3.^\circ00)$, $(5.^\circ00,\ +3.^\circ00)$, $(4.^\circ75,\ +3.^\circ25)$, and $(5.^\circ00,\ +3.^\circ25)$. The closest direction is that of the filled green squares. The other symbols/lines have the same meanings as those in Figure 5(a). Our crossing point is consistent with Marshall et al.'s (filled green squares with error bars), Özdörmez et al.'s (unfilled cyan-blue diamonds), and Chen et al.'s (cyan-blue line) distance–reddening relations.

We plot the $(B-V)_0$–$(M_V - 2.5\log f_{\rm s})$ diagram of V5589 Sgr in Figure 16(c) for $E(B-V) = 0.84$ and $(m-M')_V = 15.95$ in Equation (127). The track of V5589 Sgr follows that of V1500 Cyg and V1974 Cyg in the early phase. Thus, we regard V5589 Sgr to belong to the V1500 Cyg type. This overlapping of the V5589 Sgr track with the V1500 Cyg and V1974 Cyg tracks supports $E(B-V) = 0.84$ and $(m-M')_V = 15.95$, that is, $E(B-V) = 0.84 \pm 0.05$, $(m-M)_V = 17.6 \pm 0.1$, $d = 10 \pm 1$ kpc, and $f_{\rm s} = 0.21$ against LV Vul.

We check the distance modulus of $(m-M)_V = 17.6$ by comparing our model V light curve with the observation. Assuming that $(m-M)_V = 17.6$, we plot a V model light curve and supersoft X-ray flux (0.1–2.4 keV) of a 1.33 $M_\odot$ WD (Ne2, solid black lines; Hachisu & Kato 2010) in Figure 92(a). The V light curves reasonably reproduce the observation. This again confirms that the distance modulus of $(m-M)_V = 17.6$ is reasonable. The blue lines are the model light curves of 1.23 $M_\odot$ WD (Ne2), assuming that $(m-M)_V = 11.5$ for V382 Vel.

Weston et al. (2016) obtained $E(B-V) = 0.80 \pm 0.19$ as mentioned above and derived the distance of $d = 3.6^{+1.0}_{-2.4}$ kpc in conjunction with the 3D reddening map of Green et al. (2015). This distance estimate is not reasonable, because Green et al.'s (2015, black line) 3D reddening map deviates largely from Marshall et al.'s (2006, filled green squares) and revised Green et al.'s (2018, orange line) 3D reddening maps as shown in Figure 15(c) and the NASA/IPAC absorption map of $E(B-V) = 0.84 \pm 0.04$. The reason why Weston et al. (2016) obtained such a short distance is that they used the distance–reddening relation of Green et al. (2015), which is not consistent with other 2D and 3D dust maps.

Assuming a Hubble flow of the ejecta, Weston et al. (2016) estimated the ejecta mass as $M_{\rm ej} = 2.6 \times 10^{-5}\ M_\odot$ together with the other parameters of $d = 4$ kpc, $T = 1.2 \times 10^4$ K,

$v_{\rm HWZI} = 4000$ km s^{-1}, and $\zeta = v_{\rm min}/v_{\rm HWZI} = 0.84$. The ejected mass estimated from our model of a 1.33 $M_\odot$ WD (Figure 92) is $M_{\rm ej} = 1.7 \times 10^{-6}\ M_\odot$. Weston et al.'s value is about 10 times larger than our value. Theoretically, the ignition mass, i.e., the hydrogen-rich envelope mass at the nova ignition, is much smaller in a high-mass WD than in a low-mass WD, that is, for the 1.33 $M_\odot$ WD, $M_{\rm ig} \sim 1 \times 10^{-6}$–$3 \times 10^{-6}\ M_\odot$, depending on the mass accretion rate onto the WD (see, e.g., Figure 3 of Kato et al. 2014 for a recent estimate of ignition masses).

Weston et al. (2016) reported the *Swift* X-ray observation of V5589 Sgr. The X-ray spectrum showed an increase of soft X-ray flux (lower than 1 keV) on day 64.5 compared with the previous X-ray observation on day 53. They regarded this rise of soft X-ray flux as the appearance of the SSS phase. They further obtained the blackbody temperature of 50^{+36}_{-18} eV from the spectrum on day 68. The X-ray count rate had declined on day 78. Figure 92(a) shows our supersoft X-ray light curve (solid black lines) of a 1.33 $M_\odot$ WD, which shows a rise on day ∼55 (optically thick wind stops) and fall on day ∼75 (hydrogen-shell burning ends). These features are consistent with the *Swift*/XRT observation.

3.24. V2677 Oph 2012#2

V2677 Oph reached $m_{V,\rm max} = 11.0$ on JD 2,456,068.84 (UT 2012 May 21.34) from AAVSO data. Walter et al. (2012) identified the nova as an Fe II type. Mróz et al. (2015) presented their OGLE photometric observation of V2677 Oph and obtained a possible orbital period of $P_{\rm orb} = 8.607$ hr.

We obtain $(m-M)_B = 20.5$, $(m-M)_V = 19.18$, and $(m-M)_I = 17.1$, which broadly cross at $d = 10.7$ kpc and $E(B-V) = 1.30$, in Appendix A.24 and plot them in Figure 15(d). Thus, we have $E(B-V) = 1.30 \pm 0.10$ and $d = 10.7 \pm 2$ kpc. The distance modulus in the V band is $(m-M)_V = 19.2 \pm 0.1$.

For the reddening toward V2677 Oph, $(l,\ b) = (2\overset{\circ}{.}8584, +3\overset{\circ}{.}2550)$, the 2D NASA/IPAC galactic dust absorption map gives $E(B-V) = 1.30 \pm 0.05$, which is consistent with our value of $E(B-V) = 1.30 \pm 0.10$. We further check our result in Figure 15(d). Marshall et al.'s (2006) relations are plotted toward $(l,\ b) = (2\overset{\circ}{.}75, +3\overset{\circ}{.}25)$, $(3\overset{\circ}{.}00, +3\overset{\circ}{.}25)$, $(2\overset{\circ}{.}75, +3\overset{\circ}{.}50)$, and $(3\overset{\circ}{.}00, +3\overset{\circ}{.}50)$. The direction toward V2677 Oph is between the directions of the filled green squares and unfilled red squares. The other symbols/lines have the same meanings as those in Figure 5(a). Our crossing point is in reasonable agreement with Marshall et al.'s distance–reddening relations.

We plot the $(B-V)_0$–$(M_V - 2.5\log f_{\rm s})$ diagram of V2677 Oph in Figure 16(d) for $E(B-V) = 1.30$ and $(m-M')_V = 18.75$ in Equation (132). The track of V2677 Oph is very close to that of LV Vul and V1065 Cen (filled cyan circles). Thus, we regard V2677 Oph to belong to the LV Vul type. This similarity of the V2677 Oph track to the LV Vul track supports our values of $E(B-V) = 1.30$ and $(m-M')_V = 18.75$, that is, $E(B-V) = 1.30 \pm 0.10$, $(m-M)_V = 19.2 \pm 0.1$, $f_{\rm s} = 0.68$, and $d = 10.7 \pm 2$ kpc.

The nova had already entered the nebular phase on JD 2,456,118.5 (UT 2012 July 10) in the spectra of SMARTS (Walter et al. 2012). We specify this point in the $(B-V)_0$–$(M_V - 2.5\log f_{\rm s})$ diagram by a large unfilled red square, i.e., $(B-V)_0 = 0.974 - 1.30 = -0.33$ and $M_V = 15.84 - 19.2 = -3.36$ (Figure 16(d)).

We check the distance modulus of $(m-M)_V = 19.2$ by comparing our model V light curve with the observation (filled green circles) in Figure 96(a). Assuming $(m-M)_V = 19.2$, we plot a V model light curve of a 1.15 $M_\odot$ WD (Ne2, solid green line; Hachisu & Kato 2010). For comparison, we add the LV Vul light/color curves (unfilled blue squares). We also add the V light/color curves of V1065 Cen (unfilled magenta diamonds). The model V light curve reasonably reproduces the observation. However, the observed V magnitudes are slightly (∼0.8 mag) fainter than the model V light curve in the middle phase. The V light curve of V2677 Oph is very similar to that of V1065 Cen in the middle phase. Therefore, we suppose that a similar effect that we do not include in our model occurs for both novae. We regard our model V light curve to reproduce the V light curve of V2677 Oph except for the middle phase. This again confirms that the distance modulus of $(m-M)_V = 19.2$ is reasonable.

3.25. V1324 Sco 2012

V1324 Sco reached $m_{V,\rm max} = 9.8$ on JD 2,456,098.45 (UT 2012 June 19.95) from the AAVSO data. Wagner et al. (2012) detected a periodicity of 1.6 hr with an amplitude of 0.1 mag on UT 2012 May 28 and 31. Finzell et al. (2015) suggested a main-sequence companion if this periodicity is the orbital period ($P_{\rm orb} \sim 1.6$ hr or $P_{\rm orb} \sim 3.2$ hr for the ellipsoidal modulation). Ackermann et al. (2014) detected gamma-rays from this nova with the *Fermi*/Large Area Telescope (LAT). Assuming the distance of $d = 4.5$ kpc to V1324 Sco, they concluded that V1324 Sco is the strongest among the detected gamma-ray sources V407 Cyg (2.7 kpc), V1324 Sco (4.5 kpc), V959 Mon (3.6 kpc), and V339 Del (4.2 kpc). However, the distances of novae are always debated. For example, Hachisu & Kato (2018a) have already redetermined the distance of V959 Mon to be $d = 2.5 \pm 0.5$ kpc based on the time-stretching method and the time-stretched color–magnitude diagram. This value is much smaller than Ackerman et al.'s assumed value of 3.6 kpc for V959 Mon. Hachisu & Kato (2018b) also redetermined the distance of V407 Cyg to be $d = 3.9 \pm 0.5$ kpc, which is much larger than Ackerman et al.'s assumed value of 2.7 kpc for V407 Cyg. Ackerman et al. estimated the distance of V1324 Sco, $d = 4.5$ kpc, from various MMRD relations, but the MMRD relations are statistical relations and not that accurate for individual novae (see, e.g., Schaefer 2018). Munari et al. (2015b) obtained the reddening of $E(B-V) = 1.23 \pm 0.12$ from the colors of novae at maximum and t_2 time. Finzell et al. (2015) estimated the reddening of $E(B-V) = 1.16 \pm 0.12$ and the distance of $d > 6.5$ kpc. Finzell et al. (2018) presented the comprehensive behavior of V1324 Sco.

We obtain $(m-M)_B = 18.24$, $(m-M)_V = 16.95$, and $(m-M)_I = 14.78$, which cross at $d = 3.7$ kpc and $E(B-V) = 1.32$, in Appendix A.25 and plot them in Figure 17(a). Thus, we obtain $d = 3.7 \pm 0.6$ kpc, $E(B-V) = 1.32 \pm 0.1$, $(m-M)_V = 16.95 \pm 0.2$, and $f_{\rm s} = 2.1$ against LV Vul.

For the reddening toward V1324 Sco, i.e., $(l,\ b) = (357\overset{\circ}{.}4255, -2\overset{\circ}{.}8723)$, the 2D NASA/IPAC galactic dust absorption map gives $E(B-V) = 1.53 \pm 0.14$. We suppose that the reddening does not saturate yet at the distance of V1324 Sco as shown in Figure 17(a). Marshall et al.'s (2006) relations are plotted toward $(l,\ b) = (357\overset{\circ}{.}25, -2\overset{\circ}{.}75)$, $(357\overset{\circ}{.}50, -2\overset{\circ}{.}75)$, $(357\overset{\circ}{.}25, -3\overset{\circ}{.}00)$, and $(357\overset{\circ}{.}50, -3\overset{\circ}{.}00)$. The closest

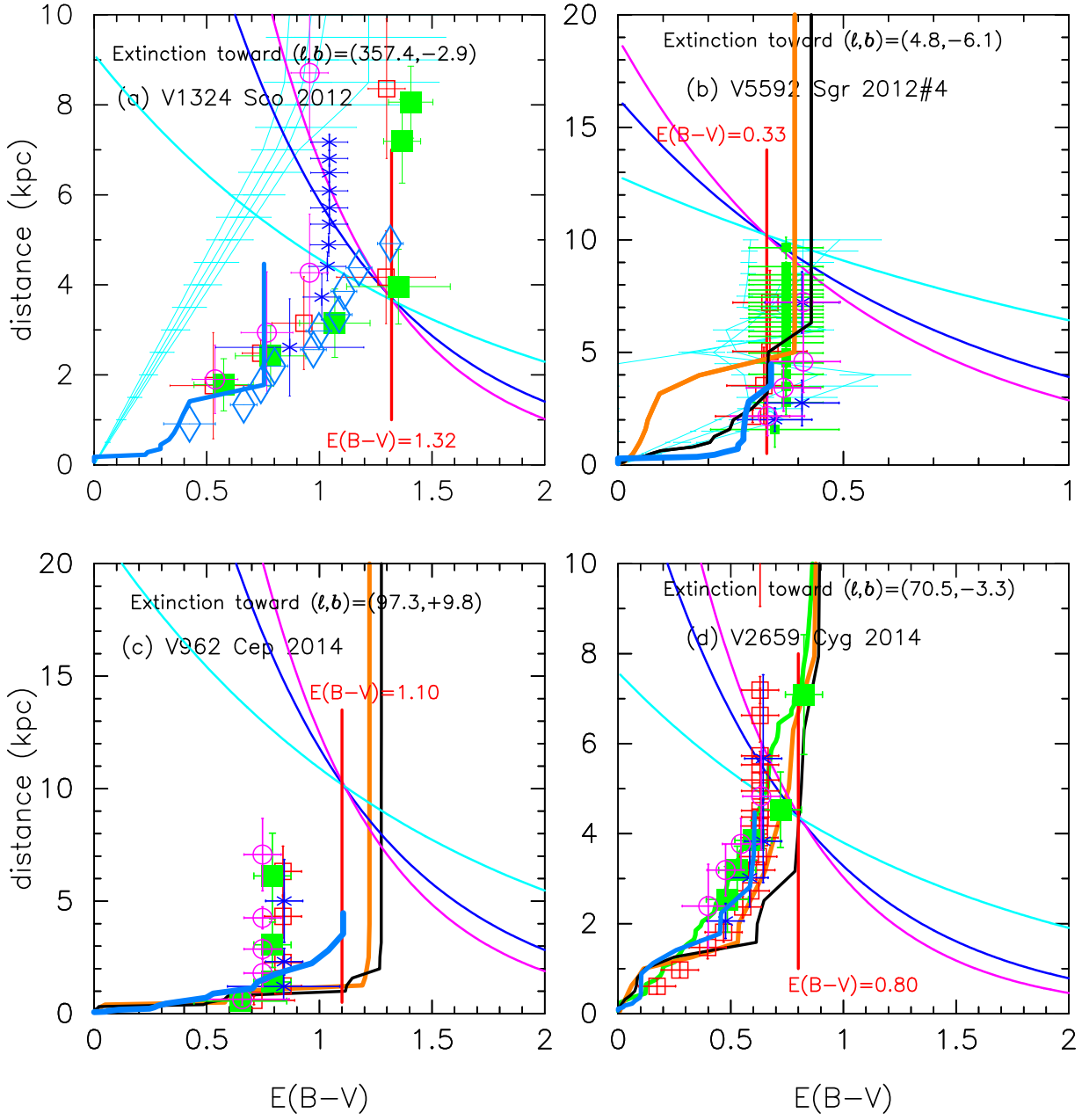

Figure 17. Same as Figure 5, but for (a) V1324 Sco, (b) V5592 Sgr, (c) V962 Cep, and (d) V2659 Cyg.

direction is that of the filled green squares. The other symbols/lines have the same meanings as those in Figure 5(a). Our crossing point of $d = 3.7$ kpc and $E(B-V) = 1.32$ is consistent with Marshall et al.'s distance–reddening relations.

Finzell et al. (2015) obtained the reddening toward V1324 Sco to be $E(B-V) = 1.16 \pm 0.12$ from five diffuse interstellar bands (DIBs) and Na I D and K I absorption features, and obtained the distance of $d > 6.5$ kpc in the conjunction with the 3D reddening map of Schultheis et al. (2014). We plot Schultheis et al.'s data by very thin cyan lines in Figure 17(a). Schultheis et al.'s distance–reddening relations show different trends from Marshall et al.'s and Özdörmez et al.'s relations. We may not use Schultheis et al.'s distance–reddening relations because their trends are sometimes largely different from the trends of Marshall et al.'s, Green et al.'s, and Özdörmez et al.'s relations.

We plot the $(B-V)_0$–$(M_V - 2.5\log f_s)$ diagram of V1324 Sco in Figure 18(a) for $E(B-V) = 1.32$ and $(m-M')_V = 17.75$ from Equation (137). The track of V1324 Sco is very close to those of LV Vul (orange line) and V496 Sct (filled cyan triangles) until the dust blackout started. Thus, we regard V1324 Sco to belong to the LV Vul type. This overlapping of V1324 Sco with LV Vul and V496 Sct supports $E(B-V) = 1.32$ and $(m-M')_V = 17.75$, that is, $E(B-V) = 1.32 \pm 0.1$, $(m-M)_V = 16.95 \pm 0.2$, $f_s = 2.1$, and $d = 3.7 \pm 0.6$ kpc.

We check the distance modulus of $(m-M)_V = 16.95$ by comparing our model V light curve with the observation in Figure 99(a). We plot a V model light curve of a 0.80 $M_\odot$ WD (CO2, solid red line; Hachisu & Kato 2010), assuming $(m-M)_V = 16.95$ for V1324 Sco. The V light curves

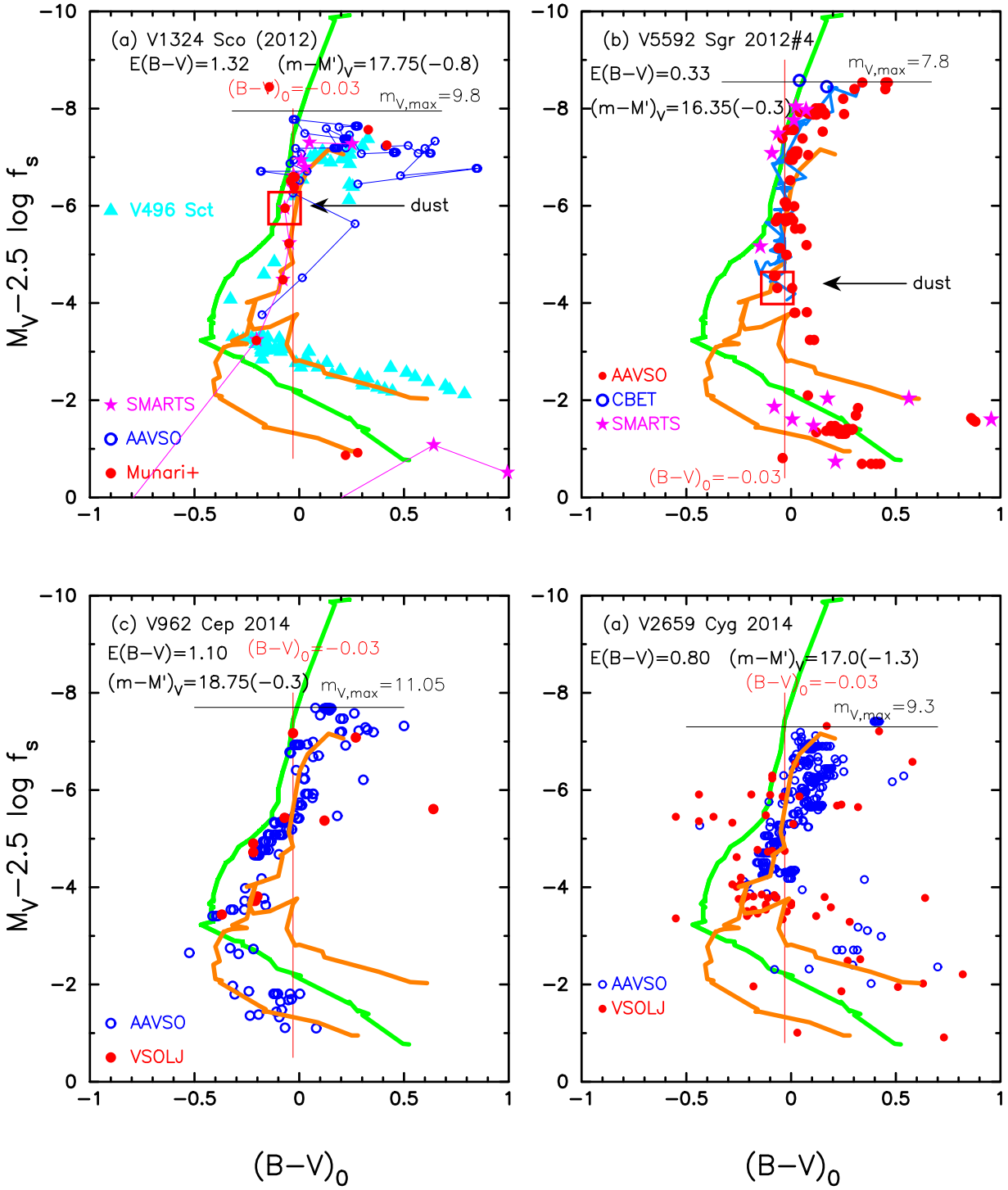

Figure 18. Same as Figure 6, but for (a) V1324 Sco, (b) V5592 Sgr, (c) V962 Cep, and (d) V2659 Cyg. The solid orange/green lines show the template tracks of LV Vul/V1500 Cyg, respectively. In panel (a), we add the track of V496 Sct with the filled cyan triangles. In panel (b), we add the tracks of V1668 Cyg with the solid cyan-blue lines.

reasonably reproduce the observation. This again confirms that the distance modulus of $(m-M)_V = 16.95$ is reasonable.

3.26. V5592 Sgr 2012#4

V5592 Sgr reached $m_{V,\max} = 7.8$ on JD 2,456,116.12 (UT 2012 July 7.62) from CBET No. 3166. The nova was identified as an Fe II type by M. Fujii (Nishiyama & Nakano 2012).

We obtain $(m-M)_B = 16.38$, $(m-M)_V = 16.06$, and $(m-M)_I = 15.59$, which cross at $d = 10$ kpc and $E(B-V) = 0.33$, in Appendix A.26 and plot them in Figure 17(b). Thus, we obtain $d = 10 \pm 1$ kpc, $E(B-V) = 0.33 \pm 0.05$, $(m-M)_V = 16.05 \pm 0.1$, and $f_s = 1.35$ against LV Vul.

For the reddening toward V5592 Sgr, $(l,\ b) = (4.^\circ8122, -6.^\circ0895)$, the 2D NASA/IPAC galactic dust absorption map gives $E(B-V) = 0.33 \pm 0.01$, which is consistent with our

crossing point. We examine our results in Figure 17(b). Marshall et al.'s (2006) relations are plotted toward (l, b) = (4.°75, −6.°00), (5.°00, −6.°00), (4.°75, −6.°25), and (5.°00, −6.°25). The closest direction is that of the unfilled red squares. The other symbols/lines have the same meanings as those in Figure 5(a). Our crossing point of $E(B-V)=0.33$ and $d=10$ kpc is consistent with Marshall et al.'s (unfilled red squares) distance–reddening relation. The reddening toward V5592 Sgr already saturates at the distance of 10 kpc.

We plot the $(B-V)_0$–$(M_V-2.5\log f_s)$ diagram of V5592 Sgr in Figure 18(b) for $E(B-V)=0.33$ and $(m-M')_V=16.35$ in Equation (142). The track of V5592 Sgr almost follows the V1668 Cyg track until the dust blackout starts. Thus, we regard V5592 Sgr to belong to the LV Vul type, because V1668 Cyg belongs to the LV Vul type (Hachisu & Kato 2019). This overlapping of V5592 Sgr with V1668 Cyg supports $E(B-V)=0.33$ and $(m-M')_V=16.35$, that is, $E(B-V)=0.33\pm0.05$, $(m-M)_V=16.05\pm0.1$, $f_s=1.35$, and $d=10\pm1$ kpc.

We check the distance modulus of $(m-M)_V=16.05$ by comparing our model V light curve with the observation in Figure 102(a). We plot a V model light curve of a 0.93 $M_\odot$ WD (CO4, solid red line; Hachisu & Kato 2015), assuming $(m-M)_V=16.05$ for V5592 Sgr. The V light curves reasonably reproduce the observation. This again confirms that the distance modulus of $(m-M)_V=16.05$ is reasonable.

3.27. V962 Cep 2014

V962 Cep reached $m_{V,\max}=11.05$ on UT 2014 March 13.92 (JD 2,456,730.42) from the AAVSO data. Then, the nova declined with $t_2=22\pm2$ days and $t_3=42\pm1$ days (Srivastava et al. 2015). Srivastava et al. (2015) obtained the reddening of $E(B-V)=0.935$ from the empirical relation of $(B-V)_0=0.23\pm0.06$ at optical maximum and $(B-V)_0=-0.02\pm0.04$ at t_2 time (van den Bergh & Younger 1987). Using the MMRD relation proposed by della Valle & Livio (1995), Srivastava et al. (2015) obtained the distance of $d=15.8\pm4$ kpc. They identified V962 Cep as an Fe II type.

We obtain $(m-M)_B=19.58$, $(m-M)_V=18.46$, and $(m-M)_I=16.67$, which cross at $d=10.2$ kpc and $E(B-V)=1.10$, in Appendix A.27 and plot them in Figure 17(c). Thus, we have $E(B-V)=1.10\pm0.1$ and $d=10.2\pm2$ kpc. The distance modulus in the V band is $(m-M)_V=18.45\pm0.2$.

For the reddening toward V962 Cep, (l, b) = (97.°3128, +9.°8202), the 2D NASA/IPAC galactic dust absorption map gives $E(B-V)=0.96\pm0.02$, which is slightly smaller than our value at the crossing point. We examine our result in Figure 17(c). Marshall et al.'s (2006) relations are plotted toward (l, b) = (97.°25, +9.°75), (97.°50, +9.°75), (97.°25, +10.°00), and (97.°50, +10.°00). The closest direction is that of the unfilled red squares. The other symbols/lines have the same meanings as those in Figure 5(a). Our crossing point at $E(B-V)=1.10$ and $d=10.2$ kpc is consistent with Chen et al.'s (cyan-blue line) but located between Marshall et al.'s (unfilled red squares with error bars) and Green et al.'s (black/orange lines) relations.

We plot the $(B-V)_0$–$(M_V-2.5\log f_s)$ diagram of V962 Cep in Figure 18(c) for $E(B-V)=1.10$ and $(m-M')_V=18.75$ in Equation (147). The track of V962 Cep almost follows the LV Vul track, although the data points are quite scattered. Thus, we regard V962 Cep to belong to the LV Vul type. This rough overlapping of V962 Cep to LV Vul supports our values of $E(B-V)=1.10$ and $(m-M')_V=18.75$, that is, $E(B-V)=1.10\pm0.1$, $(m-M)_V=18.45\pm0.2$, $d=10.2\pm2$ kpc, and $f_s=1.32$ against LV Vul.

We examine the distance modulus of $(m-M)_V=18.45$ for V962 Cep in Figure 105(a). We plot an absolute V model light curve (solid red line) of a 0.95 $M_\odot$ WD (CO3; Hachisu & Kato 2016a), assuming that $(m-M)_V=18.45$ for V962 Cep. The V light curve reasonably reproduces the observation. This confirms that the distance modulus of $(m-M)_V=18.45$ is reasonable. For comparison, we also plot a 0.98 $M_\odot$ WD model light curve (solid green lines), assuming that $(m-M)_V=14.6$ for V1668 Cyg.

3.28. V2659 Cyg 2014

V2659 Cyg reached $m_{V,\max}=9.3$ on JD 2,456,757.27 (UT 2014 April 9.77) from the VSOLJ data. The nova was identified as an Fe II type by A. Arai, K. Ayani, and M. Fujii (Nishiyama et al. 2014). Raj et al. (2014) obtained the reddening of $E(B-V)=0.63$ from the optically thin K I 7699 line. Chochol et al. (2014) obtained the reddening of $E(B-V)=0.77\pm0.06$ from the arithmetic average of the values obtained with various methods including the intrinsic colors at maximum and t_2 time (van den Bergh & Younger 1987), the equivalent widths of Na I and K I, and Raj et al.'s value. Chochol et al. (2014) also derived the distance of $d=5.5\pm0.3$ kpc from the MMRD relation (Downes & Duerbeck 2000).

We obtain $(m-M)_B=16.5$, $(m-M)_V=15.68$, and $(m-M)_I=14.41$, which cross at $d=4.4$ kpc and $E(B-V)=0.80$, in Appendix A.28 and plot them in Figure 17(d). Thus, we obtain $d=4.4\pm0.5$ kpc, $E(B-V)=0.80\pm0.05$, $(m-M)_V=15.7\pm0.1$, and $f_s=3.3$ against LV Vul.

For the reddening toward V2659 Cyg, (l, b) = (70.°5250, −3.°2860), the 2D NASA/IPAC galactic dust absorption map gives $E(B-V)=0.85\pm0.02$. This value is slightly larger than our value at the crossing point. This is because the reddening does not saturate yet at the distance of V2659 Cyg as shown in Figure 17(d). We examine our result in this plot. Marshall et al.'s (2006) relations are plotted toward (l, b) = (70.°50, −3.°25), (70.°75, −3.°25), (70.°50, −3.°50), and (70.°75, −3.°50). The closest direction is that of the unfilled red squares. The other symbols/lines have the same meanings as those in Figure 5(a). Our crossing point at $E(B-V)=0.80$ and $d=4.4$ kpc is roughly consistent with Marshall et al.'s (filled green squares) and Green et al.'s (solid black line) relations.

We plot the $(B-V)_0$–$(M_V-2.5\log f_s)$ diagram of V2659 Cyg in Figure 18(d) for $E(B-V)=0.80$ and $(m-M')_V=17.0$ in Equation (152). The track of V2659 Cyg almost follows the LV Vul track. Thus, we regard V2659 Cyg to belong to the LV Vul type in the $(B-V)_0$–$(M_V-2.5\log f_s)$ diagram. This overlapping supports $E(B-V)=0.80$ and $(m-M')_V=17.0$, that is, $E(B-V)=0.80\pm0.05$, $(m-M)_V=15.7\pm0.1$, $f_s=3.3$, and $d=4.4\pm0.5$ kpc.

We examine the distance modulus of $(m-M)_V=15.7$ for V2659 Cyg in Figure 108(a). We plot a V model light curve of a 0.75 $M_\odot$ WD (CO4, solid red line; Hachisu & Kato 2015), assuming that $(m-M)_V=15.7$ for V2659 Cyg. The V light curve reasonably reproduces the observation. This confirms that the distance modulus of $(m-M)_V=15.7\pm0.1$ is reasonable.

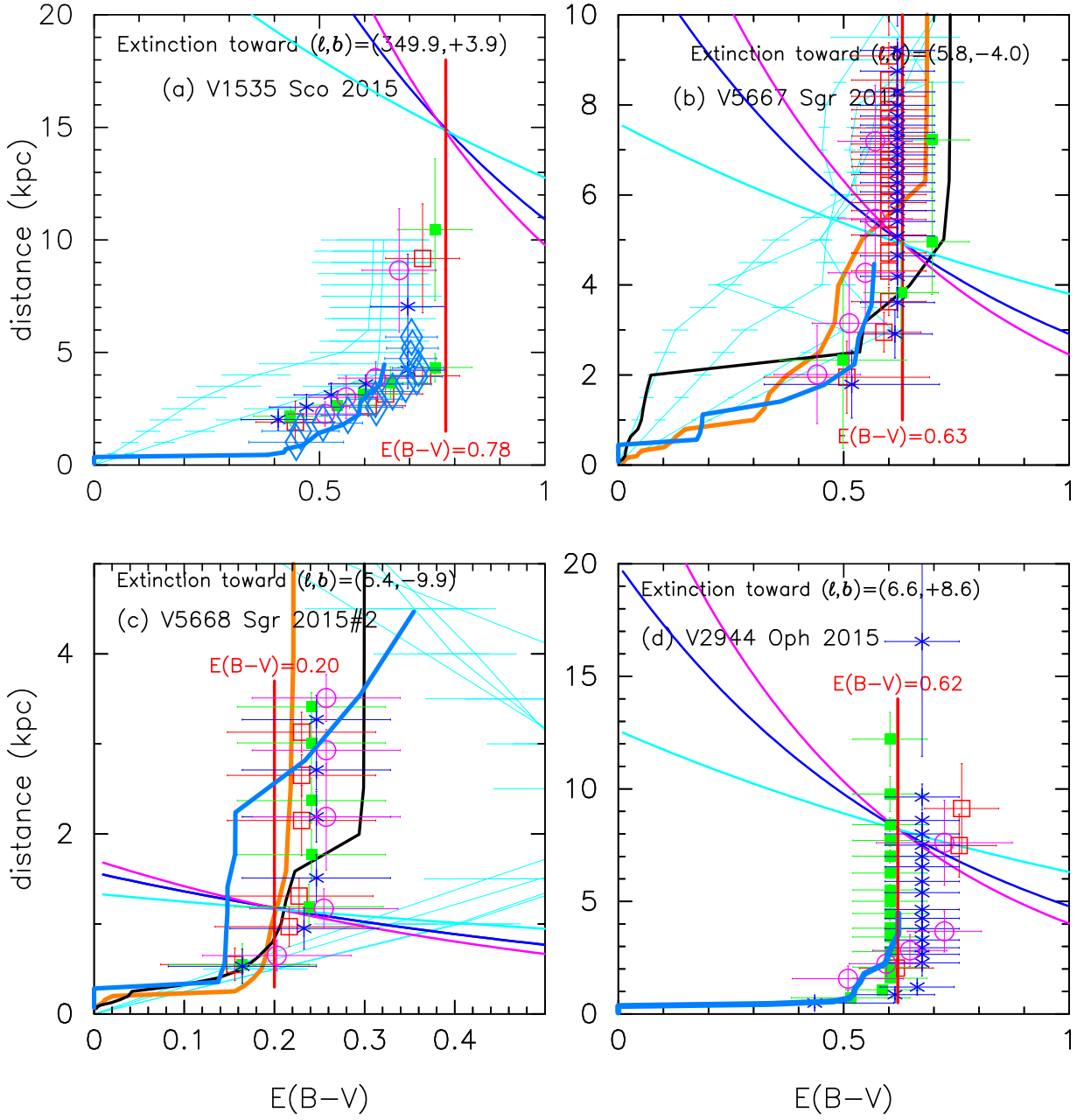

Figure 19. Same as Figure 5, but for (a) V1535 Sco, (b) V5667 Sgr, (c) V5668 Sgr, and (d) V2944 Oph.

3.29. V1535 Sco 2015

V1535 Sco reached $m_{V,\max} = 9.4$ on JD 2,457,065.34 (UT 2015 February 11.84) based on the VSOLJ data. Walter (2015a) suggested that the companion to the exploding WD is a red giant with the brightness of $J = 13.4$, $H = 12.5$, and $K = 12.2$ from the 2MASS archival database (see also Waagen et al. 2015). Srivastava et al. (2015) estimated the position in the color–color diagram ($(J-H)_0$ versus $(H-K)_0$) in quiescence, and it is consistent with a giant of type K3III/K4III, although their spectral energy distribution (SED) analysis gave a different type of giant, M4III/M5III. Nelson et al. (2015) detected hard X-rays from hot plasma, showing a strong deceleration of the ejecta by circumstellar matter (CSM). Srivastava et al. (2015) obtained $t_2 = 14 \pm 2$ days and $t_3 = 19 \pm 1$ days from the V light curve of AAVSO data and estimated the reddening of $E(B-V) = 0.72$ from the empirical relations of van den Bergh & Younger (1987). They also estimated the distance of $d = 13.7 \pm 0.4$ kpc from the MMRD relation of della Valle & Livio (1995) and $d = 14.7 \pm 3.8$ kpc from the MMRD relation of Downes & Duerbeck (2000). Linford et al. (2017) reported a comprehensive observation of V1535 Sco and concluded that a strong shock was present two weeks earlier, and the companion star is likely a K giant from the optical, NIR, and X-ray neutral hydrogen column density measurements. Munari et al. (2017) also proposed that the companion is likely a K3–4III giant from the broadband spectra of the progenitor.

We obtain $(m-M)_B = 19.04$, $(m-M)_V = 18.3$, and $(m-M)_I = 17.03$, which cross at $d = 15$ kpc and $E(B-V) = 0.78$, in Appendix A.29 and plot them in Figure 19(a). Thus, we have $E(B-V) = 0.78 \pm 0.05$ and $d = 15 \pm 2$ kpc. The distance modulus in the V band is $(m-M)_V = 18.3 \pm 0.1$.

For the reddening toward V1535 Sco, $(l, b) = (349.^{\circ}8984, +3.^{\circ}9382)$, the 2D NASA/IPAC galactic dust absorption map gives $E(B-V) = 0.65 \pm 0.04$, which is slightly smaller than our value at the crossing point. We further examine our result in Figure 19(a). Marshall et al.'s (2006) relations are plotted toward $(l, b) = (349.^{\circ}75, +3.^{\circ}75)$, $(350.^{\circ}00, +3.^{\circ}75)$, $(349.^{\circ}75, +4.^{\circ}00)$, and $(350.^{\circ}00, +4.^{\circ}00)$. The direction toward V1535 Sco is in the middle of these four directions. The other symbols/lines have the same meanings as those in Figure 5(a). Our crossing point at $E(B-V) = 0.78$ and $d = 15$ kpc is roughly consistent with Marshall et al.'s relation (filled green squares with error bars).

We plot the $(B-V)_0$–$(M_V - 2.5\log f_s)$ diagram of V1535 Sco in Figure 20(a) for $E(B-V) = 0.78$ and $(m-M')_V = 19.25$ in Equation (157). The track of V1535 Sco goes almost straight down, and this kind of behavior is common among the symbiotic classical novae that have a red-giant companion (see, e.g., Hachisu & Kato 2018b). The track of V1535 Sco follows the LV Vul and V407 Cyg tracks in the early phase, although the peak of V1535 Sco is quite bright compared with that of V407 Cyg and LV Vul. In the later phase, the track of V1535 Sco is close to the upper branch of LV Vul. These similarities and overlapping support our value of $E(B-V) = 0.78$ and $(m-M')_V = 19.25$, that is, $E(B-V) = 0.78 \pm 0.05$, $d = 15 \pm 2$ kpc, $(m-M)_V = 18.3 \pm 0.1$, and $f_s = 2.4$ against LV Vul. We regard V1535 Sco to belong to the LV Vul type.

We check the distance modulus of $(m-M)_V = 18.3$ by comparing our model light curve with the observation in Figure 111(a). We plot a model V light curve of a 0.85 $M_\odot$ WD (CO4, solid red line; Hachisu & Kato 2015), assuming $(m-M)_V = 18.3$ for V1535 Sco. The model absolute V light curve reasonably fits with the observed apparent V light curve of V1535 Sco. This again confirms that $(m-M)_V = 18.3$ is reasonable for V1535 Sco.

3.30. V5667 Sgr 2015#1

Walter identified the nova to be of Fe II type (Nishiyama et al. 2015). Rudy et al. (2015) reported the 0.38–2.5 μm spectroscopy of V5667 Sgr and V5668 Sgr. They derived the extinction of $E(B-V) = 0.2 \pm 0.15$ for V5667 Sgr and $E(B-V) = 0.5 \pm 0.2$ for V5668 Sgr, both from the O I line. However, we suppose that the reported extinctions are typographical errors and should be $E(B-V) = 0.5 \pm 0.2$ for V5667 Sgr and $E(B-V) = 0.2 \pm 0.15$ for V5668 Sgr as shown in Figures 19(b) and (c).

We obtain $(m-M)_B = 16.08$, $(m-M)_V = 15.42$, and $(m-M)_I = 14.39$, which cross at $d = 4.9$ kpc and $E(B-V) = 0.63$, in Appendix A.30 and plot them in Figure 19(b). Thus, we obtain $d = 4.9 \pm 0.5$ kpc, $E(B-V) = 0.63 \pm 0.05$, $(m-M)_V = 15.4 \pm 0.2$, and $f_s = 3.7$ against LV Vul.

For the reddening toward V5667 Sgr, $(l, b) = (5.^{\circ}8040, -4.^{\circ}0427)$, the 2D NASA/IPAC galactic dust absorption map gives $E(B-V) = 0.63 \pm 0.02$, which is consistent with our value of $E(B-V) = 0.63 \pm 0.05$. Our value of $E(B-V) = 0.63$ is also consistent with Rudy et al.'s (2015) result of $E(B-V) = 0.5 \pm 0.2$ from the O I line. We examine our results based on distance–reddening relations in Figure 19(b). Marshall et al.'s (2006) relations are plotted toward $(l, b) = (5.^{\circ}75, -4.^{\circ}00)$, $(6.^{\circ}00, -4.^{\circ}00)$, $(5.^{\circ}75, -4.^{\circ}25)$, and $(6.^{\circ}00, -4.^{\circ}25)$. The closest direction is that of the unfilled red squares. The other symbols/lines have the same meanings as those in Figure 5(a). Our crossing point at $E(B-V) = 0.63$ and $d = 4.9$ kpc is consistent with both Marshall et al.'s (unfilled red squares and blue asterisks) and Green et al.'s (orange line) relations.

We plot the $(B-V)_0$–$(M_V - 2.5\log f_s)$ diagram of V5667 Sgr in Figure 20(b) for $E(B-V) = 0.63$ and $(m-M')_V = 16.85$ in Equation (162). The track of V5667 Sgr almost follows the LV Vul track, so we regard V5667 Sgr to belong to the LV Vul type in the $(B-V)_0$–$(M_V - 2.5\log f_s)$ diagram. This overlapping supports $E(B-V) = 0.63$ and $(m-M')_V = 16.85$, that is, $E(B-V) = 0.63 \pm 0.05$, $(m-M)_V = 15.4 \pm 0.2$, $f_s = 3.7$, and $d = 4.9 \pm 0.5$ kpc.

We check the distance modulus of $(m-M)_V = 15.4$ by comparing our model light curve with the observation in Figure 114(a). We plot a model V light curve of a 0.78 $M_\odot$ WD (CO4, solid red line; Hachisu & Kato 2015), assuming that $(m-M)_V = 15.4$ for V5667 Sgr. The model absolute V light curve reasonably follows the observed apparent V light curve, although the V light curve has a wavy structure in the early phase. This again confirms that $(m-M)_V = 15.4$ is reasonable.

3.31. V5668 Sgr 2015#2

V5668 Sgr reached $m_{V,\max} = 4.05$ on JD 2,457,102.9 from the SMARTS data. Rudy et al. (2015) reported 0.38–2.5 μm spectroscopy of V5667 Sgr and V5668 Sgr and derived the extinction of $E(B-V) = 0.2 \pm 0.15$ for V5667 Sgr and $E(B-V) = 0.5 \pm 0.2$ for V5668 Sgr, both from the O I line. As mentioned in the previous subsection (Section 3.30), we assume that the reported extinctions are typographical errors and should be $E(B-V) = 0.5 \pm 0.2$ for V5667 Sgr and $E(B-V) = 0.2 \pm 0.15$ for V5668 Sgr as shown in Figures 19(b) and (c). Gamma-ray emission was detected with the *Fermi*/LAT on UT 2015 March 15.6 (JD 2,457,097.1; Cheung et al. 2016). Tajitsu et al. (2015) reported the detection of ^{7}Be in their Subaru HDS spectrum obtained on UT 2015 May 29.67 (JD 2,457,103.17). Banerjee et al. (2016) reported their NIR observation and classified the nova as an Fe II. They also estimated the distance of $d = 1.54$ kpc from the blackbody angular diameter of a dust shell, that is, 42 mas.

We obtain $(m-M)_B = 11.16$, $(m-M)_V = 10.98$, and $(m-M)_I = 10.64$, which cross at $d = 1.2$ kpc and $E(B-V) = 0.20$, in Appendix A.31 and plot them in Figure 19(c). Thus, we obtain $d = 1.2 \pm 0.2$ kpc, $E(B-V) = 0.20 \pm 0.03$, $(m-M)_V = 11.0 \pm 0.2$, and $f_s = 1.86$ against LV Vul.

For the reddening toward V5668 Sgr, $(l, b) = (5.^{\circ}3799, -9.^{\circ}8668)$, the 2D NASA/IPAC galactic dust absorption map gives $E(B-V) = 0.204 \pm 0.002$, which is consistent with our value of $E(B-V) = 0.20 \pm 0.05$. We examine our results based on the distance–reddening relations in Figure 19(c). Marshall et al.'s (2006) relations are plotted toward $(l, b) = (5.^{\circ}25, -9.^{\circ}75)$, $(5.^{\circ}50, -9.^{\circ}75)$, $(5.^{\circ}25, -10.^{\circ}00)$, and $(5.^{\circ}50, -10.^{\circ}00)$. The direction toward V5668 Sgr is in the middle of these four directions. The other symbols/lines have the same meanings as those in Figure 5(a). Our crossing point at $E(B-V) = 0.20$ and $d = 1.2$ kpc is consistent with Marshall et al.'s and Green et al.'s relations.

We plot the $(B-V)_0$–$(M_V - 2.5\log f_s)$ diagram of V5668 Sgr in Figure 20(c) for $E(B-V) = 0.20$ and $(m-M')_V = 11.65$ in Equation (167). The track of V5668 Sgr is just on the LV Vul track (thick orange lines) until the start of the dust blackout phase. Therefore, V5668 Sgr belongs to the LV Vul type. This similarity supports our adopted values of $E(B-V) = 0.20$ and $(m-$

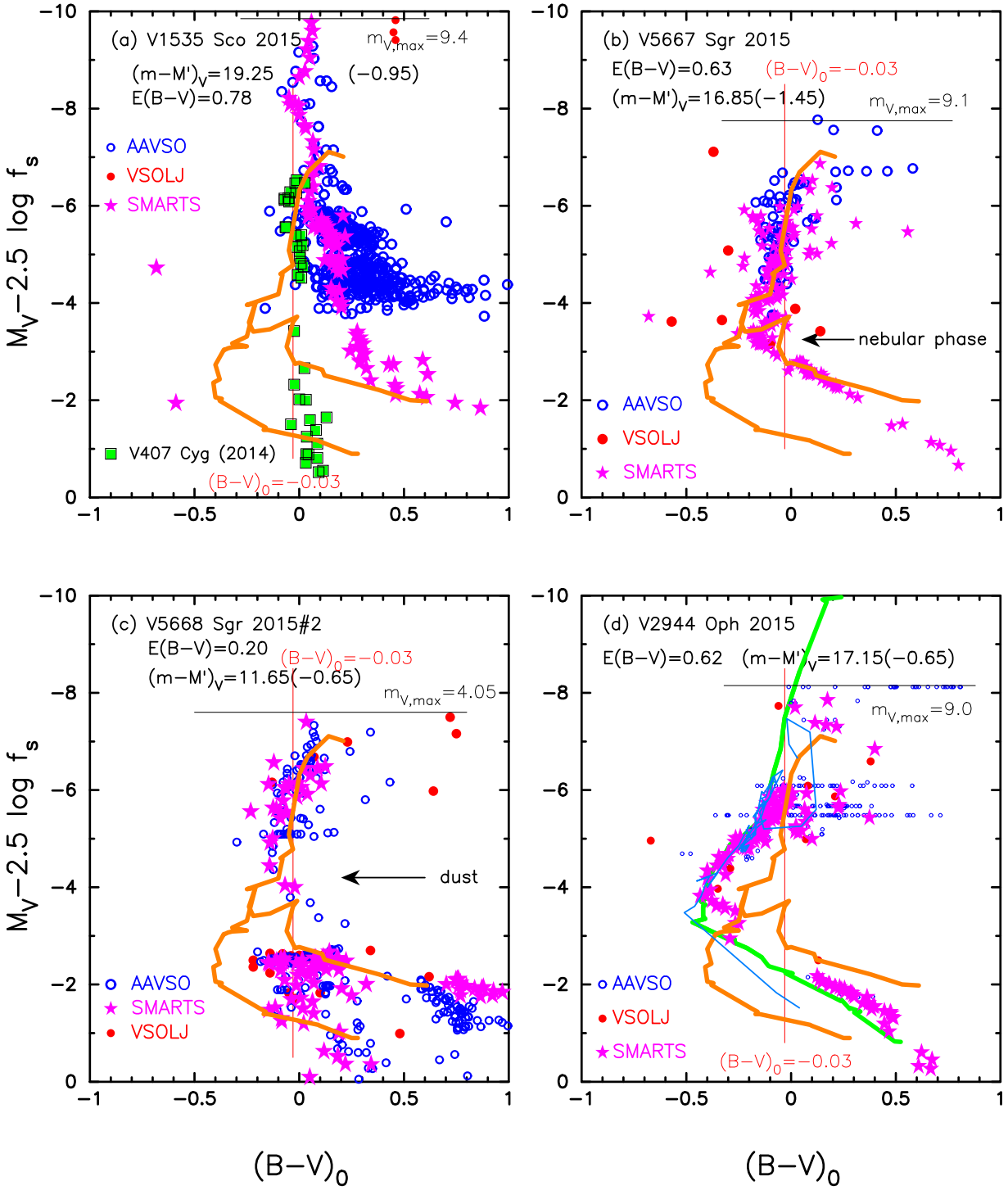

Figure 20. Same as Figure 6, but for (a) V1535 Sco, (b) V5667 Sgr, (c) V5668 Sgr, and (d) V2944 Oph. The thick solid orange lines show the template track of LV Vul. The thick solid green line shows the template track of V1500 Cyg. In panel (a), we add the track of V407 Cyg (filled green squares with black outline). In panel (d), we add the track of PW Vul (thin solid cyan-blue line), the data of which are the same as those in Figure 7(b) of Hachisu & Kato (2016b).

$M')_V = 11.65$, that is, $E(B-V) = 0.20 \pm 0.03$ and $(m-M)_V = 11.0 \pm 0.2$, $f_s = 1.86$, and $d = 1.2 \pm 0.2$ kpc.

We check the distance modulus of $(m-M)_V = 11.0$ by comparing our model light curve with the observation in Figure 117(a). We plot a model V light curve of a 0.85 $M_\odot$ WD (CO3, solid red line; Hachisu & Kato 2016a), assuming that $(m-M)_V = 11.0$ for V5668 Sgr. The model absolute V light curve reasonably follows the observed apparent V light curve, although the V light curve has a wavy structure in the early phase. This again confirms that $(m-M)_V = 11.0$ is reasonable.

3.32. V2944 Oph 2015

V2944 Oph reached $m_{V,max} = 9.0$ on JD 2,457,127.245 from the AAVSO data. The nova was identified to be of He/N type in the early pre-maximum phase (∼3 mag below the

maximum brightness; Danilet et al. 2015), but later as an Fe II type at maximum (e.g., Munari & Walter 2015). Munari & Walter (2015) obtained $E(B-V)=0.52$ from the relation of Munari (2014) or $E(B-V)=0.56$ from the relation of Kos & Zwitter (2013) between the reddening and the equivalent width of the diffuse interstellar band (DIB) at 6614 Å. Tajitsu et al. (2015) identified the line of unstable ^{7}Be in the spectrum of V2944 Oph obtained on UT 2015 July 3 (JD 2,457,206.5) about 80 days after the outburst. This clearly suggests that thermonuclear runaway occurred deep in the hydrogen-rich envelope, and its product was blown in the outburst wind. Srivastava et al. (2016) obtained NIR spectra of V2944 Oph. Their power-law fit to the spectra showed a fairly constant slope, which differs from the usual trend expected during a nova spectral evolution. They obtained $E(B-V)=0.59\pm0.04$ from the strengths of the 0.8446 μm and 1.1287 μm lines.

We obtain $(m-M)_B=17.11$, $(m-M)_V=16.5$, and $(m-M)_I=15.5$, which cross at $d=8.2$ kpc and $E(B-V)=0.62$, in Appendix A.32 and plot them in Figure 19(d). Thus, we obtain $d=8.2\pm1$ kpc, $E(B-V)=0.62\pm0.05$, $(m-M)_V=16.5\pm0.2$, and $f_s=1.78$ against LV Vul.

For the reddening toward V2944 Oph, $(l,\ b)=(6\overset{\circ}{.}6421, +8\overset{\circ}{.}5773)$, the 2D NASA/IPAC galactic dust absorption map gives $E(B-V)=0.55\pm0.02$. Munari & Walter (2015) obtained $E(B-V)=0.52$ and $E(B-V)=0.56$ from the 6614 Å diffuse interstellar band while Srivastava et al. (2016) reported $E(B-V)=0.59\pm0.04$ from the strengths of the 0.8446 μm and 1.1287 μm lines as mentioned above. These values are roughly consistent with our obtained value of $E(B-V)=0.62\pm0.05$. We examine our results in Figure 19(d). Marshall et al.'s (2006) relations are plotted toward $(l,\ b)=(6\overset{\circ}{.}50, +8\overset{\circ}{.}75)$, $(6\overset{\circ}{.}75, +8\overset{\circ}{.}75)$, $(6\overset{\circ}{.}50, +8\overset{\circ}{.}50)$, and $(6\overset{\circ}{.}75, +8\overset{\circ}{.}50)$. The direction toward V2944 Oph is in the middle of these four directions. The other symbols/lines have the same meanings as those in Figure 5(a). Our crossing point at $E(B-V)=0.62$ and $d=8.2$ kpc is consistent with Marshall et al.'s (filled green squares) and Chen et al.'s (cyan-blue line) relations.

We plot the $(B-V)_0$–$(M_V-2.5\log f_s)$ diagram of V2944 Oph in Figure 20(d) for $E(B-V)=0.62$ and $(m-M')_V=17.15$ in Equation (172). The track of V2944 Oph is almost on the V1500 Cyg (thick solid green line) and PW Vul tracks (cyan-blue lines). Therefore, V2944 Oph belongs to the V1500 Cyg type. This similarity supports our adopted values of $E(B-V)=0.62$ and $(m-M')_V=17.15$, that is, $E(B-V)=0.62\pm0.05$ and $(m-M)_V=16.5\pm0.2$, $f_s=1.78$, and $d=8.2\pm1$ kpc.

We check the distance modulus of $(m-M)_V=16.5$ by comparing our model light curve with the observation in Figure 120(a). We plot a model V light curve of a 0.85 $M_\odot$ WD (CO3, solid red line; Hachisu & Kato 2016a), assuming that $(m-M)_V=16.5$ for V2944 Oph. The model absolute V light curve reasonably follows the observed apparent V light curve, although the V light curve has a wavy structure in the early phase. This again confirms that $(m-M)_V=16.5$ is reasonable.

4. Discussion

4.1. Distance Determination

Estimating the distance to a nova is a difficult task, and the results are always debated (e.g., Schaefer 2018). Various methods have been proposed, but they often have large uncertainties (see, e.g., Hachisu & Kato 2014, 2015, 2016b). A large discrepancy is reported, especially for the MMRD relations, which may work statistically, but does not work well for individual novae (Schaefer 2018).

The present work provides an alternative method for determining the distance to a nova that has enough light/color curve data for a sufficiently long coverage of the outburst. The accuracy of the distance estimate depends mainly on the light/color curve fittings, i.e., typically $\Delta(m-M)_V=\pm0.1$ or ±0.2, and $\Delta E(B-V)=\pm0.05$ or ±0.1, which guarantee about 10%–20% of the distance accuracy.

Schaefer (2018) analyzed the results of *Gaia* data release 2 (DR2) and listed the trigonometric distances of 64 novae. Among them, his seven novae dubbed as having "very well observed light curve (<30% error)" overlap our analyzed novae in Table 1. These distances are compared with our results (object, *Gaia* DR2/the present result) as follows: CI Aql, 3.14/3.3 kpc; V705 Cas, 2.16/2.6 kpc; V1974 Cyg, 1.63/1.8 kpc; V446 Her, 1.36/1.4 kpc; V533 Her, 1.20/1.3 kpc; V382 Vel, 1.8/1.4 kpc; and PW Vul, 2.42/1.8 kpc. The present results are in good agreement with Schaefer's values within each error box.

4.2. Dependence of the WD Mass on the Chemical Composition

The largest ambiguity in our determination of the WD mass is in the choice of the chemical composition of the hydrogen-rich envelope. The chemical composition of ejecta is not well determined in many novae. In our previous work (e.g., Hachisu & Kato 2016a), we adopted several sets of chemical composition templates (CO1, CO2, CO3, and CO4 for CO novae and Ne1, Ne2, and Ne3 for neon novae) considering the degree of mixing between the mass-accreting envelope and WD core material (see Hachisu & Kato 2006, 2010, 2015, 2016a).

Figure 21 depicts our model light-curve fitting with QY Mus for three different chemical compositions (CO2, CO3, and CO4), assuming the distance modulus in the V band of $(m-M)_V=14.65$ (see Appendix A.12 for more details). Figure 21(a) shows five WD mass models, i.e., 0.65, 0.70, 0.75, 0.80, and 0.85 $M_\odot$ WDs (CO2, Hachisu & Kato 2010). The V light curve of 0.75 $M_\odot$ WD (blue line) is in best agreement with the observation among the five models. It should be noted that the V magnitude of the nova, except for the dust blackout phase until the point when the nova entered the nebular phase, decays along with the theoretical line until day ~235. In the nebular phase, however, strong emission lines make large contributions to the V band, the effect of which are not included in our model light curves. Therefore, the observed V magnitude deviates much from, and decays more slowly than, the model V light curve in the nebular phase. We select a 0.75 $M_\odot$ WD for CO2 (the hydrogen content by weight is $X=0.35$). Thus, we obtain $M_{\rm WD}=0.75\pm0.05\ M_\odot$, taking into account the fitting error.

If we increase the hydrogen content from $X=0.35$ (CO2) to $X=0.45$ (CO3, Hachisu & Kato 2016a), we obtain 0.80 $M_\odot$ among 0.75, 0.80, and 0.85 $M_\odot$ in Figure 21(b). If we further increase the hydrogen content to $X=0.55$ (CO4, Hachisu & Kato 2015), we obtain 0.85 $M_\odot$ among 0.80, 0.85, and 0.90 $M_\odot$ in Figure 21(c). Our model light-curve fitting gives a WD mass between $M_{\rm WD}=0.75$–$0.85\ M_\odot$ for the chemical compositions of $X=0.35$–0.55. These three best-fit models reasonably reproduce the V light curve of QY Mus. Thus, we are able to approximate the relation between the WD mass,

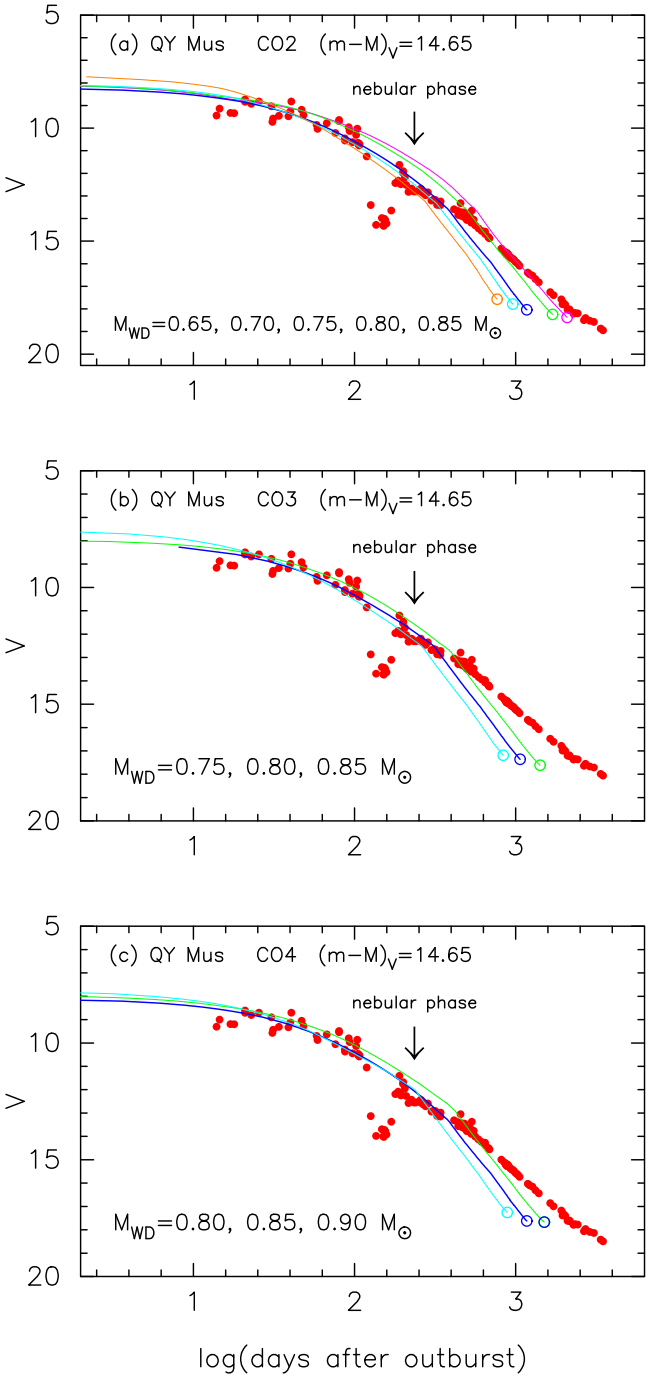

Figure 21. Model light-curve fitting with the V light curve of QY Mus for the assumed chemical composition of (a) CO nova 2 (CO2; Hachisu & Kato 2010), (b) CO nova 3 (CO3; Hachisu & Kato 2016a), and (c) CO nova 4 (CO4; Hachisu & Kato 2015). We assume that $(m-M)_V = 14.65$ for QY Mus. In panel (a), we plot five WD mass models, i.e., 0.65 (magenta), 0.70 (green), 0.75 (blue), 0.80 (cyan), and 0.85 $M_\odot$ WD (orange line). In panel (b), we plot three WD mass models, i.e., 0.75 (green), 0.80 (blue), and 0.85 $M_\odot$ WD (cyan line). In panel (c), we plot three WD mass models, i.e., 0.80 (green), 0.85 (blue), and 0.90 $M_\odot$ WD (cyan line). We denote the start of the nebular phase on day 235 with the downward arrow.

$M_{\rm WD}$, and the hydrogen content, X, as

$$M_{\rm WD}/M_\odot = 0.05(X - 0.55) + 0.85 \pm 0.05, \qquad (14)$$

for QY Mus.

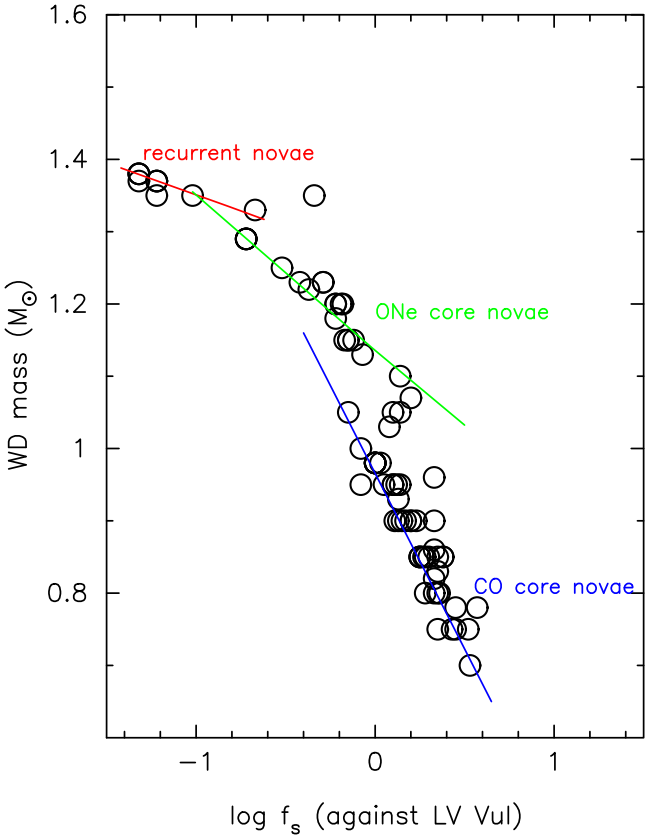

Figure 22. WD mass vs. timescaling factor $\log f_s$ for various novae. The timescaling factor is measured against that of LV Vul ($f_s = 1.0$ for LV Vul). The WD mass and f_s data are taken from Table 2. We specify three trends of $M_{\rm WD}$ vs. $\log f_s$: recurrent novae (red line), oxygen–neon (ONe) core novae (green line), and carbon–oxygen (CO) core novae (blue line).

4.3. Timescaling Factor versus WD Mass

Table 2 provides the summary of the WD masses of the novae in Table 1. The WD masses are estimated from direct comparison of our model light curves with the observation. The timescaling factor f_s of a nova is closely related to the WD mass, because a faster nova (smaller f_s) tends to host a more massive WD. Figure 22 shows the distribution of $\log f_s$–$M_{\rm WD}$ for various novae in Table 2, which includes both the present and the previous results (e.g., Hachisu & Kato 2016b, 2018a, 2018b, 2019). The three trends may represent recurrent novae (red line), oxygen–neon (ONe) novae (green line), and carbon–oxygen (CO) novae (blue line). The border between the ONe and CO cores is located around 1.0–1.1 $M_\odot$.

5. Conclusions

Our results are summarized as follows:

1. Using the time-stretching method of nova light curves (Hachisu & Kato 2010) together with the time-stretched color–magnitude diagram method (Hachisu & Kato 2019), we estimated the distance moduli $(m-M)_V$ and color excesses $E(B-V)$ of 32 recent galactic novae. Tables 1 and 2 provide a uniform data set of 73 novae obtained with a single method, including the present and previous works.

2. The present 32 nova tracks in the $(B-V)_0$–$(M_V-2.5\log f_s)$ diagram are divided into two types, LV Vul and V1500 Cyg. In general, each nova moves from the upper right (red) to the lower left (blue) and then turns toward the right (red) at the onset of the nebular phase. The LV Vul-type novae go almost straight down along the $(B-V)_0=-0.03$ line in the middle part of the track. The V1500 Cyg type novae are roughly parallel to, but bluer by $\Delta(B-V)_0\sim-0.2$ mag than, the LV Vul type track. This −0.2 mag bluer location is caused by the higher degree of ionization state (Hachisu & Kato 2019).
3. Our set of distances d and color excesses $E(B-V)$ shows a good agreement with at least one of the existing 3D dust absorption maps. Also, our distances show a good agreement with *Gaia* data release 2 (Schaefer 2018) in all seven overlapping novae, within the error box.
4. The distribution of the WD masses versus the stretching factor (i.e., decline rate) indicates three distinct tendencies that may represent recurrent novae, ONe novae, and CO novae. The border between the ONe novae and CO novae lies at 1.0–1.1 $M_\odot$.
5. Many novae, including the present 32 novae, broadly follow the universal decline law, and the present method can be applied to them. Some exceptional novae deviate greatly from the universal decline law for various physical reasons and the method cannot be directly applied to them. Hachisu & Kato (2018b) discussed some examples and proposed different novae as templates depending on the physical reason for the deviation. Appendix C explains and summarizes the results.

We thank T. Iijima and the Astronomical Observatory of Padova (Asiago) for the warm hospitality. We express our gratitude to the late A. Cassatella for providing us with UV 1455 Å data for *IUE* novae. We are also grateful to the American Association of Variable Star Observers (AAVSO) and the Variable Star Observers League of Japan (VSOLJ) for the archival data of various novae. We also thank the anonymous referee for useful comments, which improved the manuscript. This research has been supported in part by Grants-in-Aid for Scientific Research (15K05026, 16K05289) from the Japan Society for the Promotion of Science.

Appendix A
Light Curves and Distance Moduli of 32 Novae

A.1. V1663 Aql 2005

Figure 23 shows (a) the V light curve and (b) $(B-V)_0$ color evolutions of V1663 Aql. The BV data are taken from the archives of AAVSO, VSOLJ, and SMARTS. The $(B-V)_0$ is dereddened with $E(B-V)=1.88$ as obtained in Section 3.1. Figure 24 shows the light/color curves on a logarithmic timescale as well as those of LV Vul and V1668 Cyg. Each light curve is horizontally moved by $\Delta\log t=\log f_s$ and vertically shifted by ΔV with respect to that of V1663 Aql, as indicated in the figure. For example, "LV Vul V+6.1, 0.83 t" means that $\Delta V=+6.1$ and $f_s=0.83$. These three V light curves overlap each other. Applying Equation (6) to them, we have the relation

$$\begin{aligned}(m-M)_{V,\mathrm{V1663\ Aql}}&=(m-M+\Delta V)_{V,\mathrm{LV\ Vul}}-2.5\log 0.83\\&=11.85+6.1\pm0.2+0.20=18.15\pm0.2\\&=(m-M+\Delta V)_{V,\mathrm{V1668\ Cyg}}-2.5\log 0.83\\&=14.6+3.4\pm0.2+0.20=18.2\pm0.2,\end{aligned}\tag{15}$$

where we adopt $(m-M)_{V,\mathrm{LV\ Vul}}=11.85$ and $(m-M)_{V,\mathrm{V1668\ Cyg}}=14.6$, both from Hachisu & Kato (2019). Thus, we obtain $(m-M)_V=18.15\pm0.1$ for V1663 Aql and $f_s=0.83$ against that of LV Vul. The distance is estimated to be $d=2.9\pm0.3$ kpc from Equation (11). From Equations (1), (6), and (15), we have the relation

$$\begin{aligned}(m-M')_{V,\mathrm{V1663\ Aql}}&\equiv(m_V-(M_V-2.5\log f_s))_{\mathrm{V1663\ Aql}}\\&=((m-M)_V+\Delta V)_{\mathrm{LV\ Vul}}\\&=11.85+6.1\pm0.2=17.95\pm0.2.\end{aligned}\tag{16}$$

We further check the distance and reddening with the time-stretching method. Figure 25 shows the B, V, and I_C light curves of V1663 Aql together with those of the LMC novae YY Dor and LMC N 2009a. We also plot the solid blue line with the slope of $F_\nu\propto t^{-1.75}$, which is the typical decay slope of the universal decline law (Hachisu & Kato 2006). YY Dor and LMC N 2009a are members of the Large Magellanic Cloud (LMC). We adopt $\mu_{0,\mathrm{LMC}}=18.493\pm0.048$ (Pietrzyński et al. 2011) and $E(B-V)=0.12$ (Imara & Blitz 2007) for the LMC novae. Then, we obtain $(m-M)_V=\mu_0+A_V=18.49+3.1\times0.12=18.86$ toward the LMC novae. From Equation (9) for the B band in Figure 25(a), we obtain

$$\begin{aligned}(m-M)_{B,\mathrm{V1663\ Aql}}&=((m-M)_B+\Delta B)_{\mathrm{YY\ Dor}}-2.5\log 4.4\\&=18.98+2.6\pm0.2-1.6=19.98\pm0.2\\&=((m-M)_B+\Delta B)_{\mathrm{LMC\ N\ 2009a}}-2.5\log 2.8\\&=18.98+2.1\pm0.2-1.1=19.98\pm0.2.\end{aligned}\tag{17}$$

Here, we adopt $(m-M)_B=18.49+4.1\times0.12=18.98$ for the LMC novae from Equation (12). Thus, we obtain $(m-M)_{B,\mathrm{V1663\ Aql}}=19.98\pm0.2$.

For the V light curves in Figure 25(b), we similarly obtain

$$\begin{aligned}(m-M)_{V,\mathrm{V1663\ Aql}}&=((m-M)_V+\Delta V)_{\mathrm{YY\ Dor}}-2.5\log 4.4\\&=18.86+0.9\pm0.2-1.6=18.16\pm0.2\\&=((m-M)_V+\Delta V)_{\mathrm{LMC\ N\ 2009a}}-2.5\log 2.8\\&=18.86+0.4\pm0.2-1.1=18.16\pm0.2.\end{aligned}\tag{18}$$

Thus, we obtain $(m-M)_{V,\mathrm{V1663\ Aql}}=18.16\pm0.2$, which is consistent with Equation (15).

We apply Equation (10) for the I_C-band to Figure 25(c) and obtain

$$\begin{aligned}(m-M)_{I,\mathrm{V1663\ Aql}}&=((m-M)_I+\Delta I_C)_{\mathrm{YY\ Dor}}-2.5\log 4.4\\&=18.67-1.9\pm0.3-1.6=15.17\pm0.3\\&=((m-M)_I+\Delta I_C)_{\mathrm{LMC\ N\ 2009a}}-2.5\log 2.8\\&=18.67-2.4\pm0.3-1.1=15.17\pm0.3,\end{aligned}\tag{19}$$

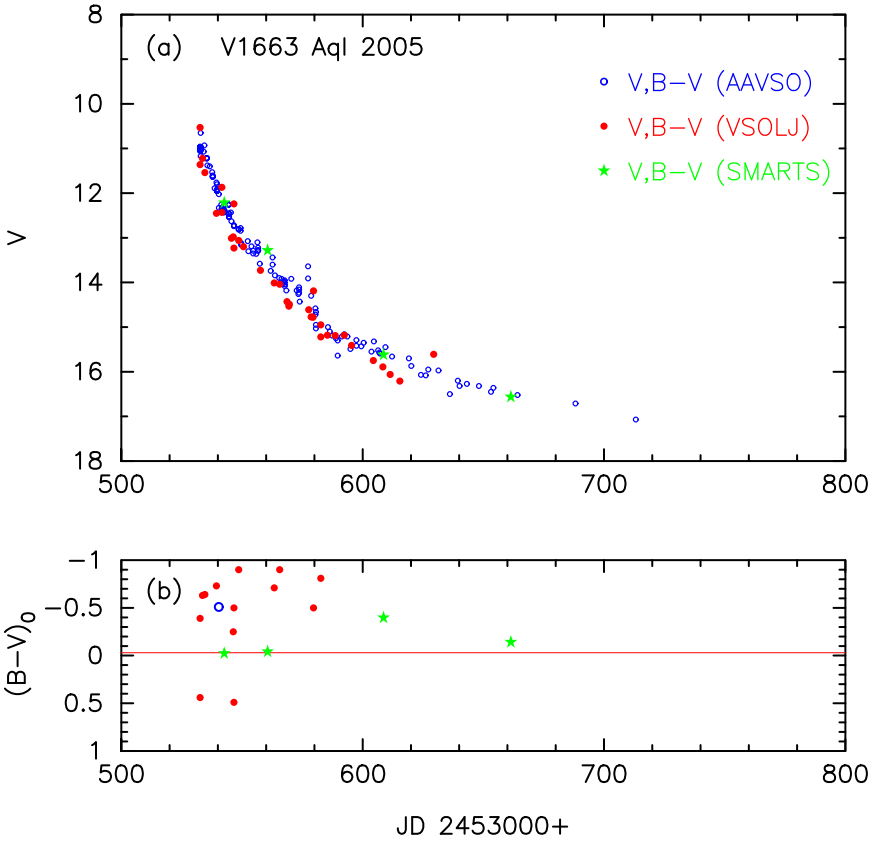

Figure 23. The light/color curves of V1663 Aql on a linear timescale. (a) The V light curve of V1663 Aql. The BV data are taken from AAVSO (unfilled blue circles), VSOLJ (filled red circles), and SMARTS (filled green stars). (b) The $(B-V)_0$ color curve of V1663 Aql. The $(B-V)_0$ are dereddened with $E(B-V)=1.88$. The horizontal red line shows $(B-V)_0=-0.03$, which is the intrinsic color of optically thick free–free emission (Hachisu & Kato 2014).

where we adopt $(m-M)_I = 18.49 + 1.5 \times 0.12 = 18.67$ for the LMC novae from Equation (13). Thus, we obtain $(m-M)_{I,\mathrm{V1663\ Aql}} = 15.17 \pm 0.2$.

We plot $(m-M)_B = 19.98$, $(m-M)_V = 18.16$, and $(m-M)_I = 15.17$ by the thin solid magenta, blue, and cyan lines, respectively, in Figure 5(a). The three lines cross at $d = 2.9$ kpc and $E(B-V) = 1.88$.

A.2. V5116 Sgr 2005#2

Figure 26 shows (a) the V, (b) $(B-V)_0$, and (c) $(U-B)_0$ evolutions of V5116 Sgr. Here, $(B-V)_0$ and $(U-B)_0$ are dereddened with $E(B-V)=0.23$ as obtained in Section 3.2. The V light curve of V5116 Sgr is similar to that of V1974 Cyg as shown in Figure 27. Here, we plot the light/color curves of V5116 Sgr, LV Vul, and V1974 Cyg on logarithmic timescales. These three V light curves overlap each other. The V magnitude has slightly different values among various observatories when strong emission lines contribute to the V filter. This is because strong [O III] lines contribute to the blue edge of V filter and a small difference in the V-filter response makes a large difference in the V magnitude and, as a result, in the $B-V$ color. This effect is clearly seen in Figure 27(b), especially in the nebular phase ($t > 100$ days). For this reason, we do not require stringent overlapping in the nebular phase. Applying Equation (6) to them, we have the relation

$$\begin{aligned}(m-M)_{V,\mathrm{V5116\ Sgr}} &= (m-M+\Delta V)_{V,\mathrm{LV\ Vul}} - 2.5\log 1.58 \\ &= 11.85 + 4.7 \pm 0.2 - 0.50 = 16.05 \pm 0.2 \\ &= (m-M+\Delta V)_{V,\mathrm{V1974\ Cyg}} - 2.5\log 1.51 \\ &= 12.2 + 4.3 \pm 0.2 - 0.45 = 16.05 \pm 0.2, \end{aligned} \quad (20)$$

where we adopt $(m-M)_{V,\mathrm{LV\ Vul}} = 11.85$ and $(m-M)_{V,\mathrm{V1974\ Cyg}} = 12.2$, both from Hachisu & Kato (2019). Thus, we obtain $(m-M)_V = 16.05 \pm 0.1$ for V5116 Sgr, consistent with Hachisu & Kato's (2010) results. From Equations (1), (6), and (20), we have the relation

$$\begin{aligned}(m-M')_{V,\mathrm{V5116\ Sgr}} &\equiv (m_V - (M_V - 2.5\log f_s))_{\mathrm{V5116\ Sgr}} \\ &= ((m-M)_V + \Delta V)_{\mathrm{LV\ Vul}} \\ &= 11.85 + 4.7 \pm 0.2 = 16.55 \pm 0.2. \end{aligned} \quad (21)$$

We obtain the distance and reddening with the time-stretching method. Figure 28 shows the B, V, and I_C light curves of V5116 Sgr together with those of V2677 Oph, V834 Car, and the LMC novae YY Dor and LMC N 2009a. We apply Equation (9) for the B band to Figure 28(a) and

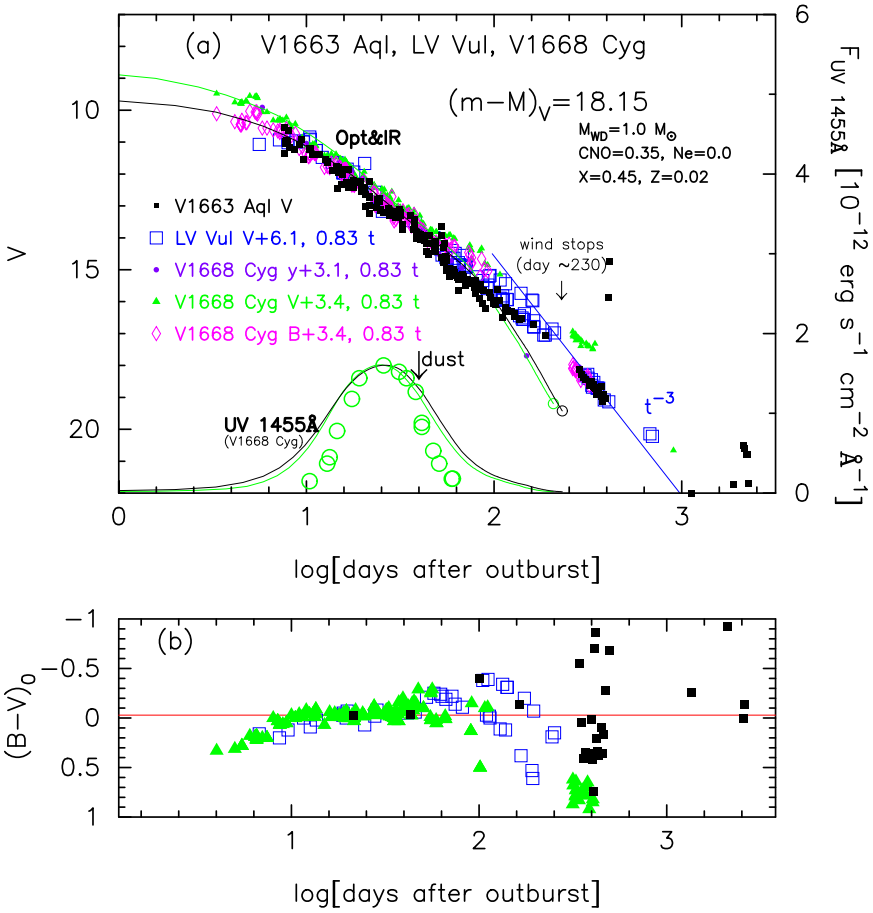

Figure 24. The light/color curves of V1663 Aql on a logarithmic timescale. The data of V1663 Aql are the same as those in Figure 23. We add the light/color curves of LV Vul and V1668 Cyg. The data of LV Vul and V1668 Cyg are the same as those in Hachisu & Kato (2016a). Each light curve is horizontally moved by $\Delta \log t = \log f_s$ and vertically shifted by ΔV with respect to that of V1663 Aql, as indicated in the figure by, for example, "LV Vul V + 6.1, 0.83 t," where $\Delta V = +6.1$ and $f_s = 0.83$. We also add the model light curve of a 1.0 $M_\odot$ WD (CO3) for V1663 Aql as well as a 0.98 $M_\odot$ WD (CO3) model for V1668 Cyg. The solid black and green lines denote the model V light curves of the 1.0 and 0.98 $M_\odot$ WDs, respectively. The solid black and green lines represent the UV 1455 Å flux based on the blackbody approximation of the 1.0 and 0.98 $M_\odot$ WDs, respectively. The UV 1455 Å flux of V1668 Cyg (unfilled green circles) is slightly smaller than the model light curve (solid green line) before the peak. This is the effect of the iron curtain (e.g., Hauschildt et al. 1995). It slightly drops on day ~60, due to the formation of an optically thin dust shell. After the optically thick winds stop, the observed V magnitude decays like the straight solid blue line of $F_\nu \propto t^{-3}$, which shows the trend of homologously expanding ejecta.

obtain

$$
\begin{aligned}
&(m-M)_{B,\mathrm{V5116\ Sgr}} \\
&= ((m-M)_B + \Delta B)_{\mathrm{V2677\ Oph}} - 2.5\log 2.3 \\
&= 20.5 - 3.3 \pm 0.2 - 0.92 = 16.28 \pm 0.2 \\
&= ((m-M)_B + \Delta B)_{\mathrm{V834\ Car}} - 2.5\log 2.5 \\
&= 17.75 - 0.5 \pm 0.2 - 0.97 = 16.28 \pm 0.2 \\
&= ((m-M)_B + \Delta B)_{\mathrm{YY\ Dor}} - 2.5\log 8.3 \\
&= 18.98 - 0.4 \pm 0.2 - 2.3 = 16.28 \pm 0.2 \\
&= ((m-M)_B + \Delta B)_{\mathrm{LMC\ N\ 2009a}} - 2.5\log 5.2 \\
&= 18.98 - 0.9 \pm 0.2 - 1.8 = 16.28 \pm 0.2, \qquad (22)
\end{aligned}
$$

where we adopt $(m-M)_{B,\mathrm{V2677\ Oph}} = 19.2 + 1.3 = 20.5$ from Appendix A.24 and $(m-M)_{B,\mathrm{V834\ Car}} = 17.25 + 0.50 = 17.75$ from Appendix A.20. Thus, we have $(m-M)_{B,\mathrm{V5116\ Sgr}} = 16.28 \pm 0.1$.

For the V light curves in Figure 28(b), we similarly obtain

$$
\begin{aligned}
&(m-M)_{V,\mathrm{V5116\ Sgr}} \\
&= ((m-M)_V + \Delta V)_{\mathrm{V2677\ Oph}} - 2.5\log 2.3 \\
&= 19.2 - 2.2 \pm 0.2 - 0.92 = 16.08 \pm 0.2 \\
&= ((m-M)_V + \Delta V)_{\mathrm{V834\ Car}} - 2.5\log 2.5 \\
&= 17.25 - 0.2 \pm 0.2 - 0.97 = 16.08 \pm 0.2 \\
&= ((m-M)_V + \Delta V)_{\mathrm{YY\ Dor}} - 2.5\log 8.3 \\
&= 18.86 - 0.5 \pm 0.2 - 2.3 = 16.06 \pm 0.2 \\
&= ((m-M)_V + \Delta V)_{\mathrm{LMC\ N\ 2009a}} - 2.5\log 5.2 \\
&= 18.86 - 1.0 \pm 0.2 - 1.8 = 16.06 \pm 0.2, \qquad (23)
\end{aligned}
$$

where we adopt $(m-M)_{V,\mathrm{V2677\ Oph}} = 19.2$ and $(m-M)_{V,\mathrm{V834\ Car}} = 17.25$ from Appendixes A.24 and A.20, respectively. We have $(m-M)_{V,\mathrm{V5116\ Sgr}} = 16.07 \pm 0.1$, which is consistent with Equation (20).

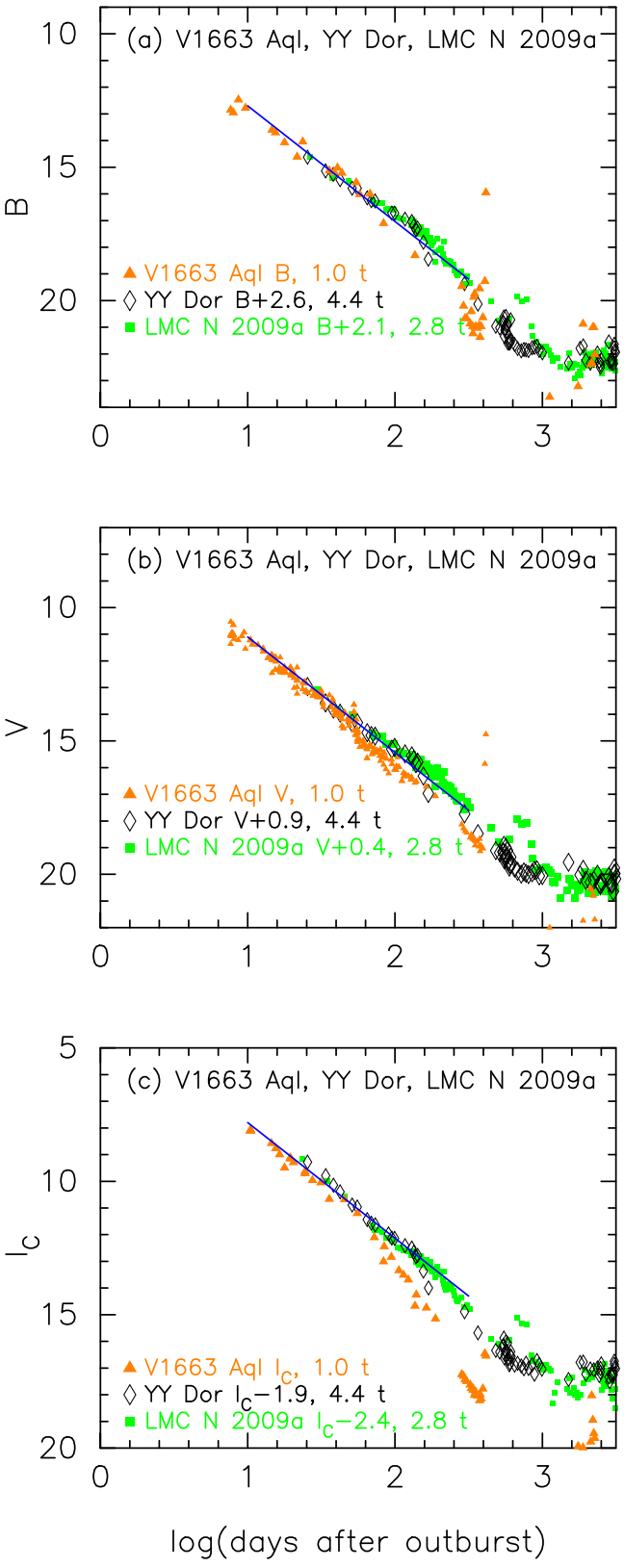

Figure 25. The (a) B, (b) V, and (c) I_C light curves of V1663 Aql, YY Dor, and LMC N 2009a. The straight solid blue lines denote the slope of $F_\nu \propto t^{-1.75}$. The BVI_C data of V1663 Aql, YY Dor, and LMC N 2009a are taken from AAVSO, VSOLJ, and SMARTS.

We apply Equation (10) for the I_C-band to Figure 28(c) and obtain

$$\begin{aligned}(m-M)_{I,\mathrm{V5116\ Sgr}} &= ((m-M)_I + \Delta I_C)_{\mathrm{V2677\ Oph}} - 2.5\log 2.3 \\ &= 17.12 - 0.5 \pm 0.2 - 0.92 = 15.7 \pm 0.2 \\ &= ((m-M)_I + \Delta I_C)_{\mathrm{V834\ Car}} - 2.5\log 2.5 \\ &= 16.45 + 0.2 \pm 0.2 - 0.97 = 15.68 \pm 0.2 \\ &= ((m-M)_I + \Delta I_C)_{\mathrm{YY\ Dor}} - 2.5\log 8.3 \\ &= 18.67 - 0.7 \pm 0.2 - 2.3 = 15.67 \pm 0.2 \\ &= ((m-M)_I + \Delta I_C)_{\mathrm{LMC\ N\ 2009a}} - 2.5\log 5.2 \\ &= 18.67 - 1.2 \pm 0.2 - 1.8 = 15.67 \pm 0.2, \end{aligned} \quad (24)$$

where we adopt $(m-M)_{I,\mathrm{V2677\ Oph}} = 19.2 - 1.6 \times 1.3 = 17.12$ from Appendix A.24 and $(m-M)_{I,\mathrm{V834\ Car}} = 17.25 - 1.6 \times 0.50 = 16.45$ from Appendix A.20. Thus, we have $(m-M)_{I,\mathrm{V5116\ Sgr}} = 15.68 \pm 0.1$.

We plot $(m-M)_B = 16.28$, $(m-M)_V = 16.07$, and $(m-M)_I = 15.68$, which cross at $d = 12$ kpc and $E(B-V) = 0.23$, in Figure 5(b). Thus, we have $E(B-V) = 0.23 \pm 0.05$ and $d = 12 \pm 2$ kpc.

A.3. V2575 Oph 2006

Figure 29 shows (a) the V and (b) $(B-V)_0$ evolutions of V2575 Oph. Here, $(B-V)_0$ are dereddened with $E(B-V) = 1.43$ as obtained in Section 3.3. The V light curve of V2575 Oph is similar to that of LV Vul and V1668 Cyg as shown in Figure 30. These three V light curves overlap each other if we properly stretch/squeeze the V and $(B-V)_0$ light/color curves. In more detail, the early V light curve shows a wavy structure during $t < 30$ days. Its upper bound follows that of LV Vul. After $t > 30$ days, the V light curve almost follows that of LV Vul. There are few observational points of $(B-V)_0$ before $t < 80$ days. The $(B-V)_0$ color curve also broadly follows the upper branch of LV Vul after $t > 80$ days. Applying Equation (6) to them, we have the relation

$$\begin{aligned}(m-M)_{V,\mathrm{V2575\ Oph}} &= (m - M + \Delta V)_{V,\mathrm{LV\ Vul}} - 2.5\log 1.29 \\ &= 11.85 + 6.3 \pm 0.2 - 0.28 = 17.87 \pm 0.2 \\ &= (m - M + \Delta V)_{V,\mathrm{V1668\ Cyg}} - 2.5\log 1.29 \\ &= 14.6 + 3.5 \pm 0.2 - 0.28 = 17.82 \pm 0.2, \end{aligned} \quad (25)$$

where we adopt $(m-M)_{V,\mathrm{LV\ Vul}} = 11.85$ and $(m-M)_{V,\mathrm{V1668\ Cyg}} = 14.6$, both from Hachisu & Kato (2019). Therefore, we adopt $(m-M)_V = 17.85 \pm 0.1$ and $f_s = 1.29$ for V2575 Oph. From Equations (1), (6), and (25), we have the relation

$$\begin{aligned}(m-M')_{V,\mathrm{V2575\ Oph}} &\equiv (m_V - (M_V - 2.5\log f_s))_{\mathrm{V2575\ Oph}} \\ &= ((m-M)_V + \Delta V)_{\mathrm{LV\ Vul}} \\ &= 11.85 + 6.3 \pm 0.2 = 18.15 \pm 0.2. \end{aligned} \quad (26)$$

We further check the distance and reddening with the time-stretching method. Figure 31 shows the B, V, and I_C light curves of V2575 Oph together with those of YY Dor and

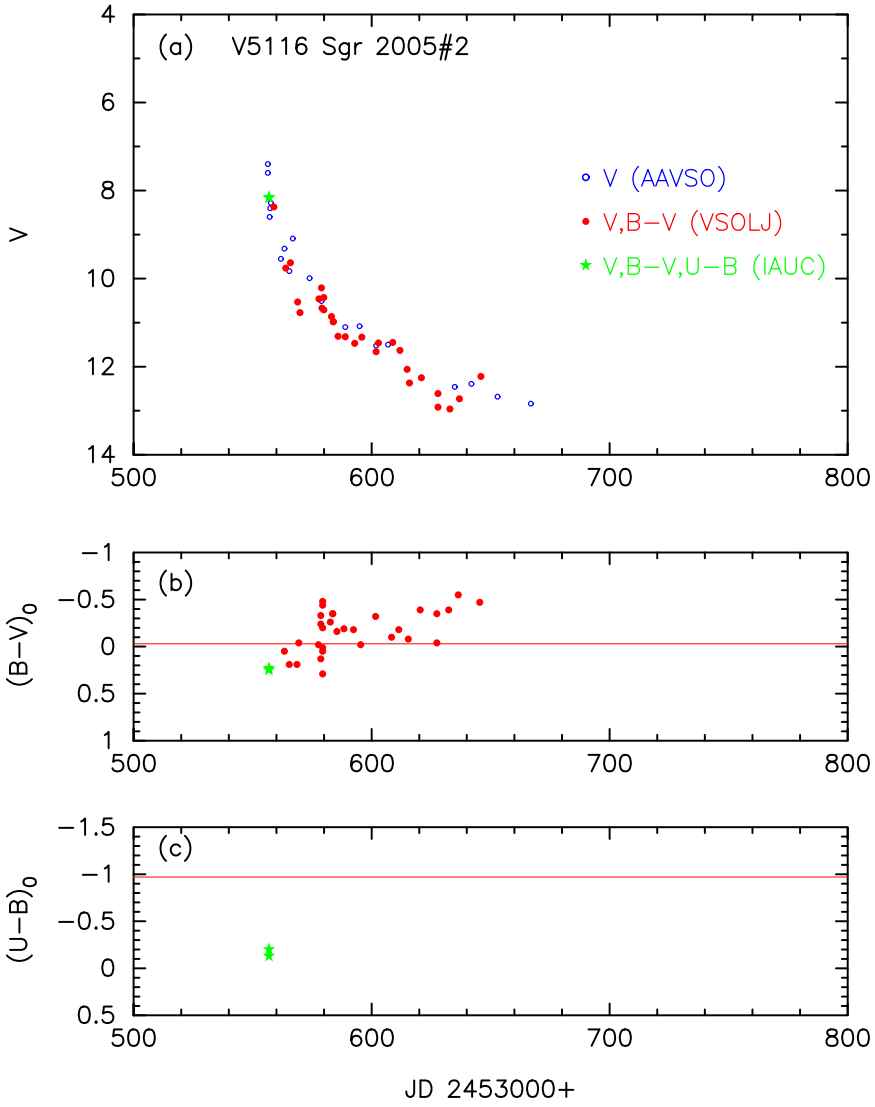

Figure 26. Same as Figure 23, but for V5116 Sgr. (a) The V data are taken from AAVSO (blue unfilled circles). The BV data are from VSOLJ (filled red circles) and the UBV data are from Gilmore & Kilmartin (2005; filled green stars). (b) The $(B-V)_0$ and (c) $(U-B)_0$ are dereddened with $E(B-V)=0.23$. The horizontal red lines show $(B-V)_0=-0.03$ and $(U-B)_0=-0.97$, which are the intrinsic colors of optically thick free–free emission (Hachisu & Kato 2014).

LMC N 2009a. We apply Equation (9) for the B band to Figure 31(a) and obtain

$$\begin{aligned}&(m-M)_{B,\mathrm{V2575\ Oph}}\\&=((m-M)_B+\Delta B)_{\mathrm{YY\ Dor}}-2.5\log 6.8\\&=18.98+2.4\pm0.2-2.08=19.3\pm0.2\\&=((m-M)_B+\Delta B)_{\mathrm{LMC\ N\ 2009a}}-2.5\log 4.3\\&=18.98+1.9\pm0.2-1.58=19.3\pm0.2.\end{aligned}\quad(27)$$

Thus, we obtain $(m-M)_{B,\mathrm{V2575\ Oph}}=19.3\pm0.1$.

For the V light curves in Figure 31(b), we similarly obtain

$$\begin{aligned}&(m-M)_{V,\mathrm{V2575\ Oph}}\\&=((m-M)_V+\Delta V)_{\mathrm{YY\ Dor}}-2.5\log 6.8\\&=18.86+1.1\pm0.2-2.08=17.88\pm0.2\\&=((m-M)_V+\Delta V)_{\mathrm{LMC\ N\ 2009a}}-2.5\log 4.3\\&=18.86+0.6\pm0.2-1.58=17.88\pm0.2.\end{aligned}\quad(28)$$

Thus, we obtain $(m-M)_{V,\mathrm{V2575\ Oph}}=17.88\pm0.1$, which is consistent with Equation (25).

We apply Equation (10) for the I_C-band to Figure 31(c) and obtain

$$\begin{aligned}&(m-M)_{I,\mathrm{V2575\ Oph}}\\&=((m-M)_I+\Delta I_C)_{\mathrm{YY\ Dor}}-2.5\log 6.8\\&=18.67-1.0\pm0.3-2.08=15.59\pm0.3\\&=((m-M)_I+\Delta I_C)_{\mathrm{LMC\ N\ 2009a}}-2.5\log 4.3\\&=18.67-1.5\pm0.3-1.58=15.59\pm0.3.\end{aligned}\quad(29)$$

Thus, we obtain $(m-M)_{I,\mathrm{V2575\ Oph}}=15.59\pm0.2$.

We plot $(m-M)_B=19.3$, $(m-M)_V=17.88$, and $(m-M)_I=15.59$, which cross at $d=4.9$ kpc and $E(B-V)=1.43$, in Figure 5(c). Thus, we obtain $E(B-V)=1.43\pm0.05$ and $d=4.9\pm0.5$ kpc.

A.4. V5117 Sgr 2006#2

Figure 32 shows (a) the V and (b) $(B-V)_0$ evolutions of V5117 Sgr. Here, $(B-V)_0$ are dereddened with $E(B-V)=0.53$ as obtained in Section 3.4. The V light curve of V5117 Sgr is similar to that of LV Vul and V1668 Cyg as

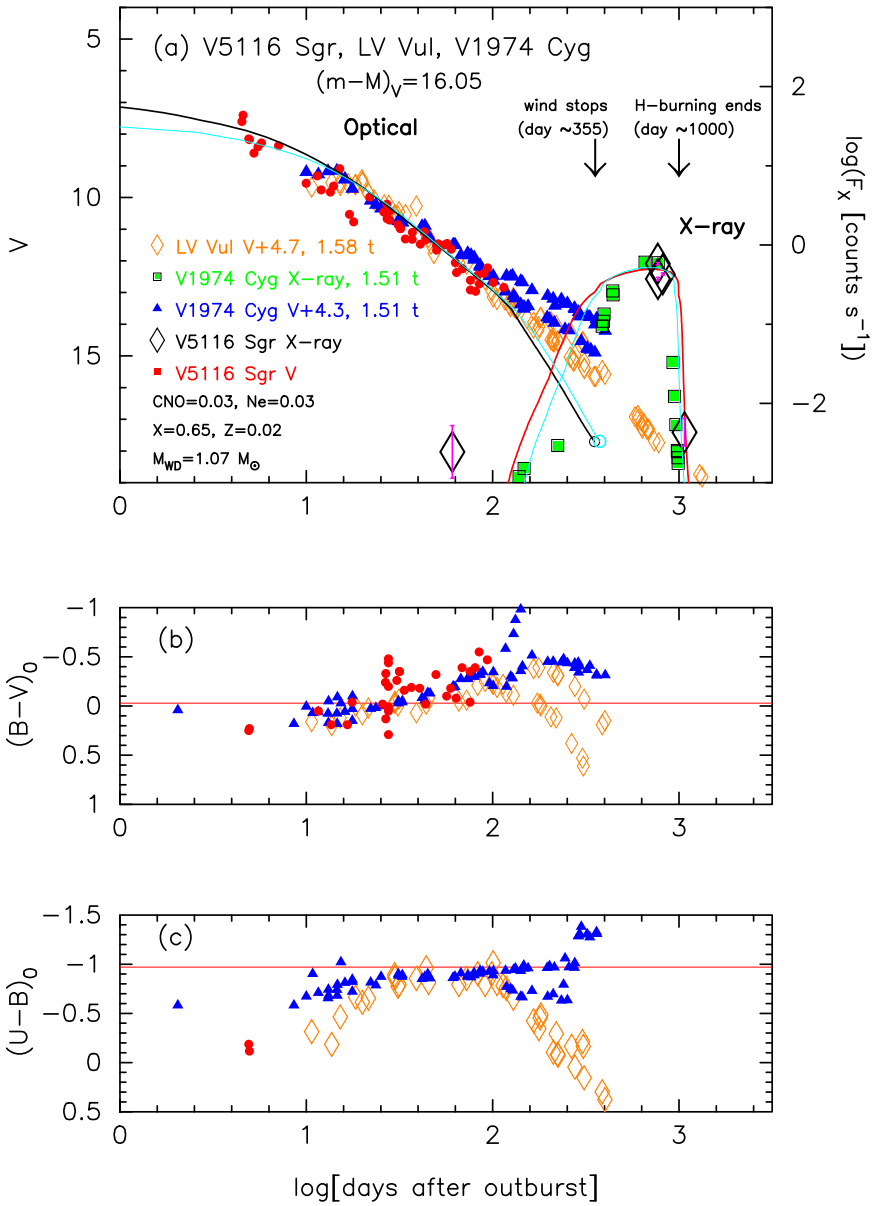

Figure 27. Same as Figure 24, but for V5116 Sgr. We add the light/color curves of LV Vul and V1974 Cyg. The data of V5116 Sgr are the same as those in Figure 26. We also add the X-ray data of V5116 Sgr and V1974 Cyg. The data of V1974 Cyg are all the same as those in Figures 38–42 of Hachisu & Kato (2016a). The timescale of V5116 Sgr is longer than that of V1974 Cyg by a factor of 1.51. We added a model light curve of a 1.07 $M_\odot$ WD (Ne3) for V5116 Sgr. The solid black line denotes our model V light curve (1.07 $M_\odot$) of photospheric plus free–free emission. The solid red line represents the supersoft X-ray flux (1.07 $M_\odot$) based on the blackbody approximation (see, e.g., Hachisu & Kato 2016a). We also add the model light curve of a 0.98 $M_\odot$ WD (CO3, solid cyan lines; Hachisu & Kato 2016a) for V1974 Cyg.

shown in Figure 33. The data of V5117 Sgr are the same as those in Figure 32. The V light curves of these three novae overlap each other. Applying Equation (6) to them, we have the relation

$$\begin{aligned}(m-M)_{V,\mathrm{V5117\ Sgr}} &= (m-M+\Delta V)_{V,\mathrm{LV\ Vul}} - 2.5\log 1.12\\ &= 11.85+4.3\pm 0.2-0.13 = 16.02\pm 0.2\\ &= (m-M+\Delta V)_{V,\mathrm{V1668\ Cyg}} - 2.5\log 1.12\\ &= 14.6+1.5\pm 0.2-0.13 = 15.97\pm 0.2,\end{aligned} \quad (30)$$

where we adopt $(m-M)_{V,\mathrm{LV\ Vul}} = 11.85$ and $(m-M)_{V,\mathrm{V1668\ Cyg}} = 14.6$, both from Hachisu & Kato (2019). Thus, we obtain $(m-M)_V = 16.0\pm 0.1$ and $f_s = 1.12$ for V5117 Sgr. From Equations (1), (6), and (30), we have the relation

$$\begin{aligned}(m-M')_{V,\mathrm{V5117\ Sgr}} &\equiv (m_V-(M_V-2.5\log f_s))_{\mathrm{V5117\ Sgr}}\\ &= ((m-M)_V+\Delta V)_{\mathrm{LV\ Vul}}\\ &= 11.85+4.3\pm 0.2 = 16.15\pm 0.2.\end{aligned} \quad (31)$$

Figure 34 shows the B, V, and I_C light curves of V5117 Sgr together with those of YY Dor and LMC N 2009a. The main part of the theoretical free–free emission light curve decays as $F_\nu \propto t^{-1.75}$ (the universal decline law of classical novae: straight solid blue line). However, the I_C light-curve matching is poor in Figure 34(c). In this case, we use only the I_C brightness near $t\sim 100$ days, because the other B and V light curves follow well the $F_\nu \propto t^{-1.75}$ law near $t\sim 100$ days, and

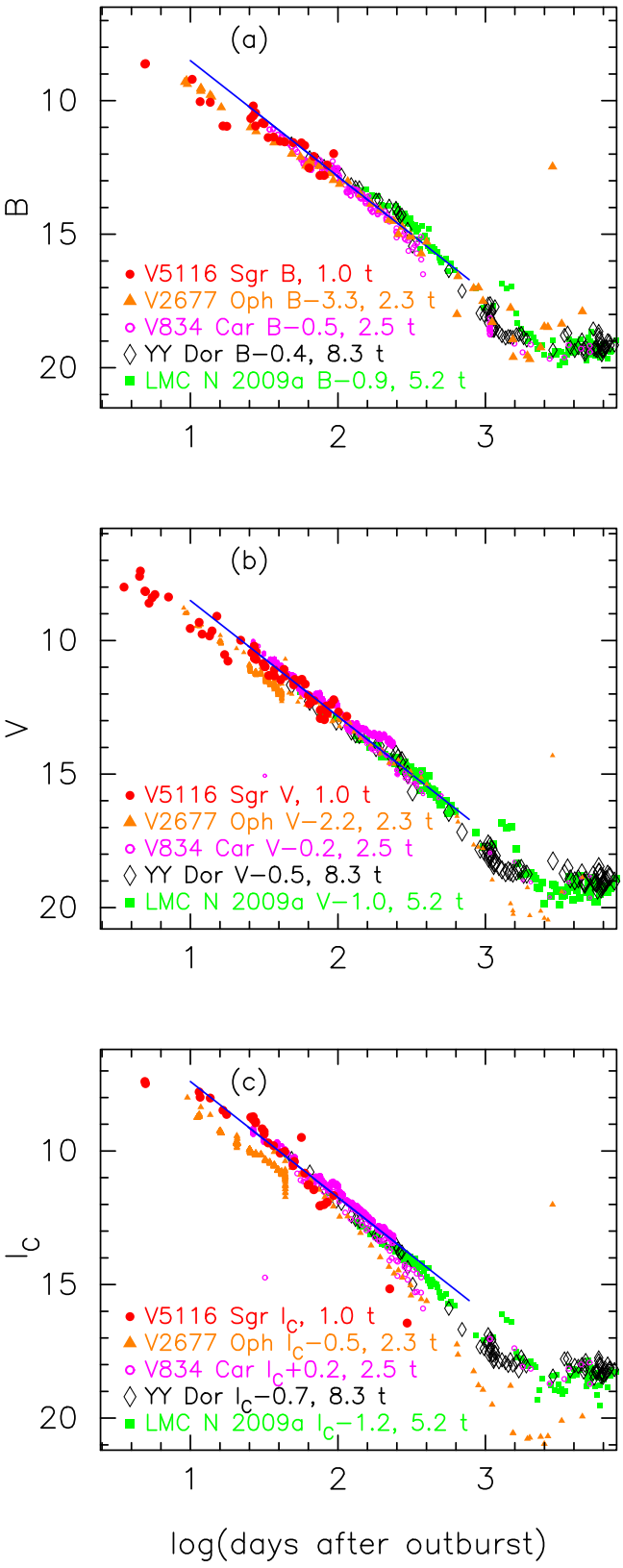

Figure 28. Same as Figure 25, but for V5116 Sgr. The (a) B, (b) V, and (c) I_C light curves of V5116 Sgr as well as those of V2677 Oph, V834 Car, YY Dor, and LMC N 2009a. The BV data of V5116 Sgr are the same as those in Figure 26. The I_C data are taken from Gilmore & Kilmartin (2005), AAVSO, and VSOLJ.

we expect that the I_C brightness represents the free–free flux around this epoch. We apply Equation (9) for the B band to Figure 34(a) and obtain

$$\begin{aligned}(m-M)_{B,\mathrm{V5117\ Sgr}} &= ((m-M)_B+\Delta B)_{\mathrm{YY\ Dor}} - 2.5\log 6.6\\ &= 18.98 - 0.4 \pm 0.2 - 2.05 = 16.53 \pm 0.2\\ &= ((m-M)_B+\Delta B)_{\mathrm{LMC\ N\ 2009a}} - 2.5\log 4.2\\ &= 18.98 - 0.9 \pm 0.2 - 1.55 = 16.53 \pm 0.2. \end{aligned} \quad (32)$$

Thus, we obtain $(m-M)_{B,\mathrm{V5117\ Sgr}} = 16.53 \pm 0.1$.

For the V light curves in Figure 34(b), we similarly obtain

$$\begin{aligned}(m-M)_{V,\mathrm{V5117\ Sgr}} &= ((m-M)_V+\Delta V)_{\mathrm{YY\ Dor}} - 2.5\log 6.6\\ &= 18.86 - 0.8 \pm 0.2 - 2.05 = 16.01 \pm 0.2\\ &= ((m-M)_V+\Delta V)_{\mathrm{LMC\ N\ 2009a}} - 2.5\log 4.2\\ &= 18.86 - 1.3 \pm 0.2 - 1.55 = 16.01 \pm 0.2. \end{aligned} \quad (33)$$

Thus, we obtain $(m-M)_{V,\mathrm{V5117\ Sgr}} = 16.01 \pm 0.1$, which is consistent with Equation (30).

We apply Equation (10) for the I_C-band to Figure 34(c) and obtain

$$\begin{aligned}(m-M)_{I,\mathrm{V5117\ Sgr}} &= ((m-M)_I+\Delta I_C)_{\mathrm{YY\ Dor}} - 2.5\log 6.6\\ &= 18.67 - 1.5 \pm 0.2 - 2.05 = 15.12 \pm 0.2\\ &= ((m-M)_I+\Delta I_C)_{\mathrm{LMC\ N\ 2009a}} - 2.5\log 4.2\\ &= 18.67 - 2.0 \pm 0.2 - 1.55 = 15.12 \pm 0.2. \end{aligned} \quad (34)$$

Thus, we obtain $(m-M)_{I,\mathrm{V5117\ Sgr}} = 15.12 \pm 0.1$.

We plot $(m-M)_B = 16.53$, $(m-M)_V = 16.01$, and $(m-M)_I = 15.12$, which cross at $d = 7.4$ kpc and $E(B-V) = 0.53$, in Figure 5(d). Thus, we obtain $E(B-V) = 0.53 \pm 0.05$ and $d = 7.4 \pm 0.8$ kpc.

A.5. V2576 Oph 2006#2

Figure 35 shows (a) the V and B, and (b) $(B-V)_0$ evolutions of V2576 Oph. Here, $(B-V)_0$ are dereddened with $E(B-V) = 0.62$ as obtained in Section 3.5. There are plenty of B and V data points from the VSOLJ archive (filled green and red circles, respectively). However, we adopt $B-V$ data only when the two (B and V) observed times are simultaneous within 0.15 days. For this constraint, we have no $B-V$ data from the VSOLJ data. The V light curve of V2576 Oph is similar to that of LV Vul and V1668 Cyg, as shown in Figure 36. The data of V2576 Oph are the same as those in Figure 35. These V light curves of the three novae overlap each other. Applying Equation (6) to them, we have the relation

$$\begin{aligned}(m-M)_{V,\mathrm{V2576\ Oph}} &= (m-M+\Delta V)_{V,\mathrm{LV\ Vul}} - 2.5\log 0.71\\ &= 11.85 + 4.4 \pm 0.2 + 0.38 = 16.63 \pm 0.2\\ &= (m-M+\Delta V)_{V,\mathrm{V1668\ Cyg}} - 2.5\log 0.71\\ &= 14.6 + 1.7 \pm 0.2 + 0.38 = 16.68 \pm 0.2. \end{aligned} \quad (35)$$

Thus, we adopt $(m-M)_V = 16.65 \pm 0.1$ and $f_s = 0.71$ for V2576 Oph. From Equations (1), (6), and (35), we have the

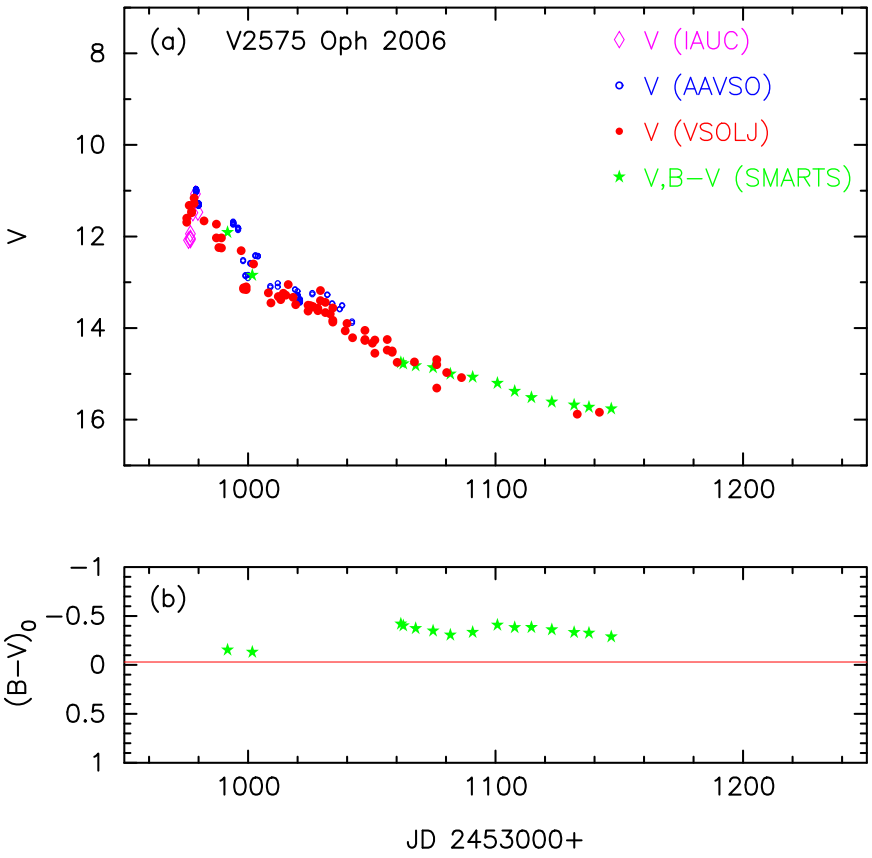

Figure 29. Same as Figure 23, but for V2575 Oph. (a) The V data are taken from IAU Circular No. 8671, 1 (unfilled magenta diamonds; Pojmanski et al. 2006), AAVSO (unfilled blue circles), and VSOLJ (filled red circles). The BV data are taken from SMARTS (filled green stars). (b) The $(B-V)_0$ are dereddened with $E(B-V)=1.43$.

relation

$$(m-M')_{V,\mathrm{V2576\ Oph}} \equiv (m_V-(M_V-2.5\log f_s))_{\mathrm{V2576\ Oph}} = ((m-M)_V+\Delta V)_{\mathrm{LV\ Vul}} = 11.85+4.4\pm0.2=16.25\pm0.2. \quad (36)$$

Figure 37 shows the B, V, and I_C light curves of V2576 Oph together with those of YY Dor and LMC N 2009a. We apply Equation (9) for the B band to Figure 37(a) and obtain

$$\begin{aligned}&(m-M)_{B,\mathrm{V2576\ Oph}}\\ &=((m-M)_B+\Delta B)_{\mathrm{YY\ Dor}}-2.5\log 3.7\\ &=18.98-0.3\pm0.2-1.43=17.25\pm0.2\\ &=((m-M)_B+\Delta B)_{\mathrm{LMC\ N\ 2009a}}-2.5\log 2.3\\ &=18.98-0.8\pm0.2-0.93=17.25\pm0.2.\end{aligned} \quad (37)$$

Thus, we have $(m-M)_{B,\mathrm{V5117\ Sgr}}=17.25\pm0.1$.

For the V light curves in Figure 37(b), we similarly obtain

$$\begin{aligned}&(m-M)_{V,\mathrm{V2576\ Oph}}\\ &=((m-M)_V+\Delta V)_{\mathrm{YY\ Dor}}-2.5\log 3.7\\ &=18.86-0.8\pm0.2-1.43=16.63\pm0.2\\ &=((m-M)_V+\Delta V)_{\mathrm{LMC\ N\ 2009a}}-2.5\log 2.3\\ &=18.86-1.3\pm0.2-0.93=16.63\pm0.2.\end{aligned} \quad (38)$$

We have $(m-M)_{V,\mathrm{V5117\ Sgr}}=16.63\pm0.1$, which is consistent with Equation (35).

We apply Equation (10) for the I_C-band to Figure 37(c) and obtain

$$\begin{aligned}&(m-M)_{I,\mathrm{V2576\ Oph}}\\ &=((m-M)_I+\Delta I_C)_{\mathrm{YY\ Dor}}-2.5\log 3.7\\ &=18.67-1.6\pm0.2-1.43=15.64\pm0.2\\ &=((m-M)_I+\Delta I_C)_{\mathrm{LMC\ N\ 2009a}}-2.5\log 2.3\\ &=18.67-2.1\pm0.2-0.93=15.64\pm0.2.\end{aligned} \quad (39)$$

Thus, we have $(m-M)_{I,\mathrm{V2576\ Oph}}=15.64\pm0.1$.

We plot $(m-M)_B=17.25$, $(m-M)_V=16.63$, and $(m-M)_I=15.64$, which cross at $d=8.8$ kpc and $E(B-V)=0.62$, in Figure 7(a). Thus, we have $E(B-V)=0.62\pm0.05$ and $d=8.8\pm1$ kpc.

A.6. V1281 Sco 2007#2

Figure 38 shows (a) the V and (b) $(B-V)_0$ evolutions of V1281 Sco. Here, $(B-V)_0$ are dereddened with $E(B-V)=0.82$ as obtained in Section 3.6. Figure 39 shows the light/color evolution of V1281 Sco as well as those of V1500 Cyg and LV Vul. The data of V1281 Sco are the same as those in Figure 38. The data of V1500 Cyg are the same as those in Figure 9 of Hachisu & Kato (2010) and Figure 6 of Hachisu & Kato (2014). The $(B-V)_0$ color curve of V1281 Sco is similar to V1500 Cyg rather than LV Vul as shown in Figure 39(b). A large part of these three V light curves overlap each other. Applying Equation (6) to them, we

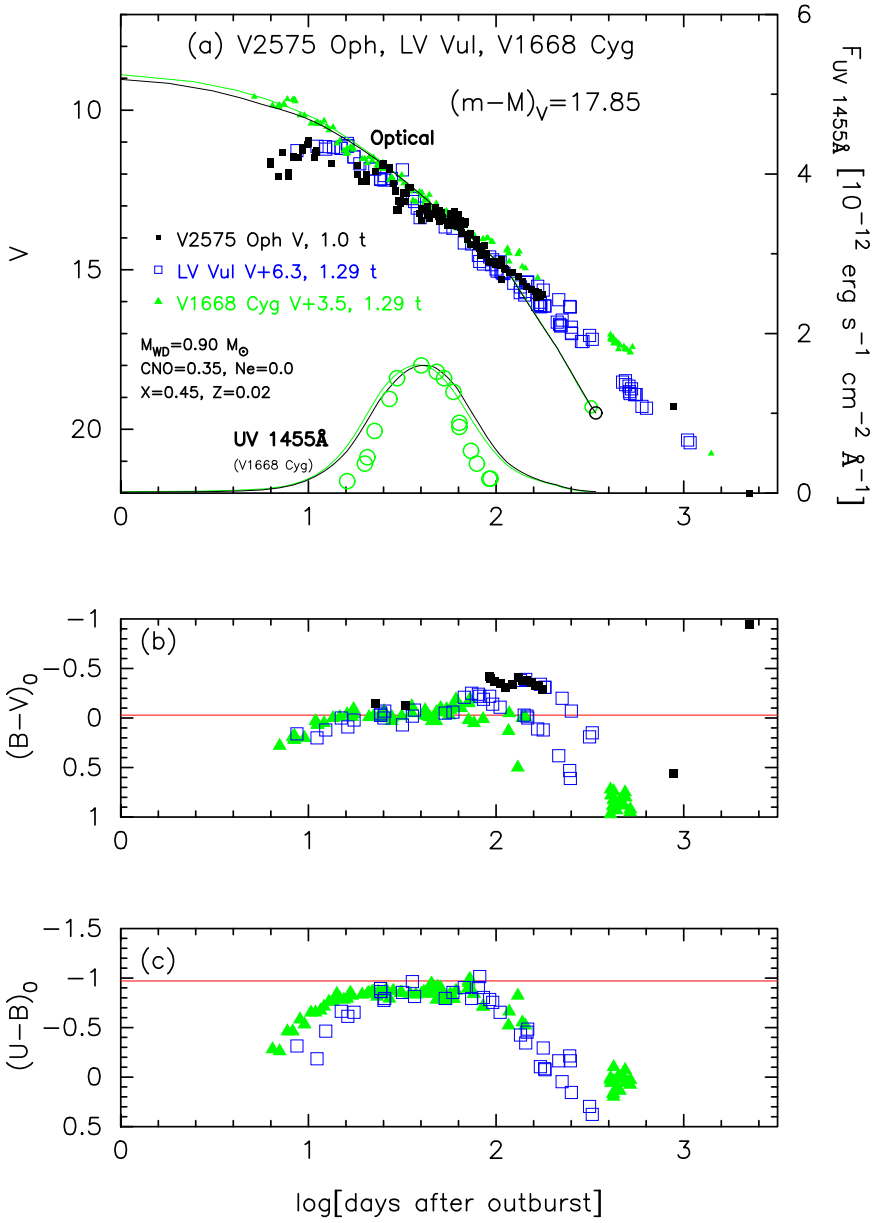

Figure 30. Same as Figure 24, but for V2575 Oph. We add the light/color curves of LV Vul and V1668 Cyg. The data of V2575 Oph are the same as those in Figure 29. The data of V1668 Cyg and LV Vul are all the same as those in Figures 1 and 4 of Hachisu & Kato (2016b). We added model light curves of a 0.90 $M_\odot$ WD (solid black lines) for V2575 Oph and a 0.98 $M_\odot$ WD (CO3, solid green lines; Hachisu & Kato 2016a) for V1668 Cyg. The upper solid black and green lines denote the V light curves of photospheric plus free–free emission for the 0.90 $M_\odot$ and 0.98 $M_\odot$ WDs. The lower solid black and green lines represent the UV 1455 Å flux based on the blackbody approximation (see, e.g., Hachisu & Kato 2016a).

have the relation

$$\begin{aligned}(m-M)_{V,\mathrm{V1281\ Sco}} &= (m-M+\Delta V)_{V,\mathrm{LV\ Vul}} - 2.5\log 0.85\\ &= 11.85 + 5.4 \pm 0.2 + 0.18 = 17.43 \pm 0.2\\ &= (m-M+\Delta V)_{V,\mathrm{V1500\ Cyg}} - 2.5\log 1.41\\ &= 12.3 + 5.5 \pm 0.2 - 0.38 = 17.42 \pm 0.2, \end{aligned} \quad (40)$$

where we adopt $(m-M)_{V,\mathrm{LV\ Vul}} = 11.85$ and $(m-M)_{V,\mathrm{V1500\ Cyg}} = 12.3$, both from Hachisu & Kato (2019). Thus, we obtained $(m-M)_V = 17.4 \pm 0.1$ and $f_s = 0.85$ against LV Vul. The newly obtained value is slightly smaller than Hachisu & Kato's (2010) value of $(m-M)_V = 17.8 \pm 0.2$. This is because Hachisu & Kato (2010) assumed $(m-M)_{V,\mathrm{V1500\ Cyg}} = 12.5$ instead of $(m-M)_{V,\mathrm{V1500\ Cyg}} = 12.3$, and we improved the vertical V fit. From Equations (1), (6), and (40), we have the relation

$$\begin{aligned}(m-M')_{V,\mathrm{V1281\ Sco}} &\equiv (m_V - (M_V - 2.5\log f_s))_{\mathrm{V1281\ Sco}}\\ &= ((m-M)_V + \Delta V)_{\mathrm{LV\ Vul}}\\ &= 11.85 + 5.4 \pm 0.2 = 17.25 \pm 0.2. \end{aligned} \quad (41)$$

Figure 40 shows the B, V, and I_C light curves of V1281 Sco together with those of YY Dor and LMC N 2009a. We apply

Equation (9) for the B band to Figure 40(a) and obtain

$$\begin{aligned}(m-M)_{B,\mathrm{V1281\ Sco}} &= ((m-M)_B+\Delta B)_{\mathrm{YY\ Dor}} - 2.5\log 4.5\\ &= 18.98+0.9\pm0.2-1.63 = 18.25\pm0.2\\ &= ((m-M)_B+\Delta B)_{\mathrm{LMC\ N\ 2009a}} - 2.5\log 2.8\\ &= 18.98+0.4\pm0.2-1.13 = 18.25\pm0.2. \end{aligned} \quad (42)$$

Thus, we have $(m-M)_{B,\mathrm{V1281\ Sco}} = 18.25\pm0.1$.

For the V light curves in Figure 40(b), we similarly obtain

$$\begin{aligned}(m-M)_{V,\mathrm{V1281\ Sco}} &= ((m-M)_V+\Delta V)_{\mathrm{YY\ Dor}} - 2.5\log 4.5\\ &= 18.86+0.2\pm0.2-1.63 = 17.43\pm0.2\\ &= ((m-M)_V+\Delta V)_{\mathrm{LMC\ N\ 2009a}} - 2.5\log 2.8\\ &= 18.86-0.3\pm0.2-1.13 = 17.43\pm0.2. \end{aligned} \quad (43)$$

We have $(m-M)_{V,\mathrm{V1281\ Sco}} = 17.43\pm0.1$, which is consistent with Equation (40).

We apply Equation (10) for the I_C-band to Figure 40(c) and obtain

$$\begin{aligned}(m-M)_{I,\mathrm{V1281\ Sco}} &= ((m-M)_I+\Delta I_C)_{\mathrm{YY\ Dor}} - 2.5\log 4.5\\ &= 18.67-0.9\pm0.2-1.63 = 16.14\pm0.2\\ &= ((m-M)_I+\Delta I_C)_{\mathrm{LMC\ N\ 2009a}} - 2.5\log 2.8\\ &= 18.67-1.4\pm0.2-1.13 = 16.14\pm0.2. \end{aligned} \quad (44)$$

Thus, we have $(m-M)_{I,\mathrm{V1281\ Sco}} = 16.14\pm0.1$.

We plot $(m-M)_B = 18.25$, $(m-M)_V = 17.43$, and $(m-M)_I = 16.14$, which broadly cross at $d = 9.4$ kpc and $E(B-V) = 0.82$, in Figure 7(b). Thus, we have $E(B-V) = 0.82\pm0.05$ and $d = 9.4\pm1$ kpc.

A.7. V390 Nor 2007

Figure 41 shows (a) the V, B, and (b) $(B-V)_0$ evolutions of V390 Nor. Here, $(B-V)_0$ are dereddened with $E(B-V) = 0.89$ as obtained in Section 3.7. The visual magnitude (magenta dots) is taken from Liller et al. (2007). The light/color curves of V390 Nor are plotted in Figure 42 together with the light/color curves of V5666 Sgr, LV Vul, and V1668 Cyg. The data of V390 Nor are the same as those in Figure 41. The BV data of V5666 Sgr are the same as those in Figure 28 of Hachisu & Kato (2019). These four V light curves roughly overlap each other. Applying Equation (6) to them, we have the relation

$$\begin{aligned}(m-M)_{V,\mathrm{V390\ Nor}} &= (m-M+\Delta V)_{V,\mathrm{LV\ Vul}} - 2.5\log 2.82\\ &= 11.85+5.9\pm0.3-1.13 = 16.62\pm0.3\\ &= (m-M+\Delta V)_{V,\mathrm{V1668\ Cyg}} - 2.5\log 2.82\\ &= 14.6+3.1\pm0.3-1.13 = 16.62\pm0.3\\ &= (m-M+\Delta V)_{V,\mathrm{V5666\ Sgr}} - 2.5\log 1.58\\ &= 15.4+1.7\pm0.3-0.50 = 16.60\pm0.3, \end{aligned} \quad (45)$$

where we adopt $(m-M)_{V,\mathrm{V5666\ Sgr}} = 15.4$ from Hachisu & Kato (2019). Thus, we obtain $(m-M)_V = 16.6\pm0.2$ and $f_s = 2.82$ against LV Vul. From Equations (1), (6), and (45),

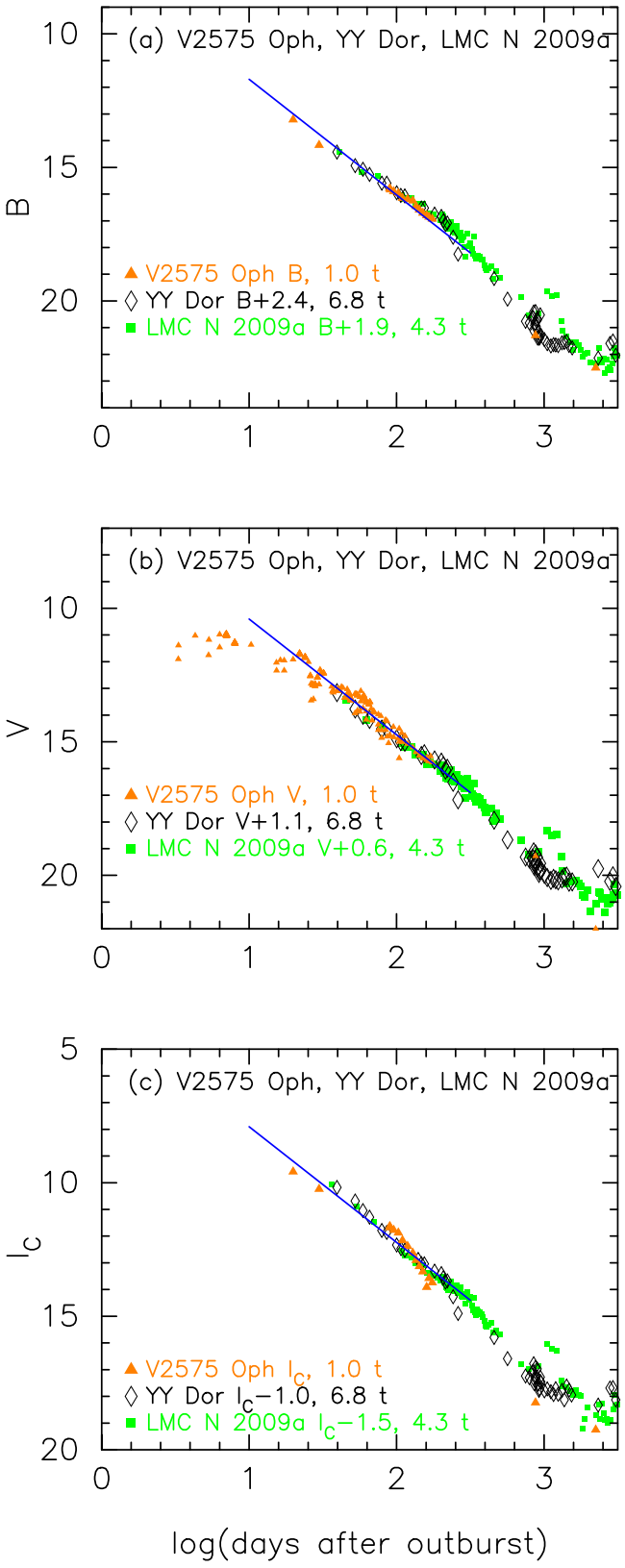

Figure 31. Same as Figure 25, but for V2575 Oph. The BVI_C data of V2575 Oph are taken from SMARTS. The V data of V2575 Oph are also taken from AAVSO and VSOLJ.

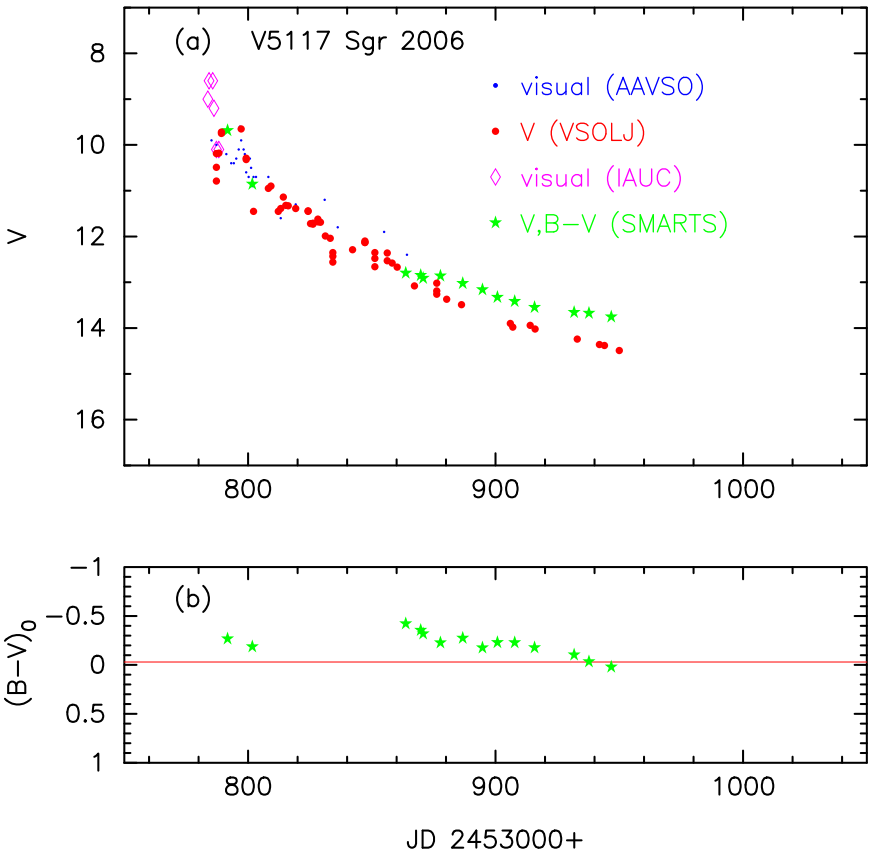

Figure 32. Same as Figure 23, but for V5117 Sgr. (a) The visual data are taken from AAVSO (blue dots) and IAU Circular 8673, 1 and 8706, 3 (unfilled magenta diamonds). The V data are from VSOLJ (filled red circles). The BV data are taken from SMARTS (filled green stars). (b) The $(B-V)_0$ are dereddened with $E(B-V)=0.53$.

we have the relation

$$(m-M')_{V,\mathrm{V390\ Nor}} \equiv (m_V-(M_V-2.5\log f_s))_{\mathrm{V390\ Nor}} = ((m-M)_V+\Delta V)_{\mathrm{LV\ Vul}} = 11.85+5.9\pm0.3=17.75\pm0.3. \quad (46)$$

Figure 43 shows the B, V, and I_C light curves of V390 Nor together with those of V1369 Cen, V496 Sct, and V5666 Sgr. In this case, the early-phase BVI_C light curves show wavy (oscillatory) structures and do not seem to follow the universal decline law. However, we can observe a moderately good overlapping of V390 Nor (filled red circles) with V496 Sct (unfilled black diamonds) and V1369 Cen (filled orange squares) especially near the straight solid blue lines of $F_\nu \propto t^{-1.75}$. We require a short period overlapping on the solid blue line because the later observational data show a long period overlapping with the other novae. Applying Equation (9) for the B band to Figure 43(a), we have the relation

$$\begin{aligned}(m-M)_{B,\mathrm{V390\ Nor}} &= ((m-M)_B+\Delta B)_{\mathrm{V1369\ Cen}}-2.5\log 1.91\\ &= 10.36+7.8\pm0.3-0.7=17.46\pm0.3\\ &= ((m-M)_B+\Delta B)_{\mathrm{V496\ Sct}}-2.5\log 1.41\\ &= 14.15+3.7\pm0.3-0.38=17.47\pm0.3\\ &= ((m-M)_B+\Delta B)_{\mathrm{V5666\ Sgr}}-2.5\log 1.58\\ &= 15.9+2.1\pm0.3-0.5=17.5\pm0.3, \end{aligned} \quad (47)$$

where we adopt $(m-M)_{B,\mathrm{V1369\ Cen}}=10.25+1.0\times0.11=10.36$, $(m-M)_{B,\mathrm{V496\ Sct}}=13.7+1.0\times0.45=14.15$, and $(m-M)_{B,\mathrm{V5666\ Sgr}}=15.4+1.0\times0.50=15.9$, all from Hachisu & Kato (2019). Thus, we obtain $(m-M)_B=17.48\pm0.2$ for V390 Nor.

Applying Equation (6) to Figure 43(b), we have the relation

$$\begin{aligned}(m-M)_{V,\mathrm{V390\ Nor}} &= ((m-M)_V+\Delta V)_{\mathrm{V1369\ Cen}}-2.5\log 1.91\\ &= 10.25+7.0\pm0.3-0.7=16.55\pm0.3\\ &= ((m-M)_V+\Delta V)_{\mathrm{V496\ Sct}}-2.5\log 1.41\\ &= 13.7+3.3\pm0.3-0.38=16.62\pm0.3\\ &= ((m-M)_V+\Delta V)_{\mathrm{V5666\ Sgr}}-2.5\log 1.58\\ &= 15.4+1.7\pm0.3-0.5=16.6\pm0.3, \end{aligned} \quad (48)$$

where we adopt $(m-M)_{V,\mathrm{V1369\ Cen}}=10.25$, $(m-M)_{V,\mathrm{V496\ Sct}}=13.7$, and $(m-M)_{V,\mathrm{V5666\ Sgr}}=15.4$, all from Hachisu & Kato (2019). Thus, we obtain $(m-M)_V=16.59\pm0.2$ for V390 Nor, which is consistent with Equation (45).

From the I_C-band data in Figure 43(c), we obtain

$$\begin{aligned}(m-M)_{I,\mathrm{V390\ Nor}} &= ((m-M)_I+\Delta I_C)_{\mathrm{V1369\ Cen}}-2.5\log 1.91\\ &= 10.07+5.8\pm0.3-0.7=15.17\pm0.3\\ &= ((m-M)_I+\Delta I_C)_{\mathrm{V496\ Sct}}-2.5\log 1.41\\ &= 12.98+2.6\pm0.3-0.38=15.2\pm0.3\\ &= ((m-M)_I+\Delta I_C)_{\mathrm{V5666\ Sgr}}-2.5\log 1.58\\ &= 14.6+1.1\pm0.3-0.5=15.2\pm0.3, \end{aligned} \quad (49)$$

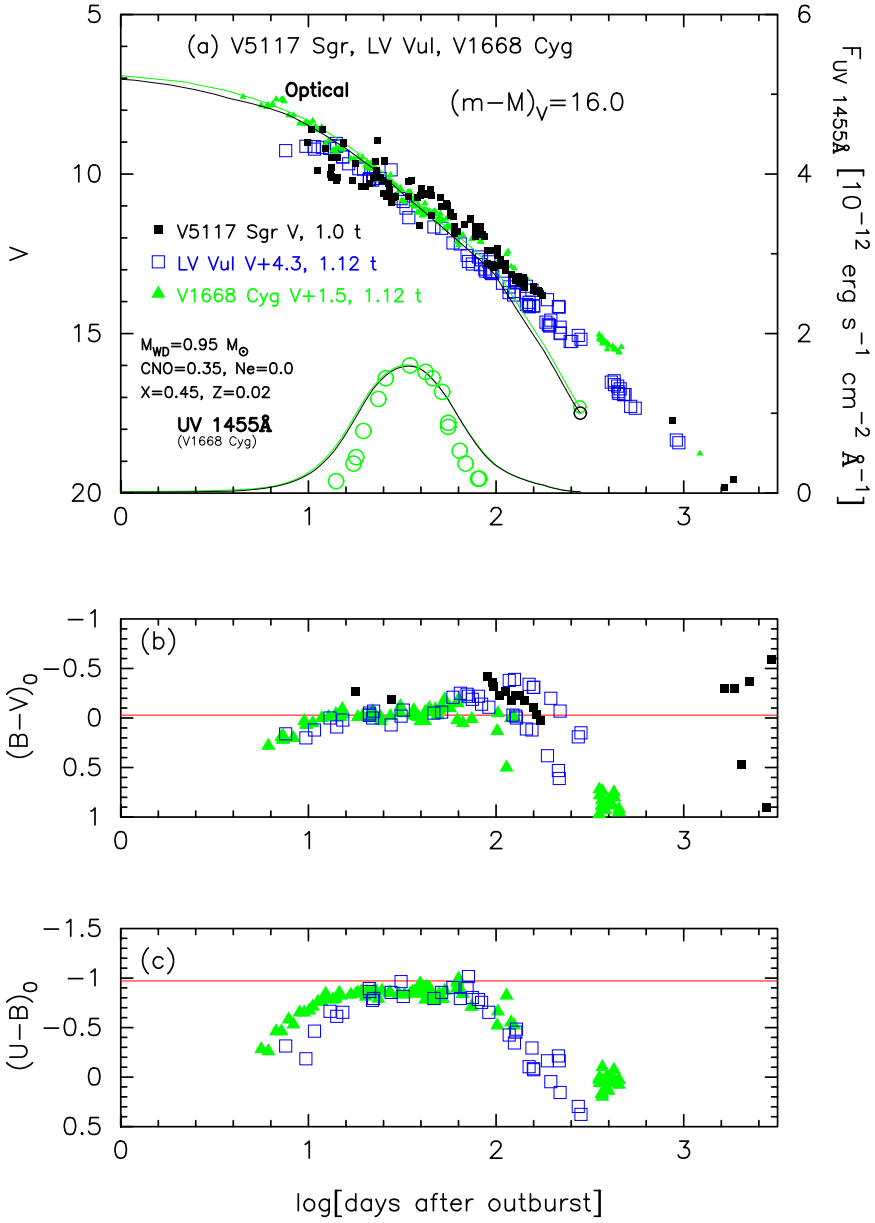

Figure 33. Same as Figures 24 and 30, but for V5117 Sgr. We add the light/color curves of LV Vul and V1668 Cyg. The data of V5117 Sgr are the same as those in Figure 32. The data of LV Vul and V1668 Cyg are all the same as those in Figure 30. Assuming that $(m-M)_V = 16.0$, we added model light curves of a 0.95 $M_\odot$ WD (CO3, Hachisu & Kato 2016a). The upper solid black line denotes the V light curve of photospheric plus free–free emission for a 0.95 $M_\odot$ WD (Hachisu & Kato 2015). The lower solid black line represents the UV 1455 Å flux based on the blackbody approximation (see, e.g., Hachisu & Kato 2016a). The green lines denote the 0.98 $M_\odot$ WD (CO3) model, assuming that $(m-M)_V = 14.6$ for V1668 Cyg.

where we adopt $(m-M)_{I,\mathrm{V1369\ Cen}} = 10.25 - 1.6 \times 0.11 = 10.07$, $(m-M)_{I,\mathrm{V496\ Sct}} = 13.7 - 1.6 \times 0.45 = 12.98$, and $(m-M)_{I,\mathrm{V5666\ Sgr}} = 15.4 - 1.6 \times 0.50 = 14.6$. Thus, we obtain $(m-M)_{I,\mathrm{V390\ Nor}} = 15.19 \pm 0.2$.

We plot $(m-M)_B = 17.48$, $(m-M)_V = 16.59$, and $(m-M)_I = 15.19$, which cross at $d = 5.8$ kpc and $E(B-V) = 0.89$, in Figure 7(c). Thus, we obtain $E(B-V) = 0.89 \pm 0.05$ and $d = 5.8 \pm 0.6$ kpc.

A.8. V597 Pup 2007

Figure 44 shows (a) the V and *SMEI* magnitudes (Hounsell et al. 2016), and (b) $(B-V)_0$ color evolutions of V597 Pup. Here, $(B-V)_0$ are dereddened with $E(B-V) = 0.24$ as obtained in Section 3.8. The V light curve of V597 Pup is similar to that of V1500 Cyg as shown in Figure 45, where we add the light/color curves of LV Vul and V1500 Cyg. The data of V597 Pup are the same as those in Figure 44. We also add two model light curves of a 1.2 $M_\odot$ WD (Ne3, solid red line) for V597 Pup and 1.2 $M_\odot$ WD (Ne2, solid blue line) for V1500 Cyg.

The optical light curve shape of V597 Pup near the peak is largely different from our model V light curve (solid red line); it is similar to the shape of V1500 Cyg (solid blue line). It is highly likely that V597 Pup is a superbright nova like V1500 Cyg (della Valle 1991). The V1500 Cyg spectra in

the superbright phase show blackbody (Gallagher & Ney 1976; Ennis et al. 1977) and the observed V brightness greatly exceeds our model V light curve. After the superbright phase, the spectra changed to free–free emission on day ∼5. After that, the V light curve is broadly approximated by our model V light curve. Thus, our time-stretching method applies to this free–free emission-dominated phase.

These V light curves overlap each other except for the superbright phase. Applying Equation (6) to them, we have the relation

$$\begin{aligned}(m-M)_{V,\mathrm{V597\ Pup}} &= (m-M+\Delta V)_{V,\mathrm{LV\ Vul}} - 2.5\log 0.66 \\ &= 11.85 + 4.1 \pm 0.2 + 0.45 = 16.4 \pm 0.2 \\ &= (m-M+\Delta V)_{V,\mathrm{V1500\ Cyg}} - 2.5\log 1.10 \\ &= 12.3 + 4.2 \pm 0.2 - 0.10 = 16.4 \pm 0.2. \end{aligned} \quad (50)$$

Thus, we obtain $(m-M)_V = 16.4 \pm 0.1$ and $f_s = 0.66$ against LV Vul. From Equations (1), (6), and (50), we have the relation

$$\begin{aligned}(m-M')_{V,\mathrm{V597\ Pup}} &\equiv (m_V - (M_V - 2.5\log f_s))_{\mathrm{V597\ Pup}} \\ &= ((m-M)_V + \Delta V)_{\mathrm{LV\ Vul}} \\ &= 11.85 + 4.1 \pm 0.2 = 15.95 \pm 0.2. \end{aligned} \quad (51)$$

Figure 46 shows the B, V, and I_C light curves of V597 Pup together with those of YY Dor and LMC N 2009a. We apply Equation (9) for the B band to Figure 46(a) and obtain

$$\begin{aligned}(m-M)_{B,\mathrm{V597\ Pup}} &= ((m-M)_B + \Delta B)_{\mathrm{YY\ Dor}} - 2.5\log 3.5 \\ &= 18.98 - 1.0 \pm 0.2 - 1.35 = 16.63 \pm 0.2 \\ &= ((m-M)_B + \Delta B)_{\mathrm{LMC\ N\ 2009a}} - 2.5\log 2.2 \\ &= 18.98 - 1.5 \pm 0.2 - 0.85 = 16.63 \pm 0.2. \end{aligned} \quad (52)$$

Thus, we have $(m-M)_{B,\mathrm{V597\ Pup}} = 16.63 \pm 0.1$.

For the V light curves in Figure 46(b), we similarly obtain

$$\begin{aligned}(m-M)_{V,\mathrm{V597\ Pup}} &= ((m-M)_V + \Delta V)_{\mathrm{YY\ Dor}} - 2.5\log 3.5 \\ &= 18.86 - 1.1 \pm 0.2 - 1.35 = 16.41 \pm 0.2 \\ &= ((m-M)_V + \Delta V)_{\mathrm{LMC\ N\ 2009a}} - 2.5\log 2.2 \\ &= 18.86 - 1.6 \pm 0.2 - 0.85 = 16.41 \pm 0.2. \end{aligned} \quad (53)$$

We have $(m-M)_{V,\mathrm{V597\ Pup}} = 16.41 \pm 0.1$, which is consistent with Equation (50).

We apply Equation (10) for the I_C band to Figure 46(c) and obtain

$$\begin{aligned}(m-M)_{I,\mathrm{V597\ Pup}} &= ((m-M)_I + \Delta I_C)_{\mathrm{YY\ Dor}} - 2.5\log 3.5 \\ &= 18.67 - 1.3 \pm 0.2 - 1.35 = 16.02 \pm 0.2 \\ &= ((m-M)_I + \Delta I_C)_{\mathrm{LMC\ N\ 2009a}} - 2.5\log 2.2 \\ &= 18.67 - 1.8 \pm 0.2 - 0.85 = 16.02 \pm 0.2. \end{aligned} \quad (54)$$

Thus, we have $(m-M)_{I,\mathrm{V597\ Pup}} = 16.02 \pm 0.1$.

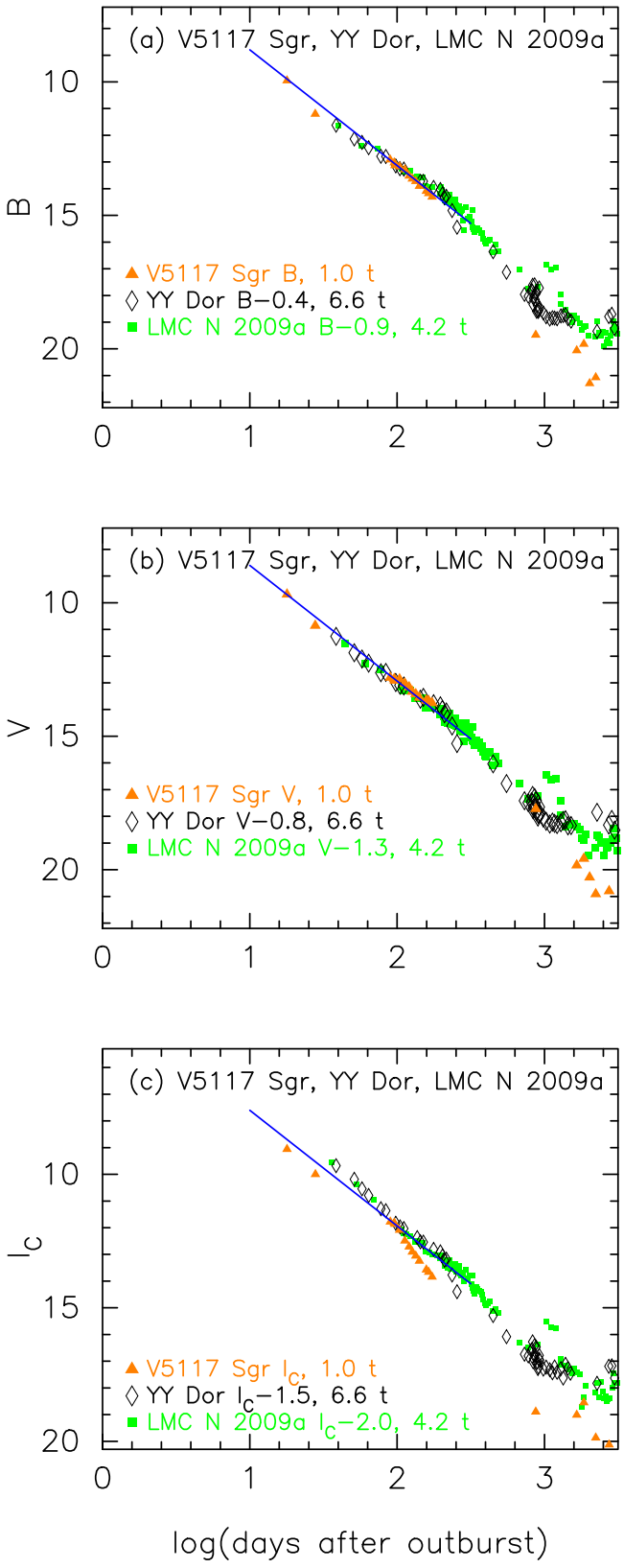

Figure 34. Same as Figure 25, but for V5117 Sgr. The BVI_C data of V5117 Sgr are taken from SMARTS.

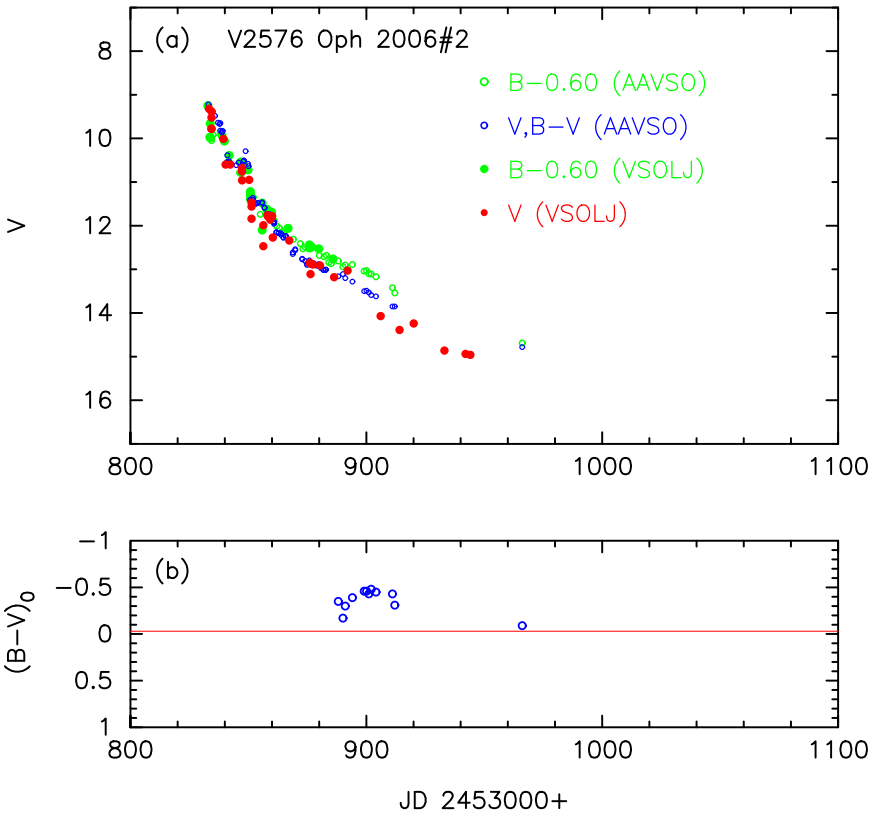

Figure 35. Same as Figure 23, but for V2576 Oph. (a) The V data are taken from AAVSO (blue unfilled circles) and VSOLJ (filled red circles). We also plot the B magnitudes of AAVSO (unfilled green circles) and VSOLJ (filled green circles), shifted up by 0.60 mag. (b) The $(B-V)_0$ are dereddened with $E(B-V)=0.62$.

We plot $(m-M)_B=16.63$, $(m-M)_V=16.41$, and $(m-M)_I=16.02$, which broadly cross at $d=13.5$ kpc and $E(B-V)=0.24$, in Figure 7(d). Thus, we have $E(B-V)=0.24\pm0.05$ and $d=13.5\pm2$ kpc.

A.9. V459 Vul 2007#2

Figure 47 shows (a) the V, *SMEI*, and B magnitudes, and (b) $(B-V)_0$ evolutions of V459 Vul. Here, $(B-V)_0$ are dereddened with $E(B-V)=0.90$ as obtained in Section 3.9. The B and V data are taken from CBET No.1183, AAVSO, and VSOLJ. We also plot the *SMEI* magnitudes taken from Hounsell et al. (2016). Figure 48 shows the V light and $(B-V)_0$ color curves of V459 Vul as well as those of LV Vul, V1668 Cyg, and V533 Her. The data of V533 Her are the same as those in Figure 33 of Hachisu & Kato (2019). The data of V459 Vul are the same as those in Figure 47. These four V light curves overlap each other. Applying Equation (6) to them, we have the relation

$$\begin{aligned}(m-M)_{V,\mathrm{V459\ Vul}}&=(m-M+\Delta V)_{V,\mathrm{LV\ Vul}}-2.5\log 0.71\\&=11.85+3.2\pm0.2+0.38=15.43\pm0.2\\&=(m-M+\Delta V)_{V,\mathrm{V1668\ Cyg}}-2.5\log 0.71\\&=14.6+0.5\pm0.2+0.38=15.48\pm0.2\\&=(m-M+\Delta V)_{V,\mathrm{V533\ Her}}-2.5\log 0.59\\&=10.65+4.2\pm0.2+0.58=15.43\pm0.2,\end{aligned}\quad(55)$$

where we adopt $(m-M)_{V,\mathrm{V533\ Her}}=10.65$ from Hachisu & Kato (2019). Thus, we obtain $(m-M)_V=15.45\pm0.1$ and $f_s=0.71$ against LV Vul. From Equations (1), (6), and (55), we have the relation

$$\begin{aligned}(m-M')_{V,\mathrm{V459\ Vul}}&\equiv(m_V-(M_V-2.5\log f_s))_{\mathrm{V459\ Vul}}\\&=((m-M)_V+\Delta V)_{\mathrm{LV\ Vul}}\\&=11.85+3.2\pm0.2=15.05\pm0.2.\end{aligned}\quad(56)$$

Figure 49 shows the B, V, and I_C light curves of V459 Vul together with those of YY Dor and LMC N 2009a. We apply Equation (9) for the B band to Figure 49(a) and obtain

$$\begin{aligned}&(m-M)_{B,\mathrm{V459\ Vul}}\\&=((m-M)_B+\Delta B)_{\mathrm{YY\ Dor}}-2.5\log 3.7\\&=18.98-1.2\pm0.2-1.43=16.35\pm0.2\\&=((m-M)_B+\Delta B)_{\mathrm{LMC\ N\ 2009a}}-2.5\log 2.3\\&=18.98-1.7\pm0.2-0.93=16.35\pm0.2.\end{aligned}\quad(57)$$

Thus, we have $(m-M)_{B,\mathrm{V459\ Vul}}=16.35\pm0.1$.

For the V light curves in Figure 49(b), we similarly obtain

$$\begin{aligned}&(m-M)_{V,\mathrm{V459\ Vul}}\\&=((m-M)_V+\Delta V)_{\mathrm{YY\ Dor}}-2.5\log 3.7\\&=18.86-2.0\pm0.2-1.43=15.43\pm0.2\\&=((m-M)_V+\Delta V)_{\mathrm{LMC\ N\ 2009a}}-2.5\log 2.3\\&=18.86-2.5\pm0.2-0.93=15.43\pm0.2.\end{aligned}\quad(58)$$

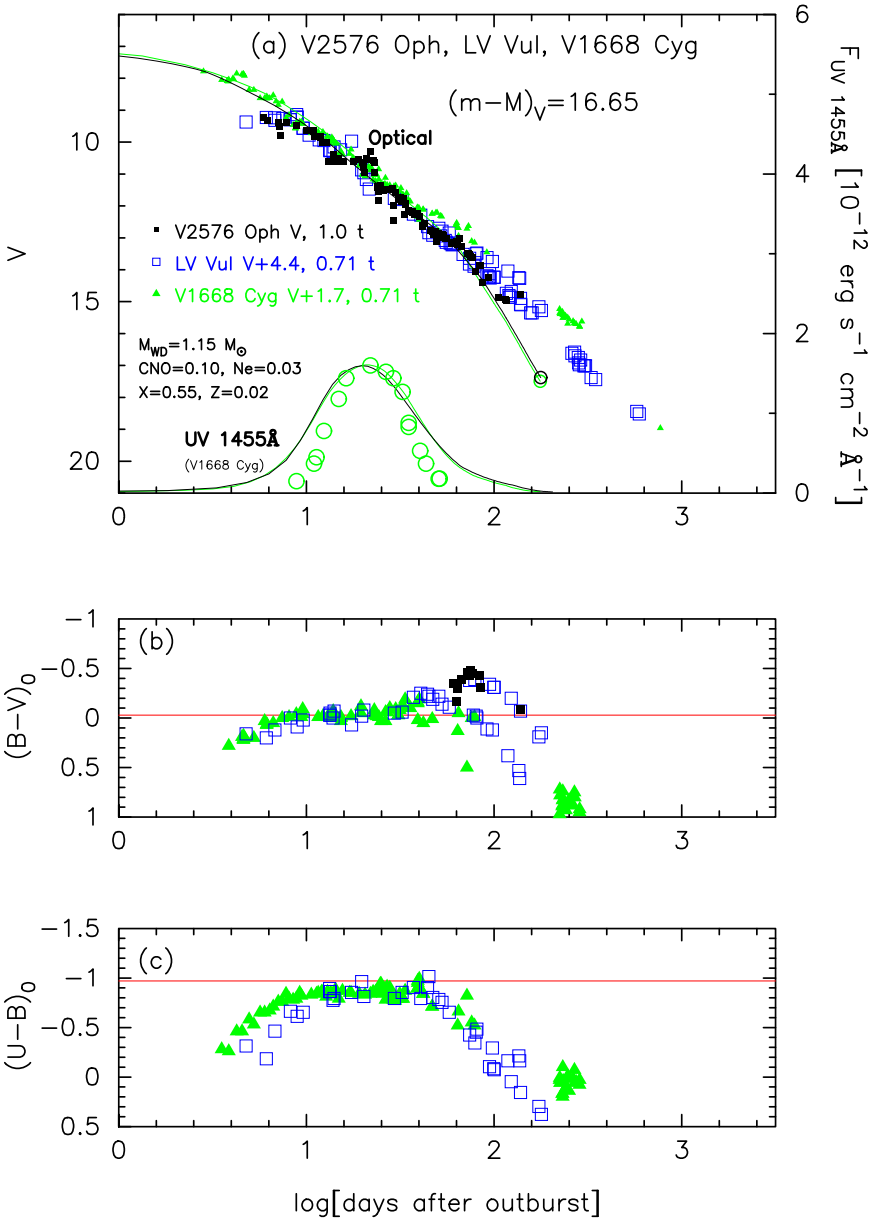

Figure 36. Same as Figure 30, but for V2576 Oph. We add the light/color curves of LV Vul and V1668 Cyg. The data of V2576 Oph are the same as those in Figure 35. We add model light curves of a 1.15 $M_\odot$ WD (Ne2, solid black lines; Hachisu & Kato 2010) for V2576 Oph and a 0.98 $M_\odot$ WD (CO3, solid green lines; Hachisu & Kato 2016a) for V1668 Cyg. The upper solid black and green lines denote the V light curves of photospheric plus free–free emission for the 1.15 $M_\odot$ WD for V2576 Oph and 0.98 $M_\odot$ WD for V1668 Cyg, respectively. The lower solid green lines represent the UV 1455 Å flux of the 0.98 $M_\odot$ WD based on the blackbody approximation (see, e.g., Hachisu & Kato 2016a).

We have $(m-M)_{V,\mathrm{V459\ Vul}} = 15.43 \pm 0.1$, which is consistent with Equation (55).

We apply Equation (10) for the I_C band to Figure 49(c) and obtain

$$\begin{aligned}(m-M)_{I,\mathrm{V459\ Vul}} &= ((m-M)_I + \Delta I_\mathrm{C})_{\mathrm{YY\ Dor}} - 2.5\log 3.7 \\ &= 18.67 - 3.2 \pm 0.3 - 1.43 = 14.04 \pm 0.3 \\ &= ((m-M)_I + \Delta I_\mathrm{C})_{\mathrm{LMC\ N\ 2009a}} - 2.5\log 2.3 \\ &= 18.67 - 3.7 \pm 0.3 - 0.93 = 14.04 \pm 0.3. \end{aligned} \quad (59)$$

Thus, we have $(m-M)_{I,\mathrm{V459\ Vul}} = 14.04 \pm 0.2$.

We plot $(m-M)_B = 16.35$, $(m-M)_V = 15.43$, and $(m-M)_I = 14.04$, which broadly cross at $d = 3.4$ kpc and $E(B-V) = 0.90$, in Figure 9(a). Thus, we obtain $E(B-V) = 0.90 \pm 0.05$ and $d = 3.4 \pm 0.5$ kpc.

A.10. V5579 Sgr 2008

Figure 50 shows (a) the V and B, and (b) $(B-V)_0$ evolutions of V5579 Sgr. Here, $(B-V)_0$ are dereddened with $E(B-V) = 0.82$ as obtained in Section 3.10. Figure 51 shows the light/color curves of V5579 Sgr as well as those of LV Vul, V1668 Cyg, and V1535 Sco. The data of V5579 Sgr are the same as those in Figure 50. The data of V1535 Sco are the

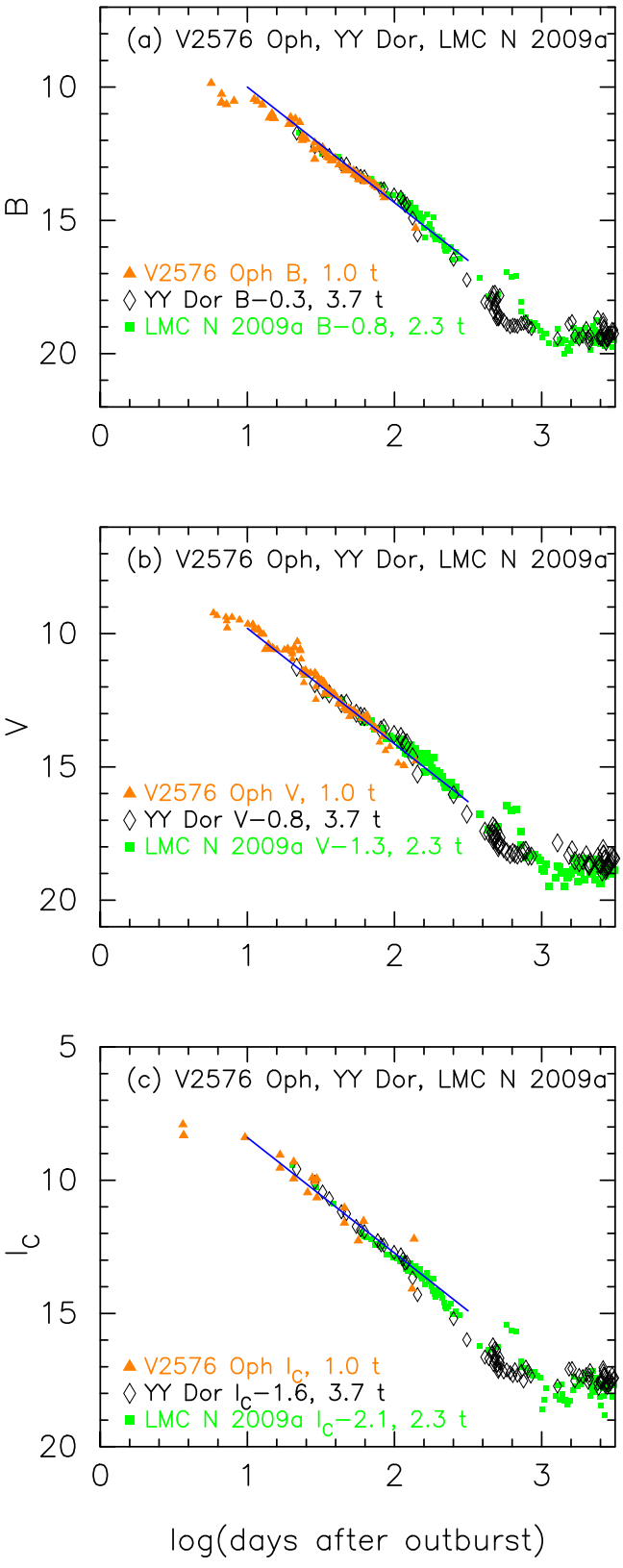

Figure 37. Same as Figure 25, but for V2576 Oph. The *BV* data of V2576 Oph are the same as those in Figure 35. The I_C data are taken from AAVSO and VSOLJ.

same as those in Figures 110 and 111. Applying Equation (6) to them, we have the relation

$$\begin{aligned}(m-M)_{V,\mathrm{V5579\ Sgr}} &= (m-M+\Delta V)_{V,\mathrm{LV\ Vul}} - 2.5\log 1.91\\ &= 11.85 + 4.8 \pm 0.2 - 0.7 = 15.95 \pm 0.2\\ &= (m-M+\Delta V)_{V,\mathrm{V1668\ Cyg}} - 2.5\log 1.91\\ &= 14.6 + 2.0 \pm 0.2 - 0.7 = 15.9 \pm 0.2\\ &= (m-M+\Delta V)_{V,\mathrm{V1535\ Sco}} - 2.5\log 0.79\\ &= 18.3 - 2.6 \pm 0.2 + 0.25 = 15.95 \pm 0.2, \end{aligned} \quad (60)$$

where we adopt $(m-M)_{V,\mathrm{V1535\ Sco}} = 18.3$ in Appendix A.29. Thus, we obtain $(m-M)_V = 15.95 \pm 0.1$ and $f_s = 1.91$ against LV Vul. From Equations (1), (6), and (60), we have the relation

$$\begin{aligned}(m-M')_{V,\mathrm{V5579\ Sgr}} &\equiv (m_V - (M_V - 2.5\log f_s))_{\mathrm{V5579\ Sgr}}\\ &= ((m-M)_V + \Delta V)_{\mathrm{LV\ Vul}}\\ &= 11.85 + 4.8 \pm 0.2 = 16.65 \pm 0.2. \end{aligned} \quad (61)$$

Figure 52 shows the *B*, *V*, and I_C light curves of V5579 Sgr together with those of V1368 Cen, YY Dor, and LMC N 2009a. We use the light curve of V1368 Cen in order to fill the gap between the light curves of YY Dor and LMC N 2009a and that of V5579 Sgr. We have already fixed the timescaling factor of V5579 Sgr, $f_s = 1.91$, against LV Vul, so we only shift the BVI_C light curves up and down, and overlap them with the other novae. Due to dust-shell formation, we only use the early-phase light-curve data. In Figure 52, we add straight solid red lines that represent the trend of the universal decline law, that is, the free–free emission model light curve decays as $F_\nu \propto t^{-1.75}$ (Hachisu & Kato 2006). We do overlap the light curves on the red lines as long as possible until the dust blackout starts. We apply Equation (9) for the *B* band to Figure 52(a) and obtain

$$\begin{aligned}(m-M)_{B,\mathrm{V5579\ Sgr}} &= ((m-M)_B + \Delta B)_{\mathrm{V1368\ Cen}} - 2.5\log 1.51\\ &= 18.53 - 1.3 \pm 0.2 - 0.45 = 16.78 \pm 0.2\\ &= ((m-M)_B + \Delta B)_{\mathrm{YY\ Dor}} - 2.5\log 10.0\\ &= 18.98 + 0.3 \pm 0.2 - 2.5 = 16.78 \pm 0.2\\ &= ((m-M)_B + \Delta B)_{\mathrm{LMC\ N\ 2009a}} - 2.5\log 6.3\\ &= 18.98 - 0.2 \pm 0.2 - 2.0 = 16.78 \pm 0.2. \end{aligned} \quad (62)$$

Thus, we have $(m-M)_{B,\mathrm{V5579\ Sgr}} = 16.78 \pm 0.1$.

For the *V* light curves in Figure 52(b), we similarly obtain

$$\begin{aligned}(m-M)_{V,\mathrm{V5579\ Sgr}} &= ((m-M)_V + \Delta V)_{\mathrm{V1368\ Cen}} - 2.5\log 1.51\\ &= 17.6 - 1.2 \pm 0.2 - 0.45 = 15.95 \pm 0.2\\ &= ((m-M)_V + \Delta V)_{\mathrm{YY\ Dor}} - 2.5\log 10.0\\ &= 18.86 - 0.4 \pm 0.2 - 2.5 = 15.96 \pm 0.2\\ &= ((m-M)_V + \Delta V)_{\mathrm{LMC\ N\ 2009a}} - 2.5\log 6.3\\ &= 18.86 - 0.9 \pm 0.2 - 2.0 = 15.96 \pm 0.2. \end{aligned} \quad (63)$$

We have $(m-M)_{V,\mathrm{V5579\ Sgr}} = 15.96 \pm 0.1$, which is consistent with Equation (60).

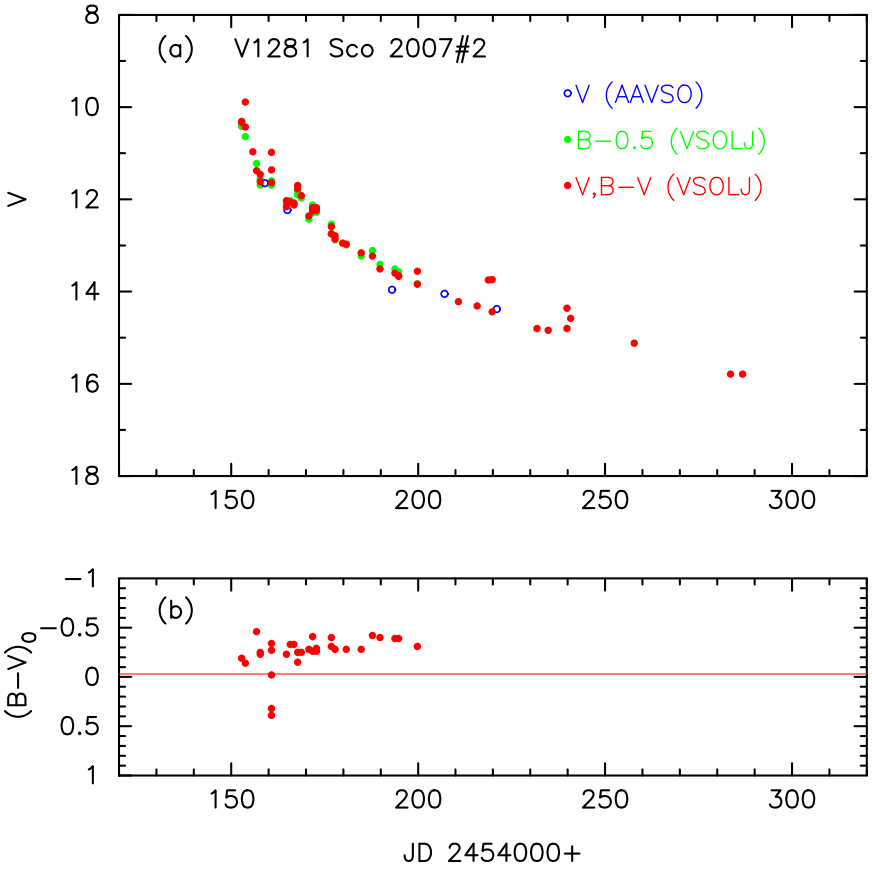

Figure 38. Same as Figure 23, but for V1281 Sco. (a) The V data are taken from AAVSO (blue unfilled circles) and VSOLJ (filled red circles). We also add the B magnitude (filled green circles) of VSOLJ, which are shifted up by 0.5 mag. (b) The $(B-V)_0$ are dereddened with $E(B-V)=0.82$.

We apply Equation (10) for the I_C band to Figure 52(c) and obtain

$$\begin{aligned}(m-M)_{I,\mathrm{V5579\ Sgr}} &= ((m-M)_I+\Delta I_C)_{\mathrm{V1368\ Cen}} - 2.5\log 1.51\\ &= 16.1 - 1.0\pm 0.2 - 0.45 = 14.65\pm 0.2\\ &= ((m-M)_I+\Delta I_C)_{\mathrm{YY\ Dor}} - 2.5\log 10.0\\ &= 18.67 - 1.5\pm 0.2 - 2.5 = 14.67\pm 0.2\\ &= ((m-M)_I+\Delta I_C)_{\mathrm{LMC\ N\ 2009a}} - 2.5\log 6.3\\ &= 18.67 - 2.0\pm 0.2 - 2.0 = 14.67\pm 0.2. \end{aligned} \quad (64)$$

Thus, we have $(m-M)_{I,\mathrm{V5579\ Sgr}}=14.67\pm 0.1$.

We plot $(m-M)_B=16.78$, $(m-M)_V=15.96$, and $(m-M)_I=14.67$, which cross at $d=4.8$ kpc and $E(B-V)=0.82$, in Figure 9(b). Thus, we obtain $E(B-V)=0.82\pm 0.05$ and $d=4.8\pm 0.5$ kpc.

A.11. V2670 Oph 2008#1

Figure 53 shows (a) the V and B, and (b) $(B-V)_0$ evolutions of V2670 Oph. Here, $(B-V)_0$ are dereddened with $E(B-V)=1.05$ as obtained in Section 3.11. Figure 54 shows the light/color curves of V2670 Oph and QU Vul. The timescales and V light curves of these two novae are very similar. The data of V2670 Oph are the same as those in Figure 53. The data of QU Vul are the same as those in Figure 10 of Hachisu & Kato (2016a). We added the UV 1455 Å light curves of QU Vul and PW Vul for comparison. The V light curves of V2670 Oph and QU Vul overlap each other. Applying Equation (6) to them, we have the relation

$$\begin{aligned}(m-M)_{V,\mathrm{V2670\ Oph}} &= (m-M+\Delta V)_{V,\mathrm{QU\ Vul}} - 2.5\log 1.0\\ &= 13.6 + 4.0\pm 0.3 - 0.0 = 17.6\pm 0.3, \end{aligned} \quad (65)$$

where we adopt $(m-M)_{V,\mathrm{QU\ Vul}}=13.6$ from Hachisu & Kato (2016a). Thus, we obtain $(m-M)_V=17.6\pm 0.3$ for V2670 Oph. The timescaling factor of QU Vul is $\log f_s=0.33$ against LV Vul, because the timescaling factor of PW Vul is $\log f_s=0.35$ against LV Vul and the timescaling factor of QU Vul is smaller by $\Delta\log f_s=-0.02$ than that of PW Vul.

Using $(m-M)_V=17.6$ and $\log f_s=0.33$ for V2670 Oph, we plot Figure 55. Here, we show three nova light/color curves, V2670 Oph, LV Vul, and V1668 Cyg. Applying Equation (6) to them, we have the relation

$$\begin{aligned}(m-M)_{V,\mathrm{V2670\ Oph}} &= (m-M+\Delta V)_{V,\mathrm{LV\ Vul}} - 2.5\log 2.1\\ &= 11.85 + 6.6\pm 0.3 - 0.83 = 17.62\pm 0.3\\ &= (m-M+\Delta V)_{V,\mathrm{V1668\ Cyg}} - 2.5\log 2.1\\ &= 14.6 + 3.8\pm 0.3 - 0.83 = 17.57\pm 0.3, \end{aligned} \quad (66)$$

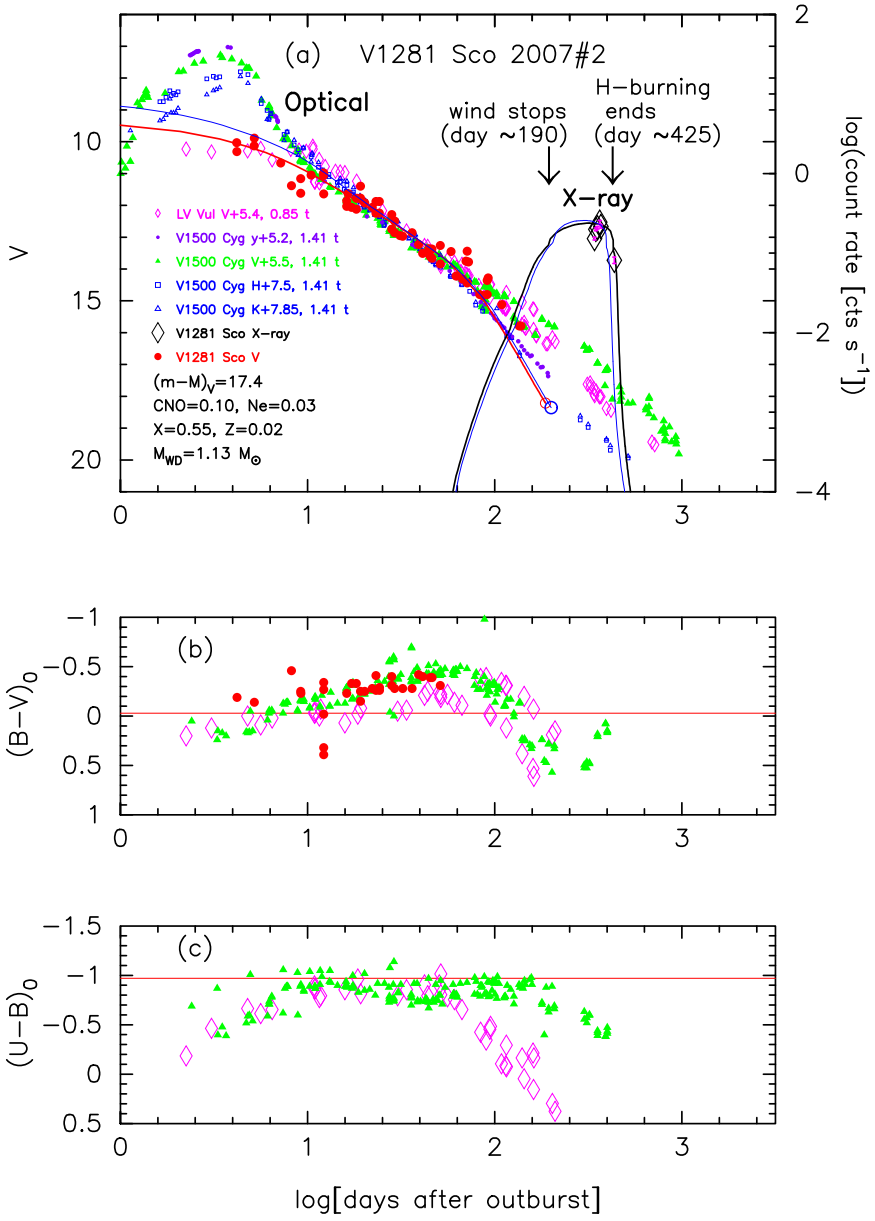

Figure 39. Same as Figure 30, but for V1281 Sco. We add the light/color curves of LV Vul and V1500 Cyg. The data of V1281 Sco are the same as those in Figure 38. Assuming $(m-M)_V = 17.4$, we added model light curves of a 1.13 $M_\odot$ WD (Ne2; Hachisu & Kato 2010). In panel (a), the solid red line denotes the V light curve of a photospheric plus free–free emission light curve while the solid black line represents the blackbody supersoft X-ray light curve, for the 1.13 $M_\odot$ WD. We also add the model light curve of a 1.20 $M_\odot$ WD (Ne2, thin solid blue lines), assuming $(m-M)_V = 12.3$ for V1500 Cyg.

where we adopt $(m-M)_{V,\mathrm{LV\ Vul}} = 11.85$ and $(m-M)_{V,\mathrm{V1668\ Cyg}} = 14.6$, both from Hachisu & Kato (2019). From Equations (1), (6), and (66), we have the relation

$$\begin{aligned}(m-M')_{V,\mathrm{V2670\ Oph}} &\equiv (m_V - (M_V - 2.5\log f_s))_{\mathrm{V2670\ Oph}} \\ &= ((m-M)_V + \Delta V)_{\mathrm{LV\ Vul}} \\ &= 11.85 + 6.6 \pm 0.3 = 18.45 \pm 0.3.\end{aligned} \tag{67}$$

Figure 56 shows the B, V, and I_C light curves of V2670 Oph together with those of QU Vul and NR TrA. We apply Equation (9) for the B band to Figure 56(a) and obtain

$$\begin{aligned}&(m-M)_{B,\mathrm{V2670\ Oph}} \\ &= ((m-M)_B + \Delta B)_{\mathrm{QU\ Vul}} - 2.5\log 1.0 \\ &= 14.15 + 4.5 \pm 0.3 - 0.0 = 18.65 \pm 0.3 \\ &= ((m-M)_B + \Delta B)_{\mathrm{NR\ TrA}} - 2.5\log 0.79 \\ &= 15.59 + 2.8 \pm 0.3 + 0.25 = 18.64 \pm 0.3,\end{aligned} \tag{68}$$

where we adopt $(m-M)_{B,\mathrm{QU\ Vul}} = 13.6 + 0.55 = 14.15$ from Hachisu & Kato (2016a) and $(m-M)_{B,\mathrm{NR\ TrA}} = 15.35 + 0.24 = 15.59$ in Appendix A.13. We obtain $(m-M)_{B,\mathrm{V2670\ Oph}} = 18.65 \pm 0.2$.

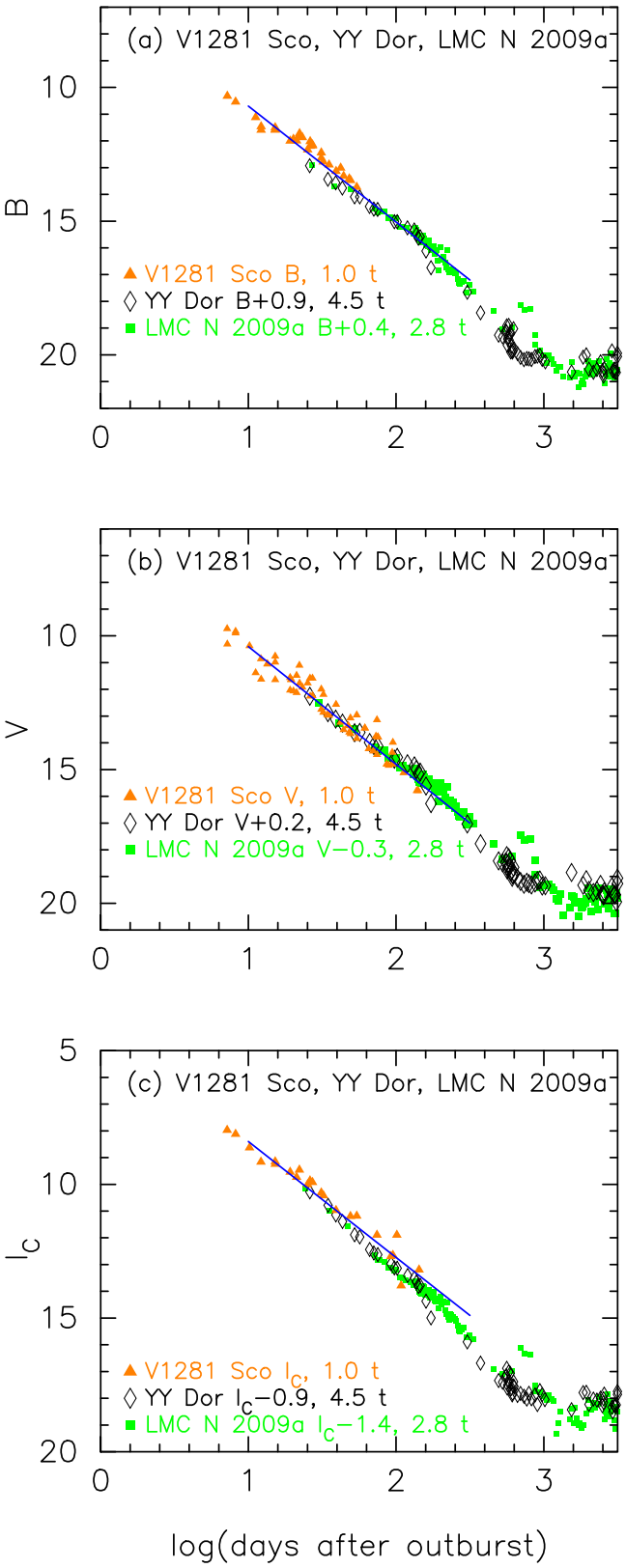

Figure 40. Same as Figure 25, but for V1281 Sco. The *BV* data of V1281 Sco are the same as those in Figure 38. The I_C data are taken from VSOLJ.

For the V light curves in Figure 63(b), we obtain

$$\begin{aligned}&(m-M)_{V,\text{V2670 Oph}}\\&=((m-M)_V+\Delta V)_{\text{QU Vul}}-2.5\log 1.0\\&=13.6+4.0\pm0.3-0.0=17.6\pm0.3\\&=((m-M)_V+\Delta V)_{\text{NR TrA}}-2.5\log 0.79\\&=15.35+2.0\pm0.3+0.25=17.6\pm0.3,\end{aligned}\tag{69}$$

where we adopt $(m-M)_{V,\text{QU Vul}}=13.6$ in Hachisu & Kato (2016a) and $(m-M)_{I,\text{NR TrA}}=15.35$ in Appendix A.13. We obtain $(m-M)_{V,\text{V2670 Oph}}=17.6\pm0.2$, which is consistent with Equations (65) and (66).

From the I_C-band data in Figure 56(c), we obtain

$$\begin{aligned}&(m-M)_{I,\text{V2670 Oph}}\\&=((m-M)_I+\Delta I_C)_{\text{QU Vul}}-2.5\log 1.0\\&=12.72+3.2\pm0.3-0.0=15.92\pm0.3\\&=((m-M)_I+\Delta I_C)_{\text{NR TrA}}-2.5\log 0.79\\&=14.97+0.7\pm0.3+0.25=15.92\pm0.3,\end{aligned}\tag{70}$$

where we adopt $(m-M)_{I,\text{QU Vul}}=13.6-1.6\times0.55=12.72$ and $(m-M)_{I,\text{NR TrA}}=15.35-1.6\times0.24=14.97$. We obtain $(m-M)_{I,\text{V2670 Oph}}=15.92\pm0.2$.

We plot $(m-M)_B=18.65$, $(m-M)_V=17.6$, and $(m-M)_I=15.92$, which broadly cross at $d=7.4$ kpc and $E(B-V)=1.05$, in Figure 9(c). Thus, we have $d=7.4\pm0.8$ kpc and $E(B-V)=1.05\pm0.1$.

A.12. QY Mus 2008

Figure 57 shows (a) the V and B, and (b) $(B-V)_0$ evolutions of QY Mus. Here, $(B-V)_0$ are dereddened with $E(B-V)=0.58$ as obtained in Section 3.12. The V light curve of QY Mus is very similar to that of V5666 Sgr. Therefore, we plot these two light/color curves in Figure 58 together with LV Vul. We overlap these three nova light/color curves. Applying Equation (6) to them, we have the relation

$$\begin{aligned}&(m-M)_{V,\text{QY Mus}}\\&=(m-M+\Delta V)_{V,\text{LV Vul}}-2.5\log 2.2\\&=11.85+3.7\pm0.2-0.88=14.67\pm0.2\\&=(m-M+\Delta V)_{V,\text{V5666 Sgr}}-2.5\log 1.26\\&=15.4-0.5\pm0.2-0.25=14.65\pm0.2,\end{aligned}\tag{71}$$

where we adopt $(m-M)_{V,\text{LV Vul}}=11.85$ and $(m-M)_{V,\text{V5666 Sgr}}=15.4$, both from Hachisu & Kato (2019). Thus, we adopt $(m-M)_V=14.65\pm0.1$ and $f_s=2.2$ against LV Vul. From Equations (1), (6), and (71), we have the relation

$$\begin{aligned}(m-M')_{V,\text{QY Mus}}&\equiv(m_V-(M_V-2.5\log f_s))_{\text{QY Mus}}\\&=((m-M)_V+\Delta V)_{\text{LV Vul}}\\&=11.85+3.7\pm0.2=15.55\pm0.2.\end{aligned}\tag{72}$$

Figure 59 shows the B, V, and I_C light curves of QY Mus together with those of V1369 Cen, V496 Sct, and V5666 Sgr.

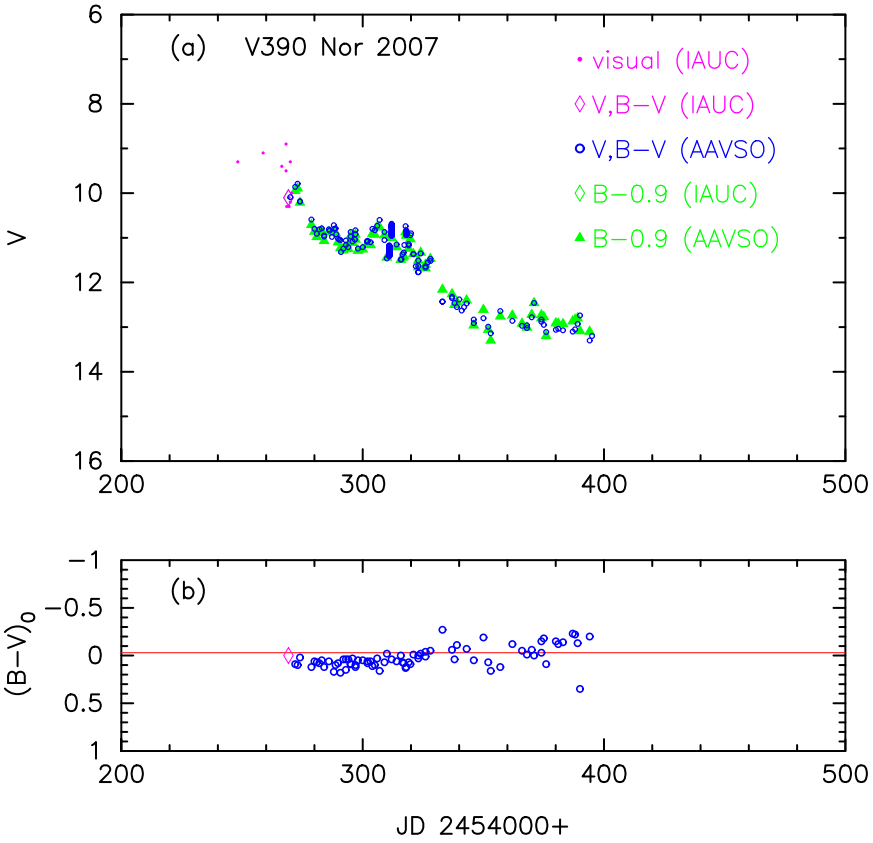

Figure 41. Same as Figure 23, but for V390 Nor. (a) The V (unfilled blue circles) and B (filled green triangles) data are taken from AAVSO. The visual (magenta dots), V (unfilled magenta diamonds), and B (unfilled green diamond) data are from IAU Circular 8850, 1. The B magnitudes are shifted up by 0.9 mag. (b) The $(B-V)_0$ are dereddened with $E(B-V)=0.89$.

The light curves overlap each other well. Applying Equation (9) for the B band to Figure 59(a), we have the relation

$$\begin{aligned}(m-M)_{B,\mathrm{QY\ Mus}} &= ((m-M)_B+\Delta B)_{\mathrm{V1369\ Cen}} - 2.5\log 1.51\\ &= 10.36+5.3\pm0.2-0.45=15.21\pm0.2\\ &= ((m-M)_B+\Delta B)_{\mathrm{V496\ Sct}} - 2.5\log 1.12\\ &= 14.15+1.2\pm0.2-0.13=15.22\pm0.2\\ &= ((m-M)_B+\Delta B)_{\mathrm{V5666\ Sgr}} - 2.5\log 1.26\\ &= 15.9-0.4\pm0.2-0.25=15.25\pm0.2, \end{aligned} \quad (73)$$

where we adopt $(m-M)_{B,\mathrm{V1369\ Cen}}=10.25+1.0\times0.11=10.36$, $(m-M)_{B,\mathrm{V496\ Sct}}=13.7+1.0\times0.45=14.15$, and $(m-M)_{B,\mathrm{V5666\ Sgr}}=15.4+1.0\times0.50=15.9$, all from Hachisu & Kato (2019). We obtain $(m-M)_B=15.23\pm0.1$ for QY Mus.

Applying Equation (6) to Figure 59(b), we have the relation

$$\begin{aligned}(m-M)_{V,\mathrm{QY\ Mus}} &= ((m-M)_V+\Delta V)_{\mathrm{V1369\ Cen}} - 2.5\log 1.51\\ &= 10.25+4.9\pm0.3-0.45=14.7\pm0.2\\ &= ((m-M)_V+\Delta V)_{\mathrm{V496\ Sct}} - 2.5\log 1.12\\ &= 13.7+1.1\pm0.3-0.13=14.67\pm0.2\\ &= ((m-M)_V+\Delta V)_{\mathrm{V5666\ Sgr}} - 2.5\log 1.26\\ &= 15.4-0.5\pm0.3-0.25=14.65\pm0.2, \end{aligned} \quad (74)$$

where we adopt $(m-M)_{V,\mathrm{V1369\ Cen}}=10.25$, $(m-M)_{V,\mathrm{V496\ Sct}}=13.7$, and $(m-M)_{V,\mathrm{V5666\ Sgr}}=15.4$, all from Hachisu & Kato (2019). We obtain $(m-M)_V=14.67\pm0.1$ for QY Mus, which is consistent with Equation (71).

From the I_C-band data in Figure 59(c), we obtain

$$\begin{aligned}(m-M)_{I,\mathrm{QY\ Mus}} &= ((m-M)_I+\Delta I_C)_{\mathrm{V1369\ Cen}} - 2.5\log 1.51\\ &= 10.07+4.1\pm0.2-0.45=13.72\pm0.2\\ &= ((m-M)_I+\Delta I_C)_{\mathrm{V496\ Sct}} - 2.5\log 1.12\\ &= 12.98+0.9\pm0.2-0.13=13.75\pm0.2\\ &= ((m-M)_I+\Delta I_C)_{\mathrm{V5666\ Sgr}} - 2.5\log 1.26\\ &= 14.6-0.6\pm0.2-0.25=13.75\pm0.2, \end{aligned} \quad (75)$$

where we adopt $(m-M)_{I,\mathrm{V1369\ Cen}}=10.25-1.6\times0.11=10.07$, $(m-M)_{I,\mathrm{V496\ Sct}}=13.7-1.6\times0.45=12.98$, and $(m-M)_{I,\mathrm{V5666\ Sgr}}=15.4-1.6\times0.50=14.6$. We obtain $(m-M)_{I,\mathrm{QY\ Mus}}=13.74\pm0.1$.

We plot $(m-M)_B=15.23$, $(m-M)_V=14.67$, and $(m-M)_I=13.74$, which cross at $d=3.7$ kpc and $E(B-V)=0.58$, in Figure 9(d). Thus, we obtain $d=3.7\pm0.4$ kpc and $E(B-V)=0.58\pm0.05$.

Our model light-curve fitting gives WD masses between $M_{\mathrm{WD}}=0.75$–$0.85\ M_\odot$ for the hydrogen content of $X=0.35$–0.55 by weight as shown in Figure 21 and as discussed in Section 4.2. It should also be noted that our model light curves reasonably reproduce the V light curve of QY Mus for $(m-M)_V=14.65\pm0.1$.

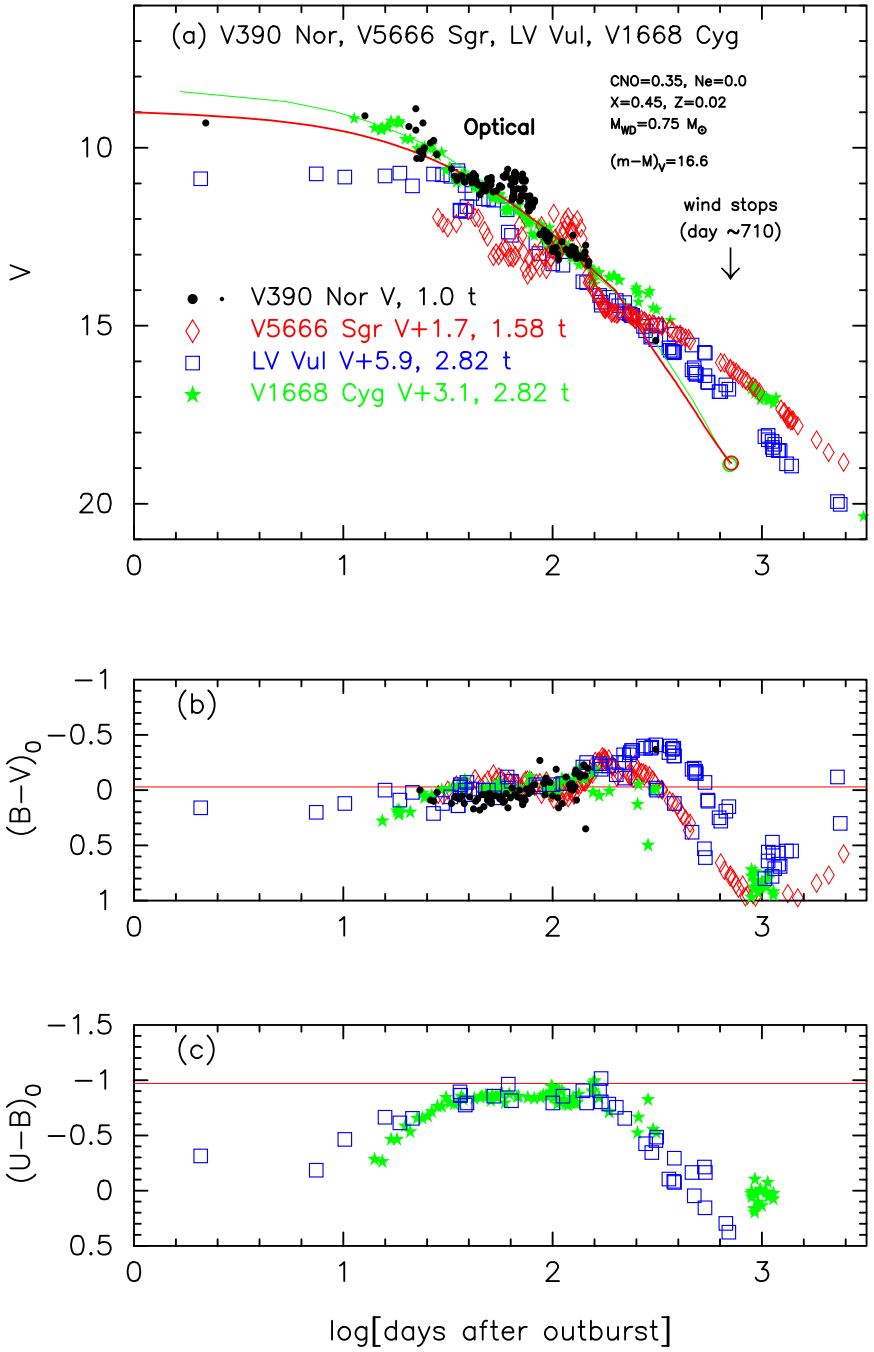

Figure 42. Same as Figure 30, but for V390 Nor. We add the light/color curves of V5666 Sgr, LV Vul, and V1668 Cyg. The data of V390 Nor are the same as those in Figure 41. The data of V5666 Sgr are the same as those in Figures 28 and 29 of Hachisu & Kato (2019). Assuming $(m-M)_V = 16.6$, we add the model light curve of a 0.75 $M_\odot$ WD (CO3, solid red line; Hachisu & Kato 2016a). We also add the model light curve of a 0.98 $M_\odot$ WD (CO3, solid green line), assuming that $(m-M)_V = 14.6$ for V1668 Cyg.

A.13. NR TrA 2008

Figure 60 shows (a) the V and B, and (b) $(B-V)_0$ evolutions of NR TrA. Here, $(B-V)_0$ are dereddened with $E(B-V) = 0.24$ as obtained in Section 3.13. We plot light curves of three novae, NR TrA, QU Vul, and V2670 Oph in Figure 61. The decay of the V light curve of NR TrA slowed down in the intermediate phase, and this slow decay is very similar to that of V2670 Oph and QU Vul. Applying Equation (6) to them, we have the relation

$$\begin{aligned}(m-M)_{V,\mathrm{NR\ TrA}} &= (m-M+\Delta V)_{V,\mathrm{QU\ Vul}} - 2.5\log 1.26 \\ &= 13.6 + 2.0 \pm 0.2 - 0.25 = 15.35 \pm 0.2 \\ &= (m-M+\Delta V)_{V,\mathrm{V2670\ Oph}} - 2.5\log 1.26 \\ &= 17.6 - 2.0 \pm 0.2 - 0.25 = 15.35 \pm 0.2, \end{aligned} \quad (76)$$

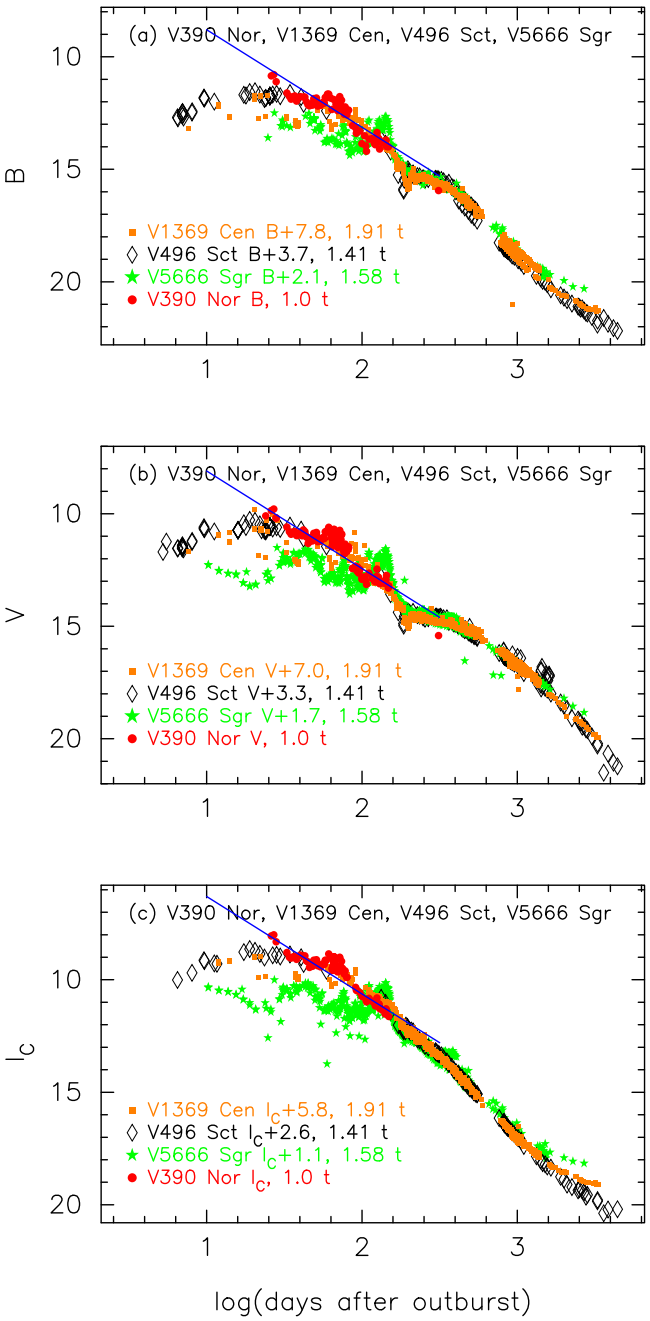

Figure 43. Same as Figure 25, but for V390 Nor. We plot the (a) B, (b) V, and (c) I_C light curves of V390 Nor as well as those of V1369 Cen, V496 Sct, and V5666 Sgr. The data of V1369 Cen, V496 Sct, and V5666 Sgr are the same as those in Figures 24, 25, 26, 28, 29, and 30 of Hachisu & Kato (2019). The straight solid blue line denotes the slope of $F_\nu \propto t^{-1.75}$. The BV data of V390 Nor are the same as those in Figure 41. The I_C data are taken from AAVSO.

where we adopt $(m-M)_{V,\mathrm{QU\ Vul}} = 13.6$ and $(m-M)_{V,\mathrm{V2670\ Oph}} = 17.6$, both from Appendix A.11. Thus, we adopt $(m-M)_V = 15.35 \pm 0.2$. The timescale of NR TrA is 1.26 times longer than those of QU Vul and V2670 Oph. This corresponds to $\log f_s = 0.43$ against LV Vul.

Using $(m-M)_V = 15.35$ and $\log f_s = 0.43$ for NR TrA, we plot Figure 62. Here, we show three nova light/color curves of NR TrA, LV Vul, and V1668 Cyg. The V light curve of NR TrA largely deviates from that of LV Vul and V1668 Cyg in the nebular phase during days 250–1000. Applying Equation (6) to them, we have the relation

$$\begin{aligned}(m-M)_{V,\mathrm{NR\ TrA}} &= (m-M+\Delta V)_{V,\mathrm{LV\ Vul}} - 2.5\log 2.7\\ &= 11.85 + 4.6 \pm 0.3 - 1.08 = 15.37 \pm 0.3\\ &= (m-M+\Delta V)_{V,\mathrm{V1668\ Cyg}} - 2.5\log 2.7\\ &= 14.6 + 1.8 \pm 0.3 - 1.08 = 15.32 \pm 0.3,\end{aligned} \quad (77)$$

where we adopt $(m-M)_{V,\mathrm{LV\ Vul}} = 11.85$ and $(m-M)_{V,\mathrm{V1668\ Cyg}} = 14.6$, both from Hachisu & Kato (2019). Thus, we adopt $(m-M)_V = 15.35 \pm 0.2$ and $f_s = 2.7$ against LV Vul. From Equations (1), (6), and (77), we have the relation

$$\begin{aligned}(m-M')_{V,\mathrm{NR\ TrA}} &\equiv (m_V - (M_V - 2.5\log f_s))_{\mathrm{NR\ TrA}}\\ &= ((m-M)_V + \Delta V)_{\mathrm{LV\ Vul}}\\ &= 11.85 + 4.6 \pm 0.3 = 16.45 \pm 0.3.\end{aligned} \quad (78)$$

Figure 63 shows the B, V, and I_C light curves of NR TrA together with those of QU Vul and V2670 Oph. We apply Equation (9) for the B band to Figure 63(a) and obtain

$$\begin{aligned}&(m-M)_{B,\mathrm{NR\ TrA}}\\ &= ((m-M)_B + \Delta B)_{\mathrm{QU\ Vul}} - 2.5\log 1.26\\ &= 14.15 + 1.7 \pm 0.3 - 0.25 = 15.6 \pm 0.3\\ &= ((m-M)_B + \Delta B)_{\mathrm{V2670\ Oph}} - 2.5\log 1.26\\ &= 18.65 - 2.8 \pm 0.3 - 0.25 = 15.6 \pm 0.3,\end{aligned} \quad (79)$$

where we adopt $(m-M)_{B,\mathrm{QU\ Vul}} = 14.15$ and $(m-M)_{B,\mathrm{V2670\ Oph}} = 17.6 + 1.05 = 18.65$ from Appendix A.11. We have $(m-M)_{B,\mathrm{NR\ TrA}} = 15.6 \pm 0.3$.

For the V band, Figure 63(b) is essentially the same as Figure 61, giving $(m-M)_{V,\mathrm{NR\ TrA}} = 15.35 \pm 0.2$.

From the I_C-band data in Figure 63(c), we obtain

$$\begin{aligned}&(m-M)_{I,\mathrm{NR\ TrA}}\\ &= ((m-M)_I + \Delta I_C)_{\mathrm{QU\ Vul}} - 2.5\log 1.26\\ &= 12.72 + 2.5 \pm 0.3 - 0.25 = 14.97 \pm 0.3\\ &= ((m-M)_I + \Delta I_C)_{\mathrm{V2670\ Oph}} - 2.5\log 1.26\\ &= 15.92 - 0.7 \pm 0.3 - 0.25 = 14.97 \pm 0.3,\end{aligned} \quad (80)$$

where we adopt $(m-M)_{I,\mathrm{QU\ Vul}} = 13.6 - 1.6 \times 0.55 = 12.72$ and $(m-M)_{I,\mathrm{V2670\ Oph}} = 17.6 - 1.6 \times 1.05 = 15.92$. We have $(m-M)_{I,\mathrm{NR\ TrA}} = 14.97 \pm 0.2$.

We plot $(m-M)_B = 15.6$, $(m-M)_V = 15.35$, and $(m-M)_I = 14.97$, which cross at $d = 8.3$ kpc and $E(B-V) = 0.24$, in Figure 11(a). Thus, we obtain $d = 8.3 \pm 1.0$ kpc and $E(B-V) = 0.24 \pm 0.05$.

A.14. V1213 Cen 2009

Figure 64 shows (a) the V and B, and (b) $(B-V)_0$ evolutions of V1213 Cen. Here, $(B-V)_0$ are dereddened with $E(B-V) = 0.78$ as obtained in Section 3.14. We plot light curves of three novae, V1213 Cen, LV Vul, and V4743 Sgr in Figure 65. The shape of the V light curve of V1213 Cen is very similar to

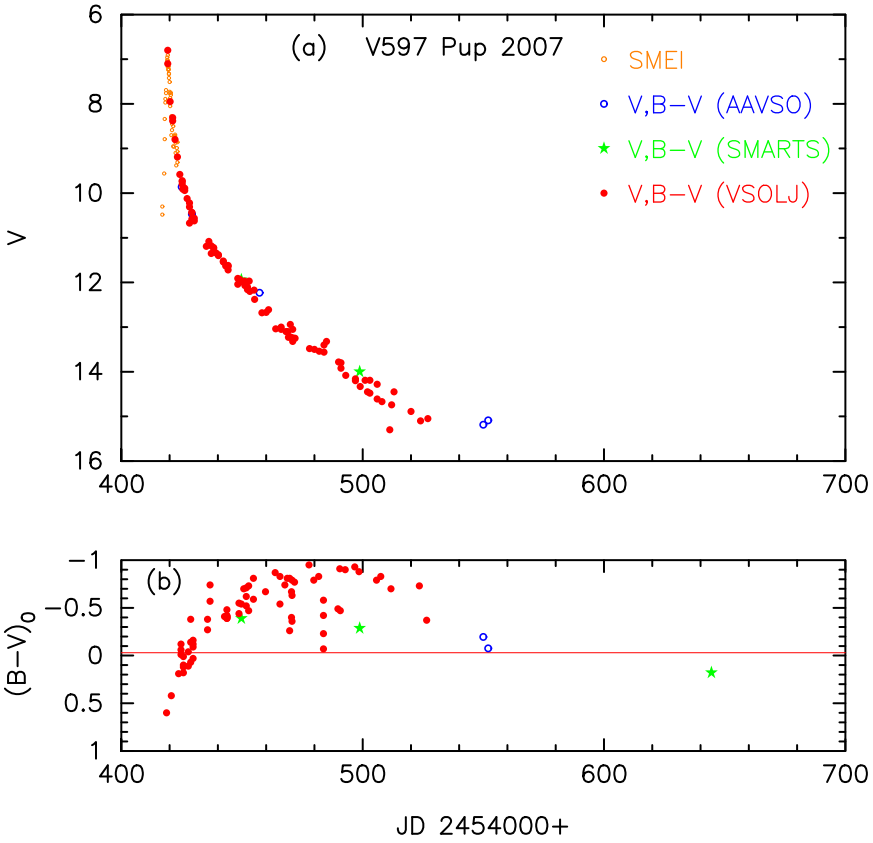

Figure 44. Same as Figure 23, but for V597 Pup. (a) The *BV* data (unfilled blue circles, filled green stars, and filled red circles) are taken from AAVSO, SMARTS, and VSOLJ, respectively. We also add the data of *SMEI* (small unfilled orange circles). (b) The $(B-V)_0$ are dereddened with $E(B-V)=0.24$.

V4743 Sgr. Applying Equation (6) to them, we have

$$\begin{aligned}(m-M)_{V,\mathrm{V1213\ Cen}} &= (m-M+\Delta V)_{V,\mathrm{LV\ Vul}} - 2.5\log 1.12 \\ &= 11.85 + 5.2 \pm 0.3 - 0.13 = 16.92 \pm 0.3 \\ &= (m-M+\Delta V)_{V,\mathrm{V4743\ Sgr}} - 2.5\log 2.0 \\ &= 13.7 + 4.0 \pm 0.3 - 0.75 = 16.95 \pm 0.3, \end{aligned} \quad (81)$$

where we adopt $(m-M)_{V,\mathrm{LV\ Vul}} = 11.85$ from Hachisu & Kato (2019) and $(m-M)_{V,\mathrm{V4743\ Sgr}} = 13.7$ from Hachisu & Kato (2010). Thus, we obtain $(m-M)_V = 16.95 \pm 0.2$ and $f_\mathrm{s} = 1.12$ against LV Vul. From Equations (1), (6), and (81), we have the relation

$$\begin{aligned}(m-M')_{V,\mathrm{V1213\ Cen}} &\equiv (m_V - (M_V - 2.5\log f_\mathrm{s}))_{\mathrm{V1213\ Cen}} \\ &= ((m-M)_V + \Delta V)_{\mathrm{LV\ Vul}} \\ &= 11.85 + 5.2 \pm 0.3 = 17.05 \pm 0.3. \end{aligned} \quad (82)$$

Figure 66 shows the *B*, *V*, and I_C light curves of V1213 Cen together with those of V382 Vel, YY Dor, and LMC N 2009a. We regard the extension of YY Dor and LMC N 2009a light curves and V382 Vel light curve to overlap with that of V1213 Cen. We apply Equation (9) for the *B* band to Figure 66(a) and obtain

$$\begin{aligned}(m-M)_{B,\mathrm{V1213\ Cen}} &= ((m-M)_B + \Delta B)_{\mathrm{V382\ Vel}} - 2.5\log 2.2 \\ &= 11.75 + 6.8 \pm 0.2 - 0.85 = 17.7 \pm 0.2 \\ &= ((m-M)_B + \Delta B)_{\mathrm{YY\ Dor}} - 2.5\log 5.9 \\ &= 18.98 + 0.7 \pm 0.2 - 1.92 = 17.76 \pm 0.2 \\ &= ((m-M)_B + \Delta B)_{\mathrm{LMC\ N\ 2009a}} - 2.5\log 3.7 \\ &= 18.98 + 0.2 \pm 0.2 - 1.42 = 17.76 \pm 0.2, \end{aligned} \quad (83)$$

where we adopt $(m-M)_{B,\mathrm{V382\ Vel}} = 11.5 + 0.25 = 11.75$ and $\log f_\mathrm{s} = -0.29$ against LV Vul for V382 Vel from Hachisu & Kato (2019). Thus, we have $(m-M)_{B,\mathrm{V1213\ Cen}} = 17.74 \pm 0.1$.

For the *V* light curves in Figure 66(b), we similarly obtain

$$\begin{aligned}(m-M)_{V,\mathrm{V1213\ Cen}} &= ((m-M)_V + \Delta V)_{\mathrm{V382\ Vel}} - 2.5\log 2.2 \\ &= 11.5 + 6.3 \pm 0.2 - 0.85 = 16.95 \pm 0.2 \\ &= ((m-M)_V + \Delta V)_{\mathrm{YY\ Dor}} - 2.5\log 5.9 \\ &= 18.86 + 0.0 \pm 0.2 - 1.92 = 16.94 \pm 0.2 \\ &= ((m-M)_V + \Delta V)_{\mathrm{LMC\ N\ 2009a}} - 2.5\log 3.7 \\ &= 18.86 - 0.5 \pm 0.2 - 1.42 = 16.94 \pm 0.2. \end{aligned} \quad (84)$$

We have $(m-M)_{V,\mathrm{V1213\ Cen}} = 16.95 \pm 0.1$, which is consistent with Equation (81).

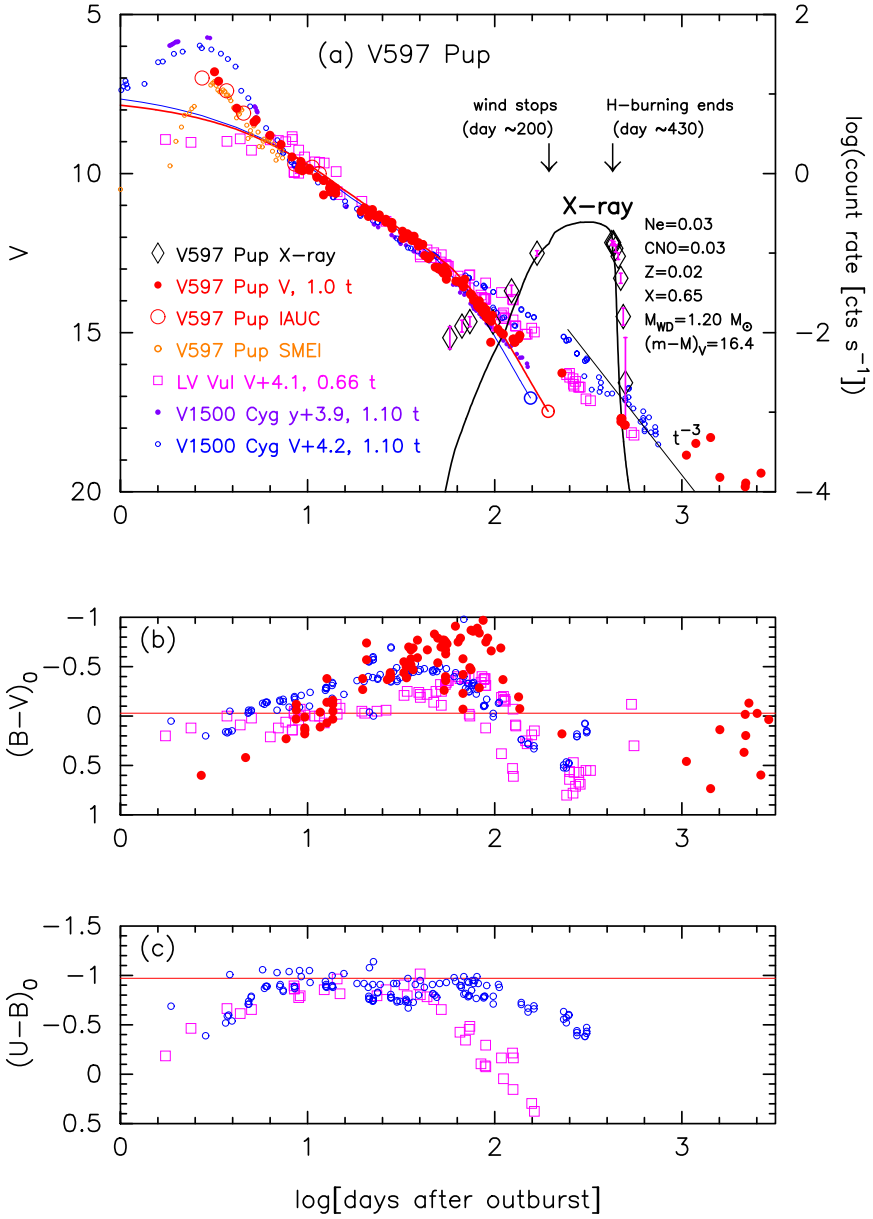

Figure 45. Same as Figure 30, but for V597 Pup. We add the light/color curves of LV Vul and V1500 Cyg. The data of V597 Pup are the same as those in Figure 44. In panel (a), assuming that $(m-M)_V = 16.4$ for V597 Pup, we added model light curves of a 1.2 $M_\odot$ WD (Ne3; Hachisu & Kato 2016a). The solid red line denotes the V light curves of blackbody plus free–free emission while the solid black line represents the blackbody supersoft X-ray light curve of the 1.2 $M_\odot$ WD. Assuming that $(m-M)_V = 12.3$ for V1500 Cyg, we add a 1.2 $M_\odot$ WD (Ne2) with the solid blue line.

We apply Equation (10) for the I_C band to Figure 66(c) and obtain

$$\begin{aligned}(m-M)_{I,\mathrm{V1213\ Cen}} &= ((m-M)_I + \Delta I_C)_{\mathrm{V382\ Vel}} - 2.5\log 2.2 \\ &= 11.1 + 5.5 \pm 0.2 - 0.85 = 15.75 \pm 0.2 \\ &= ((m-M)_I + \Delta I_C)_{\mathrm{YY\ Dor}} - 2.5\log 5.9 \\ &= 18.67 - 1.0 \pm 0.2 - 1.92 = 15.75 \pm 0.2 \\ &= ((m-M)_I + \Delta I_C)_{\mathrm{LMC\ N\ 2009a}} - 2.5\log 3.7 \\ &= 18.67 - 1.5 \pm 0.2 - 1.42 = 15.75 \pm 0.2, \end{aligned} \quad (85)$$

where we adopt $(m-M)_{I,\mathrm{V382\ Vel}} = 11.5 - 1.6 \times 0.25 = 11.1$ from Hachisu & Kato (2019). We have $(m-M)_{I,\mathrm{V1213\ Cen}} = 15.75 \pm 0.1$.

We plot $(m-M)_B = 17.74$, $(m-M)_V = 16.95$, and $(m-M)_I = 15.75$, which broadly cross at $d = 8.1$ kpc and $E(B-V) = 0.78$, in Figure 11(b). Thus, we have $E(B-V) = 0.78 \pm 0.05$ and $d = 8.1 \pm 1$ kpc.

A.15. V5583 Sgr 2009#3

Figure 67 shows (a) the visual and V, and (b) $(B-V)_0$ evolutions of V5583 Sgr. Here, $(B-V)_0$ are dereddened with $E(B-V) = 0.30$ as obtained in Section 3.15. Figure 68 shows the light/color curves of three novae, V5583 Sgr, LV Vul, and V382 Vel. The shape of the V light curve of V5583 Sgr is very similar to that of V382 Vel (Hachisu et al. 2009). The timescale of V382 Vel is almost the same as that of V5583 Sgr.

Applying Equation (6) to them, we have the relation

$$\begin{aligned}(m-M)_{V,\mathrm{V5583\ Sgr}} &= (m-M+\Delta V)_{V,\mathrm{LV\ Vul}} - 2.5\log 0.51\\ &= 11.85 + 3.7 \pm 0.2 + 0.73 = 16.28 \pm 0.2\\ &= (m-M+\Delta V)_{V,\mathrm{V382\ Vel}} - 2.5\log 1.0\\ &= 11.5 + 4.8 \pm 0.2 - 0.0 = 16.3 \pm 0.2, \end{aligned} \quad (86)$$

where we adopt $(m-M)_{V,\mathrm{LV\ Vul}} = 11.85$ and $(m-M)_{V,\mathrm{V382\ Vel}} = 11.5$, both from Hachisu & Kato (2019). Thus, we adopt $(m-M)_V = 16.3 \pm 0.1$ and $f_s = 0.51$ against LV Vul. From Equations (1), (6), and (86), we have the relation

$$\begin{aligned}(m-M')_{V,\mathrm{V5583\ Sgr}} &\equiv (m_V - (M_V - 2.5\log f_s))_{\mathrm{V5583\ Sgr}}\\ &= ((m-M)_V + \Delta V)_{\mathrm{LV\ Vul}}\\ &= 11.85 + 3.7 \pm 0.2 = 15.55 \pm 0.2. \end{aligned} \quad (87)$$

Figure 69 shows the B, V, and I_C light curves of V5583 Sgr together with those of YY Dor and LMC N 2009a. We regard the extension of the YY Dor and LMC N 2009a light curves to overlap with that of V5583 Sgr. We apply Equation (9) for the B band to Figure 69(a) and obtain

$$\begin{aligned}(m-M)_{B,\mathrm{V5583\ Sgr}} &= ((m-M)_B + \Delta B)_{\mathrm{YY\ Dor}} - 2.5\log 2.7\\ &= 18.98 - 1.3 \pm 0.2 - 1.08 = 16.6 \pm 0.2\\ &= ((m-M)_B + \Delta B)_{\mathrm{LMC\ N\ 2009a}} - 2.5\log 1.7\\ &= 18.98 - 1.8 \pm 0.2 - 0.58 = 16.6 \pm 0.2. \end{aligned} \quad (88)$$

We have $(m-M)_{B,\mathrm{V5583\ Sgr}} = 16.6 \pm 0.1$.

For the V light curves in Figure 69(b), we similarly obtain

$$\begin{aligned}(m-M)_{V,\mathrm{V5583\ Sgr}} &= ((m-M)_V + \Delta V)_{\mathrm{YY\ Dor}} - 2.5\log 2.7\\ &= 18.86 - 1.5 \pm 0.2 - 1.08 = 16.28 \pm 0.2\\ &= ((m-M)_V + \Delta V)_{\mathrm{LMC\ N\ 2009a}} - 2.5\log 1.7\\ &= 18.86 - 2.0 \pm 0.2 - 0.58 = 16.28 \pm 0.2. \end{aligned} \quad (89)$$

We have $(m-M)_{V,\mathrm{V5583\ Sgr}} = 16.28 \pm 0.1$, which is consistent with Equation (86).

We apply Equation (10) for the I_C band to Figure 69(c) and obtain

$$\begin{aligned}(m-M)_{I,\mathrm{V5583\ Sgr}} &= ((m-M)_I + \Delta I_C)_{\mathrm{YY\ Dor}} - 2.5\log 2.7\\ &= 18.67 - 1.8 \pm 0.2 - 1.08 = 15.79 \pm 0.2\\ &= ((m-M)_I + \Delta I_C)_{\mathrm{LMC\ N\ 2009a}} - 2.5\log 1.7\\ &= 18.67 - 2.3 \pm 0.2 - 0.58 = 15.79 \pm 0.2. \end{aligned} \quad (90)$$

We have $(m-M)_{I,\mathrm{V5583\ Sgr}} = 15.79 \pm 0.1$.

We plot $(m-M)_B = 16.6$, $(m-M)_V = 16.28$, and $(m-M)_I = 15.79$, which broadly cross at $d = 12$ kpc and $E(B-V) = 0.30$, in Figure 11(c). Thus, we have $E(B-V) = 0.30 \pm 0.05$ and $d = 12 \pm 2$ kpc.

A.16. V5584 Sgr 2009#4

Figure 70 shows (a) the V and B magnitudes, and (b) $(B-V)_0$ evolutions of V5584 Sgr. Here, $(B-V)_0$ are

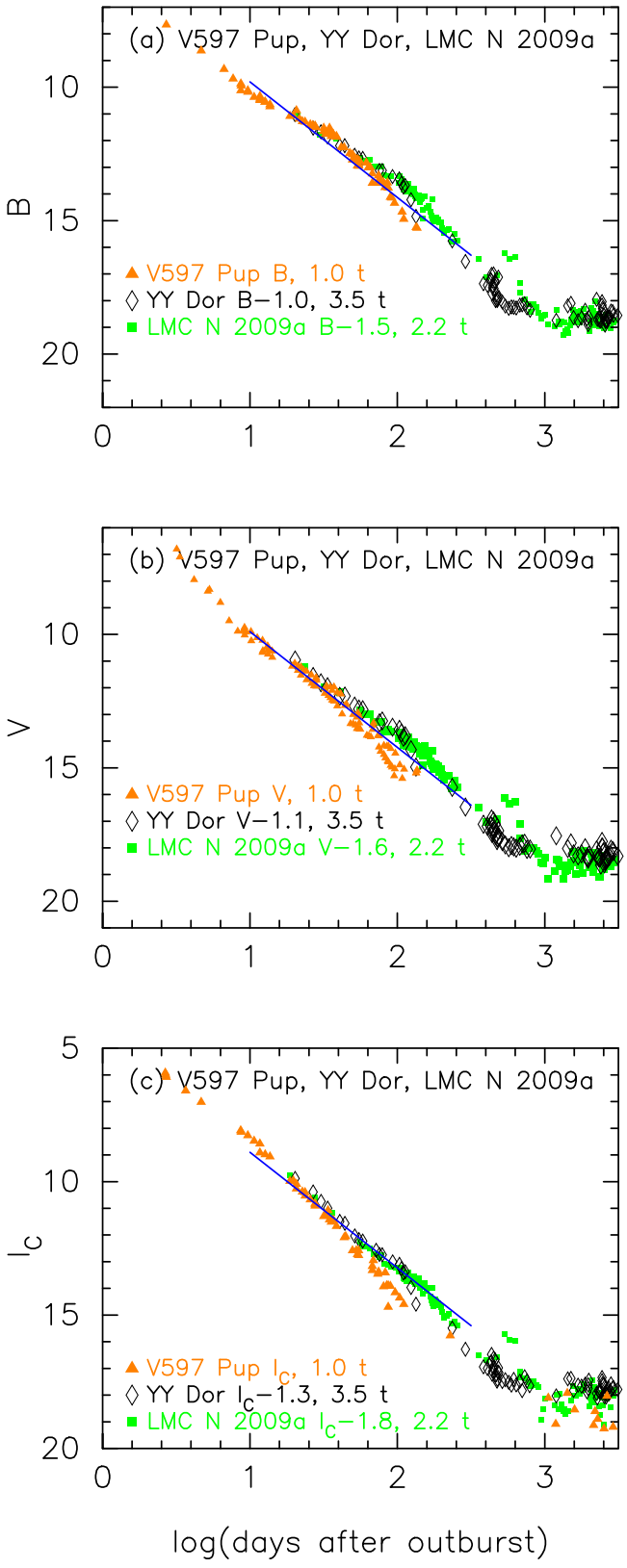

Figure 46. Same as Figure 25, but for V597 Pup. The *BV* data of V597 Pup are the same as those in Figure 44. The I_C data are taken from VSOLJ and SMARTS.

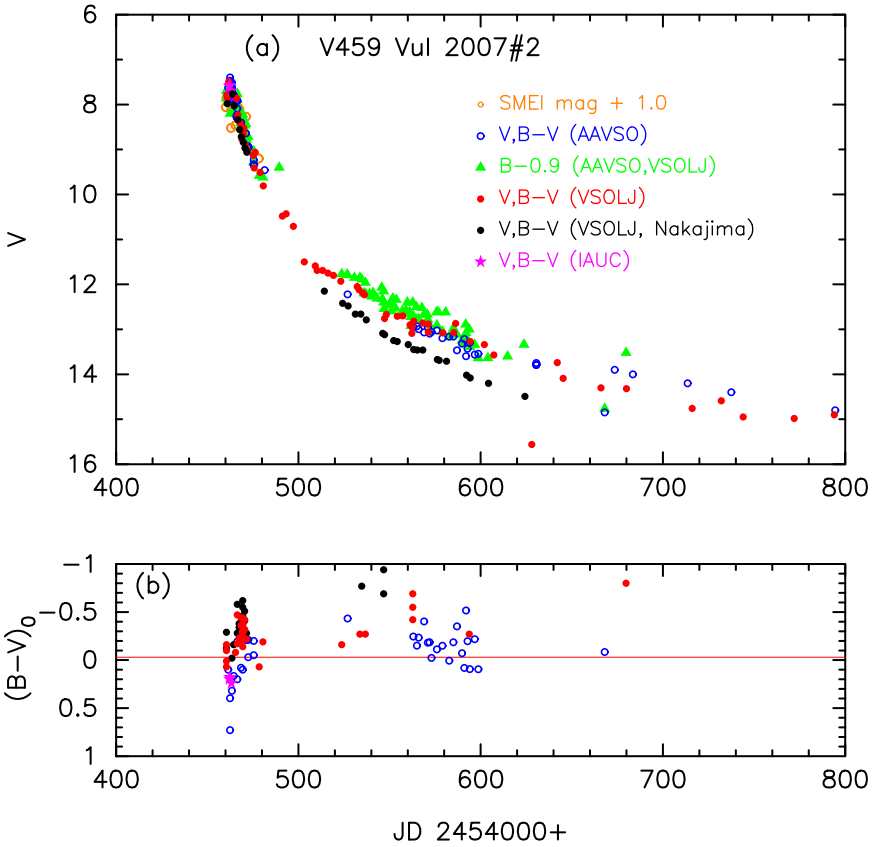

Figure 47. Same as Figure 23, but for V459 Vul. (a) The V (unfilled blue circles) and B (filled green triangles) data are taken from AAVSO. The V excluding Nakajima's data (filled red circles), V of Nakajima's data (filled black circles), and B (filled green triangles) data are from VSOLJ. The *SMEI* data (unfilled orange circles) are also plotted. (b) The $(B-V)_0$ are dereddened with $E(B-V)=0.90$.

dereddened with $E(B-V)=0.70$ as obtained in Section 3.16. Figure 71 shows the light/color curves of V5584 Sgr, LV Vul, V533 Her, V2615 Oph, and V496 Sct. Applying Equation (6) to them, we have the relation

$$\begin{aligned}(m-M)_{V,\mathrm{V5584\ Sgr}} &= (m-M+\Delta V)_{V,\mathrm{LV\ Vul}} - 2.5\log 1.35\\ &= 11.85 + 5.2 \pm 0.2 - 0.33 = 16.72 \pm 0.2\\ &= (m-M+\Delta V)_{V,\mathrm{V533\ Her}} - 2.5\log 1.12\\ &= 10.65 + 6.2 \pm 0.2 - 0.13 = 16.72 \pm 0.2\\ &= (m-M+\Delta V)_{V,\mathrm{V2615\ Oph}} - 2.5\log 0.85\\ &= 15.95 + 0.6 \pm 0.2 + 0.18 = 16.73 \pm 0.2\\ &= (m-M+\Delta V)_{V,\mathrm{V496\ Sct}} - 2.5\log 0.68\\ &= 13.7 + 2.6 \pm 0.2 + 0.43 = 16.73 \pm 0.2, \end{aligned} \quad (91)$$

where we adopt $(m-M)_{V,\mathrm{LV\ Vul}}=11.85$, $(m-M)_{V,\mathrm{V533\ Her}}=10.65$, $(m-M)_{V,\mathrm{V2615\ Oph}}=15.95$, and $(m-M)_{V,\mathrm{V496\ Sct}}=13.7$ from Hachisu & Kato (2019). Thus, we obtain $(m-M)_V=16.7\pm0.1$ and $f_s=1.35$ against LV Vul. From Equations (1), (6), and (91), we have the relation

$$\begin{aligned}(m-M')_{V,\mathrm{V5584\ Sgr}} &\equiv (m_V-(M_V-2.5\log f_s))_{\mathrm{V5584\ Sgr}}\\ &= ((m-M)_V+\Delta V)_{\mathrm{LV\ Vul}}\\ &= 11.85 + 5.2 \pm 0.2 = 17.05 \pm 0.2. \end{aligned} \quad (92)$$

Figure 72 shows the B, V, and I_C light curves of V5584 Sgr together with those of LV Vul, V1668 Cyg, and V679 Car. We apply Equation (9) for the B band to Figure 72(a) and obtain

$$\begin{aligned}(m-M)_{B,\mathrm{V5584\ Sgr}} &= ((m-M)_B+\Delta B)_{\mathrm{LV\ Vul}} - 2.5\log 1.35\\ &= 12.45 + 5.3 \pm 0.2 - 0.33 = 17.42 \pm 0.2\\ &= ((m-M)_B+\Delta B)_{\mathrm{V1668\ Cyg}} - 2.5\log 1.35\\ &= 14.9 + 2.8 \pm 0.2 - 0.33 = 17.37 \pm 0.2\\ &= ((m-M)_B+\Delta B)_{\mathrm{V679\ Car}} - 2.5\log 1.35\\ &= 16.79 + 0.9 \pm 0.2 - 0.33 = 17.36 \pm 0.2, \end{aligned} \quad (93)$$

where we adopt $(m-M)_{B,\mathrm{LV\ Vul}}=11.85+0.60=12.45$, $(m-M)_{B,\mathrm{V1668\ Cyg}}=14.6+0.30=14.9$, and $(m-M)_{B,\mathrm{V679\ Car}}=16.1+0.69=16.79$, all from Hachisu & Kato (2019). We have $(m-M)_{B,\mathrm{V5584\ Sgr}}=17.39\pm0.1$.

For the V light curves in Figure 72(b), we similarly obtain

$$\begin{aligned}(m-M)_{V,\mathrm{V5584\ Sgr}} &= ((m-M)_V+\Delta V)_{\mathrm{LV\ Vul}} - 2.5\log 1.35\\ &= 11.85 + 5.2 \pm 0.2 - 0.33 = 16.72 \pm 0.2\\ &= ((m-M)_V+\Delta V)_{\mathrm{V1668\ Cyg}} - 2.5\log 1.35\\ &= 14.6 + 2.4 \pm 0.2 - 0.33 = 16.67 \pm 0.2\\ &= ((m-M)_V+\Delta V)_{\mathrm{V679\ Car}} - 2.5\log 1.35\\ &= 16.1 + 0.9 \pm 0.2 - 0.33 = 16.67 \pm 0.2, \end{aligned} \quad (94)$$

where we adopt $(m-M)_{V,\mathrm{V679\ Car}}=16.1$ from Hachisu & Kato (2019). We have $(m-M)_{V,\mathrm{V5584\ Sgr}}=16.69\pm0.1$, which is consistent with Equation (91).

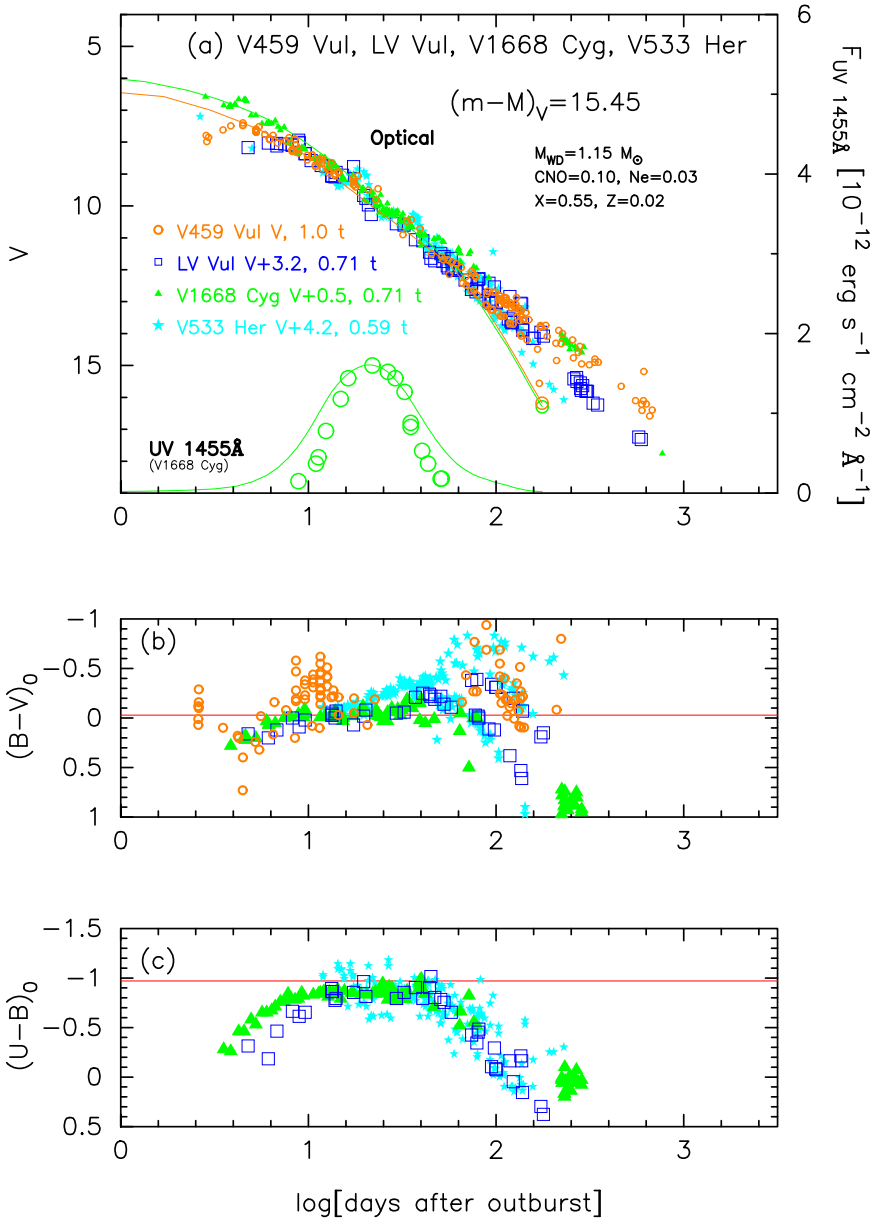

Figure 48. Same as Figure 30, but for V459 Vul. We add the light/color curves of LV Vul, V1668 Cyg, and V533 Her. The data of V459 Vul are the same as those in Figure 47. We added model light curves (solid orange lines) of a 1.15 $M_\odot$ WD (Ne2; Hachisu & Kato 2010), assuming that $(m-M)_V = 15.45$ for V459 Vul. We also add a 0.98 $M_\odot$ WD (CO3, solid green lines; Hachisu & Kato 2016a), assuming that $(m-M)_V = 14.6$ for V1668 Cyg.

We apply Equation (10) for the I_C band to Figure 72(c) and obtain

$$\begin{aligned}(m-M)_{I,\mathrm{V5584\ Sgr}} &= ((m-M)_I + \Delta I_C)_{\mathrm{V1668\ Cyg}} - 2.5\log 1.35 \\ &= 14.12 + 1.8 \pm 0.2 - 0.33 = 15.59 \pm 0.2 \\ &= ((m-M)_I + \Delta I_C)_{\mathrm{V679\ Car}} - 2.5\log 1.35 \\ &= 15.0 + 0.9 \pm 0.2 - 0.33 = 15.57 \pm 0.2, \end{aligned} \quad (95)$$

where we adopt $(m-M)_{I,\mathrm{V1668\ Cyg}} = 14.6 - 1.6 \times 0.30 = 14.12$ and $(m-M)_{I,\mathrm{V679\ Car}} = 16.1 - 1.6 \times 0.69 = 15.0$, both from Hachisu & Kato (2019). Unfortunately, no I_C or I data of LV Vul are available. We have $(m-M)_{I,\mathrm{V5584\ Sgr}} = 15.58 \pm 0.1$.

We plot $(m-M)_B = 17.39$, $(m-M)_V = 16.69$, and $(m-M)_I = 15.58$ in Figure 11(d), which cross at d =8.0 kpc and $E(B-V) = 0.70$. Thus, we obtain $E(B-V) = 0.70 \pm 0.05$ and $d = 8.0 \pm 1$ kpc.

A.17. V5585 Sgr 2010

Figure 73 shows the (a) V and B, and (b) $(B-V)_0$ evolutions of V5585 Sgr. Here, $(B-V)_0$ are dereddened with $E(B-V) = 0.47$ as obtained in Section 3.17. Figure 74 shows the light/color curves of V5585 Sgr, LV Vul, V1668 Cyg, and V2576 Oph. Applying Equation (6) to them, we have the

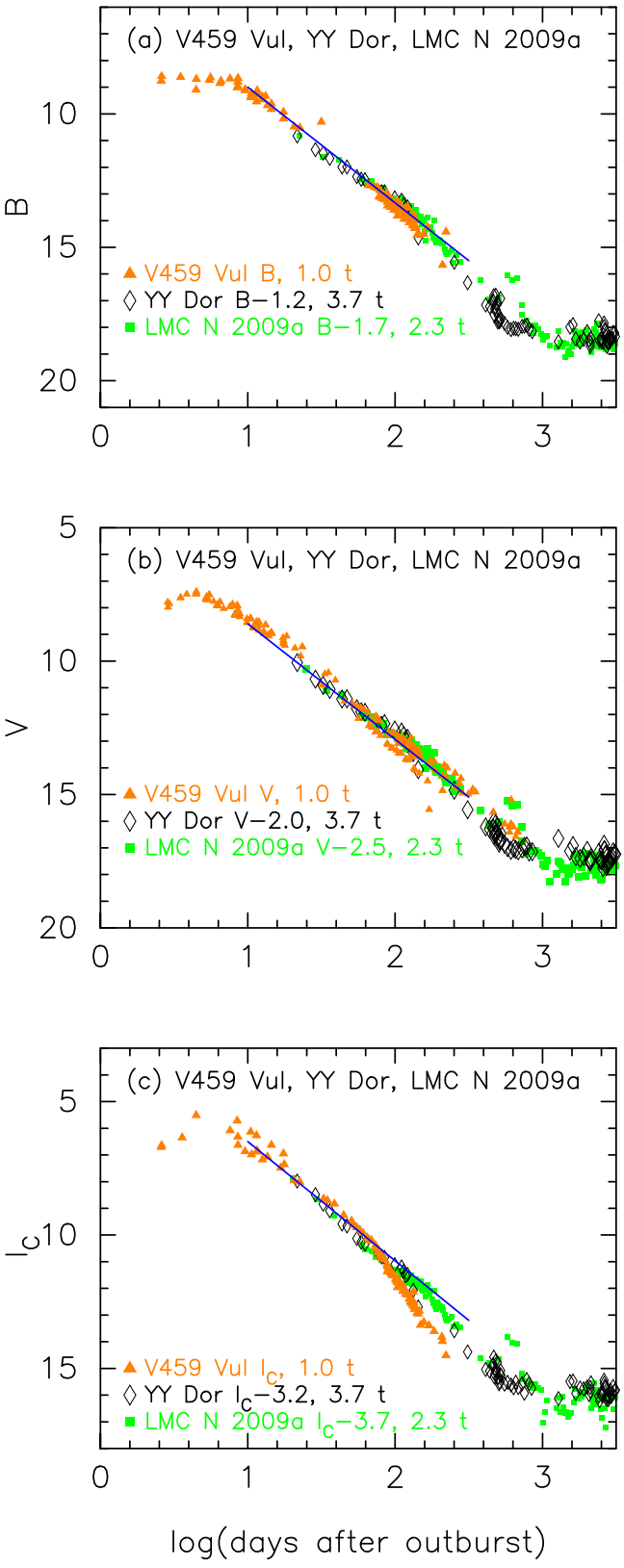

Figure 49. Same as Figure 25, but for V459 Vul. The *BV* data of V459 Vul are the same as those in Figure 47. The I_C data are taken from AAVSO and VSOLJ.

relation

$$
\begin{aligned}
&(m-M)_{V,\mathrm{V5585\ Sgr}}\\
&=(m-M+\Delta V)_{V,\mathrm{LV\ Vul}}-2.5\log 1.26\\
&=11.85+5.1\pm 0.3-0.25=16.7\pm 0.3\\
&=(m-M+\Delta V)_{V,\mathrm{V1668\ Cyg}}-2.5\log 1.26\\
&=14.6+2.4\pm 0.3-0.25=16.75\pm 0.3\\
&=(m-M+\Delta V)_{V,\mathrm{V2576\ Oph}}-2.5\log 1.78\\
&=16.65+0.7\pm 0.2-0.63=16.72\pm 0.2, \qquad (96)
\end{aligned}
$$

where we adopt $(m-M)_{V,\mathrm{LV\ Vul}}=11.85$ and $(m-M)_{V,\mathrm{V1668\ Cyg}}=14.6$, both from Hachisu & Kato (2019), and $(m-M)_{V,\mathrm{V2576\ Oph}}=16.65$ in Appendix A.5. Thus, we obtain $(m-M)_V=16.7\pm 0.2$ and $f_s=1.26$ against LV Vul. From Equations (1), (6), and (96), we have the relation

$$
\begin{aligned}
(m-M')_{V,\mathrm{V5585\ Sgr}}&\equiv(m_V-(M_V-2.5\log f_s))_{\mathrm{V5585\ Sgr}}\\
&=((m-M)_V+\Delta V)_{\mathrm{LV\ Vul}}\\
&=11.85+5.1\pm 0.3=16.95\pm 0.3. \qquad (97)
\end{aligned}
$$

Figure 75 shows the B, V, and I_C light curves of V5585 Sgr together with those of V2677 Oph, V834 Car, YY Dor, and LMC N 2009a. We apply Equation (9) for the B band to Figure 75(a) and obtain

$$
\begin{aligned}
&(m-M)_{B,\mathrm{V5585\ Sgr}}\\
&=((m-M)_B+\Delta B)_{\mathrm{V2677\ Oph}}-2.5\log 1.86\\
&=20.5-2.6\pm 0.2-0.67=17.23\pm 0.2\\
&=((m-M)_B+\Delta B)_{\mathrm{V834\ Car}}-2.5\log 1.95\\
&=17.75+0.2\pm 0.2-0.72=17.23\pm 0.2\\
&=((m-M)_B+\Delta B)_{\mathrm{YY\ Dor}}-2.5\log 6.6\\
&=18.98+0.3\pm 0.2-2.05=17.23\pm 0.2\\
&=((m-M)_B+\Delta B)_{\mathrm{LMC\ N\ 2009a}}-2.5\log 4.2\\
&=18.98-0.2\pm 0.2-1.55=17.23\pm 0.2, \qquad (98)
\end{aligned}
$$

where we adopt $(m-M)_{B,\mathrm{V2677\ Oph}}=19.2+1.3=20.5$ from Appendix A.24 and $(m-M)_{B,\mathrm{V834\ Car}}=17.25+0.50=17.75$ from Appendix A.20. We have $(m-M)_{B,\mathrm{V5585\ Sgr}}=17.23\pm 0.1$.

For the V light curves in Figure 75(b), we similarly obtain

$$
\begin{aligned}
&(m-M)_{V,\mathrm{V5585\ Sgr}}\\
&=((m-M)_V+\Delta V)_{\mathrm{V2677\ Oph}}-2.5\log 1.86\\
&=19.2-1.8\pm 0.2-0.67=16.73\pm 0.2\\
&=((m-M)_V+\Delta V)_{\mathrm{V834\ Car}}-2.5\log 1.95\\
&=17.25+0.2\pm 0.2-0.72=16.73\pm 0.2\\
&=((m-M)_V+\Delta V)_{\mathrm{YY\ Dor}}-2.5\log 6.6\\
&=18.86-0.1\pm 0.2-2.05=16.71\pm 0.2\\
&=((m-M)_V+\Delta V)_{\mathrm{LMC\ N\ 2009a}}-2.5\log 4.2\\
&=18.86-0.6\pm 0.2-1.55=16.71\pm 0.2. \qquad (99)
\end{aligned}
$$

We have $(m-M)_{V,\mathrm{V5585\ Sgr}}=16.72\pm 0.1$, which is consistent with Equation (96).

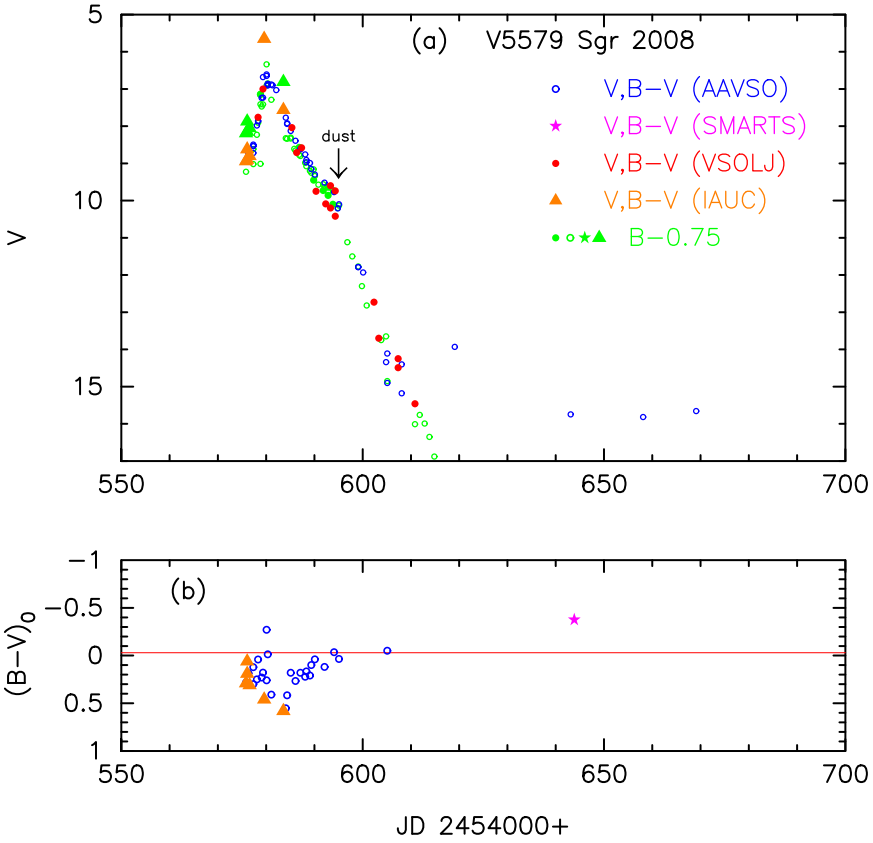

Figure 50. Same as Figure 23, but for V5579 Sgr. (a) The V (unfilled blue circles) and B (unfilled green circles) data are taken from AAVSO. The V (filled red circles) and B (filled green circles) data are from VSOLJ. The V (filled magenta stars) and B (filled green stars) from SMARTS are also plotted. (b) The $(B-V)_0$ are dereddened with $E(B-V)=0.82$.

We apply Equation (10) for the I_C band to Figure 75(c) and obtain

$$\begin{aligned}(m-M)_{I,\mathrm{V5585\ Sgr}} &= ((m-M)_I+\Delta I_C)_{\mathrm{V2677\ Oph}} - 2.5\log 1.86\\ &= 17.12 - 0.5\pm 0.2 - 0.67 = 15.95\pm 0.2\\ &= ((m-M)_I+\Delta I_C)_{\mathrm{V834\ Car}} - 2.5\log 1.95\\ &= 16.45 + 0.2\pm 0.2 - 0.72 = 15.93\pm 0.2\\ &= ((m-M)_I+\Delta I_C)_{\mathrm{YY\ Dor}} - 2.5\log 6.6\\ &= 18.67 - 0.7\pm 0.2 - 2.05 = 15.92\pm 0.2\\ &= ((m-M)_I+\Delta I_C)_{\mathrm{LMC\ N\ 2009a}} - 2.5\log 4.2\\ &= 18.67 - 1.2\pm 0.2 - 1.55 = 15.92\pm 0.2, \end{aligned} \quad (100)$$

where we adopt $(m-M)_{I,\mathrm{V2677\ Oph}} = 19.2 - 1.6\times 1.3 = 17.12$ from Appendix A.24 and $(m-M)_{I,\mathrm{V834\ Car}} = 17.25 - 1.6\times 0.50 = 16.45$ from Appendix A.20. We have $(m-M)_{I,\mathrm{V5585\ Sgr}} = 15.93\pm 0.1$.

We plot $(m-M)_B = 17.23$, $(m-M)_V = 16.72$, and $(m-M)_I = 15.93$, which broadly cross at $d = 11$ kpc and $E(B-V) = 0.47$, in Figure 13(a). Thus, we have $E(B-V) = 0.47\pm 0.05$ and $d = 11\pm 2$ kpc.

A.18. PR Lup 2011

Figure 76 shows the (a) visual, V, and K_s, and (b) $(B-V)_0$ evolutions of PR Lup. Here, $(B-V)_0$ are dereddened with $E(B-V)=0.74$ as obtained in Section 3.18. Figure 77 shows the light/color curves of PR Lup, LV Vul, V496 Sct, and V1369 Cen. Here we assume that PR Lup outbursted on JD 2,455,766.0 (Day 0). These V light and $(B-V)_0$ color curves overlap each other. Applying Equation (6) to them, we have the relation

$$\begin{aligned}(m-M)_{V,\mathrm{PR\ Lup}} &= (m-M+\Delta V)_{V,\mathrm{LV\ Vul}} - 2.5\log 1.70\\ &= 11.85 + 4.8\pm 0.2 - 0.58 = 16.07\pm 0.2\\ &= (m-M+\Delta V)_{V,\mathrm{V496\ Sct}} - 2.5\log 0.85\\ &= 13.7 + 2.2\pm 0.2 + 0.18 = 16.08\pm 0.2\\ &= (m-M+\Delta V)_{V,\mathrm{V1369\ Cen}} - 2.5\log 1.15\\ &= 10.25 + 6.0\pm 0.2 - 0.15 = 16.1\pm 0.2, \end{aligned} \quad (101)$$

where we adopt $(m-M)_{V,\mathrm{LV\ Vul}} = 11.85$, $(m-M)_{V,\mathrm{V496\ Sct}} = 13.7$, and $(m-M)_{V,\mathrm{V1369\ Cen}} = 10.25$ all from Hachisu & Kato (2019). Thus, we obtain $(m-M)_V = 16.1\pm 0.1$ and $f_s = 1.70$ against LV Vul. From Equations (1), (6), and (101), we have the relation

$$\begin{aligned}(m-M')_{V,\mathrm{PR\ Lup}} &\equiv (m_V - (M_V - 2.5\log f_s))_{\mathrm{PR\ Lup}}\\ &= ((m-M)_V+\Delta V)_{\mathrm{LV\ Vul}}\\ &= 11.85 + 4.8\pm 0.2 = 16.65\pm 0.2. \end{aligned} \quad (102)$$

Figure 78 shows the B, V, and I_C light curves of PR Lup together with those of V1369 Cen, V496 Sct, and V5666 Sgr. The light curves overlap each other well. Applying Equation (9) for the B band to Figure 78(a), we have the

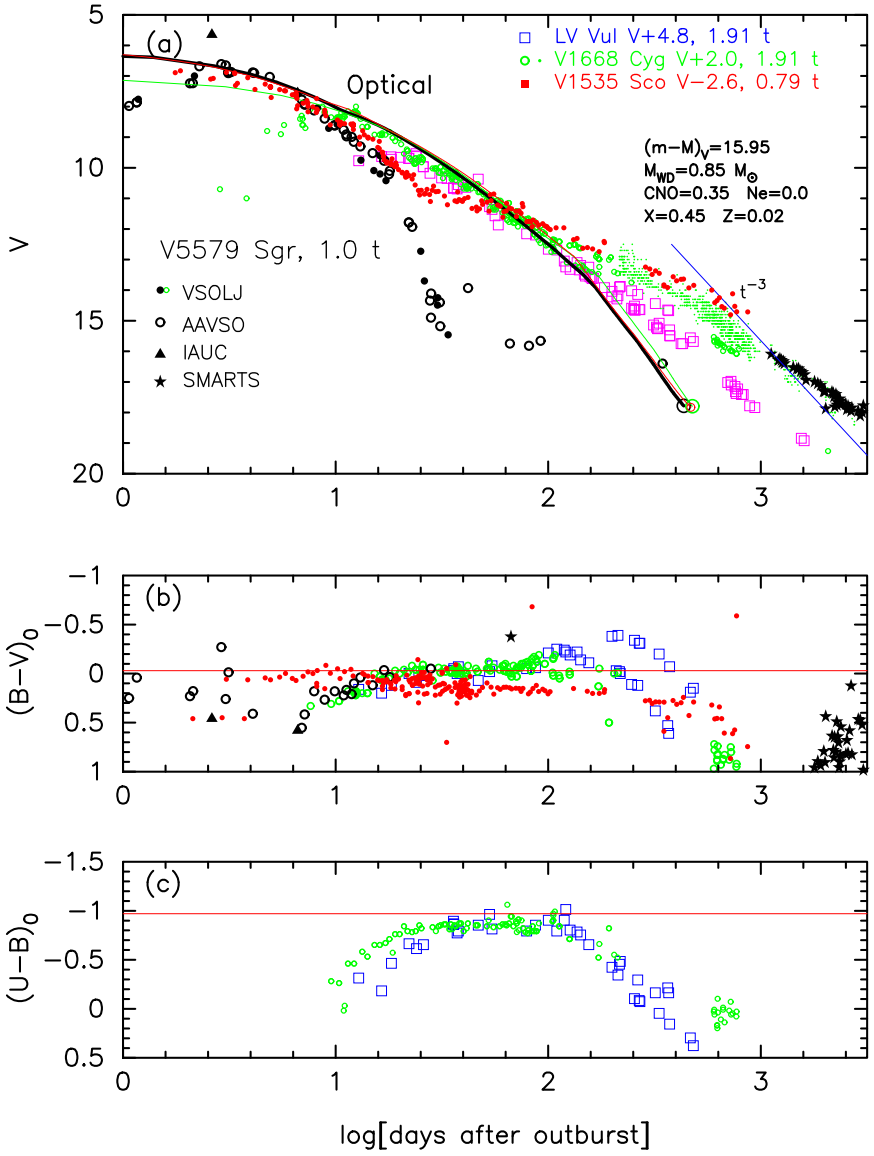

Figure 51. Same as Figure 30, but for V5579 Sgr (black symbols). We add the data of LV Vul, V1668 Cyg, and V1535 Sco. The data of V5579 Sgr are the same as those in Figure 50. The data of V1535 Sco are the same as those in Figure 110. In panel (a), we added a model absolute V light curve (solid black line) of a 0.85 $M_\odot$ WD (CO3; Hachisu & Kato 2016a), adopting $(m-M)_V = 15.95$ for V5579 Sgr. The solid green line denotes the V light curve of a 0.98 $M_\odot$ WD (CO3) for V1668 Cyg, while the solid red line represents the V light curve of a 0.85 $M_\odot$ WD (CO4) for V1535 Sco. Here, we assume $(m-M)_V = 14.6$ for V1668 Cyg and $(m-M)_V = 18.3$ for V1535 Sco.

relation

$$\begin{aligned}(m-M)_{B,\mathrm{PR\ Lup}} &= ((m-M)_B + \Delta B)_{\mathrm{V1369\ Cen}} - 2.5\log 1.15 \\ &= 10.36 + 6.6 \pm 0.2 - 0.15 = 16.81 \pm 0.2 \\ &= ((m-M)_B + \Delta B)_{\mathrm{V496\ Sct}} - 2.5\log 0.85 \\ &= 14.15 + 2.5 \pm 0.2 + 0.18 = 16.83 \pm 0.2 \\ &= ((m-M)_B + \Delta B)_{\mathrm{V5666\ Sgr}} - 2.5\log 0.95 \\ &= 15.9 + 0.9 \pm 0.2 + 0.05 = 16.88 \pm 0.2, \end{aligned} \quad (103)$$

where we adopt $(m-M)_{B,\mathrm{V1369\ Cen}} = 10.36$, $(m-M)_{B,\mathrm{V496\ Sct}} = 14.15$, and $(m-M)_{B,\mathrm{V5666\ Sgr}} = 15.9$ from Appendix A.12. We have $(m-M)_B = 16.84 \pm 0.1$ for PR Lup.

Applying Equation (6) to Figure 78(b), we have the relation

$$\begin{aligned}(m-M)_{V,\mathrm{PR\ Lup}} &= ((m-M)_V + \Delta V)_{\mathrm{V1369\ Cen}} - 2.5\log 1.15 \\ &= 10.25 + 6.0 \pm 0.3 - 0.15 = 16.1 \pm 0.2 \\ &= ((m-M)_V + \Delta V)_{\mathrm{V496\ Sct}} - 2.5\log 0.85 \\ &= 13.7 + 2.2 \pm 0.3 + 0.18 = 16.08 \pm 0.2 \\ &= ((m-M)_V + \Delta V)_{\mathrm{V5666\ Sgr}} - 2.5\log 0.95 \\ &= 15.4 + 0.7 \pm 0.3 + 0.05 = 16.15 \pm 0.2, \end{aligned} \quad (104)$$

where we adopt $(m-M)_{V,\mathrm{V1369\ Cen}} = 10.25$, $(m-M)_{V,\mathrm{V496\ Sct}} = 13.7$, and $(m-M)_{V,\mathrm{V5666\ Sgr}} = 15.4$ from Hachisu & Kato (2019). We have $(m-M)_V = 16.1 \pm 0.1$, which is consistent with Equation (101).

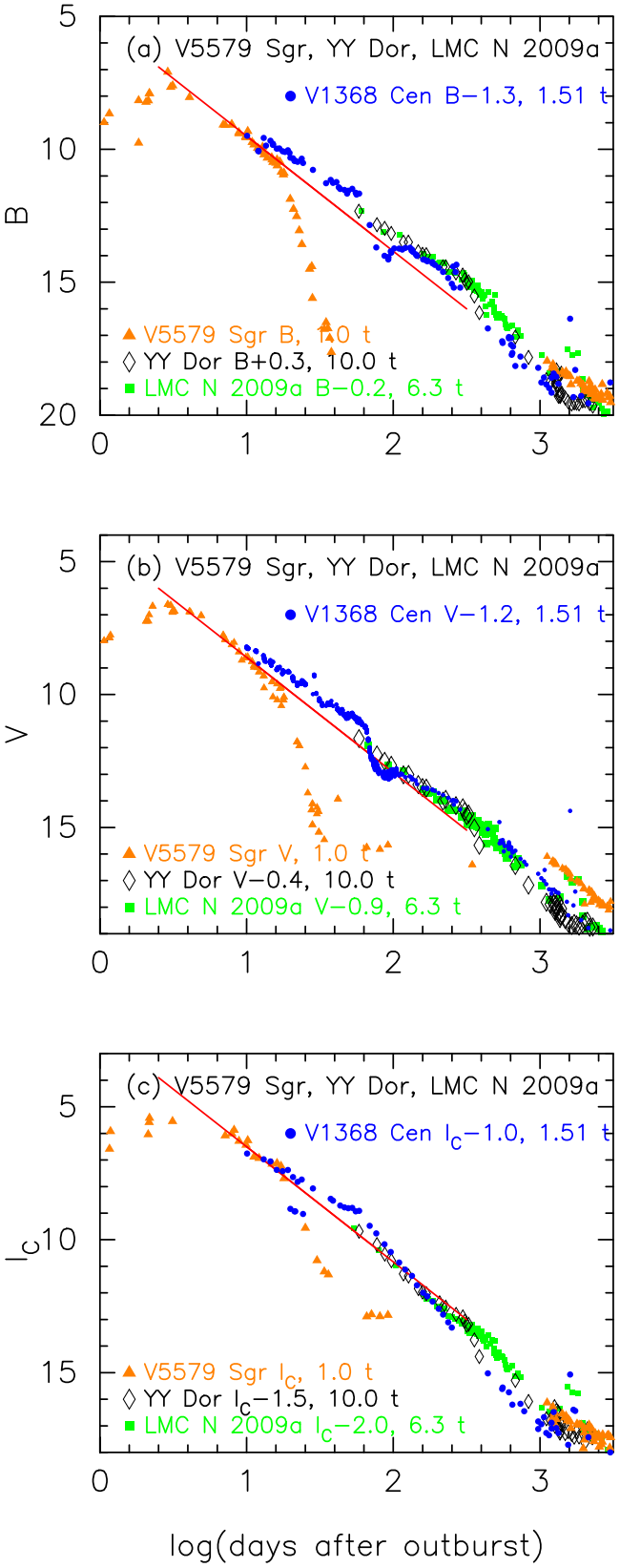

Figure 52. Same as Figure 25, but for V5579 Sgr. We added the data of V1368 Cen, YY Dor, and LMC N 2009a. The *BV* data of V5579 Sgr are the same as those in Figure 50. The I_C data are taken from AAVSO, VSOLJ, and SMARTS. The data of V1368 Cen are the same as those in Figures 85, 86, and 87.

From the I_C band data in Figure 78(c), we obtain

$$\begin{aligned}(m-M)_{I,\mathrm{PR\ Lup}} &= ((m-M)_I + \Delta I_C)_{\mathrm{V1369\ Cen}} - 2.5\log 1.15 \\ &= 10.07 + 5.0 \pm 0.2 - 0.15 = 14.92 \pm 0.2 \\ &= ((m-M)_I + \Delta I_C)_{\mathrm{V496\ Sct}} - 2.5\log 0.85 \\ &= 12.98 + 1.8 \pm 0.2 + 0.18 = 14.96 \pm 0.2 \\ &= ((m-M)_I + \Delta I_C)_{\mathrm{V5666\ Sgr}} - 2.5\log 0.95 \\ &= 14.6 + 0.3 \pm 0.2 + 0.05 = 14.95 \pm 0.2, \end{aligned} \quad (105)$$

where we adopt $(m-M)_{I,\mathrm{V1369\ Cen}} = 10.07$, $(m-M)_{I,\mathrm{V496\ Sct}} = 12.98$, and $(m-M)_{I,\mathrm{V5666\ Sgr}} = 14.6$ from Appendix A.12. We have $(m-M)_I = 14.94 \pm 0.1$.

We plot $(m-M)_B = 16.84$, $(m-M)_V = 16.1$, $(m-M)_I = 14.94$, which cross at $d = 5.8$ kpc and $E(B-V) = 0.74$, in Figure 13(b). Thus, we obtain $d = 5.8 \pm 0.6$ kpc and $E(B-V) = 0.74 \pm 0.05$.

A.19. V1313 Sco 2011#2

Figure 79 shows the (a) visual and V, and (b) $(B-V)_0$ evolutions of V1313 Sco. Here, $(B-V)_0$ are dereddened with $E(B-V) = 1.30$ as obtained in Section 3.19. Figure 80 shows the light/color curves of V1313 Sco, LV Vul, V1668 Cyg, V533 Her, and V2676 Oph. Applying Equation (6) to them, we have the relation

$$\begin{aligned}(m-M)_{V,\mathrm{V1313\ Sco}} &= (m - M + \Delta V)_{V,\mathrm{LV\ Vul}} - 2.5\log 0.60 \\ &= 11.85 + 6.6 \pm 0.2 + 0.55 = 19.0 \pm 0.2 \\ &= (m - M + \Delta V)_{V,\mathrm{V1668\ Cyg}} - 2.5\log 0.60 \\ &= 14.6 + 3.9 \pm 0.2 + 0.55 = 19.05 \pm 0.2 \\ &= (m - M + \Delta V)_{V,\mathrm{V533\ Her}} - 2.5\log 0.50 \\ &= 10.65 + 7.6 \pm 0.2 + 0.75 = 19.0 \pm 0.2 \\ &= (m - M + \Delta V)_{V,\mathrm{V2576\ Oph}} - 2.5\log 0.85 \\ &= 16.65 + 2.2 \pm 0.2 + 0.18 = 19.03 \pm 0.2, \end{aligned} \quad (106)$$

where we adopt $(m-M)_{V,\mathrm{LV\ Vul}} = 11.85$, $(m-M)_{V,\mathrm{V1668\ Cyg}} = 14.6$, and $(m-M)_{V,\mathrm{V533\ Her}} = 10.65$ from Hachisu & Kato (2019), and $(m-M)_{V,\mathrm{V2576\ Oph}} = 16.65$ in Appendix A.5. Thus, we obtain $(m-M)_V = 19.0 \pm 0.1$ and $f_s = 0.60$ against LV Vul. From Equations (1), (6), and (106), we have the relation

$$\begin{aligned}(m-M')_{V,\mathrm{V1313\ Sco}} &\equiv (m_V - (M_V - 2.5\log f_s))_{\mathrm{V1313\ Sco}} \\ &= ((m-M)_V + \Delta V)_{\mathrm{LV\ Vul}} \\ &= 11.85 + 6.6 \pm 0.2 = 18.45 \pm 0.2. \end{aligned} \quad (107)$$

Figure 81 shows the B, V, and I_C light curves of V1313 Sco together with those of YY Dor and LMC N 2009a. We regard the extension of the YY Dor and LMC N 2009a light curves to overlap with that of V1313 Sco. We apply Equation (9) for the

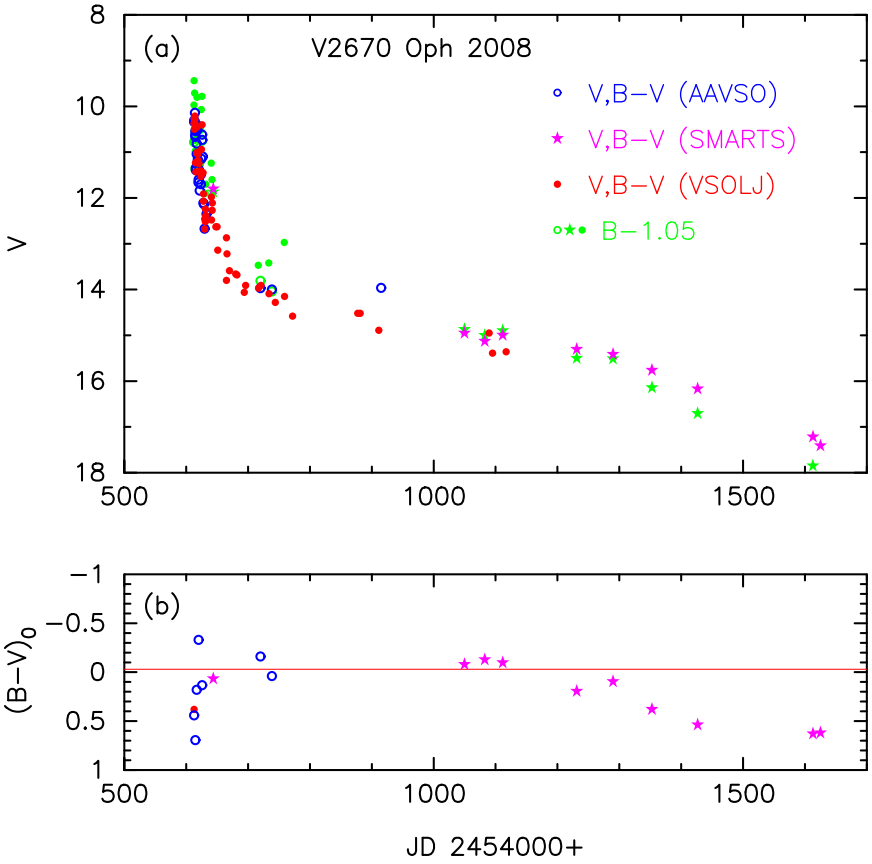

Figure 53. Same as Figure 23, but for V2670 Oph. (a) The V (unfilled blue circles) and B (unfilled green circles) data are taken from AAVSO. The V (filled red circles) and B (filled green circles) data are from VSOLJ. The SMARTS data of V (filled magenta stars) and B (filled green stars) are also plotted. (b) The $(B-V)_0$ are dereddened with $E(B-V)=1.05$.

B band to Figure 81(a) and obtain

$$\begin{aligned}(m-M)_{B,\mathrm{V1313\ Sco}}&=((m-M)_B+\Delta B)_{\mathrm{YY\ Dor}}-2.5\log 3.2\\&=18.98+2.6\pm0.2-1.25=20.33\pm0.2\\&=((m-M)_B+\Delta B)_{\mathrm{LMC\ N\ 2009a}}-2.5\log 2.0\\&=18.98+2.1\pm0.2-0.75=20.33\pm0.2.\end{aligned}\quad(108)$$

We have $(m-M)_{B,\mathrm{V1313\ Sco}}=20.33\pm0.1$.

For the V light curves in Figure 81(b), we similarly obtain

$$\begin{aligned}(m-M)_{V,\mathrm{V1313\ Sco}}&=((m-M)_V+\Delta V)_{\mathrm{YY\ Dor}}-2.5\log 3.2\\&=18.86+1.4\pm0.2-1.25=19.01\pm0.2\\&=((m-M)_V+\Delta V)_{\mathrm{LMC\ N\ 2009a}}-2.5\log 2.0\\&=18.86+0.9\pm0.2-0.75=19.01\pm0.2.\end{aligned}\quad(109)$$

We have $(m-M)_{V,\mathrm{V1313\ Sco}}=19.01\pm0.1$, which is consistent with Equation (106).

We apply Equation (10) for the I_C band to Figure 81(c) and obtain

$$\begin{aligned}(m-M)_{I,\mathrm{V1313\ Sco}}&=((m-M)_I+\Delta I_C)_{\mathrm{YY\ Dor}}-2.5\log 3.2\\&=18.67-0.5\pm0.2-1.25=16.92\pm0.2\\&=((m-M)_I+\Delta I_C)_{\mathrm{LMC\ N\ 2009a}}-2.5\log 2.0\\&=18.67-1.0\pm0.2-0.75=16.92\pm0.2.\end{aligned}\quad(110)$$

We have $(m-M)_{I,\mathrm{V1313\ Sco}}=16.92\pm0.1$.

We plot $(m-M)_B=20.33$, $(m-M)_V=19.01$, and $(m-M)_I=16.92$, which broadly cross at $d=9.9$ kpc and $E(B-V)=1.30$, in Figure 13(c). Thus, we obtain $E(B-V)=1.30\pm0.1$ and $d=9.9\pm2$ kpc.

A.20. V834 Car 2012

Figure 82 shows the (a) V and visual, and (b) $(B-V)_0$ evolutions of V834 Car. Here, $(B-V)_0$ are dereddened with $E(B-V)=0.50$ as obtained in Section 3.20. Figure 83 shows the light/color curves of V834 Car, LV Vul, V1668 Cyg, V533 Her, and V2576 Oph. Applying Equation (6) to them, we have the relation

$$\begin{aligned}(m-M)_{V,\mathrm{V834\ Car}}&=(m-M+\Delta V)_{V,\mathrm{LV\ Vul}}-2.5\log 0.65\\&=11.85+4.9\pm0.2+0.48=17.23\pm0.2\\&=(m-M+\Delta V)_{V,\mathrm{V1668\ Cyg}}-2.5\log 0.65\\&=14.6+2.2\pm0.2+0.48=17.28\pm0.2\\&=(m-M+\Delta V)_{V,\mathrm{V533\ Her}}-2.5\log 0.54\\&=10.65+5.9\pm0.2+0.68=17.23\pm0.2\\&=(m-M+\Delta V)_{V,\mathrm{V2576\ Oph}}-2.5\log 0.91\\&=16.65+0.5\pm0.2+0.10=17.25\pm0.2,\end{aligned}\quad(111)$$

where we adopt $(m-M)_{V,\mathrm{LV\ Vul}}=11.85$, $(m-M)_{V,\mathrm{V1668\ Cyg}}=14.6$, and $(m-M)_{V,\mathrm{V533\ Her}}=10.65$ from Hachisu & Kato (2019), and $(m-M)_{V,\mathrm{V2576\ Oph}}=16.65$ in Appendix A.5. Thus, we obtain $(m-M)_V=17.25\pm0.1$ and $f_s=0.65$ against

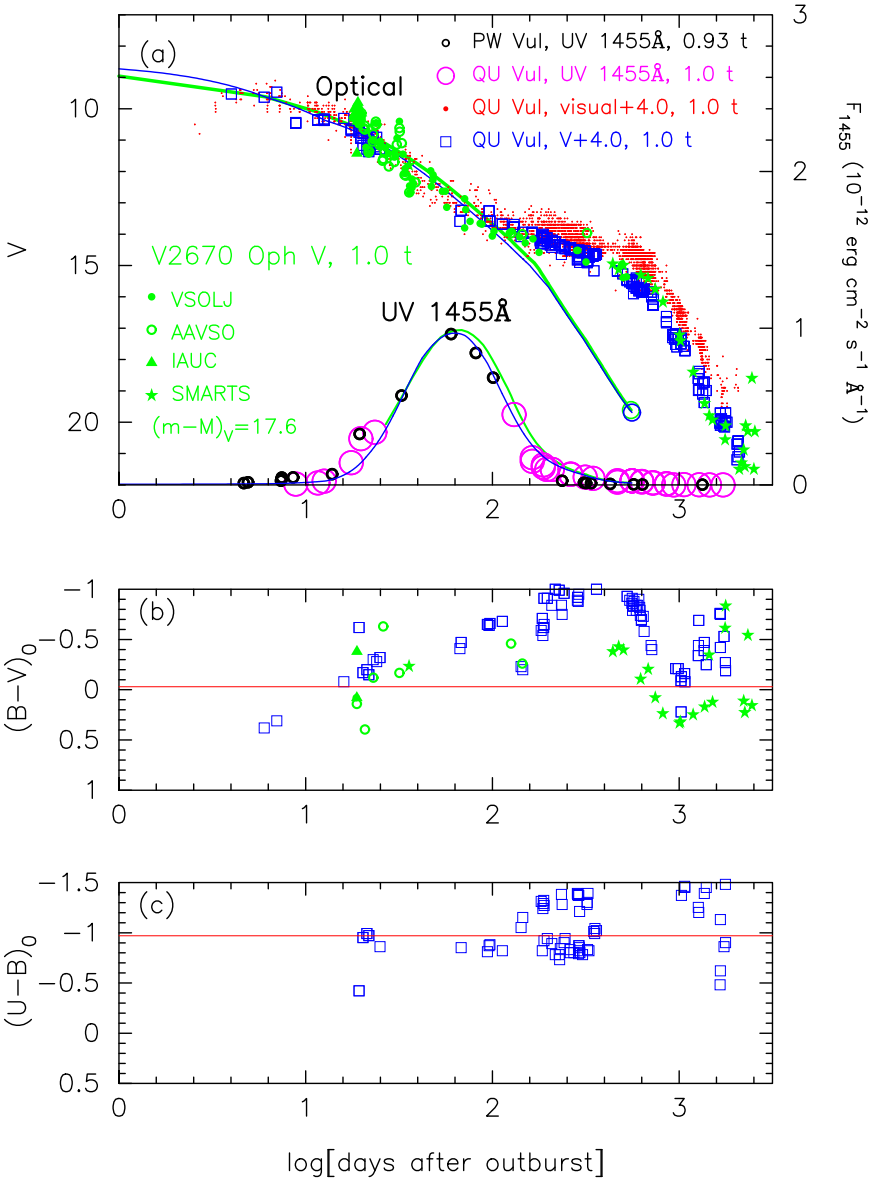

Figure 54. The light/color curves of V2670 Oph as well as those of QU Vul. The data of V2670 Oph are the same as those in Figure 53. The data of QU Vul are the same as those in Figure 10 of Hachisu & Kato (2016a). In panel (a), we added model light curves (solid green lines) of a 0.80 $M_\odot$ WD (CO3; Hachisu & Kato 2016a), assuming that $(m-M)_V = 17.6$ for V2670 Oph. The solid blue lines denote the V and UV 1455 Å light curve of a 0.86 $M_\odot$ WD (Ne3; Hachisu & Kato 2015), assuming that $(m-M)_V = 13.6$ for QU Vul (Hachisu & Kato 2016a).

LV Vul. From Equations (1), (6), and (111), we have the relation

$$\begin{aligned}(m-M')_{V,\mathrm{V834\ Car}} &\equiv (m_V - (M_V - 2.5\log f_s))_{\mathrm{V834\ Car}} \\ &= ((m-M)_V + \Delta V)_{\mathrm{LV\ Vul}} \\ &= 11.85 + 4.9 \pm 0.2 = 16.75 \pm 0.2. \end{aligned} \quad (112)$$

Figure 84 shows the B, V, and I_C light curves of V834 Car together with those of YY Dor and LMC N 2009a. We regard the extension of the YY Dor and LMC N 2009a light curves to overlap with that of V834 Car. We apply Equation (9) for the B band to Figure 84(a) and obtain

$$\begin{aligned}&(m-M)_{B,\mathrm{V834\ Car}} \\ &= ((m-M)_B + \Delta B)_{\mathrm{YY\ Dor}} - 2.5\log 3.4 \\ &= 18.98 + 0.1 \pm 0.2 - 1.33 = 17.75 \pm 0.2 \\ &= ((m-M)_B + \Delta B)_{\mathrm{LMC\ N\ 2009a}} - 2.5\log 2.1 \\ &= 18.98 - 0.4 \pm 0.2 - 0.83 = 17.75 \pm 0.2. \end{aligned} \quad (113)$$

We have $(m-M)_{B,\mathrm{V834\ Car}} = 17.75 \pm 0.1$.

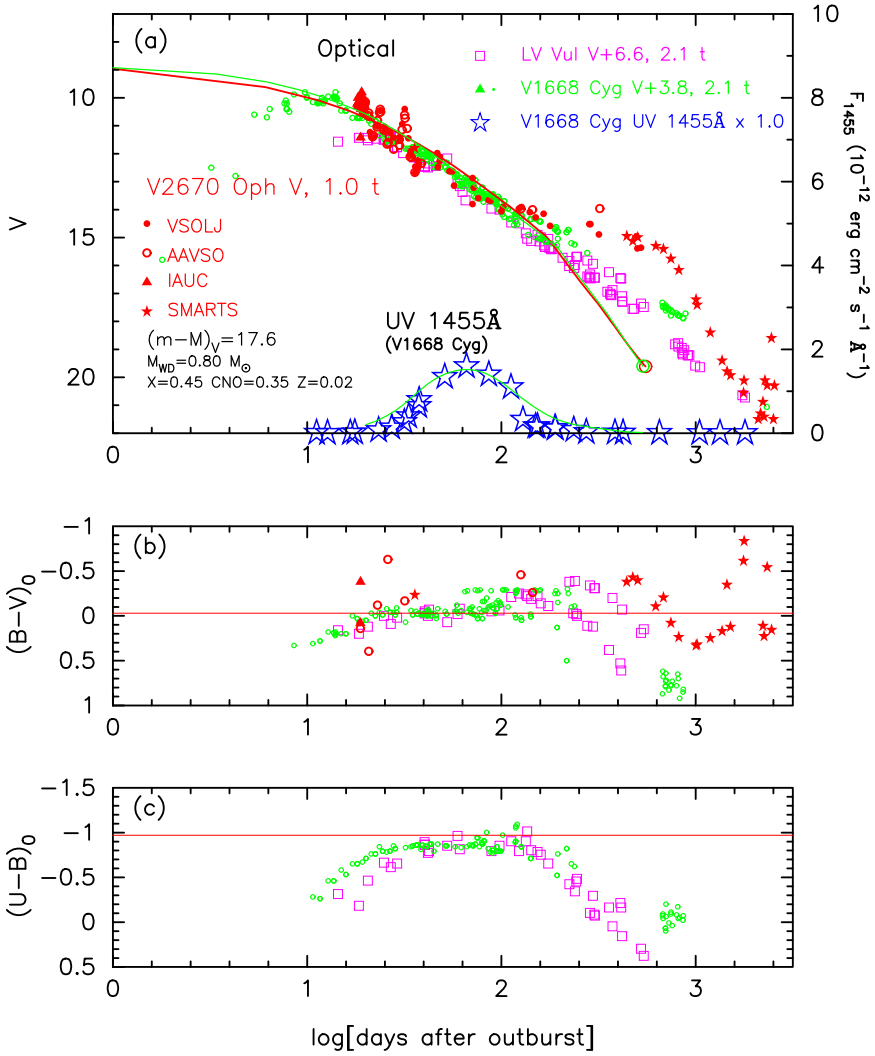

Figure 55. Same as Figure 30, but for V2670 Oph (red symbols). The data of V2670 Oph are the same as those in Figure 53. In panel (a), we added model light curves (solid red lines) of a 0.80 $M_\odot$ WD (CO3, Hachisu & Kato 2016a), assuming that $(m-M)_V = 17.6$ for V2670 Oph. The solid green lines denote the V and UV 1455 Å light curve of a 0.98 $M_\odot$ WD (CO3), assuming that $(m-M)_V = 14.6$ for V1668 Cyg.

For the V light curves in Figure 84(b), we similarly obtain

$$\begin{aligned}(m-M)_{V,\mathrm{V834\ Car}} &= ((m-M)_V + \Delta V)_{\mathrm{YY\ Dor}} - 2.5\log 3.4 \\ &= 18.86 - 0.3 \pm 0.2 - 1.33 = 17.23 \pm 0.2 \\ &= ((m-M)_V + \Delta V)_{\mathrm{LMC\ N\ 2009a}} - 2.5\log 2.1 \\ &= 18.86 - 0.8 \pm 0.2 - 0.83 = 17.23 \pm 0.2. \end{aligned} \quad (114)$$

We have $(m-M)_{V,\mathrm{V834\ Car}} = 17.23 \pm 0.1$, which is consistent with Equation (111).

We apply Equation (10) for the I_C band to Figure 84(c) and obtain

$$\begin{aligned}(m-M)_{I,\mathrm{V834\ Car}} &= ((m-M)_I + \Delta I_C)_{\mathrm{YY\ Dor}} - 2.5\log 3.4 \\ &= 18.67 - 0.9 \pm 0.2 - 1.33 = 16.44 \pm 0.2 \\ &= ((m-M)_I + \Delta I_C)_{\mathrm{LMC\ N\ 2009a}} - 2.5\log 2.1 \\ &= 18.67 - 1.4 \pm 0.2 - 0.83 = 16.44 \pm 0.2. \end{aligned} \quad (115)$$

We have $(m-M)_{I,\mathrm{V834\ Car}} = 16.44 \pm 0.1$.

We plot $(m-M)_B = 17.75$, $(m-M)_V = 17.23$, and $(m-M)_I = 16.44$, which broadly cross at $d = 14$ kpc and $E(B-V) = 0.50$, in Figure 13(d). Thus, we obtain $E(B-V) = 0.50 \pm 0.05$ and $d = 14 \pm 2$ kpc.

A.21. V1368 Cen 2012

Figure 85 shows the (a) V and K_s, and (b) $(B-V)_0$ evolutions of V1368 Cen. Here, $(B-V)_0$ are dereddened with $E(B-V) = 0.93$ as obtained in Section 3.21. Figure 86 shows the light/color curves of V1368 Cen, LV Vul, V1668 Cyg, and OS And. They overlap each other. Applying Equation (6) to them, we have the relation

$$\begin{aligned}(m-M)_{V,\mathrm{V1368\ Cen}} &= (m-M+\Delta V)_{V,\mathrm{LV\ Vul}} - 2.5\log 1.26 \\ &= 11.85 + 6.0 \pm 0.2 - 0.25 = 17.6 \pm 0.2 \\ &= (m-M+\Delta V)_{V,\mathrm{V1668\ Cyg}} - 2.5\log 1.26 \\ &= 14.6 + 3.3 \pm 0.2 - 0.25 = 17.65 \pm 0.2 \\ &= (m-M+\Delta V)_{V,\mathrm{OS\ And}} - 2.5\log 1.78 \\ &= 14.8 + 3.4 \pm 0.2 - 0.63 = 17.57 \pm 0.2, \end{aligned} \quad (116)$$

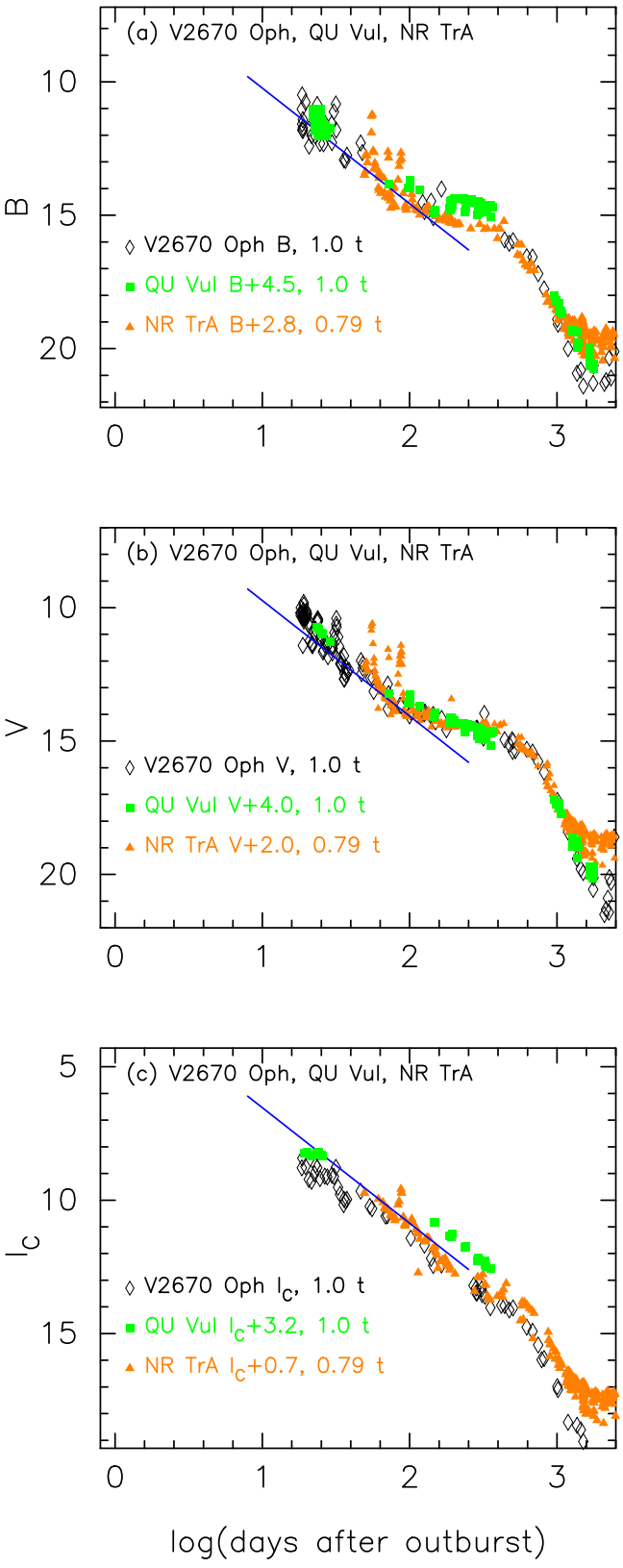

Figure 56. Same as Figure 25, but for V2670 Oph. The *BV* data of V2670 Oph are the same as those in Figure 53. The *BV* data of QU Vul are the same as those in Figure 10 of Hachisu & Kato (2016a). The *BV* data of NR TrA are the same as those in Figure 60. The I_C data are taken from AAVSO, VSOLJ, and SMARTS.

where we adopt $(m-M)_{V,\mathrm{LV\ Vul}} = 11.85$ and $(m-M)_{V,\mathrm{V1668\ Cyg}} = 14.6$ from Hachisu & Kato (2019), and $(m-M)_{V,\mathrm{OS\ And}} = 14.8$ from Hachisu & Kato (2016b). Thus, we obtain $(m-M)_V = 17.6 \pm 0.1$ and $f_s = 1.26$ against LV Vul. From Equations (1), (6), and (116), we have the relation

$$\begin{aligned}(m-M')_{V,\mathrm{V1368\ Cen}} &\equiv (m_V - (M_V - 2.5\log f_s))_{\mathrm{V1368\ Cen}} \\ &= ((m-M)_V + \Delta V)_{\mathrm{LV\ Vul}} \\ &= 11.85 + 6.0 \pm 0.2 = 17.85 \pm 0.2.\end{aligned} \tag{117}$$

Figure 87 shows the *B*, *V*, and I_C light curves of V1368 Cen together with those of V834 Car, YY Dor, and LMC N 2009a. We apply Equation (9) for the *B* band to Figure 87(a) and obtain

$$\begin{aligned}&(m-M)_{B,\mathrm{V1368\ Cen}} \\ &= ((m-M)_B + \Delta B)_{\mathrm{V834\ Car}} - 2.5\log 1.95 \\ &= 17.75 + 1.5 \pm 0.2 - 0.73 = 18.52 \pm 0.2 \\ &= ((m-M)_B + \Delta B)_{\mathrm{YY\ Dor}} - 2.5\log 6.6 \\ &= 18.98 + 1.6 \pm 0.2 - 2.05 = 18.53 \pm 0.2 \\ &= ((m-M)_B + \Delta B)_{\mathrm{LMC\ N\ 2009a}} - 2.5\log 4.2 \\ &= 18.98 + 1.1 \pm 0.2 - 1.55 = 18.53 \pm 0.2.\end{aligned} \tag{118}$$

We have $(m-M)_{B,\mathrm{V1368\ Cen}} = 18.53 \pm 0.1$.

For the *V* light curves in Figure 87(b), we similarly obtain

$$\begin{aligned}&(m-M)_{V,\mathrm{V1368\ Cen}} \\ &= ((m-M)_V + \Delta V)_{\mathrm{V834\ Car}} - 2.5\log 1.95 \\ &= 17.3 - 1.0 \pm 0.2 - 0.73 = 17.57 \pm 0.2 \\ &= ((m-M)_V + \Delta V)_{\mathrm{YY\ Dor}} - 2.5\log 6.6 \\ &= 18.86 + 0.8 \pm 0.2 - 2.05 = 17.61 \pm 0.2 \\ &= ((m-M)_V + \Delta V)_{\mathrm{LMC\ N\ 2009a}} - 2.5\log 4.2 \\ &= 18.86 + 0.3 \pm 0.2 - 1.55 = 17.61 \pm 0.2.\end{aligned} \tag{119}$$

We have $(m-M)_{V,\mathrm{V1368\ Cen}} = 17.6 \pm 0.1$, which is consistent with Equation (116).

We apply Equation (10) for the I_C band to Figure 87(c) and obtain

$$\begin{aligned}&(m-M)_{I,\mathrm{V1368\ Cen}} \\ &= ((m-M)_I + \Delta I_C)_{\mathrm{V834\ Car}} - 2.5\log 1.95 \\ &= 16.45 + 0.4 \pm 0.2 - 0.73 = 16.12 \pm 0.2 \\ &= ((m-M)_I + \Delta I_C)_{\mathrm{YY\ Dor}} - 2.5\log 6.6 \\ &= 18.67 - 0.5 \pm 0.2 - 2.05 = 16.12 \pm 0.2 \\ &= ((m-M)_I + \Delta I_C)_{\mathrm{LMC\ N\ 2009a}} - 2.5\log 4.2 \\ &= 18.67 - 1.0 \pm 0.2 - 1.55 = 16.12 \pm 0.2.\end{aligned} \tag{120}$$

We have $(m-M)_{I,\mathrm{V1368\ Cen}} = 16.12 \pm 0.1$.

We plot $(m-M)_B = 18.53$, $(m-M)_V = 17.6$, and $(m-M)_I = 16.12$, which broadly cross at $d = 8.8$ kpc and $E(B-V) = 0.93$, in Figure 15(a). Thus, we obtain $E(B-V) = 0.93 \pm 0.05$ and $d = 8.8 \pm 1.0$ kpc.

A.22. V2676 Oph 2012

Figure 88 shows the (a) visual, *V*, and K_s, and (b) $(B-V)_0$ evolutions of V2676 Oph. Here, $(B-V)_0$ are dereddened with $E(B-V) = 0.90$ as obtained in Section 3.22. Figure 89 shows the light/color curves of V2676 Oph as well as those of

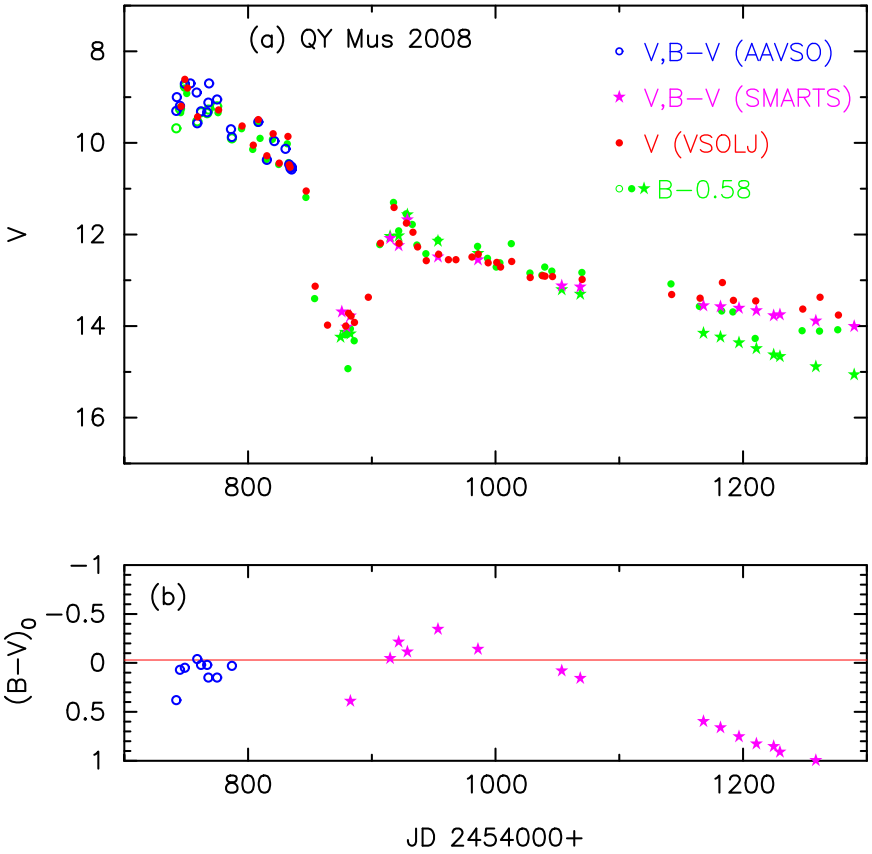

Figure 57. Same as Figure 23, but for QY Mus. (a) The V (unfilled blue circles) and B (unfilled green circles) data are taken from AAVSO. The V (filled red circles) and B (filled green circles) data are from VSOLJ. The SMARTS data of V (filled magenta stars) and B (filled green stars) are also plotted. (b) The $(B-V)_0$ are dereddened with $E(B-V)=0.58$.

QY Mus, V496 Sct, V475 Sct, and LV Vul. The V light curve of V2676 Oph overlaps well with that of V475 Sct. Applying Equation (6) to them, we have the relation

$$\begin{aligned}(m-M)_{V,\mathrm{V2676\ Oph}} &= (m-M+\Delta V)_{V,\mathrm{LV\ Vul}} - 2.5\log 3.4\\ &= 11.85+6.8\pm 0.3-1.33 = 17.32\pm 0.3\\ &= (m-M+\Delta V)_{V,\mathrm{V496\ Sct}} - 2.5\log 1.7\\ &= 13.7+4.2\pm 0.3-0.58 = 17.32\pm 0.3\\ &= (m-M+\Delta V)_{V,\mathrm{QY\ Mus}} - 2.5\log 1.51\\ &= 14.65+3.1\pm 0.3-0.45 = 17.3\pm 0.3\\ &= (m-M+\Delta V)_{V,\mathrm{V475\ Sct}} - 2.5\log 1.48\\ &= 15.4+2.3\pm 0.3-0.43 = 17.27\pm 0.3, \end{aligned} \quad (121)$$

where we adopt $(m-M)_{V,\mathrm{LV\ Vul}}=11.85$ and $(m-M)_{V,\mathrm{V496\ Sct}}=13.7$ from Hachisu & Kato (2019), $(m-M)_{V,\mathrm{QY\ Mus}}=14.65$ from Section 3.12, and $(m-M)_{V,\mathrm{V475\ Sct}}=15.4$ from Hachisu & Kato (2016b). Thus, we obtain $(m-M)_V=17.3\pm 0.2$ and $f_s=3.4$ against LV Vul. From Equations (1), (6), and (121), we have the relation

$$\begin{aligned}(m-M')_{V,\mathrm{V2676\ Oph}} &\equiv (m_V-(M_V-2.5\log f_s))_{\mathrm{V2676\ Oph}}\\ &= ((m-M)_V+\Delta V)_{\mathrm{LV\ Vul}}\\ &= 11.85+6.8\pm 0.3 = 18.65\pm 0.3. \end{aligned} \quad (122)$$

Figure 90 shows the B, V, and I_C light curves of V2676 Oph together with those of V5584 Sgr, V679 Car, LV Vul, and V1668 Cyg. We apply Equation (9) for the B band to Figure 90(a) and obtain

$$\begin{aligned}(m-M)_{B,\mathrm{V2676\ Oph}} &= ((m-M)_B+\Delta B)_{\mathrm{LV\ Vul}} - 2.5\log 3.4\\ &= 12.45+7.1\pm 0.2-1.32 = 18.23\pm 0.2\\ &= ((m-M)_B+\Delta B)_{\mathrm{V1668\ Cyg}} - 2.5\log 3.4\\ &= 14.9+4.6\pm 0.2-1.32 = 18.18\pm 0.2\\ &= ((m-M)_B+\Delta B)_{\mathrm{V679\ Car}} - 2.5\log 3.4\\ &= 16.79+2.7\pm 0.2-1.32 = 18.17\pm 0.2\\ &= ((m-M)_B+\Delta B)_{\mathrm{V5584\ Sgr}} - 2.5\log 2.5\\ &= 17.4+1.8\pm 0.2-1.0 = 18.2\pm 0.2, \end{aligned} \quad (123)$$

where we adopt $(m-M)_{B,\mathrm{LV\ Vul}}=11.85+0.60=12.45$, $(m-M)_{B,\mathrm{V1668\ Cyg}}=14.6+0.30=14.9$, and $(m-M)_{B,\mathrm{V679\ Car}}=16.1+0.69=16.79$ from Hachisu & Kato (2019), and $(m-M)_{B,\mathrm{V5584\ Sgr}}=16.7+0.70=17.4$ from Appendix A.16. We have $(m-M)_{B,\mathrm{V2676\ Oph}}=18.2\pm 0.1$.

For the V light curves in Figure 90(b), we similarly obtain

$$\begin{aligned}(m-M)_{V,\mathrm{V2676\ Oph}} &= ((m-M)_V+\Delta V)_{\mathrm{LV\ Vul}} - 2.5\log 3.4\\ &= 11.85+6.8\pm 0.2-1.32 = 17.33\pm 0.2\\ &= ((m-M)_V+\Delta V)_{\mathrm{V1668\ Cyg}} - 2.5\log 3.4\\ &= 14.6+4.0\pm 0.2-1.32 = 17.28\pm 0.2\\ &= ((m-M)_V+\Delta V)_{\mathrm{V679\ Car}} - 2.5\log 3.4\\ &= 16.1+2.5\pm 0.2-1.32 = 17.28\pm 0.2\\ &= ((m-M)_V+\Delta V)_{\mathrm{V5584\ Sgr}} - 2.5\log 2.5\\ &= 16.7+1.6\pm 0.2-1.0 = 17.3\pm 0.2, \end{aligned} \quad (124)$$

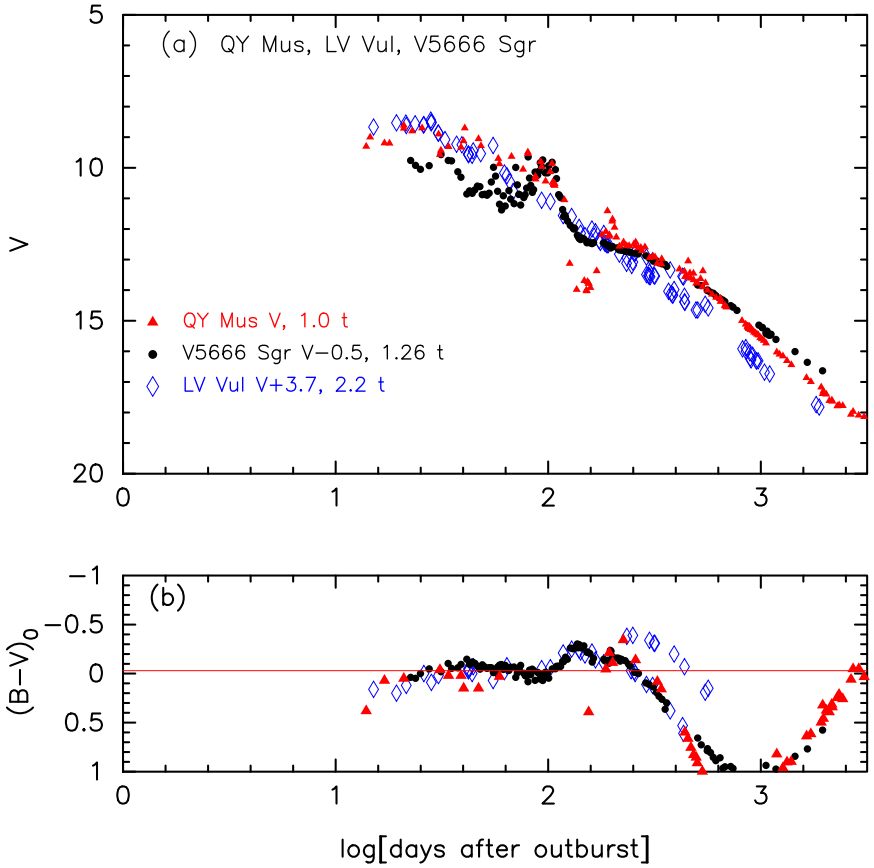

Figure 58. Same as Figure 30, but for QY Mus (filled red triangles). We added the V5666 Sgr (filled black circles) and LV Vul (unfilled blue diamonds) light/color curves. The data of QY Mus are the same as those in Figure 57.

where we adopt $(m-M)_{V,\mathrm{LV\ Vul}}=11.85$, $(m-M)_{V,\mathrm{V1668\ Cyg}}=14.6$, and $(m-M)_{V,\mathrm{V679\ Car}}=16.1$ from Hachisu & Kato (2019), and $(m-M)_{V,\mathrm{V5584\ Sgr}}=16.7$ from Appendix A.16. We have $(m-M)_{V,\mathrm{V2676\ Oph}}=17.3\pm0.1$, which is consistent with Equation (121).

We apply Equation (10) for the I_{C} band to Figure 90(c) and obtain

$$\begin{aligned}(m-M)_{I,\mathrm{V2676\ Oph}}&=((m-M)_I+\Delta I_{\mathrm{C}})_{\mathrm{V1668\ Cyg}}-2.5\log 3.4\\&=14.12+3.1\pm0.2-1.32=15.9\pm0.2\\&=((m-M)_I+\Delta I_{\mathrm{C}})_{\mathrm{V679\ Car}}-2.5\log 3.4\\&=15.0+2.2\pm0.2-1.32=15.88\pm0.2\\&=((m-M)_I+\Delta I_{\mathrm{C}})_{\mathrm{V5584\ Sgr}}-2.5\log 2.5\\&=15.58+1.3\pm0.2-1.0=15.88\pm0.2,\end{aligned}\tag{125}$$

where we adopt $(m-M)_{I,\mathrm{V1668\ Cyg}}=14.6-1.6\times0.30=14.12$ and $(m-M)_{I,\mathrm{V679\ Car}}=16.1-1.6\times0.69=15.0$ from Hachisu & Kato (2019), and $(m-M)_{I,\mathrm{V5584\ Sgr}}=16.7-1.6\times0.70=15.58$ from Appendix A.16. Unfortunately, neither I_{C} nor I data of LV Vul are available. We have $(m-M)_{I,\mathrm{V2676\ Oph}}=15.88\pm0.1$.

We plot $(m-M)_B=18.2$, $(m-M)_V=17.3$, and $(m-M)_I=15.88$, which cross at $d=8.0$ kpc and $E(B-V)=0.90$, in Figure 15(b). Thus, we obtain $E(B-V)=0.90\pm0.05$ and $d=8.0\pm1$ kpc.

A.23. V5589 Sgr 2012#1

Figure 91 shows the (a) visual and V, and (b) $(B-V)_0$ evolutions of V5589 Sgr. Here, $(B-V)_0$ are dereddened with $E(B-V)=0.84$ as obtained in Section 3.23. Figure 92 shows the light/color curves of V5589 Sgr, V5583 Sgr, V382 Vel, and LV Vul. Applying Equation (6) to them, we have the relation

$$\begin{aligned}(m-M)_{V,\mathrm{V5589\ Sgr}}&=(m-M+\Delta V)_{V,\mathrm{LV\ Vul}}-2.5\log 0.21\\&=11.85+4.1\pm0.2+1.68=17.63\pm0.2\\&=(m-M+\Delta V)_{V,\mathrm{V382\ Vel}}-2.5\log 0.42\\&=11.5+5.1\pm0.2+0.95=17.55\pm0.2\\&=(m-M+\Delta V)_{V,\mathrm{V5583\ Sgr}}-2.5\log 0.42\\&=16.3+0.3\pm0.2+0.95=17.55\pm0.2,\end{aligned}\tag{126}$$

where we adopt $(m-M)_{V,\mathrm{LV\ Vul}}=11.85$ and $(m-M)_{V,\mathrm{V382\ Vel}}=11.5$ from Hachisu & Kato (2019), and $(m-M)_{V,\mathrm{V5583\ Sgr}}=16.3$ in Section 3.15. Thus, we adopt $(m-M)_V=17.6\pm0.1$ and $f_{\mathrm{s}}=0.21$ against LV Vul. From Equations (1), (6), and (126), we have the relation

$$\begin{aligned}(m-M')_{V,\mathrm{V5589\ Sgr}}&\equiv(m_V-(M_V-2.5\log f_{\mathrm{s}}))_{\mathrm{V5589\ Sgr}}\\&=((m-M)_V+\Delta V)_{\mathrm{LV\ Vul}}\\&=11.85+4.1\pm0.2=15.95\pm0.2.\end{aligned}\tag{127}$$

Figure 93 shows the B, V, and I_C light curves of V5589 Sgr together with those of V834 Car, YY Dor, and LMC N 2009a. We apply Equation (9) for the B band to Figure 93(a) and obtain

$$\begin{aligned}(m-M)_{B,\mathrm{V5589\ Sgr}} &= ((m-M)_B+\Delta B)_{\mathrm{V834\ Car}} - 2.5\log 0.33\\ &= 17.75 - 0.5 \pm 0.2 + 1.2 = 18.45 \pm 0.2\\ &= ((m-M)_B+\Delta B)_{\mathrm{YY\ Dor}} - 2.5\log 1.12\\ &= 18.98 - 0.4 \pm 0.2 - 0.13 = 18.45 \pm 0.2\\ &= ((m-M)_B+\Delta B)_{\mathrm{LMC\ N\ 2009a}} - 2.5\log 0.71\\ &= 18.98 - 0.9 \pm 0.2 + 0.37 = 18.45 \pm 0.2. \end{aligned} \quad (128)$$

We have $(m-M)_{B,\mathrm{V5589\ Sgr}} = 18.45 \pm 0.1$.

For the V light curves in Figure 93(b), we similarly obtain

$$\begin{aligned}(m-M)_{V,\mathrm{V5589\ Sgr}} &= ((m-M)_V+\Delta V)_{\mathrm{V834\ Car}} - 2.5\log 0.33\\ &= 17.3 - 0.9 \pm 0.2 + 1.2 = 17.6 \pm 0.2\\ &= ((m-M)_V+\Delta V)_{\mathrm{YY\ Dor}} - 2.5\log 1.12\\ &= 18.86 - 1.1 \pm 0.2 - 0.13 = 17.63 \pm 0.2\\ &= ((m-M)_V+\Delta V)_{\mathrm{LMC\ N\ 2009a}} - 2.5\log 0.71\\ &= 18.86 - 1.6 \pm 0.2 + 0.37 = 17.63 \pm 0.2. \end{aligned} \quad (129)$$

We have $(m-M)_{V,\mathrm{V5589\ Sgr}} = 17.62 \pm 0.1$, which is consistent with Equation (116).

We apply Equation (10) for the I_C band to Figure 93(c) and obtain

$$\begin{aligned}(m-M)_{I,\mathrm{V5589\ Sgr}} &= ((m-M)_I+\Delta I_C)_{\mathrm{V834\ Car}} - 2.5\log 0.33\\ &= 16.45 - 1.4 \pm 0.2 + 1.2 = 16.25 \pm 0.2\\ &= ((m-M)_I+\Delta I_C)_{\mathrm{YY\ Dor}} - 2.5\log 1.12\\ &= 18.67 - 2.3 \pm 0.2 - 0.13 = 16.24 \pm 0.2\\ &= ((m-M)_I+\Delta I_C)_{\mathrm{LMC\ N\ 2009a}} - 2.5\log 0.71\\ &= 18.67 - 2.8 \pm 0.2 + 0.37 = 16.24 \pm 0.2. \end{aligned} \quad (130)$$

We have $(m-M)_{I,\mathrm{V5589\ Sgr}} = 16.25 \pm 0.1$.

We plot $(m-M)_B = 18.45$, $(m-M)_V = 17.62$, and $(m-M)_I = 16.25$, which cross at $d = 10$ kpc and $E(B-V) = 0.84$, in Figure 15(c). Thus, we obtain $E(B-V) = 0.84 \pm 0.05$ and $d = 10 \pm 1$ kpc.

The orbital period of V5589 Sgr is $P_{\mathrm{orb}} = 1.5923$ days, and its companion is a subgiant (Mróz et al. 2015). This binary parameter reminds us of U Sco, the orbital period of which is $P_{\mathrm{orb}} = 1.23$ days (e.g., Schaefer 2011). We plot the color–magnitude diagram of (a) V5589 Sgr as well as that of the recurrent novae (b) CI Aql, (c) U Sco, and (d) LMC N 2009a in Figure 94. The orbital periods of CI Aql and LMC N 2009a are $P_{\mathrm{orb}} = 0.618$ days (e.g., Schaefer 2011) and $P_{\mathrm{orb}} = 1.19$ days (Bode et al. 2016), respectively. The track of V5589 Sgr is very close to the U Sco track in the color–magnitude diagram. In these binary systems, the accretion disk is so bright in the SSS phase, and it makes the $B-V$ color blue, $(B-V)_0 \sim -0.2$ to 0.0 in the later phase ($M_V \gtrsim -2$).

Hachisu & Kato (2016b) empirically found that the turning point (or inflection point) of nova tracks in the color–magnitude diagram can be clearly identified in many of the V1500 Cyg-type novae, and that the start of the nebular phase almost coincides with the turning point, and that they are located on the two-headed black arrow in Figure 94. The turning point of V5589 Sgr is not clearly identified, but its location is almost on the two-headed arrow. This may support that our distance modulus of $(m-M)_V = 17.6$ is reasonable.

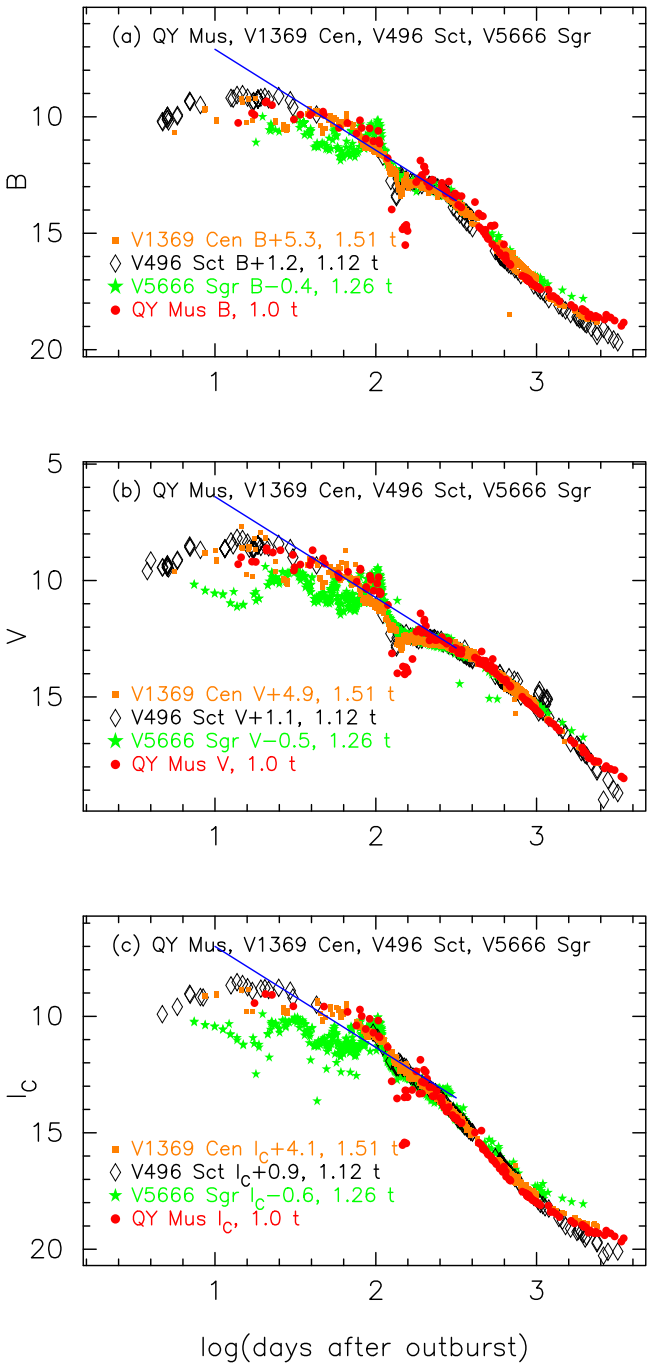

Figure 59. Same as Figure 25, but for QY Mus. The (a) B, (b) V, and (c) I_C light curves of QY Mus as well as those of V1369 Cen, V496 Sct, and V5666 Sgr. The BV data of QY Mus are the same as those in Figure 57. The I_C data of QY Mus are taken from AAVSO and SMARTS.

A.24. V2677 Oph 2012#2

Figure 95 shows the (a) visual, V, and (b) $(B-V)_0$ evolutions of V2677 Oph. Here, $(B-V)_0$ are dereddened with $E(B-V) = 1.30$ as explained in Section 3.24. Figure 96

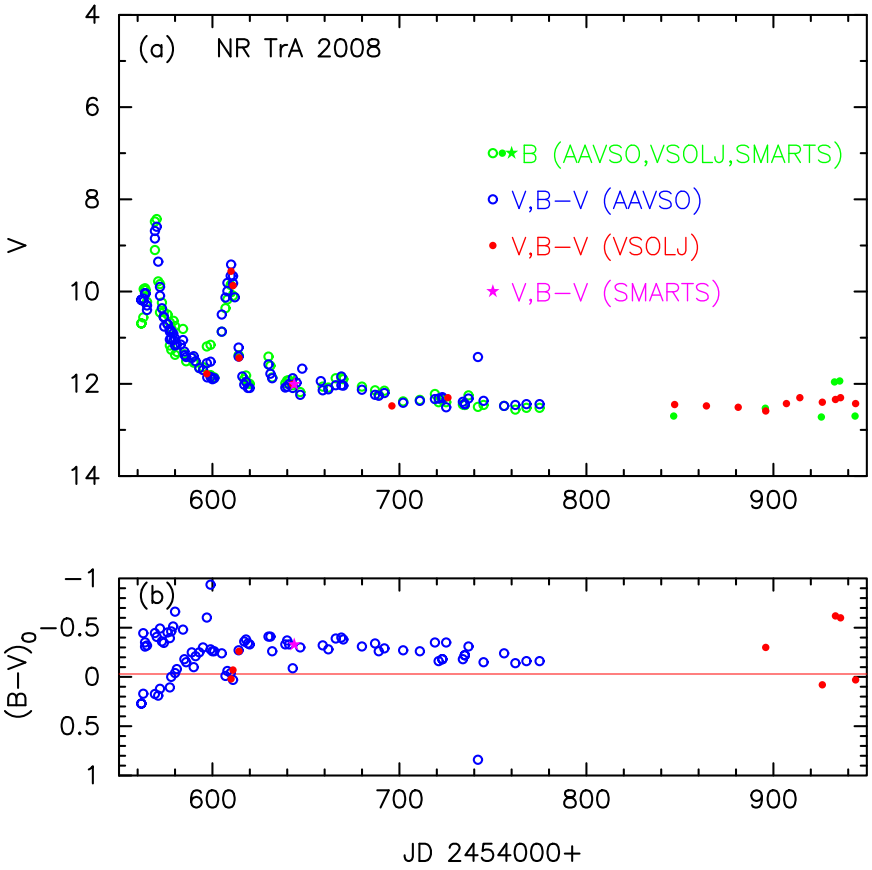

Figure 60. Same as Figure 23, but for NR TrA. (a) The V (unfilled blue circles) and B (unfilled green circles) data are taken from AAVSO. The V (filled red circles) and B (filled green circles) data are from VSOLJ. The V (filled magenta stars) and B (filled green stars) data are from SMARTS. (b) The $(B-V)_0$ are dereddened with $E(B-V)=0.24$.

shows the light/color curves of V2677 Oph, LV Vul, and V1065 Cen. Applying Equation (6) to them, we have the relation

$$\begin{aligned}(m-M)_{V,\mathrm{V2677\ Oph}} &= (m-M+\Delta V)_{V,\mathrm{LV\ Vul}} - 2.5\log 0.68\\ &= 11.85 + 6.9 \pm 0.2 + 0.43 = 19.18 \pm 0.2\\ &= (m-M+\Delta V)_{V,\mathrm{V1065\ Cen}} - 2.5\log 0.68\\ &= 15.0 + 3.8 \pm 0.2 + 0.43 = 19.23 \pm 0.2, \end{aligned} \quad (131)$$

where we adopt $(m-M)_{V,\mathrm{LV\ Vul}} = 11.85$ from Hachisu & Kato (2019) and $(m-M)_{V,\mathrm{V1065\ Cen}} = 15.0$ from Hachisu & Kato (2018a). Thus, we obtain $(m-M)_V = 19.2 \pm 0.1$ and $f_s = 0.68$ against LV Vul. From Equations (1), (6), and (131), we have the relation

$$\begin{aligned}(m-M')_{V,\mathrm{V2677\ Oph}} &\equiv (m_V - (M_V - 2.5\log f_s))_{\mathrm{V2677\ Oph}}\\ &= ((m-M)_V + \Delta V)_{\mathrm{LV\ Vul}}\\ &= 11.85 + 6.9 \pm 0.2 = 18.75 \pm 0.2. \end{aligned} \quad (132)$$

Figure 97 shows the B, V, and I_C light curves of V2677 Oph together with those of V834 Car, YY Dor, and LMC N 2009a. We apply Equation (9) for the B band to Figure 97(a) and obtain

$$\begin{aligned}&(m-M)_{B,\mathrm{V2677\ Oph}}\\ &= ((m-M)_B + \Delta B)_{\mathrm{V834\ Car}} - 2.5\log 1.05\\ &= 17.75 + 2.8 \pm 0.2 - 0.05 = 20.5 \pm 0.2\\ &= ((m-M)_B + \Delta B)_{\mathrm{YY\ Dor}} - 2.5\log 3.5\\ &= 18.98 + 2.9 \pm 0.2 - 1.38 = 20.5 \pm 0.2\\ &= ((m-M)_B + \Delta B)_{\mathrm{LMC\ N\ 2009a}} - 2.5\log 2.24\\ &= 18.98 + 2.4 \pm 0.2 - 0.88 = 20.5 \pm 0.2. \end{aligned} \quad (133)$$

We have $(m-M)_{B,\mathrm{V2677\ Oph}} = 20.5 \pm 0.1$.

For the V light curves in Figure 97(b), we similarly obtain

$$\begin{aligned}&(m-M)_{V,\mathrm{V2677\ Oph}}\\ &= ((m-M)_V + \Delta V)_{\mathrm{V834\ Car}} - 2.5\log 1.05\\ &= 17.25 + 2.0 \pm 0.2 - 0.05 = 19.2 \pm 0.2\\ &= ((m-M)_V + \Delta V)_{\mathrm{YY\ Dor}} - 2.5\log 3.5\\ &= 18.86 + 1.7 \pm 0.2 - 1.38 = 19.18 \pm 0.2\\ &= ((m-M)_V + \Delta V)_{\mathrm{LMC\ N\ 2009a}} - 2.5\log 2.24\\ &= 18.86 + 1.2 \pm 0.2 - 0.88 = 19.18 \pm 0.2. \end{aligned} \quad (134)$$

We have $(m-M)_{V,\mathrm{V2677\ Oph}} = 19.18 \pm 0.1$, which is consistent with Equation (131).

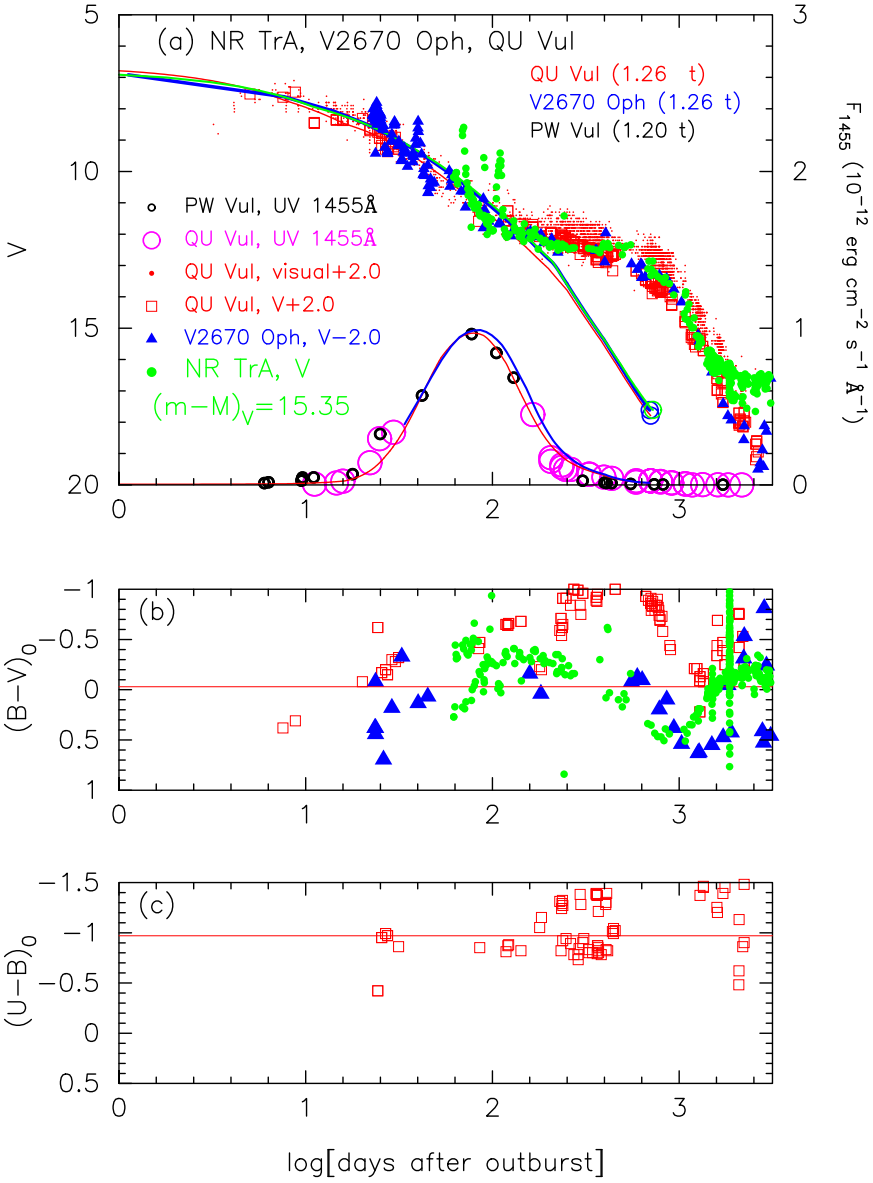

Figure 61. Same as Figure 54, but for NR TrA (filled green circles). The data of NR TrA are the same as those in Figure 60. The timescales of QU Vul and V2670 Oph are stretched by 1.26. The timescale of PW Vul is also stretched by 1.20. In panel (a), we added model light curves (solid green lines) of a 0.75 $M_\odot$ WD (CO3, Hachisu & Kato 2016a), assuming that $(m-M)_V = 15.35$ for NR TrA. The solid blue lines denote the V and UV 1455 Å light curve of a 0.80 $M_\odot$ WD (CO3), assuming that $(m-M)_V = 17.6$ for V2670 Oph. The solid red lines denote the V and UV 1455 Å light curve of a 0.86 $M_\odot$ WD (CO4), assuming that $(m-M)_V = 13.6$ for QU Vul.

We apply Equation (10) for the I_C band to Figure 97(c) and obtain

$$\begin{aligned}
&(m-M)_{I,\mathrm{V2677\ Oph}} \\
&= ((m-M)_I + \Delta I_C)_{\mathrm{V834\ Car}} - 2.5\log 1.05 \\
&= 16.45 + 0.7 \pm 0.2 - 0.05 = 17.1 \pm 0.2 \\
&= ((m-M)_I + \Delta I_C)_{\mathrm{YY\ Dor}} - 2.5\log 3.5 \\
&= 18.67 - 0.2 \pm 0.2 - 1.38 = 17.09 \pm 0.2 \\
&= ((m-M)_I + \Delta I_C)_{\mathrm{LMC\ N\ 2009a}} - 2.5\log 2.24 \\
&= 18.67 - 0.7 \pm 0.2 - 0.88 = 17.09 \pm 0.2. \qquad (135)
\end{aligned}$$

We have $(m-M)_{I,\mathrm{V2677\ Oph}} = 17.1 \pm 0.1$.

We plot $(m-M)_B = 20.5$, $(m-M)_V = 19.18$, and $(m-M)_I = 17.1$, which cross at $d = 10.7$ kpc and $E(B-V) = 1.30$, in Figure 15(d). Thus, we obtain $E(B-V) = 1.30 \pm 0.10$ and $d = 10.7 \pm 2$ kpc.

A.25. V1324 Sco 2012

Figure 98 shows the (a) visual, V, K_s, and (b) $(B-V)_0$ evolutions of V1324 Sco. Here, $(B-V)_0$ are dereddened with $E(B-V) = 1.32$ as obtained in Section 3.25. Figure 99 shows the light/color curves of V1324 Sco as well as those of LV Vul, V496 Sct, and V1369 Cen. The V light and $(B-V)_0$ color curves of these four novae overlap each other except for the dust blackout phase. Applying Equation (6) to them, we

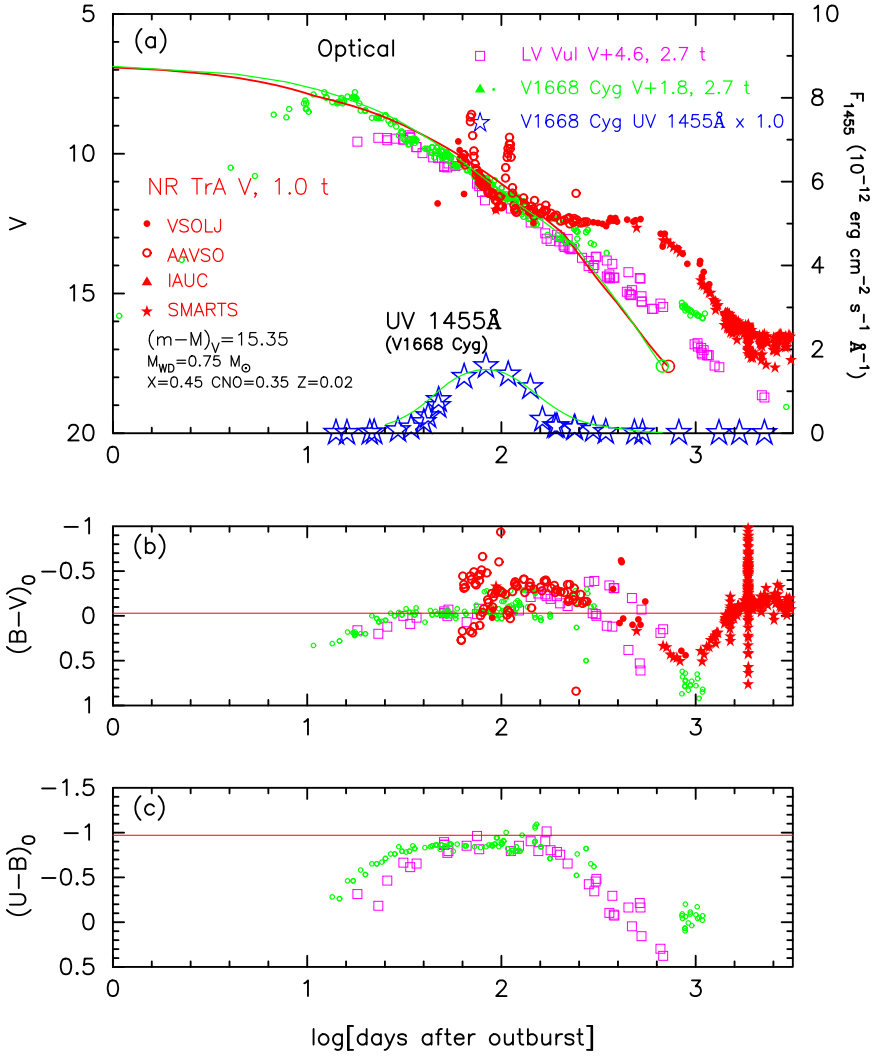

Figure 62. Same as Figure 55, but for NR TrA (red symbols). In panel (a), we added model light curves (solid red lines) of a 0.75 $M_\odot$ WD (CO3; Hachisu & Kato 2016a), assuming that $(m-M)_V = 15.35$ for NR TrA. The solid green lines denote the V and UV 1455 Å light curve of a 0.98 $M_\odot$ WD (CO3), assuming that $(m-M)_V = 14.6$ for V1668 Cyg.

have the relation

$$\begin{aligned}(m-M)_{V,\mathrm{V1324\ Sco}} &= (m-M+\Delta V)_{V,\mathrm{LV\ Vul}} - 2.5\log 2.1 \\ &= 11.85 + 5.9 \pm 0.3 - 0.82 = 16.93 \pm 0.3 \\ &= (m-M+\Delta V)_{V,\mathrm{V496\ Sct}} - 2.5\log 1.07 \\ &= 13.7 + 3.3 \pm 0.3 - 0.07 = 16.93 \pm 0.3 \\ &= (m-M+\Delta V)_{V,\mathrm{V1369\ Cen}} - 2.5\log 1.45 \\ &= 10.25 + 7.1 \pm 0.3 - 0.4 = 16.95 \pm 0.3, \end{aligned} \quad (136)$$

where we adopt $(m-M)_{V,\mathrm{LV\ Vul}} = 11.85$, $(m-M)_{V,\mathrm{V496\ Sct}} = 13.7$, and $(m-M)_{V,\mathrm{V1369\ Cen}} = 10.25$ from Hachisu & Kato (2019). Thus, we obtain $(m-M)_V = 16.95 \pm 0.2$ for V1324 Sco. From Equations (1), (6), and (136), we have the relation

$$\begin{aligned}(m-M')_{V,\mathrm{V1324\ Sco}} &\equiv (m_V - (M_V - 2.5\log f_s))_{\mathrm{V1324\ Sco}} \\ &= ((m-M)_V + \Delta V)_{\mathrm{LV\ Vul}} \\ &= 11.85 + 5.9 \pm 0.3 = 17.75 \pm 0.3. \end{aligned} \quad (137)$$

Figure 100 shows the B, V, and I_C light curves of V1324 Sco together with those of V679 Car, V5584 Sgr, LV Vul, and V1668 Cyg. We apply Equation (9) for the B band to Figure 100(a) and obtain

$$\begin{aligned}(m-M)_{B,\mathrm{V1324\ Sco}} &= ((m-M)_B + \Delta B)_{\mathrm{LV\ Vul}} - 2.5\log 2.1 \\ &= 12.45 + 6.6 \pm 0.2 - 0.82 = 18.23 \pm 0.2 \\ &= ((m-M)_B + \Delta B)_{\mathrm{V1668\ Cyg}} - 2.5\log 2.1 \\ &= 14.9 + 4.2 \pm 0.2 - 0.82 = 18.28 \pm 0.2 \\ &= ((m-M)_B + \Delta B)_{\mathrm{V679\ Car}} - 2.5\log 2.1 \\ &= 16.79 + 2.3 \pm 0.2 - 0.82 = 18.27 \pm 0.2 \\ &= ((m-M)_B + \Delta B)_{\mathrm{V5584\ Sgr}} - 2.5\log 1.58 \\ &= 17.4 + 1.3 \pm 0.2 - 0.5 = 18.2 \pm 0.2, \end{aligned} \quad (138)$$

where we adopt $(m-M)_{B,\mathrm{LV\ Vul}} = 11.85 + 0.60 = 12.45$, $(m-M)_{B,\mathrm{V1668\ Cyg}} = 14.6 + 0.30 = 14.9$, and $(m-M)_{B,\mathrm{V679\ Car}} = 16.1 + 0.69 = 16.79$ from Hachisu & Kato (2019), and $(m-M)_{B,\mathrm{V5584\ Sgr}} = 16.7 + 0.70 = 17.4$ from Appendix A.16. We have $(m-M)_{B,\mathrm{V1324\ Sco}} = 18.24 \pm 0.1$.

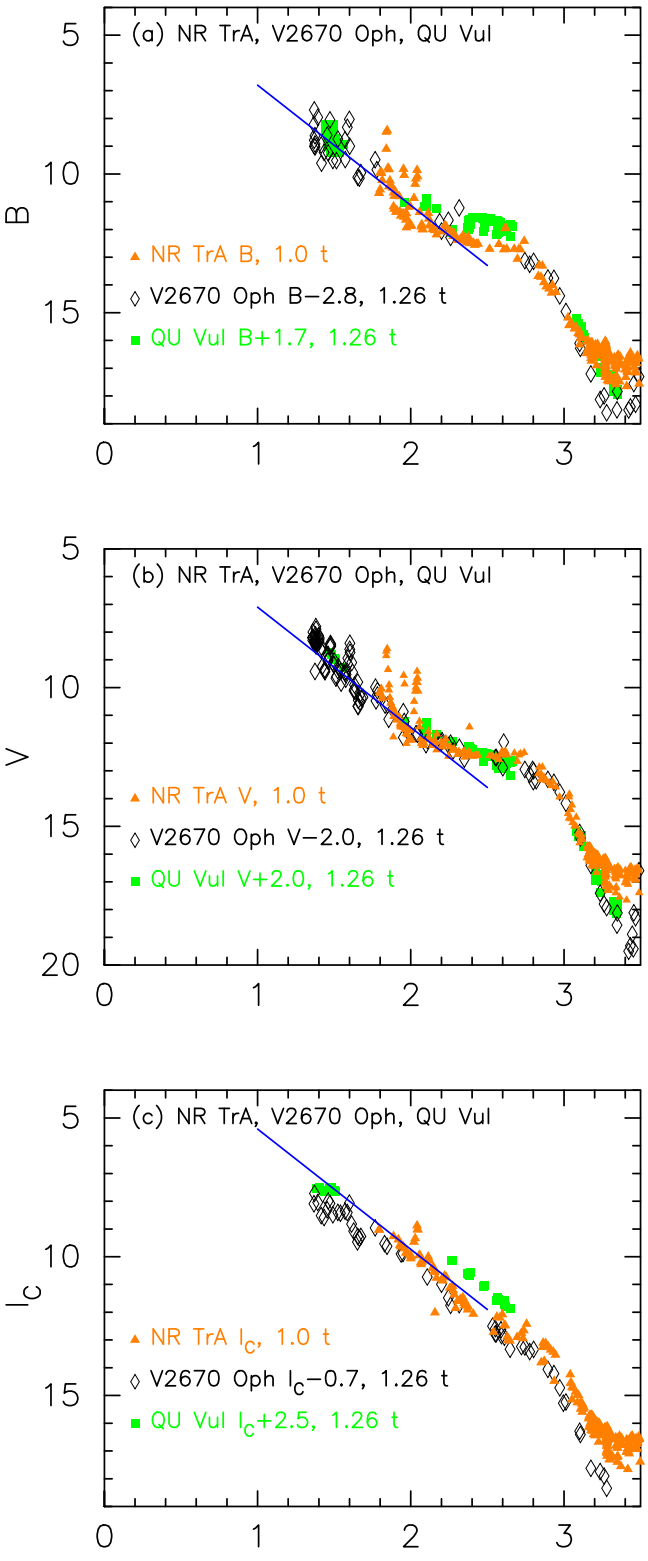

Figure 63. Same as Figure 25, but for NR TrA. The (a) B, (b) V, and (c) I_C light curves of NR TrA as well as those of QU Vul and V2670 Oph. The BV data of NR TrA are the same as those in Figure 60. The I_C data of NR TrA are taken from AAVSO, VSOLJ, and SMARTS.

For the V light curves in Figure 100(b), we similarly obtain

$$\begin{aligned}(m-M)_{V,\mathrm{V1324\ Sco}} &= ((m-M)_V+\Delta V)_{\mathrm{LV\ Vul}} - 2.5\log 2.1\\ &= 11.85+5.9\pm0.2-0.82 = 16.93\pm0.2\\ &= ((m-M)_V+\Delta V)_{\mathrm{V1668\ Cyg}} - 2.5\log 2.1\\ &= 14.6+3.2\pm0.2-0.82 = 16.98\pm0.2\\ &= ((m-M)_V+\Delta V)_{\mathrm{V679\ Car}} - 2.5\log 2.1\\ &= 16.1+1.7\pm0.2-0.82 = 16.98\pm0.2\\ &= ((m-M)_V+\Delta V)_{\mathrm{V5584\ Sgr}} - 2.5\log 1.58\\ &= 16.7+0.7\pm0.2-0.5 = 16.9\pm0.2, \end{aligned} \quad (139)$$

where we adopt $(m-M)_{V,\mathrm{LV\ Vul}} = 11.85$, $(m-M)_{V,\mathrm{V1668\ Cyg}} = 14.6$, $(m-M)_{V,\mathrm{V679\ Car}} = 16.1$ from Hachisu & Kato (2019), and $(m-M)_{V,\mathrm{V5584\ Sgr}} = 16.7$ from Appendix A.16. We have $(m-M)_{V,\mathrm{V1324\ Sco}} = 16.95\pm0.1$, which is consistent with Equation (136).

We apply Equation (10) for the I_C band to Figure 100(c) and obtain

$$\begin{aligned}(m-M)_{I,\mathrm{V1324\ Sco}} &= ((m-M)_I+\Delta I_C)_{\mathrm{V1668\ Cyg}} - 2.5\log 2.1\\ &= 14.12+1.5\pm0.2-0.82 = 14.8\pm0.2\\ &= ((m-M)_I+\Delta I_C)_{\mathrm{V679\ Car}} - 2.5\log 2.1\\ &= 15.0+0.6\pm0.2-0.82 = 14.78\pm0.2\\ &= ((m-M)_I+\Delta I_C)_{\mathrm{V5584\ Sgr}} - 2.5\log 1.58\\ &= 15.58-0.3\pm0.2-0.5 = 14.78\pm0.2, \end{aligned} \quad (140)$$

where we adopt $(m-M)_{I,\mathrm{V1668\ Cyg}} = 14.6-1.6\times0.30 = 14.12$ and $(m-M)_{I,\mathrm{V679\ Car}} = 16.1-1.6\times0.69 = 15.0$ from Hachisu & Kato (2019), and $(m-M)_{I,\mathrm{V5584\ Sgr}} = 16.7-1.6\times0.70 = 15.58$ from Appendix A.16. Unfortunately, neither I_C nor I data of LV Vul are available. We have $(m-M)_{I,\mathrm{V1324\ Sco}} = 14.78\pm0.2$.

We plot $(m-M)_B = 18.24$, $(m-M)_V = 16.95$, and $(m-M)_I = 14.78$, which cross at $d = 3.7$ kpc and $E(B-V)$ =1.32, in Figure 17(a). Thus, we obtain $E(B-V) = 1.32\pm0.1$ and $d = 3.7\pm0.6$ kpc.

A.26. V5592 Sgr 2012#4

Figure 101 shows the (a) visual, V, and (b) $(B-V)_0$ evolutions of V5592 Sgr. Here, $(B-V)_0$ are dereddened with $E(B-V) = 0.33$ as obtained in Section 3.26. The BJAA's (observer's ID) $B-V$ data of AAVSO are systematically bluer by 0.20 mag than the other $B-V$ data in AAVSO, so we shifted BJAA's $B-V$ data by 0.20 mag redder in the figure. As a result, these two $B-V$ data in the AAVSO archive overlap each other in Figure 101(b).

Figure 102 shows the light/color curves of V5592 Sgr as well as those of LV Vul and V705 Cas. We overlap these V light and $(B-V)_0$ color curves. Applying Equation (6) to

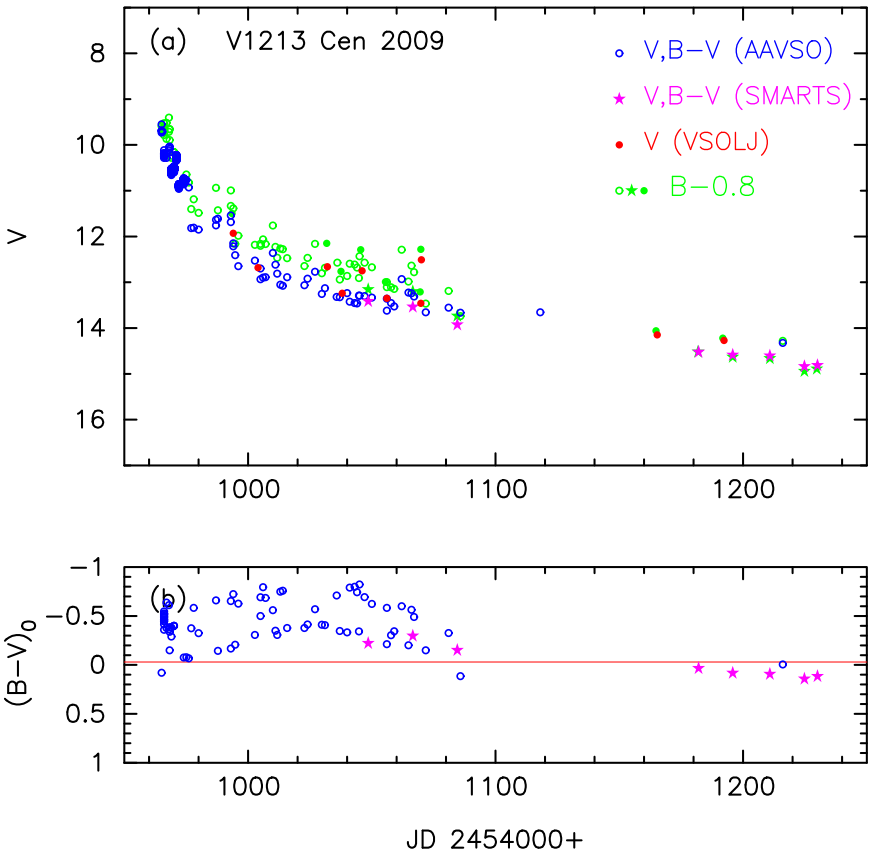

Figure 64. Same as Figure 23, but for V1213 Cen. (a) The V (unfilled blue circles) and B (unfilled green circles) data are taken from AAVSO. The V (filled red circles) and B (filled green circles) data are from VSOLJ. The SMARTS data of V (filled magenta stars) and B (filled green stars) are also plotted. (b) The $(B-V)_0$ are dereddened with $E(B-V)=0.78$.

them, we have the relation

$$\begin{aligned}(m-M)_{V,\mathrm{V5592\ Sgr}} &= (m-M+\Delta V)_{V,\mathrm{LV\ Vul}} - 2.5\log 1.35\\ &= 11.85+4.5\pm 0.3-0.33 = 16.02\pm 0.3\\ &= (m-M+\Delta V)_{V,\mathrm{V705\ Cas}} - 2.5\log 0.52\\ &= 13.45+1.9\pm 0.3+0.7 = 16.05\pm 0.3, \end{aligned} \quad (141)$$

where we adopt $(m-M)_{V,\mathrm{LV\ Vul}}=11.85$ and $(m-M)_{V,\mathrm{V705\ Cas}}=13.45$ from Hachisu & Kato (2019). Thus, we obtain $(m-M)_V=16.05\pm 0.2$ and $f_\mathrm{s}=1.35$ against LV Vul. From Equations (1), (6), and (141), we have the relation

$$\begin{aligned}(m-M')_{V,\mathrm{V5592\ Sgr}} &\equiv (m_V-(M_V-2.5\log f_\mathrm{s}))_{\mathrm{V5592\ Sgr}}\\ &= ((m-M)_V+\Delta V)_{\mathrm{LV\ Vul}}\\ &= 11.85+4.5\pm 0.3 = 16.35\pm 0.3. \end{aligned} \quad (142)$$

Figure 103 shows the B, V, and I_C light curves of V5592 Sgr together with those of V1369 Cen, V496 Sct, and V5666 Sgr. The light curves overlap each other. Applying Equation (9) for the B band to Figure 103(a), we have the relation

$$\begin{aligned}(m-M)_{B,\mathrm{V5592\ Sgr}} &= ((m-M)_B+\Delta B)_{\mathrm{V1369\ Cen}} - 2.5\log 0.91\\ &= 10.36+5.9\pm 0.2+0.1 = 16.36\pm 0.2\\ &= ((m-M)_B+\Delta B)_{\mathrm{V496\ Sct}} - 2.5\log 0.68\\ &= 14.15+1.8\pm 0.2+0.43 = 16.38\pm 0.2\\ &= ((m-M)_B+\Delta B)_{\mathrm{V5666\ Sgr}} - 2.5\log 0.76\\ &= 15.9+0.2\pm 0.2+0.3 = 16.4\pm 0.2, \end{aligned} \quad (143)$$

where we adopt $(m-M)_{B,\mathrm{V1369\ Cen}}=10.36$, $(m-M)_{B,\mathrm{V496\ Sct}}=14.15$, and $(m-M)_{B,\mathrm{V5666\ Sgr}}=15.9$ from Appendix A.12. We have $(m-M)_B=16.38\pm 0.1$ for V5592 Sgr.

Applying Equation (6) to Figure 103(b), we have the relation

$$\begin{aligned}(m-M)_{V,\mathrm{V5592\ Sgr}} &= ((m-M)_V+\Delta V)_{\mathrm{V1369\ Cen}} - 2.5\log 0.91\\ &= 10.25+5.7\pm 0.3+0.1 = 16.05\pm 0.2\\ &= ((m-M)_V+\Delta V)_{\mathrm{V496\ Sct}} - 2.5\log 0.68\\ &= 13.7+1.9\pm 0.3+0.43 = 16.03\pm 0.2\\ &= ((m-M)_V+\Delta V)_{\mathrm{V5666\ Sgr}} - 2.5\log 0.76\\ &= 15.4+0.4\pm 0.3+0.3 = 16.1\pm 0.2, \end{aligned} \quad (144)$$

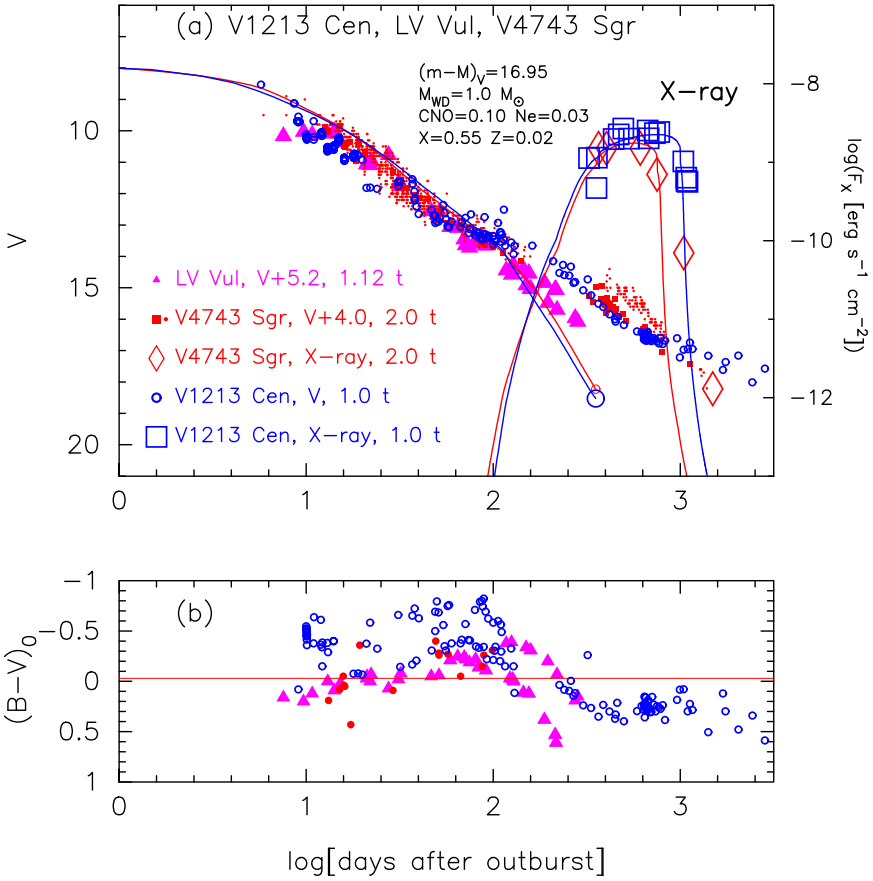

Figure 65. Same as Figure 30, but for V1213 Cen. We add the V light curves of LV Vul and V4743 Sgr. The data of V1213 Cen are the same as those in Figure 64. The data of V4743 Sgr are the same as those in Figures 18 of Hachisu & Kato (2010). In panel (a), we add model light curves (solid blue lines) of a 1.0 $M_\odot$ WD (Ne2; Hachisu & Kato 2010) both for the V and X-ray (0.2–2.0 keV), assuming that $(m-M)_V = 16.95$ for V1213 Cen. The solid red lines denote the model light curves of a 1.15 $M_\odot$ WD (Ne2), assuming $(m-M)_V = 13.7$ for V4743 Sgr (Hachisu & Kato 2010).

where we adopt $(m-M)_{V,\mathrm{V1369\ Cen}} = 10.25$, $(m-M)_{V,\mathrm{V496\ Sct}} = 13.7$, and $(m-M)_{V,\mathrm{V5666\ Sgr}} = 15.4$ from Hachisu & Kato (2019). We have $(m-M)_V = 16.06 \pm 0.1$, which is consistent with Equation (141).

From the I_C-band data in Figure 103(c), we obtain

$$\begin{aligned}(m-M)_{I,\mathrm{V5592\ Sgr}} &= ((m-M)_I + \Delta I_C)_{\mathrm{V1369\ Cen}} - 2.5\log 0.91\\ &= 10.07 + 5.4 \pm 0.2 + 0.1 = 15.57 \pm 0.2\\ &= ((m-M)_I + \Delta I_C)_{\mathrm{V496\ Sct}} - 2.5\log 0.68\\ &= 12.98 + 2.2 \pm 0.2 + 0.43 = 15.61 \pm 0.2\\ &= ((m-M)_I + \Delta I_C)_{\mathrm{V5666\ Sgr}} - 2.5\log 0.76\\ &= 14.6 + 0.7 \pm 0.2 + 0.3 = 15.6 \pm 0.2, \end{aligned} \quad (145)$$

where we adopt $(m-M)_{I,\mathrm{V1369\ Cen}} = 10.07$, $(m-M)_{I,\mathrm{V496\ Sct}} = 12.98$, and $(m-M)_{I,\mathrm{V5666\ Sgr}} = 14.6$ from Appendix A.12. We obtain $(m-M)_{I,\mathrm{V5592\ Sgr}} = 15.59 \pm 0.1$.

We plot $(m-M)_B = 16.38$, $(m-M)_V = 16.06$, and $(m-M)_I = 15.59$, which cross at $d = 10$ kpc and $E(B-V) = 0.33$, in Figure 17(b). Thus, we obtain $d = 10 \pm 1$ kpc and $E(B-V) = 0.33 \pm 0.05$.

A.27. V962 Cep 2014

Figure 104 shows the (a) visual, V, and (b) $(B-V)_0$ evolutions of V962 Cep. Here, $(B-V)_0$ are dereddened with $E(B-V) = 1.10$ as obtained in Section 3.27. Figure 105 shows the light/color curves of V962 Cep as well as those of LV Vul and V1668 Cyg. Applying Equation (6) to them, we have the relation

$$\begin{aligned}(m-M)_{V,\mathrm{V962\ Cep}} &= (m - M + \Delta V)_{V,\mathrm{LV\ Vul}} - 2.5\log 1.32\\ &= 11.85 + 6.9 \pm 0.2 - 0.30 = 18.45 \pm 0.2\\ &= (m - M + \Delta V)_{V,\mathrm{V1668\ Cyg}} - 2.5\log 1.32\\ &= 14.6 + 4.2 \pm 0.2 - 0.30 = 18.50 \pm 0.2, \end{aligned} \quad (146)$$

where we adopt $(m-M)_{V,\mathrm{LV\ Vul}} = 11.85$ and $(m-M)_{V,\mathrm{V1668\ Cyg}} = 14.6$ from Hachisu & Kato (2019). Thus, we obtain $(m-M)_V = 18.45 \pm 0.1$ and $f_s = 1.32$ against LV Vul. From Equations (1), (6), and (146), we have the relation

$$\begin{aligned}(m-M')_{V,\mathrm{V962\ Cep}} &\equiv (m_V - (M_V - 2.5\log f_s))_{\mathrm{V962\ Cep}}\\ &= ((m-M)_V + \Delta V)_{\mathrm{LV\ Vul}}\\ &= 11.85 + 6.9 \pm 0.2 = 18.75 \pm 0.2. \end{aligned} \quad (147)$$

Figure 106 shows the B, V, and I_C light curves of V962 Cep together with those of V834 Car, YY Dor, and LMC N 2009a. We apply Equation (9) for the B band to Figure 106(a) and

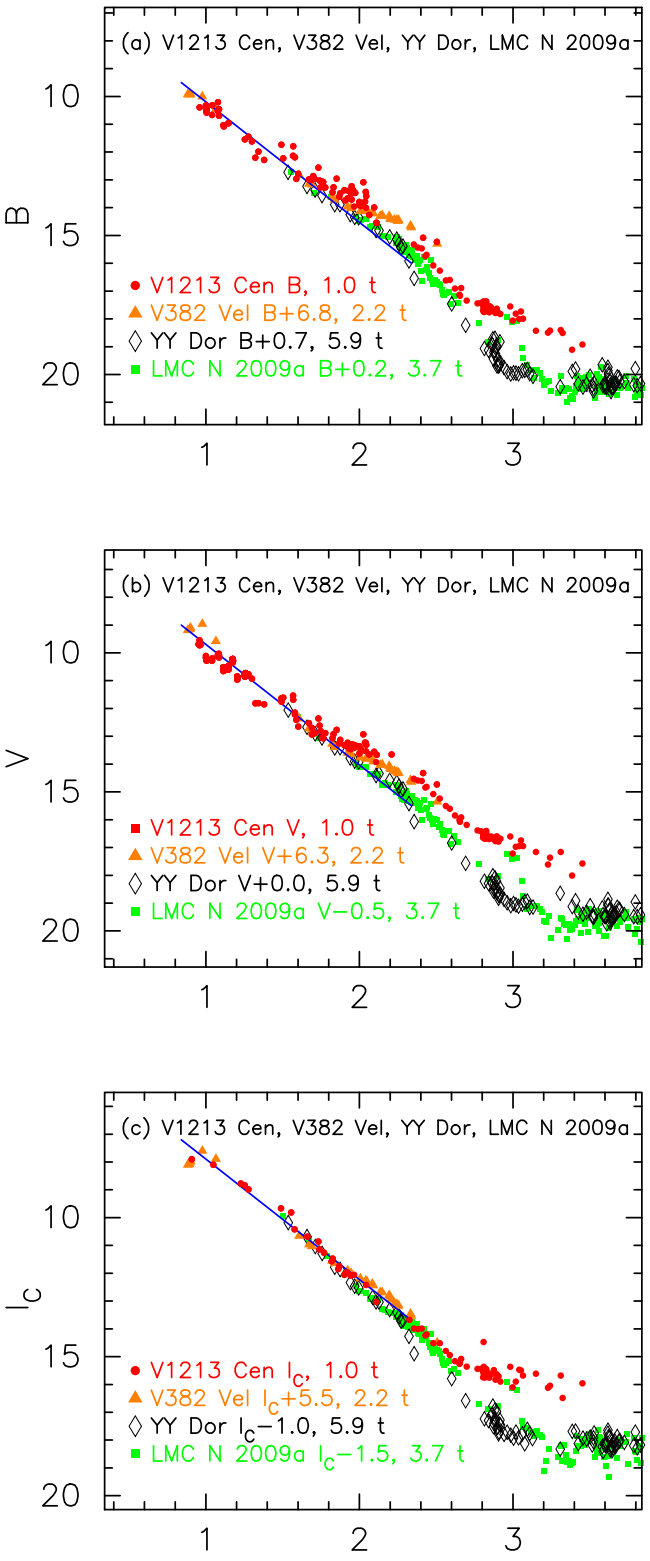

Figure 66. Same as Figure 25, but for V1213 Cen. The (a) B, (b) V, and (c) I_C light curves of V1213 Cen as well as those of V382 Vel, YY Dor, and LMC N 2009a. The BV data of V1213 Cen are the same as those in Figure 64. The I_C data of V1213 Cen are taken from AAVSO, VSOLJ, and SMARTS. The BVI_C data of V382 Vel are the same as those in Figure 40 of Hachisu & Kato (2019).

obtain

$$\begin{aligned}(m-M)_{B,\mathrm{V962\ Cep}} &= ((m-M)_B+\Delta B)_{\mathrm{V834\ Car}} - 2.5\log 2.0\\ &= 17.75 + 2.6 \pm 0.2 - 0.78 = 19.57 \pm 0.2\\ &= ((m-M)_B+\Delta B)_{\mathrm{YY\ Dor}} - 2.5\log 6.9\\ &= 18.98 + 2.7 \pm 0.2 - 2.1 = 19.58 \pm 0.2\\ &= ((m-M)_B+\Delta B)_{\mathrm{LMC\ N\ 2009a}} - 2.5\log 4.4\\ &= 18.98 + 2.2 \pm 0.2 - 1.6 = 19.58 \pm 0.2, \end{aligned} \quad (148)$$

where we adopt $(m-M)_{B,\mathrm{V834\ Car}} = 17.25 + 0.50 = 17.75$. We have $(m-M)_{B,\mathrm{V962\ Cep}} = 19.58 \pm 0.1$.

For the V light curves in Figure 106(b), we similarly obtain

$$\begin{aligned}(m-M)_{V,\mathrm{V962\ Cep}} &= ((m-M)_V+\Delta V)_{\mathrm{V834\ Car}} - 2.5\log 2.0\\ &= 17.25 + 2.0 \pm 0.2 - 0.78 = 18.47 \pm 0.2\\ &= ((m-M)_V+\Delta V)_{\mathrm{YY\ Dor}} - 2.5\log 6.9\\ &= 18.86 + 1.7 \pm 0.2 - 2.1 = 18.46 \pm 0.2\\ &= ((m-M)_V+\Delta V)_{\mathrm{LMC\ N\ 2009a}} - 2.5\log 4.4\\ &= 18.86 + 1.2 \pm 0.2 - 1.6 = 18.46 \pm 0.2, \end{aligned} \quad (149)$$

where we adopt $(m-M)_{V,\mathrm{V834\ Car}} = 17.25$. We have $(m-M)_{V,\mathrm{V962\ Cep}} = 18.46 \pm 0.1$, which is consistent with Equation (146).

We apply Equation (10) for the I_C band to Figure 106(c) and obtain

$$\begin{aligned}(m-M)_{I,\mathrm{V962\ Cep}} &= ((m-M)_I+\Delta I_C)_{\mathrm{V834\ Car}} - 2.5\log 2.0\\ &= 16.45 + 1.0 \pm 0.2 - 0.78 = 16.67 \pm 0.2\\ &= ((m-M)_I+\Delta I_C)_{\mathrm{YY\ Dor}} - 2.5\log 6.9\\ &= 18.67 + 0.1 \pm 0.2 - 2.1 = 16.67 \pm 0.2\\ &= ((m-M)_I+\Delta I_C)_{\mathrm{LMC\ N\ 2009a}} - 2.5\log 4.4\\ &= 18.67 - 0.4 \pm 0.2 - 1.6 = 16.67 \pm 0.2, \end{aligned} \quad (150)$$

where we adopt $(m-M)_{I,\mathrm{V834\ Car}} = 17.25 - 1.6 \times 0.50 = 16.45$. We have $(m-M)_{I,\mathrm{V962\ Cep}} = 16.67 \pm 0.1$.

We plot $(m-M)_B = 19.58$, $(m-M)_V = 18.46$, and $(m-M)_I = 16.67$, which cross at $d = 10.2$ kpc and $E(B-V) = 1.10$, in Figure 17(c). Thus, we obtain $E(B-V) = 1.10 \pm 0.10$ and $d = 10.2 \pm 2$ kpc.

A.28. V2659 Cyg 2014

Figure 107 shows (a) the V light and (b) $(B-V)_0$ color curves of V2659 Cyg on a linear timescale. Here, $(B-V)_0$ are dereddened with $E(B-V) = 0.80$ as explained in Section 3.28. Figure 108 shows the V light and $(B-V)_0$ color curves of V2659 Cyg, LV Vul, V5666 Sgr, V1369 Cen, and V496 Sct. The light curves of V2659 Cyg, V5666 Sgr, V1369 Cen, and V496 Sct are so similar to each other.

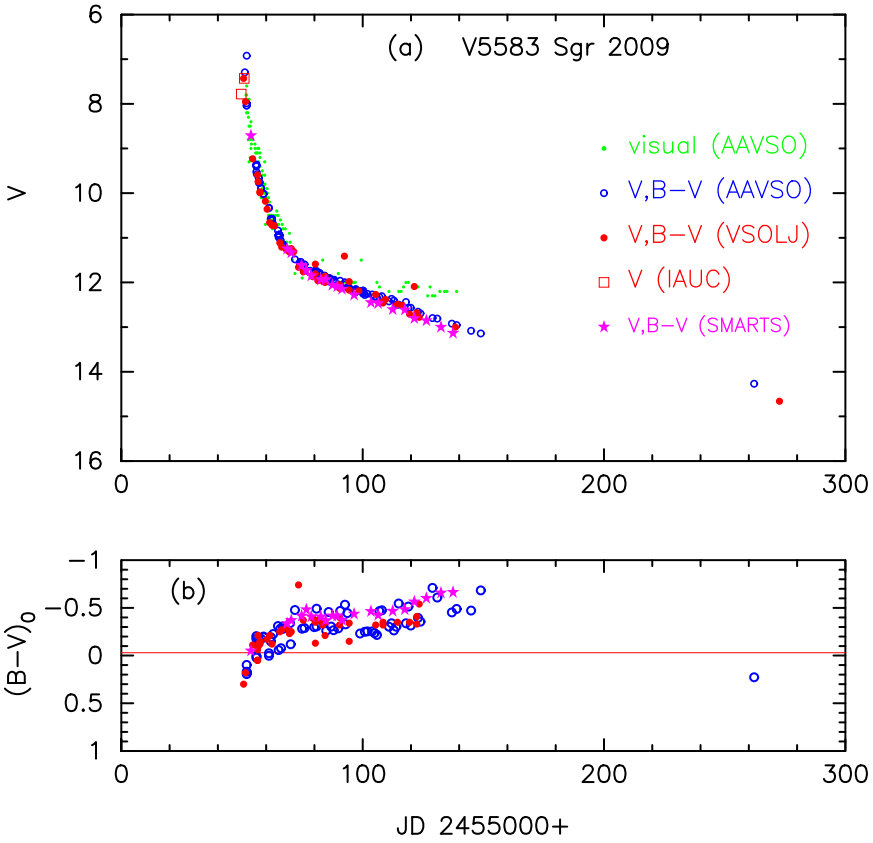

Figure 67. Same as Figure 23, but for V5583 Sgr. The V and $B-V$ (unfilled blue circles) and visual (green dots) data are taken from AAVSO. The V and $B-V$ (filled red circles) data are from VSOLJ. The V (unfilled red squares) data are from IAU Circulars. The SMARTS data of V and $B-V$ (filled magenta stars) are also plotted. In panel (b), the $(B-V)_0$ colors are dereddened with $E(B-V)=0.30$.

Applying Equation (6) to them, we have the relation

$$\begin{aligned}(m-M)_{V,\mathrm{V2659\ Cyg}} &= (m-M+\Delta V)_{V,\mathrm{LV\ Vul}} - 2.5\log 3.3\\ &= 11.85+5.1\pm0.3-1.30=15.65\pm0.3\\ &= (m-M+\Delta V)_{V,\mathrm{V5666\ Sgr}} - 2.5\log 1.86\\ &= 15.4+1.0\pm0.3-0.68=15.72\pm0.3\\ &= (m-M+\Delta V)_{V,\mathrm{V1369\ Cen}} - 2.5\log 2.24\\ &= 10.25+6.3\pm0.3-0.88=15.67\pm0.3\\ &= (m-M+\Delta V)_{V,\mathrm{V496\ Sct}} - 2.5\log 1.66\\ &= 13.7+2.5\pm0.3-0.55=15.65\pm0.3, \end{aligned} \quad (151)$$

where we adopt $(m-M)_{V,\mathrm{LV\ Vul}}=11.85$, $(m-M)_{V,\mathrm{V5666\ Sgr}}=15.4$, $(m-M)_{V,\mathrm{V1369\ Cen}}=10.25$, and $(m-M)_{V,\mathrm{V496\ Sct}}=13.7$ in Hachisu & Kato (2019). Thus, we obtained $(m-M)_V=15.65\pm0.1$ and $f_\mathrm{s}=3.3$ against LV Vul. From Equations (1), (6), and (151), we have the relation

$$\begin{aligned}(m-M')_{V,\mathrm{V2659\ Cyg}} &\equiv (m_V-(M_V-2.5\log f_\mathrm{s}))_{\mathrm{V2659\ Cyg}}\\ &= ((m-M)_V+\Delta V)_{\mathrm{LV\ Vul}}\\ &= 11.85+5.1\pm0.3=16.95\pm0.3. \end{aligned} \quad (152)$$

Figure 109 shows the B, V, and I_C light curves of V2659 Cyg together with those of V1369 Cen, V496 Sct, and V5666 Sgr. The light curves overlap each other. Applying Equation (9) for the B band to Figure 109(a), we have the relation

$$\begin{aligned}(m-M)_{B,\mathrm{V2659\ Cyg}} &= ((m-M)_B+\Delta B)_{\mathrm{V1369\ Cen}} - 2.5\log 2.24\\ &= 10.36+7.0\pm0.2-0.88=16.48\pm0.2\\ &= ((m-M)_B+\Delta B)_{\mathrm{V496\ Sct}} - 2.5\log 1.66\\ &= 14.15+2.9\pm0.2-0.55=16.5\pm0.2\\ &= ((m-M)_B+\Delta B)_{\mathrm{V5666\ Sgr}} - 2.5\log 1.86\\ &= 15.9+1.3\pm0.2-0.68=16.52\pm0.2, \end{aligned} \quad (153)$$

where we adopt $(m-M)_{B,\mathrm{V1369\ Cen}}=10.25+0.11=10.36$, $(m-M)_{B,\mathrm{V496\ Sct}}=13.7+0.45=14.15$, and $(m-M)_{B,\mathrm{V5666\ Sgr}}=15.4+0.50=15.9$ from Appendix A.12. We have $(m-M)_B=16.5\pm0.1$ for V2659 Cyg.

Applying Equation (6) to Figure 109(b), we have the relation

$$\begin{aligned}(m-M)_{V,\mathrm{V2659\ Cyg}} &= ((m-M)_V+\Delta V)_{\mathrm{V1369\ Cen}} - 2.5\log 2.24\\ &= 10.25+6.3\pm0.2-0.88=15.67\pm0.2\\ &= ((m-M)_V+\Delta V)_{\mathrm{V496\ Sct}} - 2.5\log 1.66\\ &= 13.7+2.5\pm0.2-0.55=15.65\pm0.2\\ &= ((m-M)_V+\Delta V)_{\mathrm{V5666\ Sgr}} - 2.5\log 1.86\\ &= 15.4+1.0\pm0.2-0.68=15.72\pm0.2, \end{aligned} \quad (154)$$

where we adopt $(m-M)_{V,\mathrm{V1369\ Cen}}=10.25$, $(m-M)_{V,\mathrm{V496\ Sct}}=13.7$, and $(m-M)_{V,\mathrm{V5666\ Sgr}}=15.4$ from Hachisu & Kato (2019).

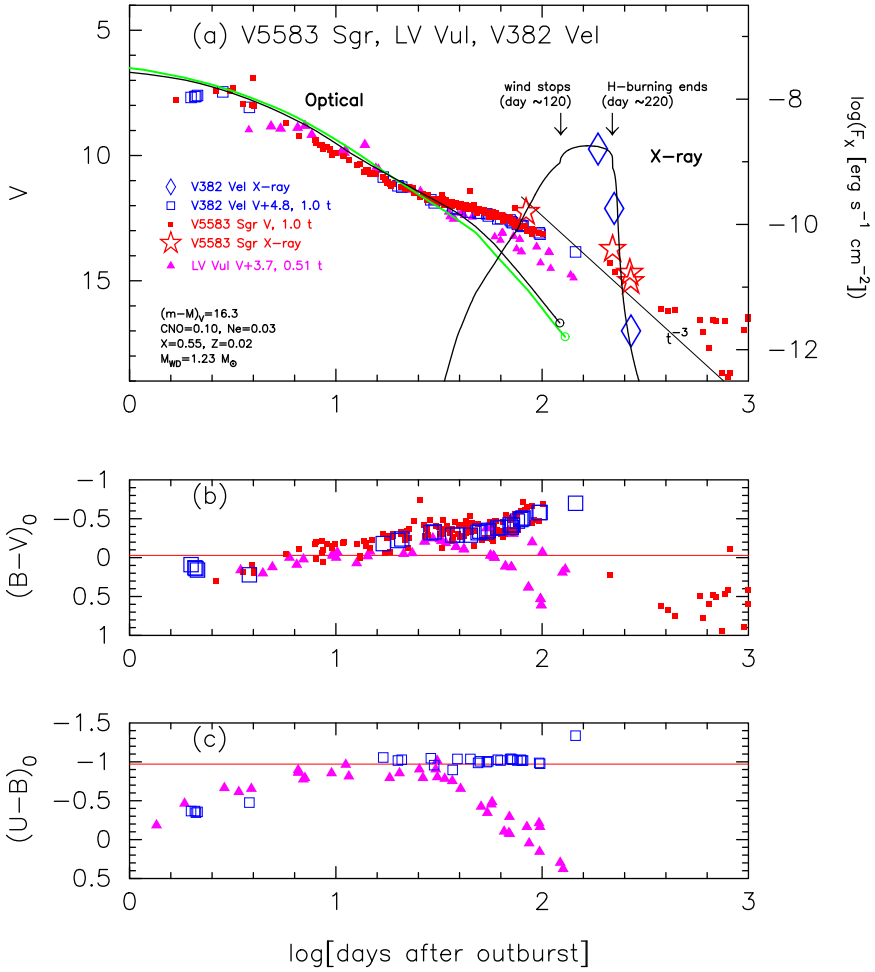

Figure 68. Same as Figure 30, but for V5583 Sgr (filled red squares). We overplot the V382 Vel light curves by unfilled blue squares. The data of V5583 Sgr are the same as those in Figure 67. The data of V382 Vel are the same as those in Figures 25–29 of Hachisu & Kato (2016a) and Figure 39 of Hachisu & Kato (2016b). We assume that the timescale of V382 Vel is the same as that of V5583 Sgr, but shift down the V magnitude of V382 Vel by 4.8 mag. In panel (a), we added model light curves (solid black lines) of a 1.23 $M_\odot$ WD (Ne2; Hachisu & Kato 2010, 2016a) both for the V and X-ray, assuming that $(m-M)_V = 16.3$ for V5583 Sgr and $(m-M)_V = 11.5$ for V382 Vel (Hachisu & Kato 2019). For comparison, we add the light curve of a 0.98 $M_\odot$ WD (CO3, solid green line), assuming that $(m-M)_V = 11.85$ for LV Vul.

We have $(m-M)_V = 15.68 \pm 0.1$, which is consistent with Equation (151).

From the I_C-band data in Figure 109(c), we obtain

$$\begin{aligned}(m-M)_{I,\mathrm{V2659\ Cyg}} &= ((m-M)_I + \Delta I_C)_{\mathrm{V1369\ Cen}} - 2.5\log 2.24 \\ &= 10.07 + 5.2 \pm 0.2 - 0.88 = 14.39 \pm 0.2 \\ &= ((m-M)_I + \Delta I_C)_{\mathrm{V496\ Sct}} - 2.5\log 1.66 \\ &= 12.98 + 2.0 \pm 0.2 - 0.55 = 14.43 \pm 0.2 \\ &= ((m-M)_I + \Delta I_C)_{\mathrm{V5666\ Sgr}} - 2.5\log 1.86 \\ &= 14.6 + 0.5 \pm 0.2 - 0.68 = 14.42 \pm 0.2, \end{aligned} \quad (155)$$

where we adopt $(m-M)_{I,\mathrm{V1369\ Cen}} = 10.07$, $(m-M)_{I,\mathrm{V496\ Sct}} = 12.98$, and $(m-M)_{I,\mathrm{V5666\ Sgr}} = 14.6$ from Appendix A.12. We have $(m-M)_{I,\mathrm{V2659\ Cyg}} = 14.41 \pm 0.1$.

We plot $(m-M)_B = 16.5$, $(m-M)_V = 15.68$, and $(m-M)_I = 14.41$, which cross at $d = 4.4$ kpc and $E(B-V) = 0.80$, in Figure 17(d). Thus, we obtain $d = 4.4 \pm 0.5$ kpc, $E(B-V) = 0.80 \pm 0.05$.

A.29. V1535 Sco 2015

Figure 110 shows the (a) V light and (b) $(B-V)_0$ color curves of V1535 Sco. Here, $(B-V)_0$ are dereddened with $E(B-V) = 0.78$ as obtained in Section 3.29. Figure 111 shows the V light and $(B-V)_0$ color curves of V1535 Sco as well as those of LV Vul, V1668 Cyg, and V2468 Cyg. Applying Equation (6) to them, we have the relation

$$\begin{aligned}(m-M)_{V,\mathrm{V1535\ Sco}} &= (m-M+\Delta V)_{V,\mathrm{LV\ Vul}} - 2.5\log 2.4 \\ &= 11.85 + 7.4 \pm 0.2 - 0.95 = 18.3 \pm 0.2 \\ &= (m-M+\Delta V)_{V,\mathrm{V1668\ Cyg}} - 2.5\log 2.4 \\ &= 14.6 + 4.7 \pm 0.2 - 0.95 = 18.35 \pm 0.2 \\ &= (m-M+\Delta V)_{V,\mathrm{V2468\ Cyg}} - 2.5\log 1.0 \\ &= 16.2 + 2.1 \pm 0.2 - 0.0 = 18.3 \pm 0.2, \end{aligned} \quad (156)$$

where we adopt $(m-M)_{V,\mathrm{LV\ Vul}} = 11.85$, $(m-M)_{V,\mathrm{V1668\ Cyg}} = 14.6$, and $(m-M)_{V,\mathrm{V2468\ Cyg}} = 16.2$ in Hachisu & Kato (2019). Thus, we obtain $(m-M)_V = 18.3 \pm 0.1$ and $f_s = 2.4$ against

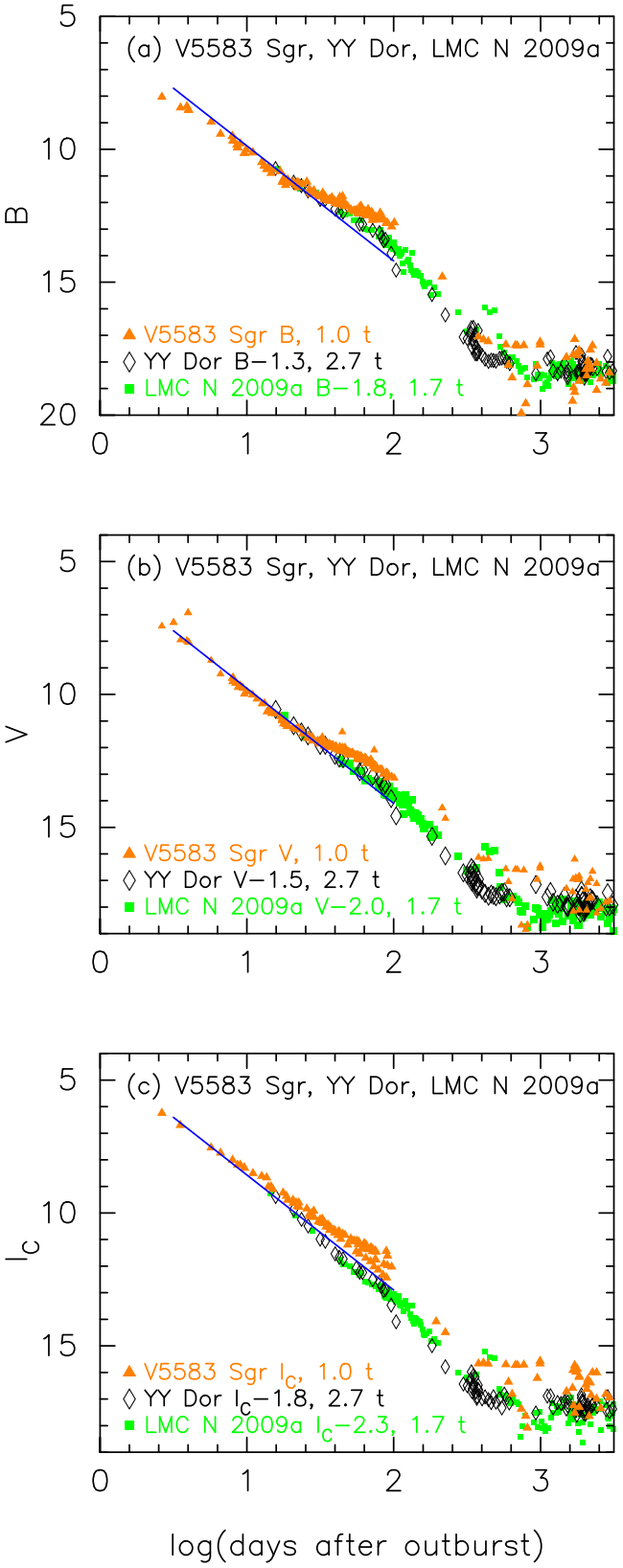

Figure 69. Same as Figure 25, but for V5583 Sgr. The *BV* data of V5583 Sgr are the same as those in Figure 67. The I_C data of V5583 Sgr are taken from AAVSO, VSOLJ, and SMARTS.

LV Vul. From Equations (1), (6), and (156), we have the relation

$$\begin{aligned}(m - M')_{V,\mathrm{V1535\ Sco}} &\equiv (m_V - (M_V - 2.5\log f_s))_{\mathrm{V1535\ Sco}} \\ &= ((m-M)_V + \Delta V)_{\mathrm{LV\ Vul}} \\ &= 11.85 + 7.4 \pm 0.2 = 19.25 \pm 0.2.\end{aligned} \tag{157}$$

Figure 112 shows the B, V, and I_C light curves of V1535 Sco together with those of V2468 Cyg, V834 Car, YY Dor, and LMC N 2009a. We apply Equation (9) for the B band to Figures 112(a) and (d) and obtain

$$\begin{aligned}&(m - M)_{B,\mathrm{V1535\ Sco}} \\ &= ((m-M)_B + \Delta B)_{\mathrm{V2468\ Cyg}} - 2.5\log 1.0 \\ &= 16.85 + 2.2 \pm 0.2 - 0.0 = 19.05 \pm 0.2 \\ &= ((m-M)_B + \Delta B)_{\mathrm{V834\ Car}} - 2.5\log 3.7 \\ &= 17.75 + 2.7 \pm 0.2 - 1.43 = 19.02 \pm 0.2 \\ &= ((m-M)_B + \Delta B)_{\mathrm{YY\ Dor}} - 2.5\log 12.6 \\ &= 18.98 + 2.8 \pm 0.2 - 2.75 = 19.03 \pm 0.2 \\ &= ((m-M)_B + \Delta B)_{\mathrm{LMC\ N\ 2009a}} - 2.5\log 7.9 \\ &= 18.98 + 2.3 \pm 0.2 - 2.25 = 19.03 \pm 0.2.\end{aligned} \tag{158}$$

We have $(m-M)_{B,\mathrm{V1535\ Sco}} = 19.04 \pm 0.1$.

For the V light curves in Figures 112(b) and (e), we similarly obtain

$$\begin{aligned}&(m - M)_{V,\mathrm{V1535\ Sco}} \\ &= ((m-M)_V + \Delta V)_{\mathrm{V2468\ Cyg}} - 2.5\log 1.0 \\ &= 16.2 + 2.1 \pm 0.2 - 0.0 = 18.3 \pm 0.2 \\ &= ((m-M)_V + \Delta V)_{\mathrm{V834\ Car}} - 2.5\log 3.7 \\ &= 17.3 + 2.4 \pm 0.2 - 1.43 = 18.27 \pm 0.2 \\ &= ((m-M)_V + \Delta V)_{\mathrm{YY\ Dor}} - 2.5\log 12.6 \\ &= 18.86 + 2.2 \pm 0.2 - 2.75 = 18.31 \pm 0.2 \\ &= ((m-M)_V + \Delta V)_{\mathrm{LMC\ N\ 2009a}} - 2.5\log 7.9 \\ &= 18.86 + 1.7 \pm 0.2 - 2.25 = 18.31 \pm 0.2.\end{aligned} \tag{159}$$

We have $(m-M)_{V,\mathrm{V1535\ Sco}} = 18.3 \pm 0.1$, which is consistent with Equation (156).

We apply Equation (10) for the I_C band to Figures 112(c) and (f) and obtain

$$\begin{aligned}&(m - M)_{I,\mathrm{V1535\ Sco}} \\ &= ((m-M)_I + \Delta I_C)_{\mathrm{V2468\ Cyg}} - 2.5\log 1.0 \\ &= 15.16 + 1.9 \pm 0.2 - 0.0 = 17.06 \pm 0.2 \\ &= ((m-M)_I + \Delta I_C)_{\mathrm{V834\ Car}} - 2.5\log 3.7 \\ &= 16.45 + 2.0 \pm 0.2 - 1.43 = 17.02 \pm 0.2 \\ &= ((m-M)_I + \Delta I_C)_{\mathrm{YY\ Dor}} - 2.5\log 12.6 \\ &= 18.67 + 1.1 \pm 0.2 - 2.75 = 17.02 \pm 0.2 \\ &= ((m-M)_I + \Delta I_C)_{\mathrm{LMC\ N\ 2009a}} - 2.5\log 7.9 \\ &= 18.67 + 0.6 \pm 0.2 - 2.25 = 17.02 \pm 0.2.\end{aligned} \tag{160}$$

We have $(m-M)_{I,\mathrm{V1535\ Sco}} = 17.03 \pm 0.1$.

We plot $(m-M)_B = 19.04$, $(m-M)_V = 18.3$, and $(m-M)_I = 17.03$, which broadly cross at $d = 15$ kpc and $E(B-V) = 0.78$, in Figure 19(a). Thus, we obtain $E(B-V) = 0.78 \pm 0.05$ and $d = 15 \pm 2$ kpc.

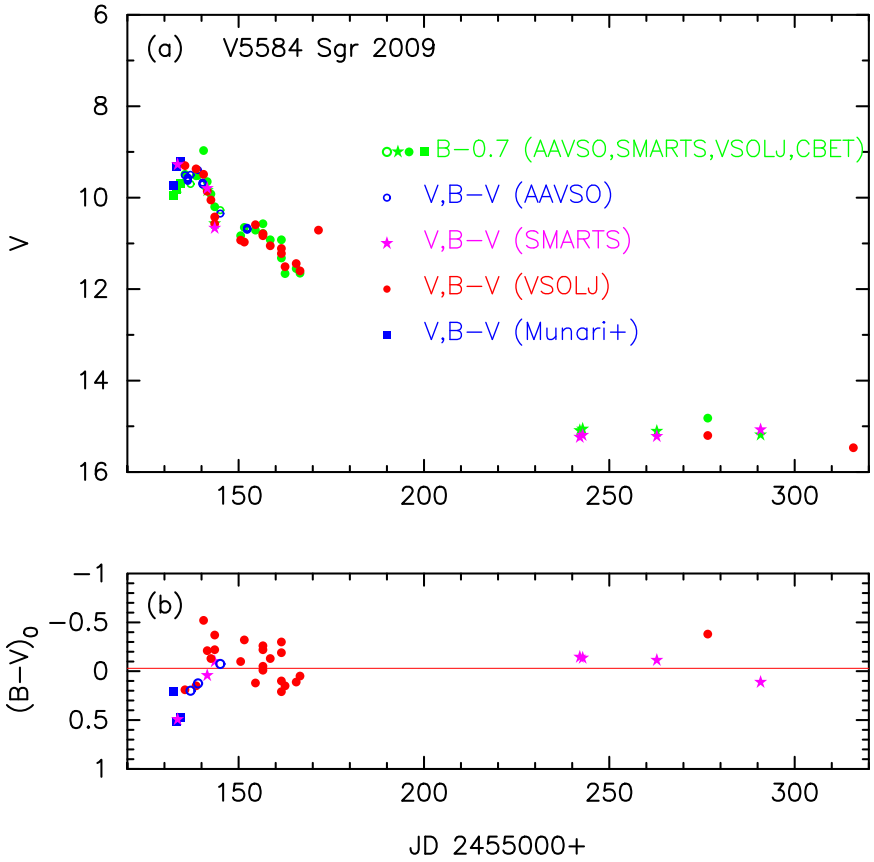

Figure 70. Same as Figure 23, but for V5584 Sgr. (a) The V (unfilled blue circles) and B (unfilled green circles) data are taken from AAVSO. The V (filled magenta stars) and B (filled green stars) data are taken from SMARTS. The V (filled red circles) and B (filled green circles) data are taken from VSOLJ. The V (filled blue squares) and B (filled green squares) data are taken from Munari et al. (2009). (b) The $(B-V)_0$ are dereddened with $E(B-V)=0.70$.

A.30. V5667 Sgr 2015#1

Figure 113 shows the (a) V and (b) $(B-V)_0$ evolutions of V5667 Sgr. Here, $(B-V)_0$ are dereddened with $E(B-V)=0.63$ as obtained in Section 3.30. Figure 114 shows the V light and $(B-V)_0$ color curves of V5667 Sgr as well as those of LV Vul, V5666 Sgr, V1369 Cen, and V496 Sct. Applying Equation (6) to them, we have the relation

$$\begin{aligned}(m-M)_{V,\mathrm{V5667\ Sgr}} &= (m-M+\Delta V)_{V,\mathrm{LV\ Vul}} - 2.5\log 3.7\\ &= 11.85+5.0\pm 0.3-1.43 = 15.37\pm 0.3\\ &= (m-M+\Delta V)_{V,\mathrm{V496\ Sct}} - 2.5\log 1.86\\ &= 13.7+2.4\pm 0.3-0.68 = 15.43\pm 0.3\\ &= (m-M+\Delta V)_{V,\mathrm{V1369\ Cen}} - 2.5\log 2.5\\ &= 10.25+6.2\pm 0.3-1.0 = 15.45\pm 0.3\\ &= (m-M+\Delta V)_{V,\mathrm{V5666\ Sgr}} - 2.5\log 2.1\\ &= 15.4+0.8\pm 0.3-0.8 = 15.4\pm 0.3, \end{aligned} \quad (161)$$

where we adopt $(m-M)_{V,\mathrm{LV\ Vul}}=11.85$, $(m-M)_{V,\mathrm{V496\ Sct}}=13.7$, $(m-M)_{V,\mathrm{V1369\ Cen}}=10.25$, and $(m-M)_{V,\mathrm{V5666\ Sgr}}=15.4$ from Hachisu & Kato (2019). Thus, we obtained $f_s=3.7$ against LV Vul and $(m-M)_{V,\mathrm{V5667\ Sgr}}=15.4\pm 0.2$. From Equations (1), (6), and (161), we have the relation

$$\begin{aligned}(m-M')_{V,\mathrm{V5667\ Sgr}} &\equiv (m_V-(M_V-2.5\log f_s))_{\mathrm{V5667\ Sgr}}\\ &= ((m-M)_V+\Delta V)_{\mathrm{LV\ Vul}}\\ &= 11.85+5.0\pm 0.3 = 16.85\pm 0.3. \end{aligned} \quad (162)$$

Figure 115 shows the B, V, and I_C light curves of V5667 Sgr together with those of V1369 Cen, V496 Sct, and V5666 Sgr. Applying Equation (9) for the B band to Figure 115(a), we have the relation

$$\begin{aligned}(m-M)_{B,\mathrm{V5667\ Sgr}} &= ((m-M)_B+\Delta B)_{\mathrm{V1369\ Cen}} - 2.5\log 2.5\\ &= 10.36+6.7\pm 0.3-1.0 = 16.06\pm 0.3\\ &= ((m-M)_B+\Delta B)_{\mathrm{V496\ Sct}} - 2.5\log 1.86\\ &= 14.15+2.6\pm 0.3-0.68 = 16.07\pm 0.3\\ &= ((m-M)_B+\Delta B)_{\mathrm{V5666\ Sgr}} - 2.5\log 2.1\\ &= 15.9+1.0\pm 0.3-0.8 = 16.1\pm 0.3, \end{aligned} \quad (163)$$

where we adopt $(m-M)_{B,\mathrm{V1369\ Cen}}=10.36$, $(m-M)_{B,\mathrm{V496\ Sct}}=14.15$, and $(m-M)_{B,\mathrm{V5666\ Sgr}}=15.9$ from Appendix A.12. We have $(m-M)_B=16.08\pm 0.2$ for V5667 Sgr.

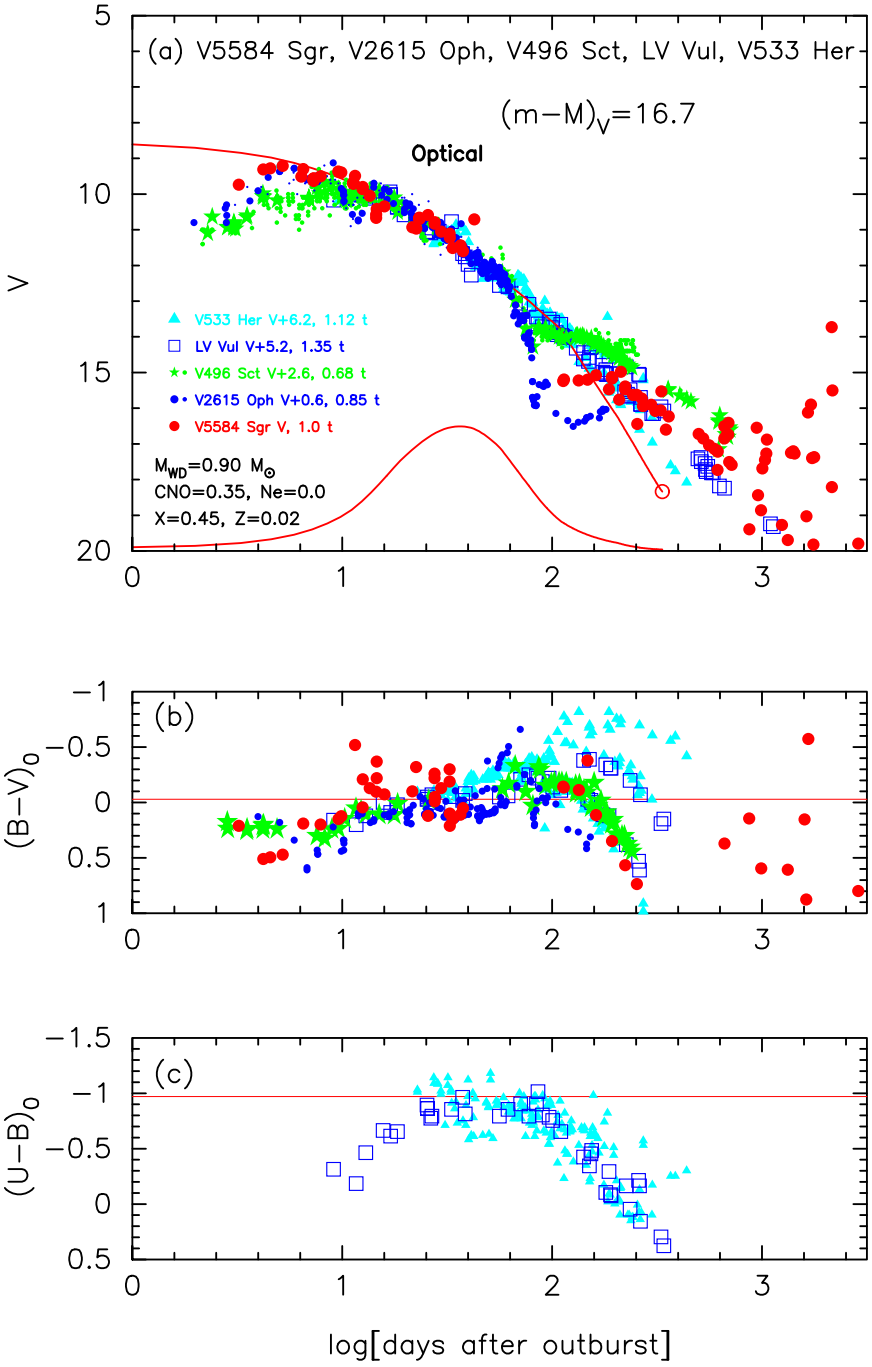

Figure 71. Same as Figure 30, but for V5584 Sgr (filled red circles). We add the light/color curves of LV Vul, V533 Her, V2615 Oph, and V496 Sct. The data of V5584 Sgr are the same as those in Figure 70. In panel (a), we added model light curves (solid red lines) of a 0.90 $M_\odot$ WD (CO3, Hachisu & Kato 2016a) for the V (upper red line) and UV 1455 Å (lower red line), assuming that $(m-M)_V = 16.7$ for V5584 Sgr.

Applying Equation (6) to Figure 115(b), we have the relation

$$\begin{aligned}(m-M)_{V,\mathrm{V5667\ Sgr}} &= ((m-M)_V + \Delta V)_{\mathrm{V1369\ Cen}} - 2.5\log 2.5 \\ &= 10.25 + 6.2 \pm 0.3 - 1.0 = 15.45 \pm 0.3 \\ &= ((m-M)_V + \Delta V)_{\mathrm{V496\ Sct}} - 2.5\log 1.86 \\ &= 13.7 + 2.4 \pm 0.3 - 0.68 = 15.42 \pm 0.3 \\ &= ((m-M)_V + \Delta V)_{\mathrm{V5666\ Sgr}} - 2.5\log 2.1 \\ &= 15.4 + 0.8 \pm 0.3 - 0.8 = 15.4 \pm 0.3, \end{aligned} \quad (164)$$

where we adopt $(m-M)_{V,\mathrm{V1369\ Cen}} = 10.25$, $(m-M)_{V,\mathrm{V496\ Sct}} = 13.7$, and $(m-M)_{V,\mathrm{V5666\ Sgr}} = 15.4$ from Hachisu & Kato (2019). We have $(m-M)_V = 15.42 \pm 0.2$, which is essentially the same as Equation (161).

From the I_C-band data in Figure 115(c), we obtain

$$\begin{aligned}(m-M)_{I,\mathrm{V5667\ Sgr}} &= ((m-M)_I + \Delta I_C)_{\mathrm{V1369\ Cen}} - 2.5\log 2.5 \\ &= 10.07 + 5.3 \pm 0.3 - 1.0 = 14.37 \pm 0.3 \\ &= ((m-M)_I + \Delta I_C)_{\mathrm{V496\ Sct}} - 2.5\log 1.86 \\ &= 12.98 + 2.1 \pm 0.3 - 0.68 = 14.4 \pm 0.3 \\ &= ((m-M)_I + \Delta I_C)_{\mathrm{V5666\ Sgr}} - 2.5\log 2.1 \\ &= 14.6 + 0.6 \pm 0.3 - 0.8 = 14.4 \pm 0.3, \end{aligned} \quad (165)$$

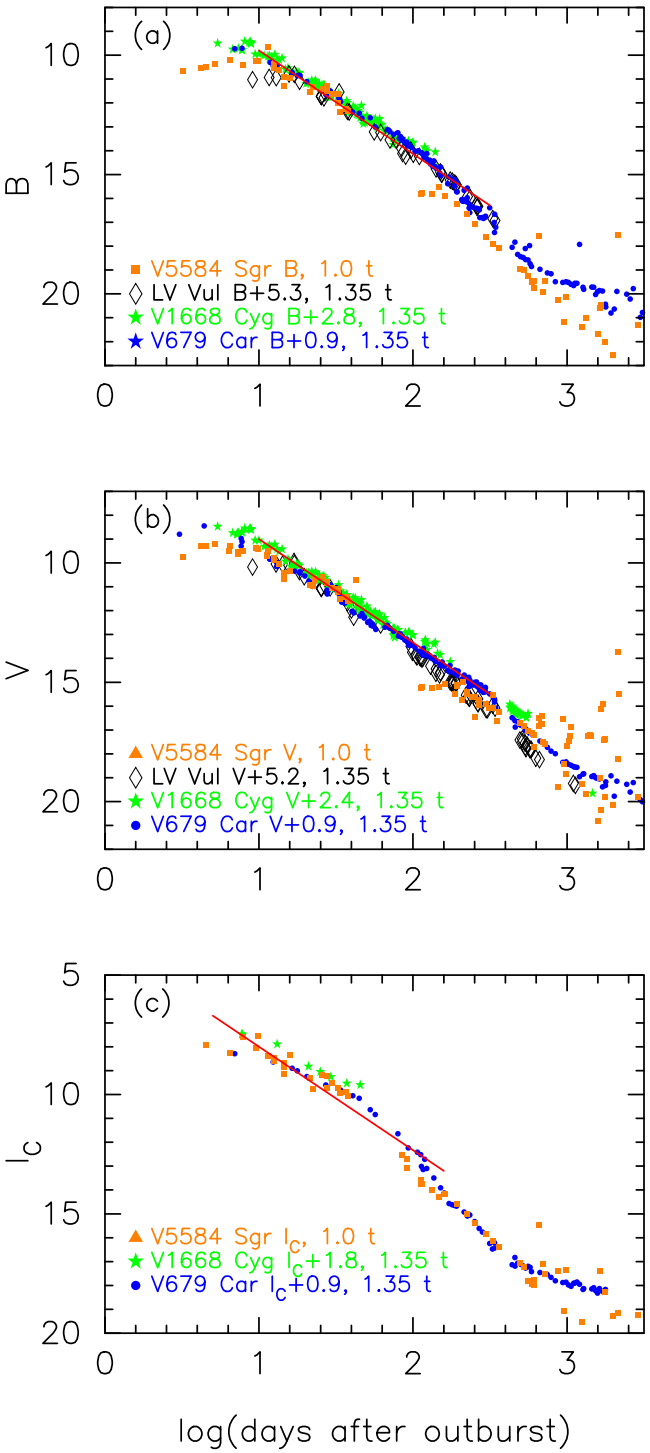

Figure 72. Same as Figure 25, but for V5584 Sgr. The (a) B, (b) V, and (c) I_C light curves of V5584 Sgr as well as those of LV Vul, V1668 Cyg, and V679 Car. The BV data of V5584 Sgr are the same as those in Figure 70. The I_C data of V5584 Sgr are taken from AAVSO, VSOLJ, and SMARTS. The BVI_C data of V679 Car are the same as those in Figure 21 of Hachisu & Kato (2019). Neither I_C nor I data are available for LV Vul.

where we adopt $(m-M)_{I,\mathrm{V1369\ Cen}} = 10.07$, $(m-M)_{I,\mathrm{V496\ Sct}} = 12.98$, and $(m-M)_{I,\mathrm{V5666\ Sgr}} = 14.6$ from Appendix A.12. We have $(m-M)_{I,\mathrm{V5667\ Sgr}} = 14.39 \pm 0.2$.

We plot $(m-M)_B = 16.08$, $(m-M)_V = 15.42$, and $(m-M)_I = 14.39$, which cross at $d = 4.9$ kpc and $E(B-V) = 0.63$, in Figure 19(b). Thus, we obtain $d = 4.9 \pm 0.5$ kpc and $E(B-V) = 0.63 \pm 0.05$.

A.31. V5668 Sgr 2015#2

Figure 116 shows (a) the V, K_s, and (b) $(B-V)_0$ evolutions of V5668 Sgr. Here, $(B-V)_0$ are dereddened with $E(B-V) = 0.20$ as obtained in Section 3.31. Figure 117 shows the light/color curves of V5668 Sgr as well as those of LV Vul, V496 Sct, and V1369 Cen. Applying Equation (6) to them, we have the relation

$$\begin{aligned}
&(m-M)_{V,\mathrm{V5668\ Sgr}} \\
&= (m-M+\Delta V)_{V,\mathrm{LV\ Vul}} - 2.5\log 1.86 \\
&= 11.85 - 0.2 \pm 0.2 - 0.68 = 10.97 \pm 0.2 \\
&= (m-M+\Delta V)_{V,\mathrm{V496\ Sct}} - 2.5\log 0.93 \\
&= 13.7 - 2.8 \pm 0.2 + 0.08 = 10.98 \pm 0.2 \\
&= (m-M+\Delta V)_{V,\mathrm{V1369\ Cen}} - 2.5\log 1.26 \\
&= 10.25 + 1.0 \pm 0.2 - 0.25 = 11.0 \pm 0.2, \qquad (166)
\end{aligned}$$

where we adopt $(m-M)_{V,\mathrm{LV\ Vul}} = 11.85$ and $(m-M)_{V,\mathrm{V496\ Sct}} = 13.7$, and $(m-M)_{V,\mathrm{V1369\ Cen}} = 10.25$ from Hachisu & Kato (2019). Thus, we obtain $(m-M)_V = 11.0 \pm 0.1$ and $f_s = 1.86$ against LV Vul. From Equations (1), (6), and (166), we have the relation

$$\begin{aligned}
(m-M')_{V,\mathrm{V5668\ Sgr}} &\equiv (m_V - (M_V - 2.5\log f_s))_{\mathrm{V5668\ Sgr}} \\
&= ((m-M)_V + \Delta V)_{\mathrm{LV\ Vul}} \\
&= 11.85 - 0.2 \pm 0.2 = 11.65 \pm 0.2. \qquad (167)
\end{aligned}$$

Figure 118 shows the B, V, and I_C light curves of V5668 Sgr together with those of V1369 Cen, V496 Sct, and V5666 Sgr. Applying Equation (9) for the B band to Figure 118(a), we have the relation

$$\begin{aligned}
&(m-M)_{B,\mathrm{V5668\ Sgr}} \\
&= ((m-M)_B + \Delta B)_{\mathrm{V1369\ Cen}} - 2.5\log 1.26 \\
&= 10.36 + 1.1 \pm 0.3 - 0.25 = 11.21 \pm 0.3 \\
&= ((m-M)_B + \Delta B)_{\mathrm{V496\ Sct}} - 2.5\log 0.93 \\
&= 14.15 - 3.1 \pm 0.3 + 0.08 = 11.13 \pm 0.3 \\
&= ((m-M)_B + \Delta B)_{\mathrm{V5666\ Sgr}} - 2.5\log 1.05 \\
&= 15.9 - 4.7 \pm 0.3 - 0.05 = 11.15 \pm 0.3, \qquad (168)
\end{aligned}$$

where we adopt $(m-M)_{B,\mathrm{V1369\ Cen}} = 10.36$, $(m-M)_{B,\mathrm{V496\ Sct}} = 14.15$, and $(m-M)_{B,\mathrm{V5666\ Sgr}} = 15.9$ from Appendix A.12. We have $(m-M)_B = 11.16 \pm 0.2$ for V5668 Sgr.

Applying Equation (6) to Figure 118(b), we have the relation

$$\begin{aligned}
&(m-M)_{V,\mathrm{V5668\ Sgr}} \\
&= ((m-M)_V + \Delta V)_{\mathrm{V1369\ Cen}} - 2.5\log 1.26 \\
&= 10.25 + 1.0 \pm 0.3 - 0.25 = 11.0 \pm 0.3 \\
&= ((m-M)_V + \Delta V)_{\mathrm{V496\ Sct}} - 2.5\log 0.93 \\
&= 13.7 - 2.8 \pm 0.3 + 0.08 = 10.98 \pm 0.3 \\
&= ((m-M)_V + \Delta V)_{\mathrm{V5666\ Sgr}} - 2.5\log 1.05 \\
&= 15.4 - 4.4 \pm 0.3 - 0.05 = 10.95 \pm 0.3, \qquad (169)
\end{aligned}$$

where we adopt $(m-M)_{V,\mathrm{V1369\ Cen}} = 10.25$, $(m-M)_{V,\mathrm{V496\ Sct}} = 13.7$, and $(m-M)_{V,\mathrm{V5666\ Sgr}} = 15.4$ from Hachisu & Kato (2019). We have $(m-M)_V = 10.98 \pm 0.2$, being essentially the same as Equation (166).

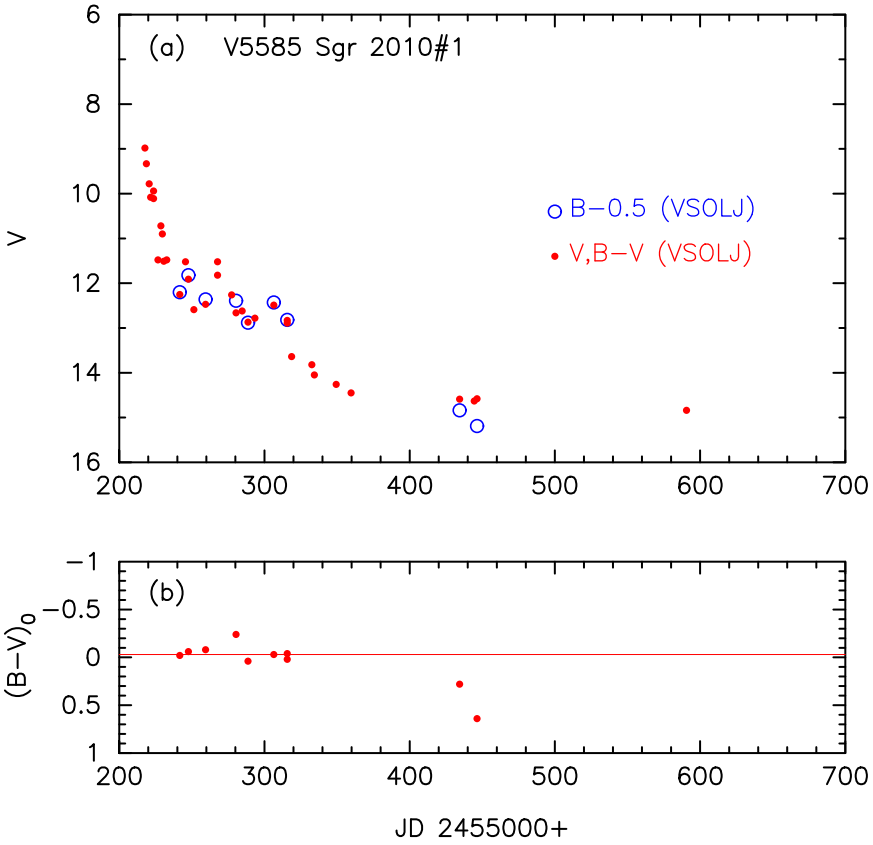

Figure 73. Same as Figure 23, but for V5585 Sgr. (a) The V (filled red circles) and B (unfilled blue circles) data are taken from VSOLJ. (b) The $(B-V)_0$ are dereddened with $E(B-V)=0.47$.

From the I_C band data in Figure 118(c), we obtain

$$\begin{aligned}(m-M)_{I,\mathrm{V5668\ Sgr}} &= ((m-M)_I+\Delta I_C)_{\mathrm{V1369\ Cen}} - 2.5\log 1.26\\ &= 10.07+0.8\pm0.3-0.25=10.62\pm0.3\\ &= ((m-M)_I+\Delta I_C)_{\mathrm{V496\ Sct}} - 2.5\log 0.93\\ &= 12.98-2.4\pm0.3+0.08=10.66\pm0.3\\ &= ((m-M)_I+\Delta I_C)_{\mathrm{V5666\ Sgr}} - 2.5\log 1.05\\ &= 14.6-3.9\pm0.3-0.05=10.65\pm0.3, \end{aligned} \quad (170)$$

where we adopt $(m-M)_{I,\mathrm{V1369\ Cen}}=10.07$, $(m-M)_{I,\mathrm{V496\ Sct}}=12.98$, and $(m-M)_{I,\mathrm{V5666\ Sgr}}=14.6$ from Appendix A.12. We have $(m-M)_{I,\mathrm{V5668\ Sgr}}=10.64\pm0.2$.

We plot $(m-M)_B=11.16$, $(m-M)_V=10.98$, and $(m-M)_I=10.64$, which cross at $d=1.2$ kpc and $E(B-V)=0.20$, in Figure 19(c). Thus, we obtain $d=1.2\pm0.2$ kpc and $E(B-V)=0.20\pm0.03$.

A.32. V2944 Oph 2015

Figure 119 shows (a) the V and (b) $(B-V)_0$ evolutions of V2944 Oph. Here, $(B-V)_0$ are dereddened with $E(B-V)=0.62$ as obtained in Section 3.32. Figure 120 shows the V light and $(B-V)_0$ color curves of V2944 Oph, V5666 Sgr, V1369 Cen, V496 Sct, and LV Vul. Applying Equation (6) to them, we have the relation

$$\begin{aligned}(m-M)_{V,\mathrm{V2944\ Oph}} &= (m-M+\Delta V)_{V,\mathrm{LV\ Vul}} - 2.5\log 1.78\\ &= 11.85+5.3\pm0.3-0.63=16.52\pm0.3\\ &= (m-M+\Delta V)_{V,\mathrm{V496\ Sct}} - 2.5\log 0.89\\ &= 13.7+2.7\pm0.3+0.13=16.53\pm0.3\\ &= (m-M+\Delta V)_{V,\mathrm{V1369\ Cen}} - 2.5\log 1.20\\ &= 10.25+6.5\pm0.3-0.2=16.55\pm0.3\\ &= (m-M+\Delta V)_{V,\mathrm{V5666\ Sgr}} - 2.5\log 1.0\\ &= 15.4+1.1\pm0.3+0.0=16.5\pm0.3, \end{aligned} \quad (171)$$

where we adopt $(m-M)_{V,\mathrm{LV\ Vul}}=11.85$, $(m-M)_{V,\mathrm{V496\ Sct}}=13.7$, $(m-M)_{V,\mathrm{V1369\ Cen}}=10.25$, and $(m-M)_{V,\mathrm{V5666\ Sgr}}=15.4$ from Hachisu & Kato (2019), Thus, we obtained $f_s=1.78$ against LV Vul and $(m-M)_{V,\mathrm{V2944\ Oph}}=16.5\pm0.2$. From Equations (1), (6), and (171), we have the relation

$$\begin{aligned}(m-M')_{V,\mathrm{V2944\ Oph}} &\equiv (m_V-(M_V-2.5\log f_s))_{\mathrm{V2944\ Oph}}\\ &= ((m-M)_V+\Delta V)_{\mathrm{LV\ Vul}}\\ &= 11.85+5.3\pm0.3=17.15\pm0.3. \end{aligned} \quad (172)$$

Figure 121 shows the B, V, and I_C light curves of V2944 Oph together with those of V1369 Cen, V496 Sct, and V5666 Sgr. Applying Equation (9) for the B band to

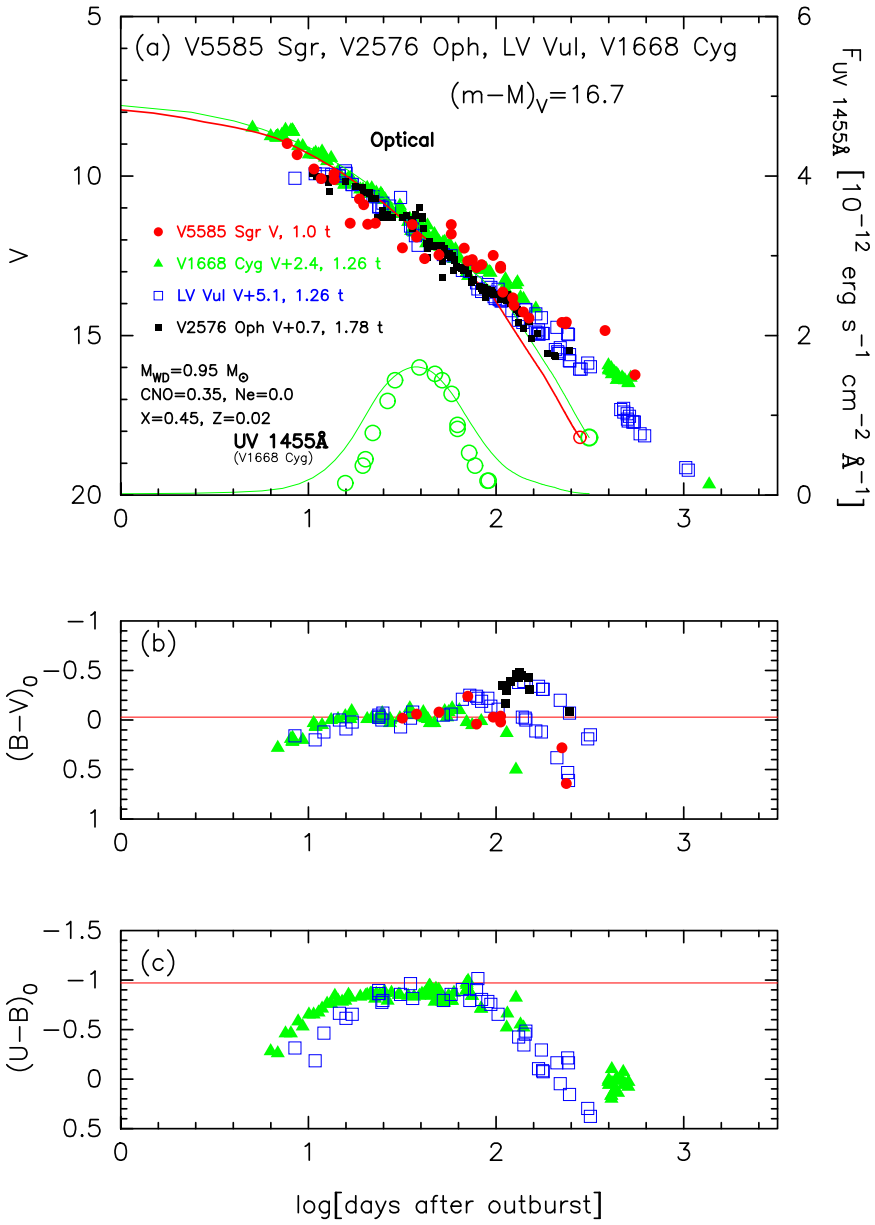

Figure 74. Same as Figure 30, but for V5585 Sgr (filled red circles). We plot the V1668 Cyg light curves by filled green triangles, LV Vul by unfilled blue squares, and V2576 Oph by filled black squares. The data of V5585 Sgr are the same as those in Figure 73. In panel (a), we added a V model light curve (solid red lines) of a 0.95 $M_\odot$ WD (CO3; Hachisu & Kato 2016a), assuming that $(m-M)_V = 16.7$ for V5585 Sgr. The solid green lines denote the model light curves of a 0.98 $M_\odot$ WD (CO3) for both the V and UV 1455 Å light curves, assuming $(m-M)_V = 14.6$ for V1668 Cyg.

Figure 121(a), we have the relation

$$\begin{aligned}(m-M)_{B,\mathrm{V2944\ Oph}} &= ((m-M)_B + \Delta B)_{\mathrm{V1369\ Cen}} - 2.5\log 1.20 \\ &= 10.36 + 7.0 \pm 0.3 - 0.2 = 17.16 \pm 0.3 \\ &= ((m-M)_B + \Delta B)_{\mathrm{V496\ Sct}} - 2.5\log 0.89 \\ &= 14.15 + 2.8 \pm 0.3 + 0.13 = 17.08 \pm 0.3 \\ &= ((m-M)_B + \Delta B)_{\mathrm{V5666\ Sgr}} - 2.5\log 1.0 \\ &= 15.9 + 1.2 \pm 0.3 - 0.0 = 17.1 \pm 0.3, \end{aligned} \quad (173)$$

where we adopt $(m-M)_{B,\mathrm{V1369\ Cen}} = 10.36$, $(m-M)_{B,\mathrm{V496\ Sct}} = 14.15$, and $(m-M)_{B,\mathrm{V5666\ Sgr}} = 15.9$ from Appendix A.12. We have $(m-M)_B = 17.11 \pm 0.2$ for V2944 Oph.

Applying Equation (6) to Figure 121(b), we have the relation

$$\begin{aligned}(m-M)_{V,\mathrm{V2944\ Oph}} &= ((m-M)_V + \Delta V)_{\mathrm{V1369\ Cen}} - 2.5\log 1.20 \\ &= 10.25 + 6.5 \pm 0.3 - 0.2 = 16.55 \pm 0.3 \\ &= ((m-M)_V + \Delta V)_{\mathrm{V496\ Sct}} - 2.5\log 0.89 \\ &= 13.7 + 2.7 \pm 0.3 + 0.13 = 16.53 \pm 0.3 \\ &= ((m-M)_V + \Delta V)_{\mathrm{V5666\ Sgr}} - 2.5\log 1.0 \\ &= 15.4 + 1.1 \pm 0.3 - 0.0 = 16.5 \pm 0.3, \end{aligned} \quad (174)$$

where we adopt $(m-M)_{V,\mathrm{V1369\ Cen}} = 10.25$, $(m-M)_{V,\mathrm{V496\ Sct}} = 13.7$, and $(m-M)_{V,\mathrm{V5666\ Sgr}} = 15.4$ from Hachisu & Kato (2019). We have $(m-M)_{V,\mathrm{V2944\ Oph}} = 16.5 \pm 0.2$, which is essentially the same as Equation (171).

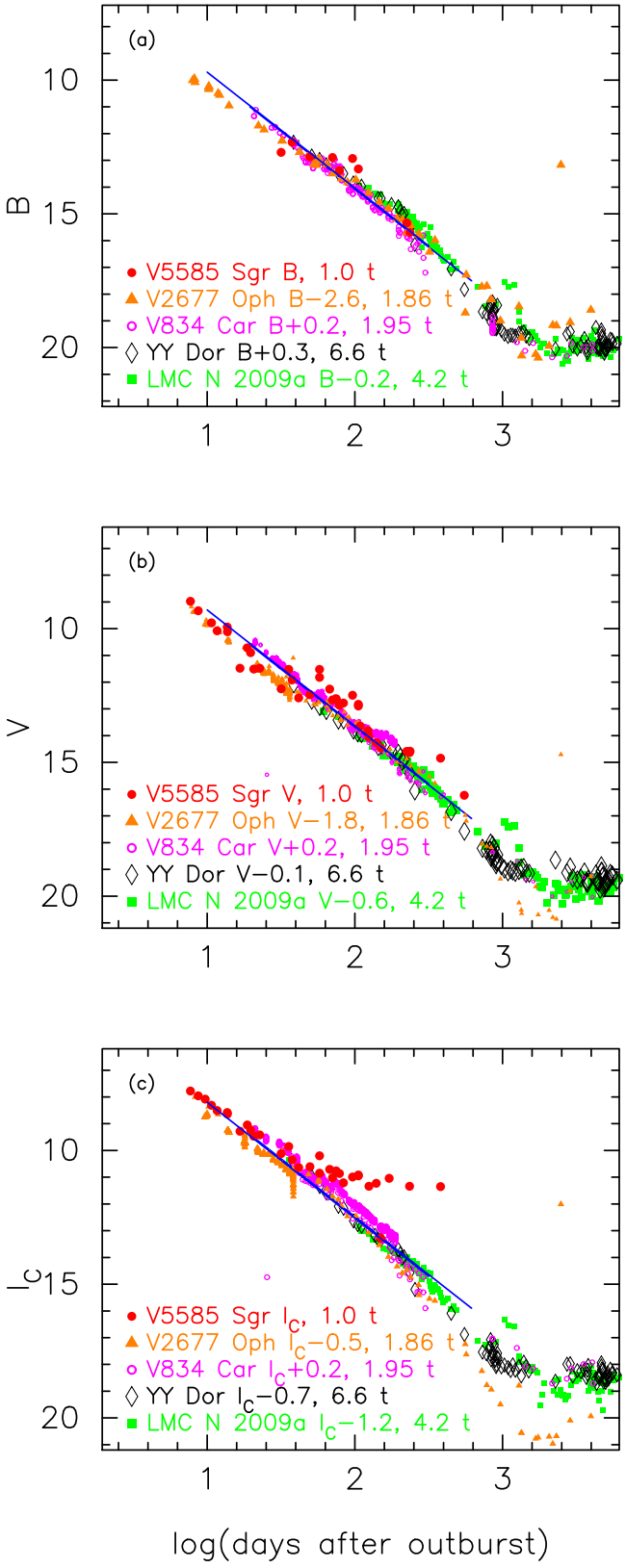

Figure 75. Same as Figure 25, but for V5585 Sgr. The (a) *B*, (b) *V*, and (c) I_C light curves of V5585 Sgr as well as those of V2677 Oph, V834 Car, YY Dor, and LMC N 2009a. The *BV* data of V5585 Sgr are the same as those in Figure 73. The I_C data of V5585 Sgr are taken from VSOLJ. The BVI_C data of V2677 Oph are the same as those in Figures 95, 96, and 97.

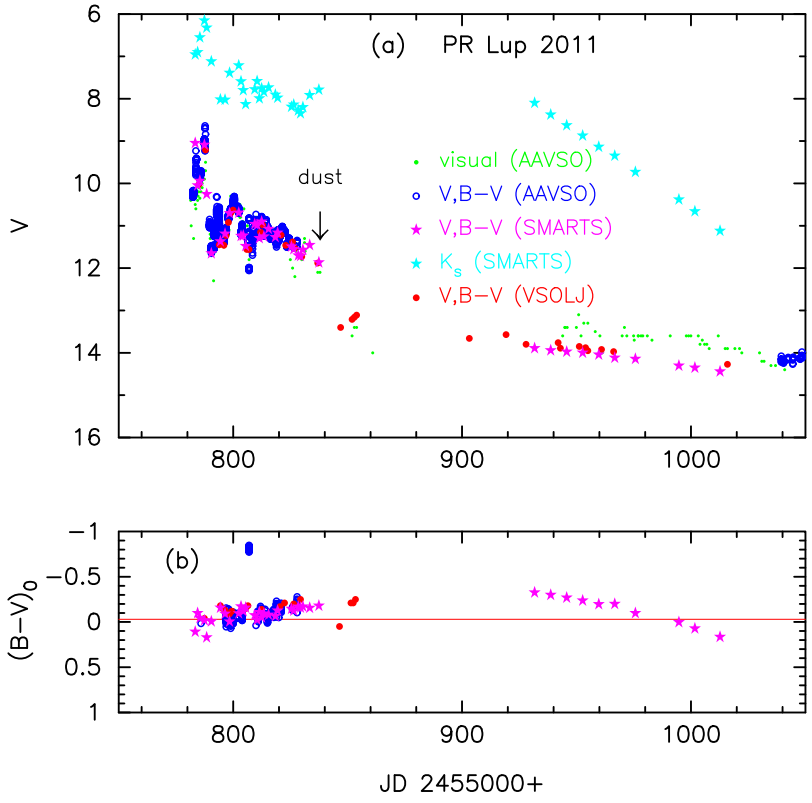

Figure 76. Same as Figure 23, but for PR Lup. (a) The visual data (green dots) are taken from AAVSO. The *BV* data are taken from AAVSO (unfilled blue circles), SMARTS (filled magenta stars), and VSOLJ (filled red circles). We add the K_s magnitudes (filled cyan stars) which are taken from SMARTS. A dust shell formed around the time indicated by the arrow labeled dust. (b) The $(B-V)_0$ are dereddened with $E(B-V)=0.74$.

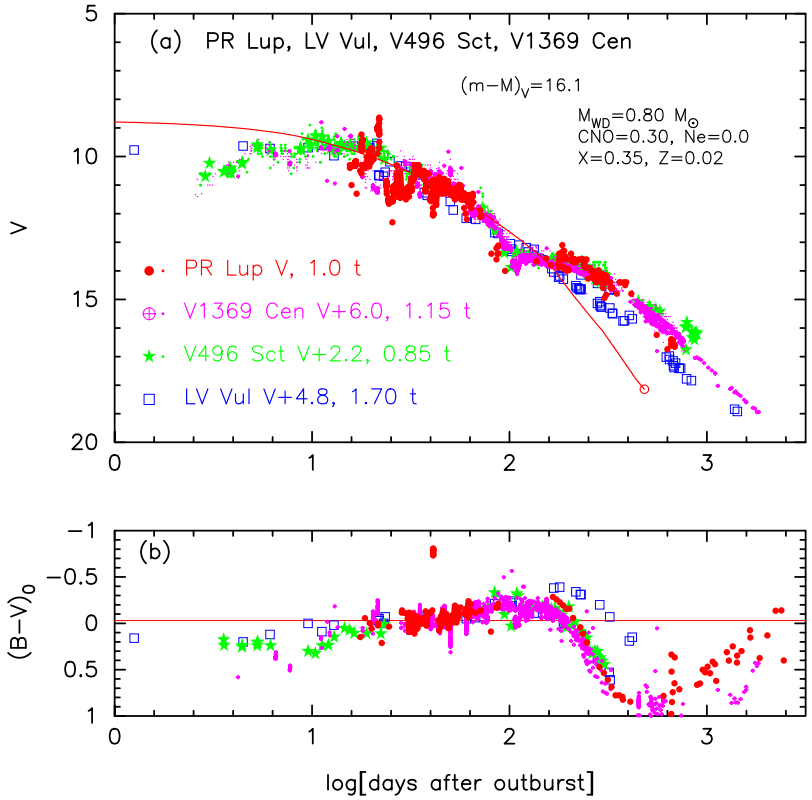

Figure 77. Same as Figure 30, but for PR Lup (filled red circles for *V* and red dots for visual). We add the V1369 Cen light curves with the unfilled magenta encircled plus (*V*) and by magenta dots (visual), V496 Sct by filled green stars (*V*) and by green dots (visual), and LV Vul by unfilled blue squares (*V*). The data of PR Lup are the same as those in Figure 76. The data of V1369 Cen and V496 Sct are the same as those in Figure 15 of Hachisu & Kato (2019). In panel (a), we add the model light curve of a 0.80 $M_\odot$ WD (CO2, solid red line; Hachisu & Kato 2010), assuming that $(m-M)_V=16.1$ for PR Lup.

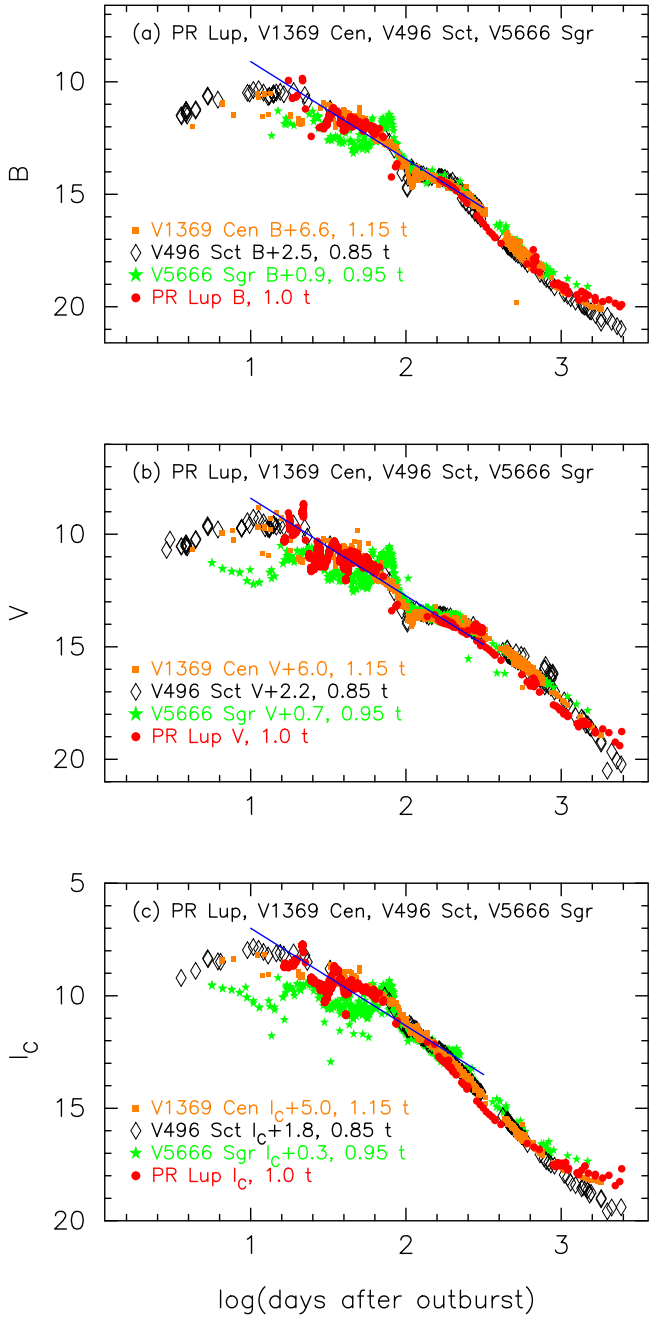

Figure 78. Same as Figure 25, but for PR Lup. We plot the (a) *B*, (b) *V*, and (c) I_C light curves of PR Lup as well as those of V1369 Cen, V496 Sct, and V5666 Sgr. The *BV* data of PR Lup are the same as those in Figure 76. The I_C data of PR Lup are taken from AAVSO, VSOLJ, and SMARTS.

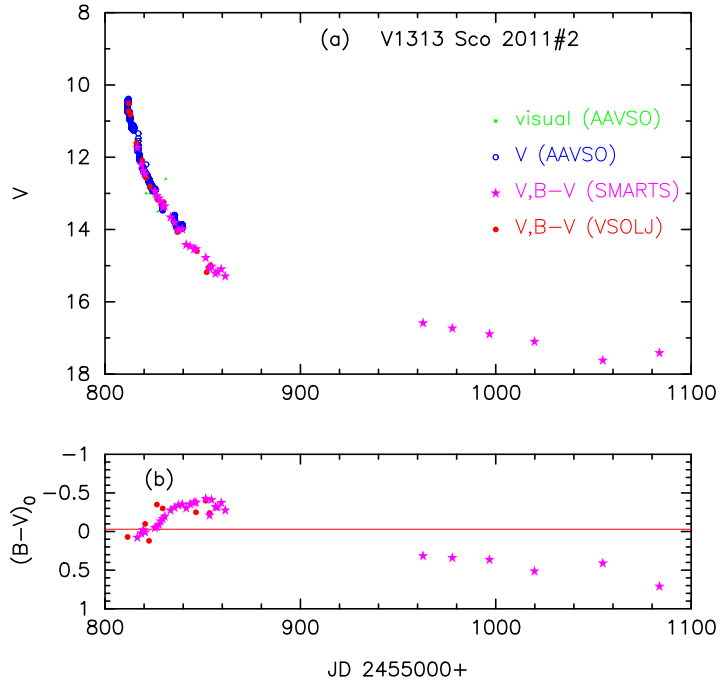

Figure 79. Same as Figure 23, but for V1313 Sco. (a) The visual data (green dots) are taken from AAVSO. The V data are taken from AAVSO (unfilled blue circles), SMARTS (filled magenta stars), and VSOLJ (filled red circles). (b) The $(B-V)_0$ are dereddened with $E(B-V)=1.30$.

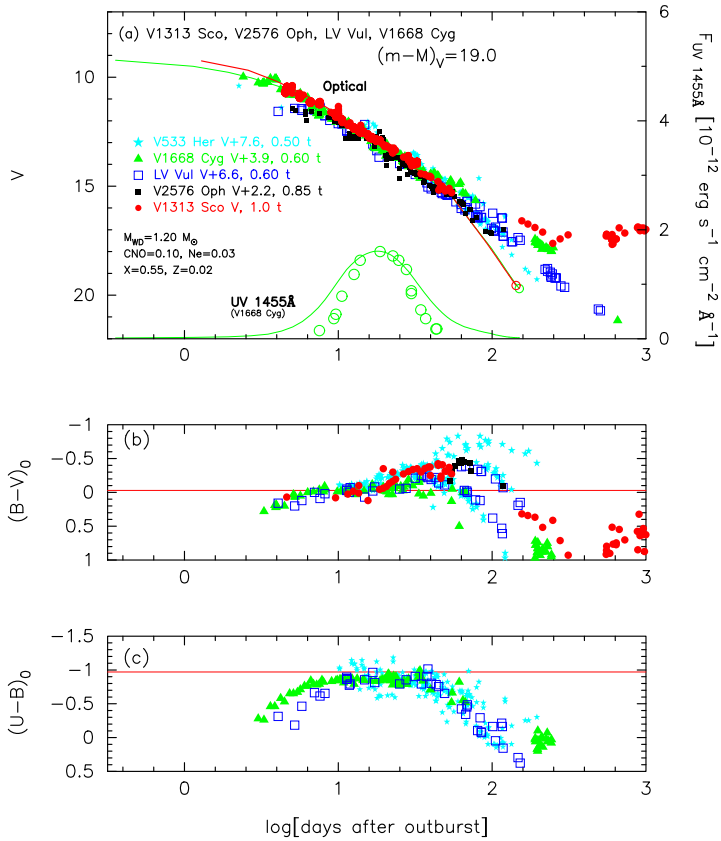

Figure 80. Same as Figure 30, but for V1313 Sco (filled red circles). The data of V1313 Sco are the same as those in Figure 79. In panel (a), we add the model V light curve (solid red line) of a 1.20 $M_\odot$ WD (Ne2; Hachisu & Kato 2010), assuming that $(m-M)_V=19.0$ for V1313 Sco. The solid green lines denote the model V and UV 1455 Å light curves of a 0.98 $M_\odot$ WD (CO3), assuming $(m-M)_V=14.6$ for V1668 Cyg.

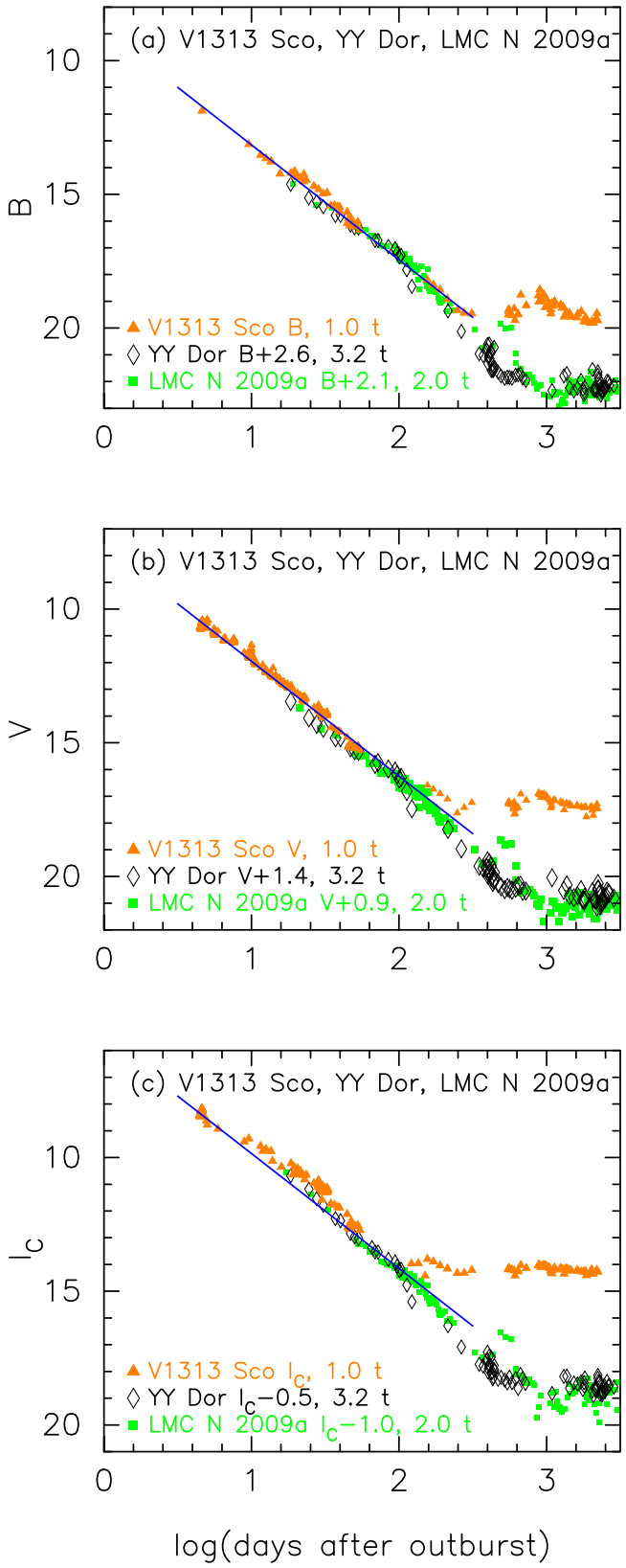

Figure 81. Same as Figure 25, but for V1313 Sco. The *BV* data of V1313 Sco are the same as those in Figure 79. The I_C data of V1313 Sco are taken from AAVSO, VSOLJ, and SMARTS.

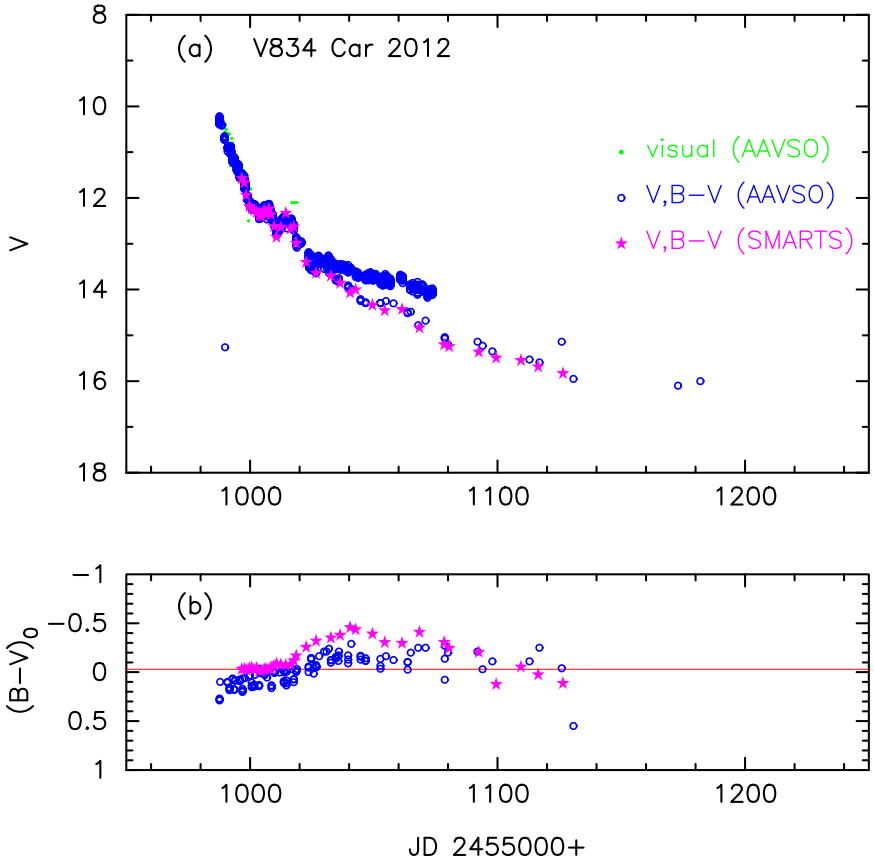

Figure 82. Same as Figure 23, but for V834 Car. (a) The visual data (green dots) are taken from AAVSO. The V data are taken from AAVSO (unfilled blue circles) and SMARTS (filled magenta stars). (b) The $(B-V)_0$ are dereddened with $E(B-V)=0.50$.

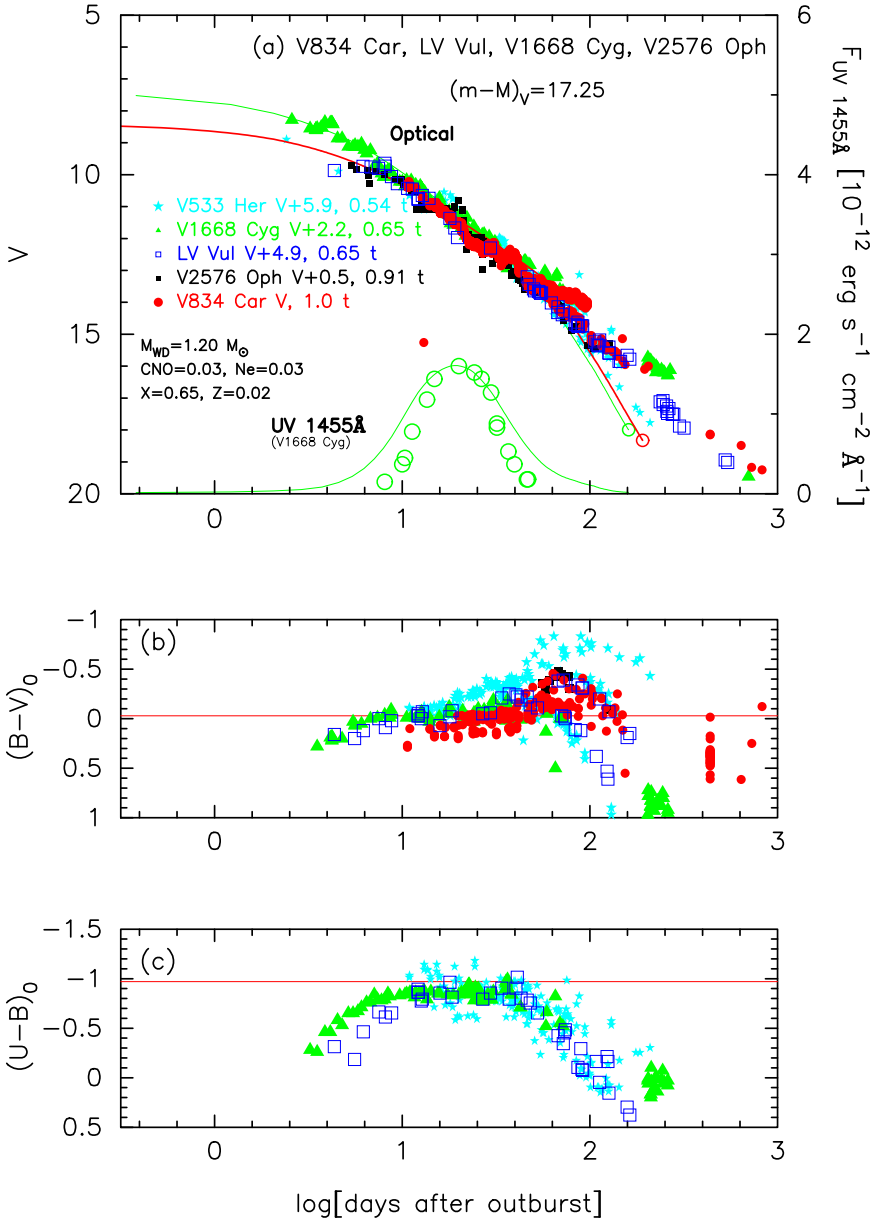

Figure 83. Same as Figure 30, but for V834 Car (filled red circles). The data of V834 Car are the same as those in Figure 82. In panel (a), we added the model V light curve (solid red line) of a 1.20 $M_\odot$ WD (Ne3; Hachisu & Kato 2016a), assuming that $(m - M)_V = 17.25$ for V834 Car. The solid green lines denote the model light curves of a 0.98 $M_\odot$ WD (CO3) both for the V and UV 1455 Å light curves, assuming $(m - M)_V = 14.6$ for V1668 Cyg.

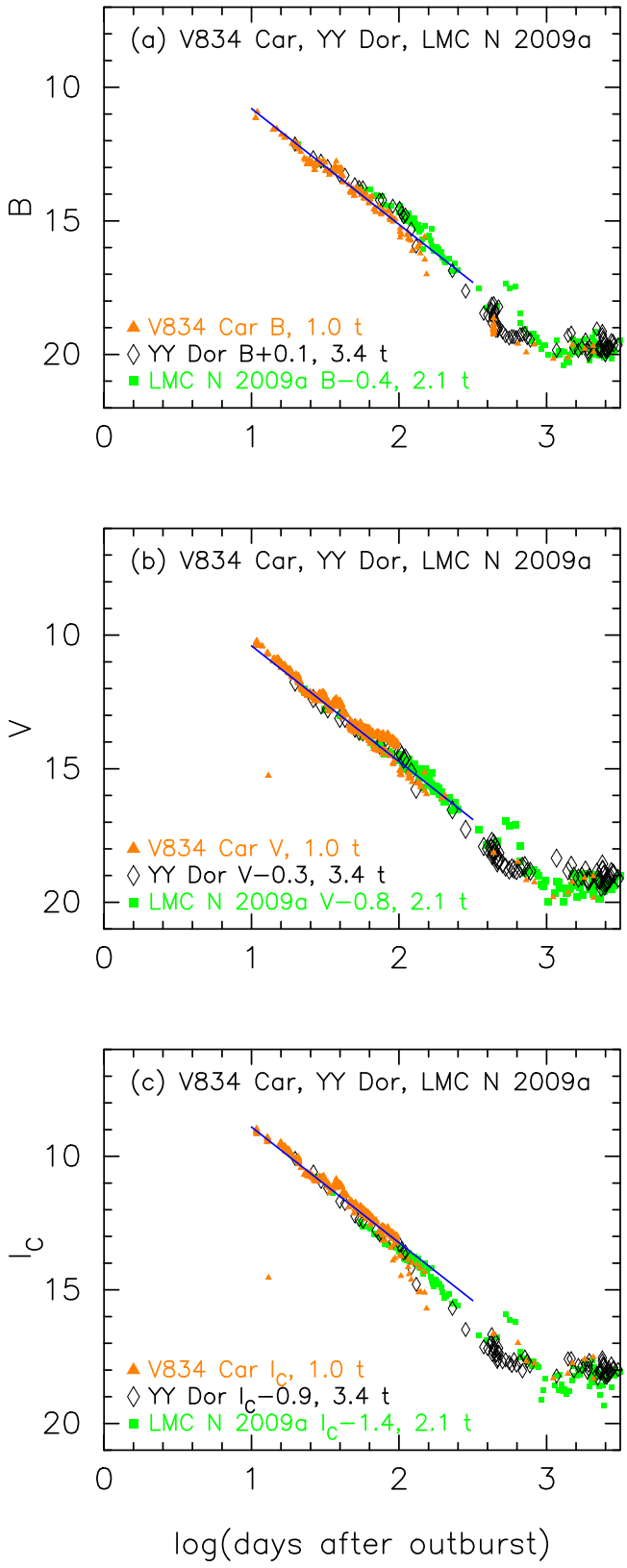

Figure 84. Same as Figure 25, but for V834 Car. The *BV* data of V834 Car are the same as those in Figure 82. The I_C data of V834 Car are taken from AAVSO and SMARTS.

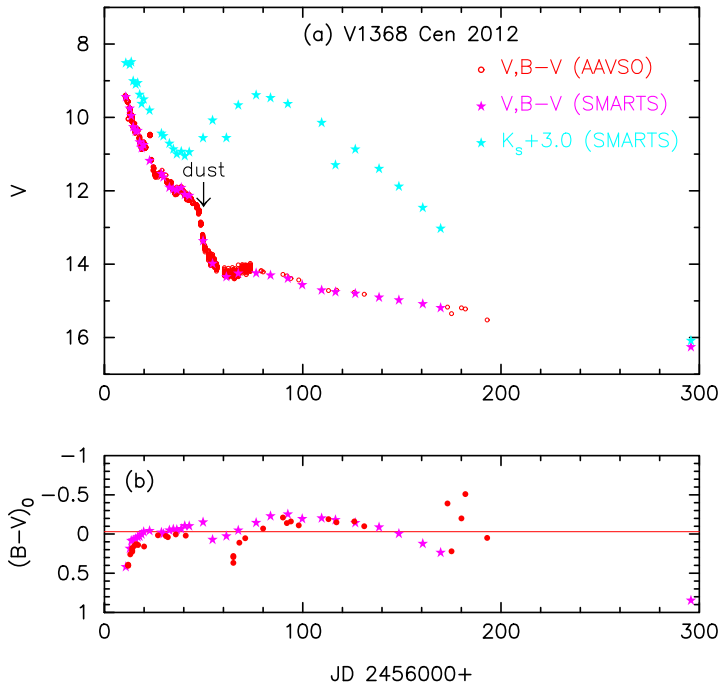

Figure 85. Same as Figure 23, but for V1368 Cen. (a) The V data are taken from AAVSO (unfilled red circles) and SMARTS (filled magenta stars). The K_s data are taken from SMARTS (filled cyan stars). A dust shell formed around the time indicated by the arrow labeled dust. (b) The $(B-V)_0$ are dereddened with $E(B-V)=0.93$.

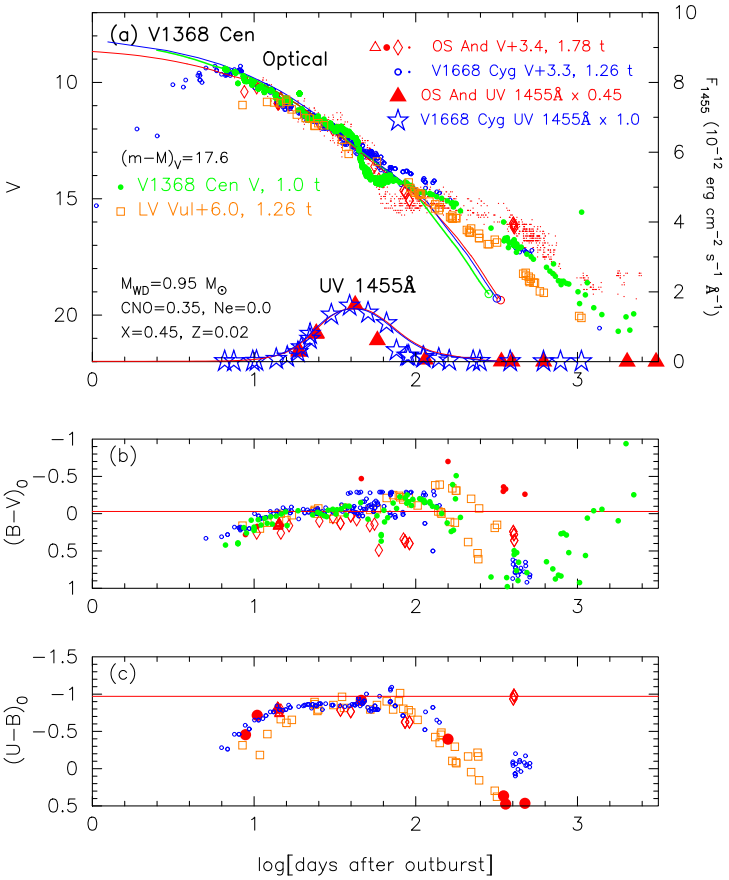

Figure 86. Same as Figure 30, but for V1368 Cen (filled green circles). The data of V1368 Cen are the same as those in Figure 85. In panel (a), we added a model V light curve of a 0.95 $M_\odot$ WD (CO3, solid green lines; Hachisu & Kato 2016a), assuming that $(m-M)_V=17.6$ for V1368 Cen. The solid blue lines denotes the V and UV 1455 Å light curve of a 0.98 $M_\odot$ WD (CO3), assuming $(m-M)_V=14.6$ for V1668 Cyg, while the solid red lines represent the V and UV 1455 Å light curves of a 1.05 $M_\odot$ WD (CO3), assuming $(m-M)_V=14.8$ for OS And.

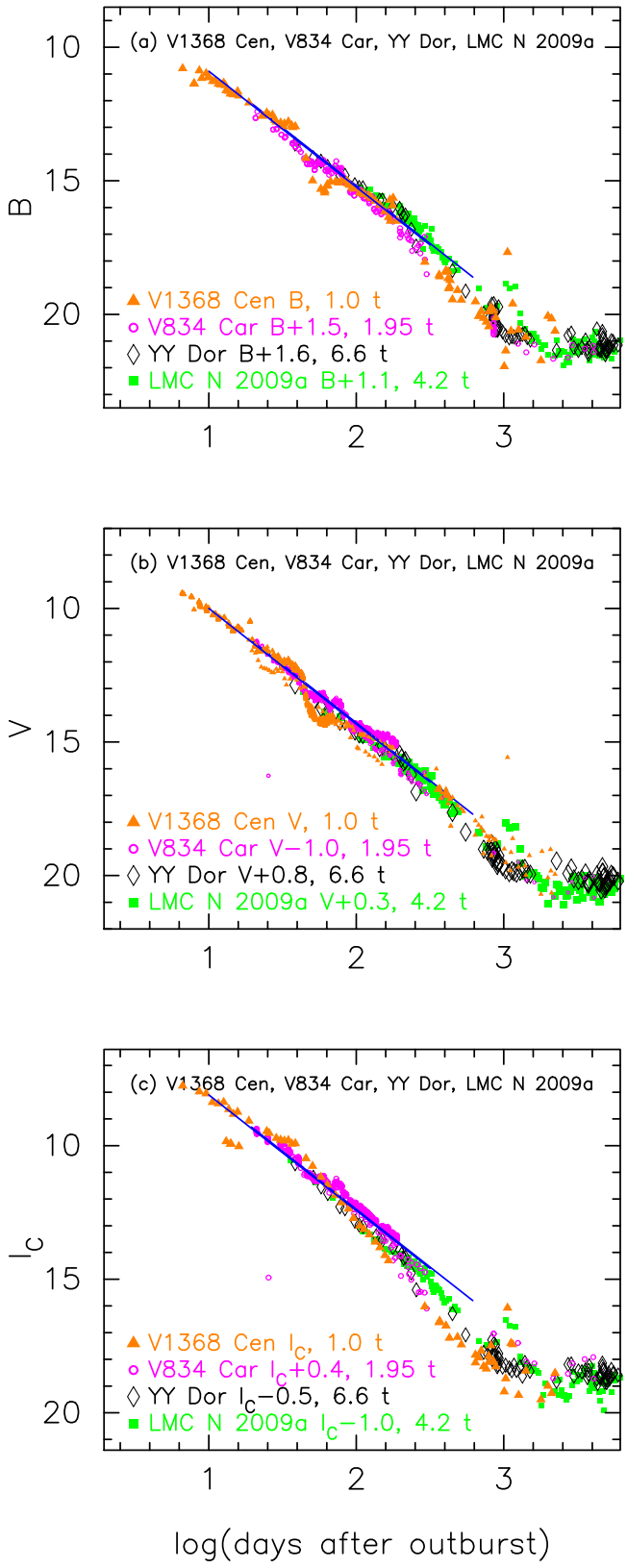

Figure 87. Same as Figure 25, but for V1368 Cen. The *BV* data of V1368 Cen are the same as those in Figure 85. The I_C data of V1368 Cen are taken from AAVSO and SMARTS.

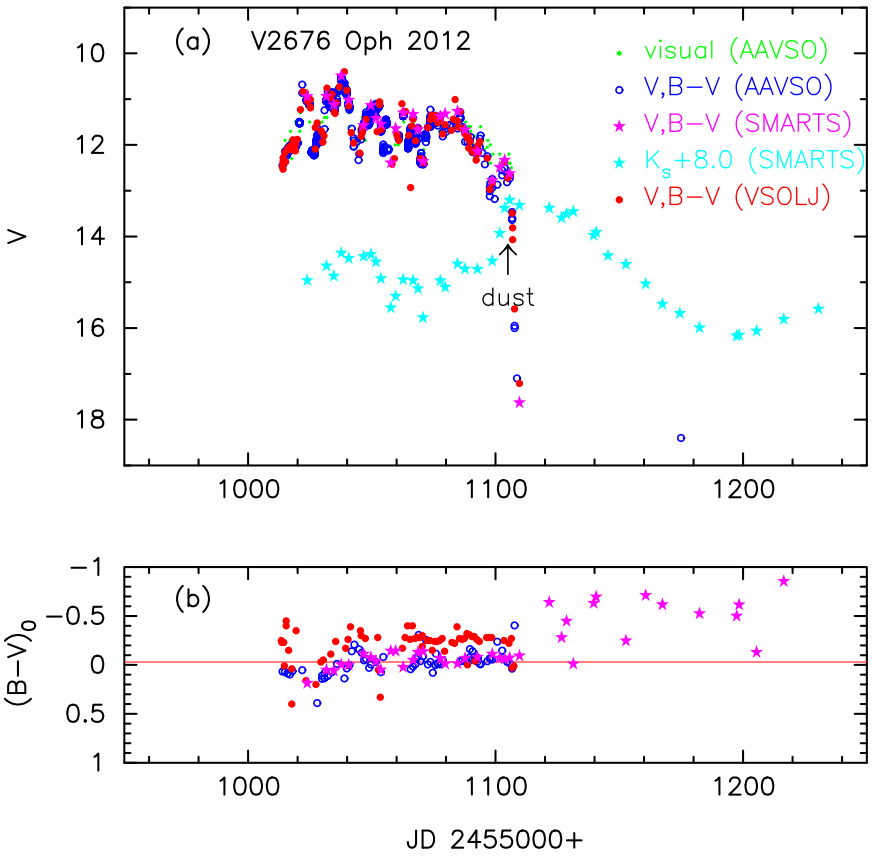

Figure 88. Same as Figure 23, but for V2676 Oph. (a) The visual data (green dots) are taken from AAVSO. The V data are taken from AAVSO (unfilled blue circles), SMARTS (filled magenta stars), and VSOLJ (filled red circles). We add the K_s data (filled cyan stars) from SMARTS. The dust formation epoch is denoted by the arrow labeled dust. (b) The $(B-V)_0$ are dereddened with $E(B-V)=0.90$.

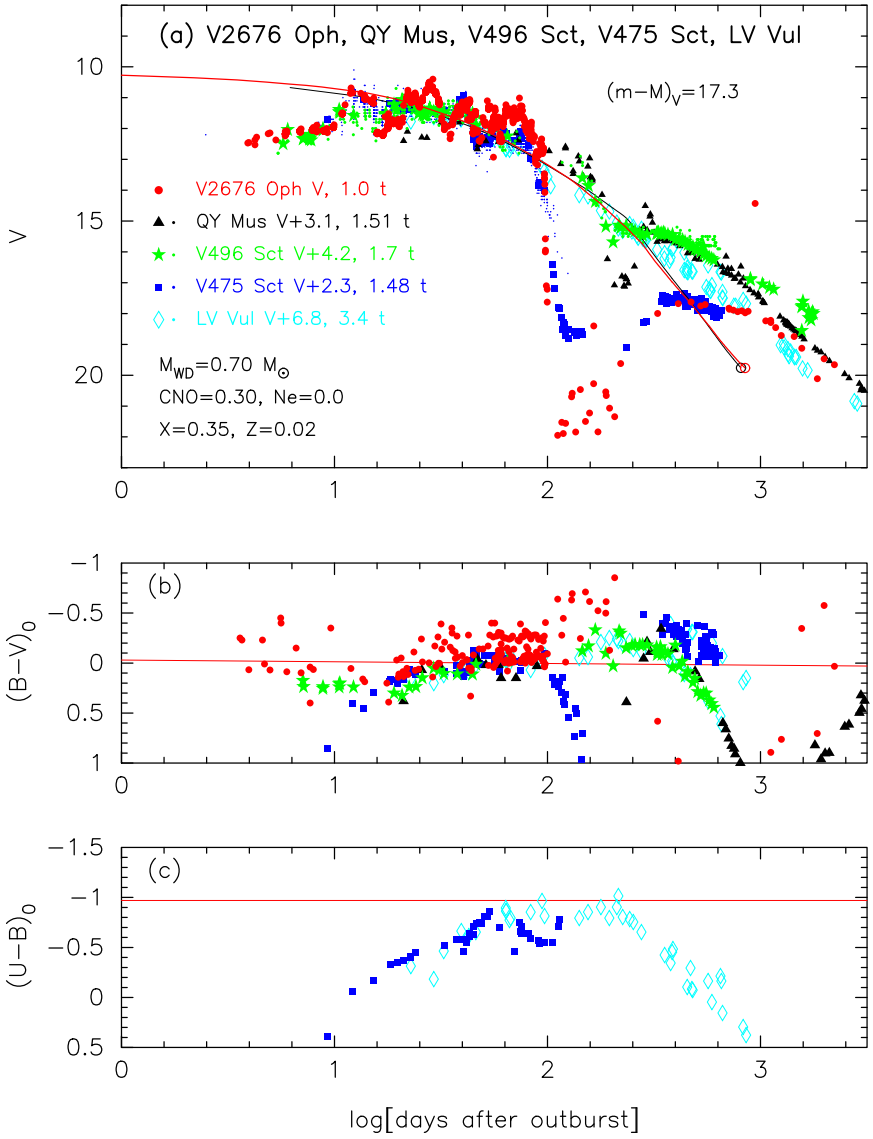

Figure 89. Same as Figure 30, but for V2676 Oph (filled red circles). The data of V2676 Oph are the same as those in Figure 88. The data of V475 Sct are the same as those in Figures 49 and 50 of Hachisu & Kato (2016b). In panel (a), we added the model V light curve of a 0.70 $M_\odot$ WD (CO2, solid red line; Hachisu & Kato 2010), assuming that $(m-M)_V = 17.3$ for V2676 Oph. The solid black line denotes the V light curve of a 0.80 $M_\odot$ WD (CO3; Hachisu & Kato 2016a), assuming $(m-M)_V = 14.65$ for QY Mus.

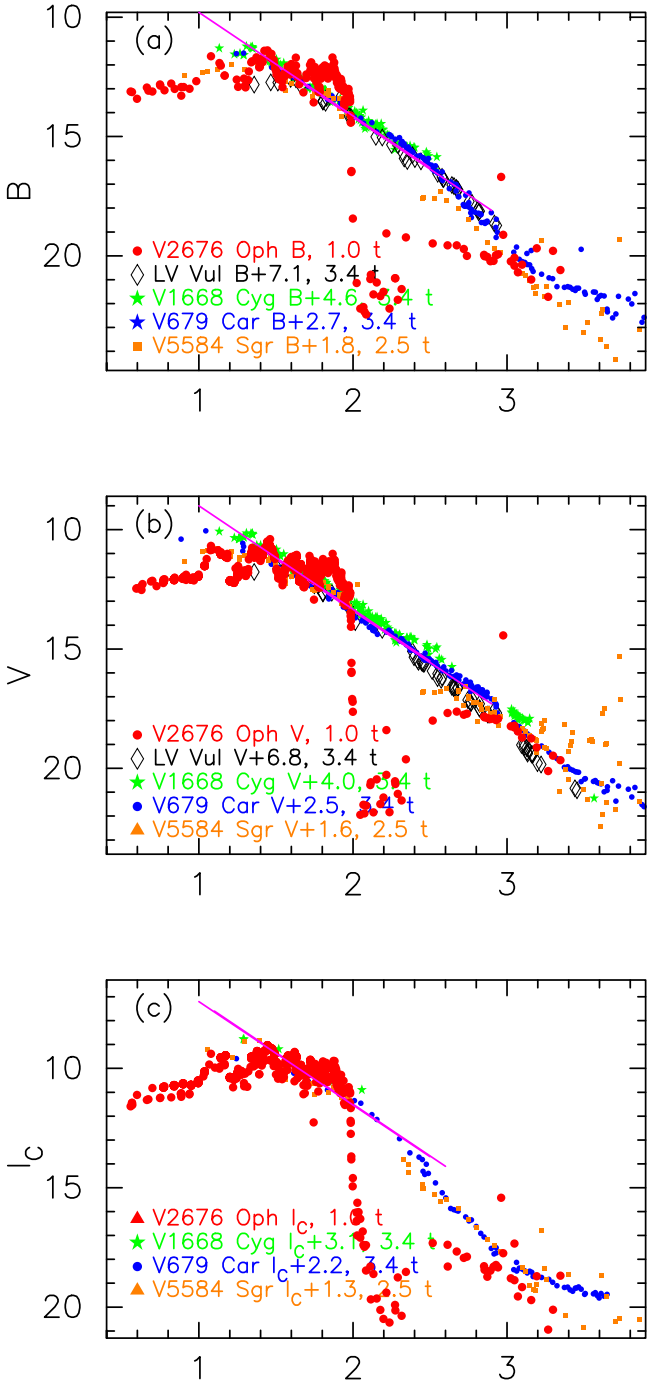

Figure 90. Same as Figure 25, but for V2676 Oph. The (a) *B*, (b) *V*, and (c) I_C light curves of V2676 Oph as well as those of V5584 Sgr, 679 Car, LV Vul, and V1668 Cyg. The *BV* data of V2676 Oph are the same as those in Figure 88. The I_C data of V2676 Oph are taken from AAVSO, VSOLJ, and SMARTS.

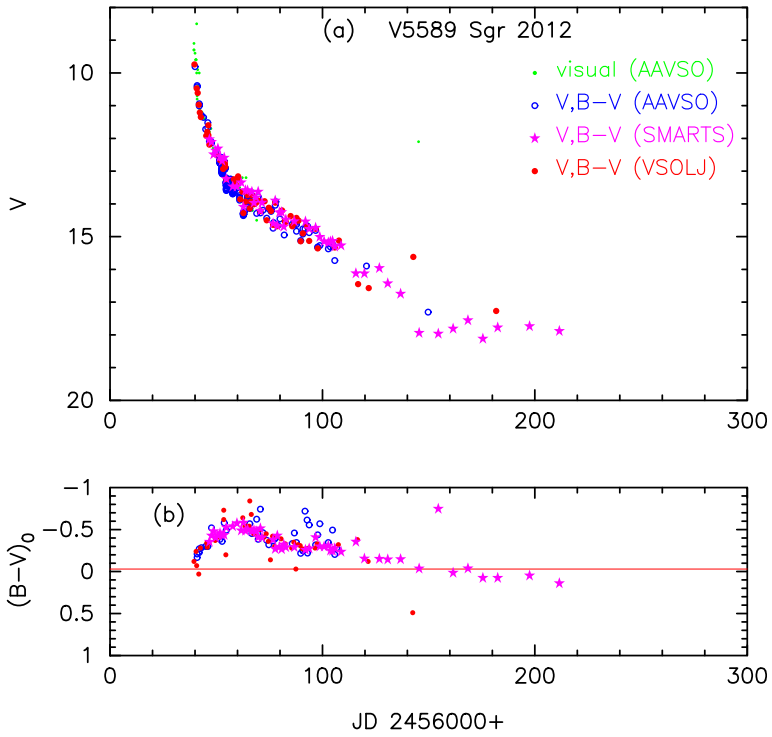

Figure 91. Same as Figure 23, but for V5589 Sgr. (a) The visual data (green dots) are taken from AAVSO. The V data are taken from AAVSO (unfilled blue circles), SMARTS (filled magenta stars), and VSOLJ (filled red circles). (b) The $(B-V)_0$ are dereddened with $E(B-V)=0.84$.

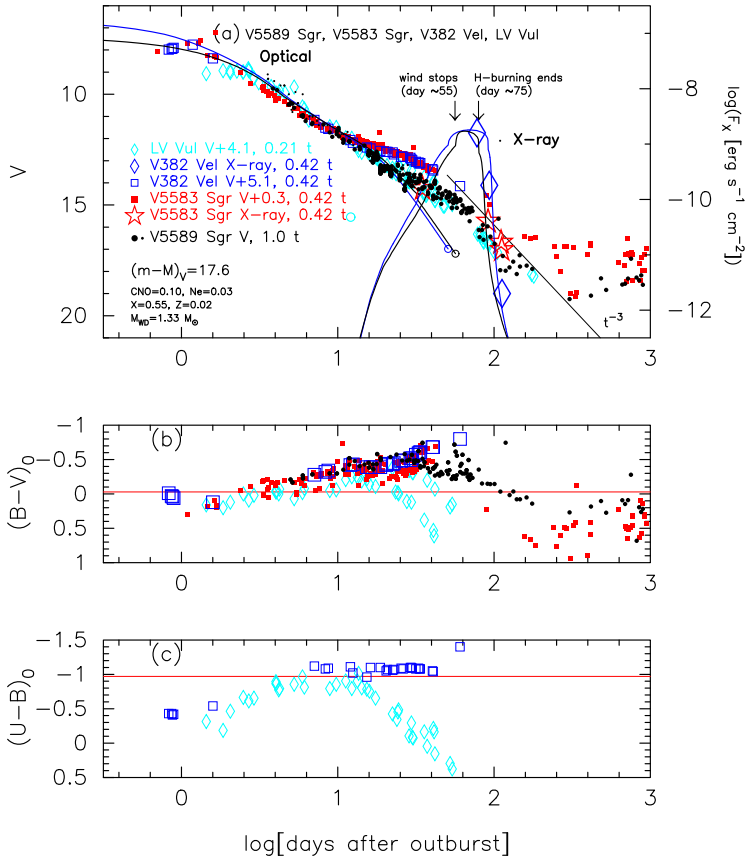

Figure 92. Same as Figure 30, but for V5589 Sgr (black dots for visual and filled black circles for V and $B-V$). We add three novae, V5583 Sgr, V382 Vel, and LV Vul, the V light curves of which are similar to those of V5589 Sgr. The data of V5589 Sgr are the same as those in Figure 91. In panel (a), we add the model light curve (solid black lines) of a 1.33 $M_\odot$ WD (Ne2; Hachisu & Kato 2010), assuming that $(m-M)_V=17.6$ for V5589 Sgr. We also add the model light curves (solid blue lines) of a 1.23 $M_\odot$ WD (Ne2), assuming that $(m-M)_V=11.5$ for V382 Vel (Hachisu & Kato 2016a).

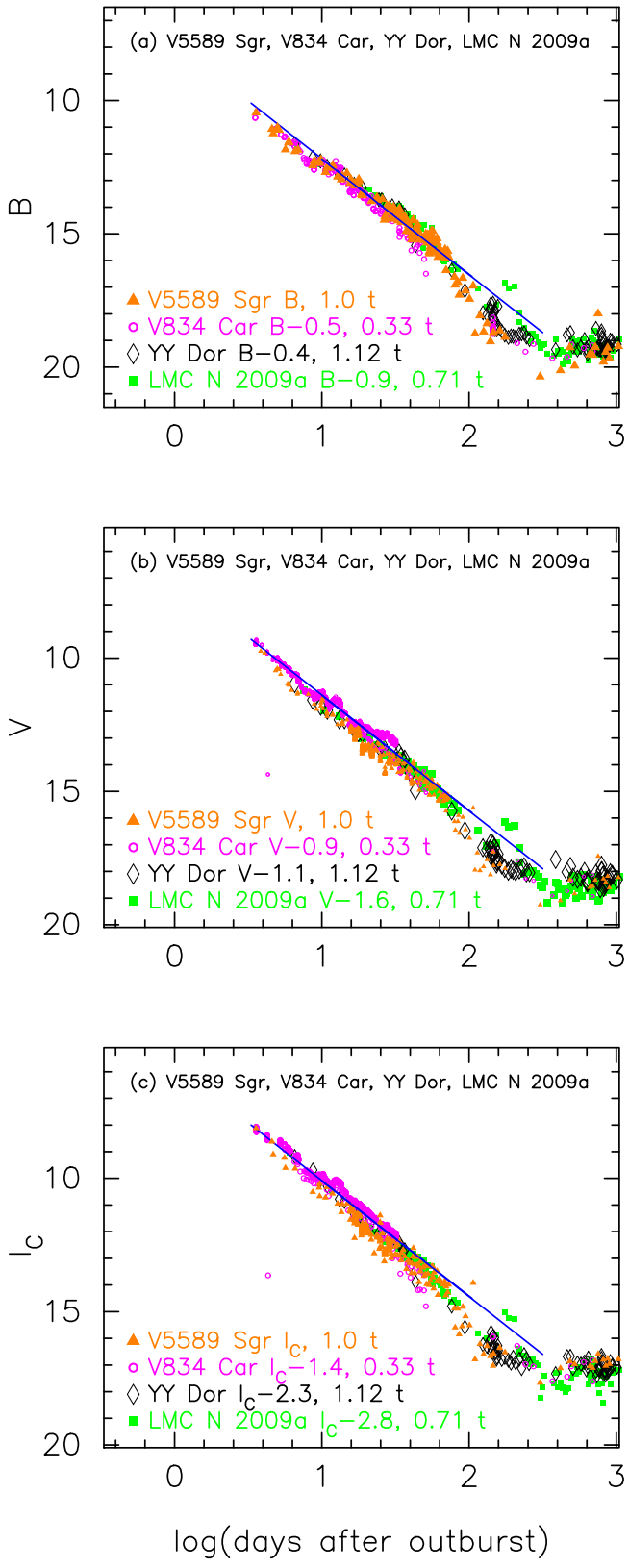

Figure 93. Same as Figure 25, but for V5589 Sgr. The *BV* data of V5589 Sgr are the same as those in Figure 91. The I_C data of V5589 Sgr are taken from AAVSO, VSOLJ, and SMARTS.

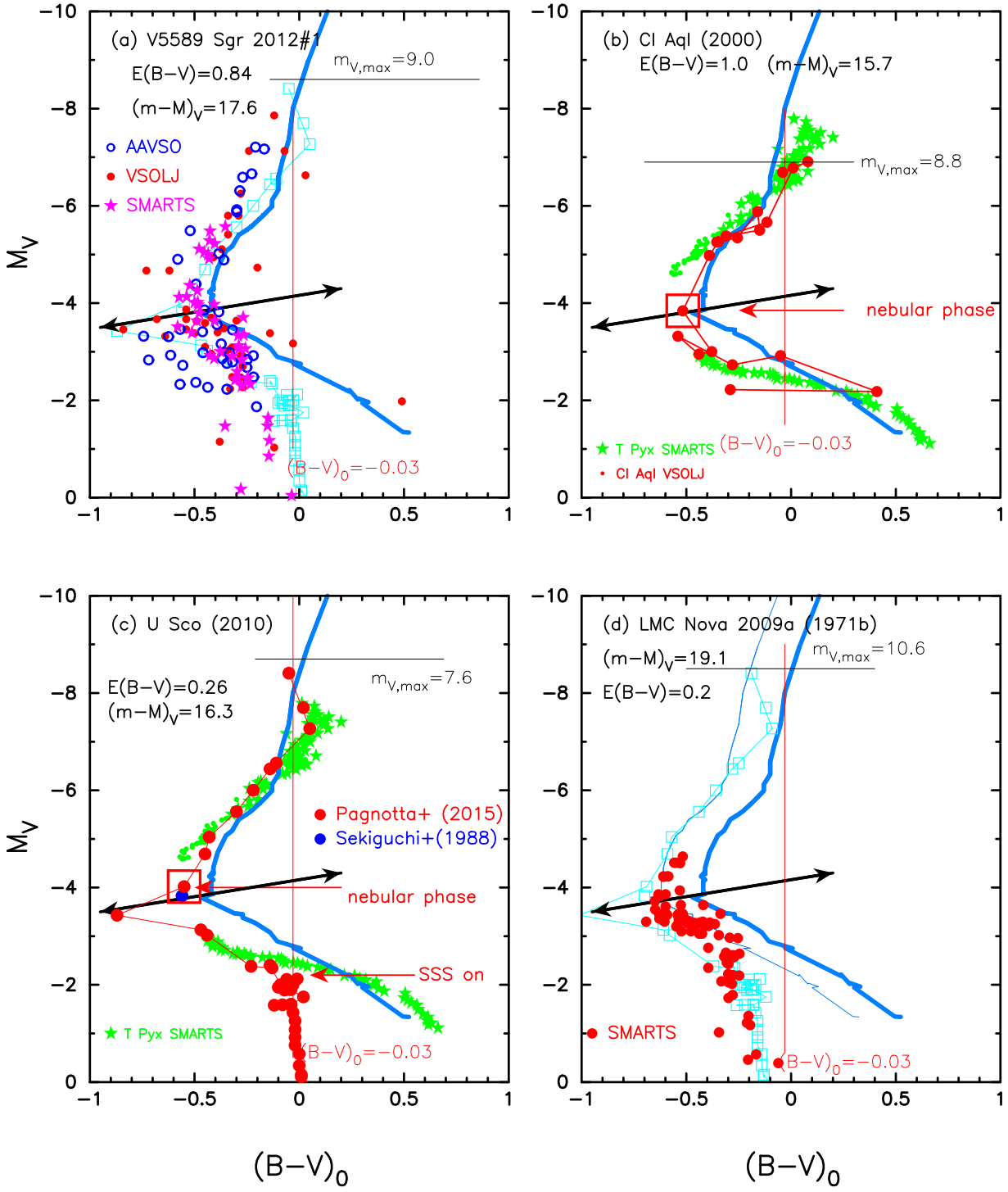

Figure 94. Color−magnitude diagram for (a) V5589 Sgr, (b) CI Aql, (c) U Sco, and (d) LMC N 2009a. The thick solid cyan-blue line is the V1500 Cyg track. The two-headed black arrow represents the locations of the turning point of the tracks (Hachisu & Kato 2016b). In panel (a), we add the track of U Sco with the unfilled cyan squares connected by the solid cyan line. In panels (b) and (c), we also plot the T Pyx (2011) outburst (filled green stars, taken from SMARTS). In panel (d), the very thin solid cyan-blue line corresponds to the V1500 Cyg track, which is blueshifted by $\Delta(B-V)_0 = -0.2$. The unfilled cyan squares connected by a thin solid cyan line represent the U Sco track, which is blueshifted by $\Delta(B-V)_0 = -0.14$. The blueshifted nature of LMC N 2009a is due to the low (subsolar) metallicity of the LMC (e.g., Hachisu & Kato 2018b).

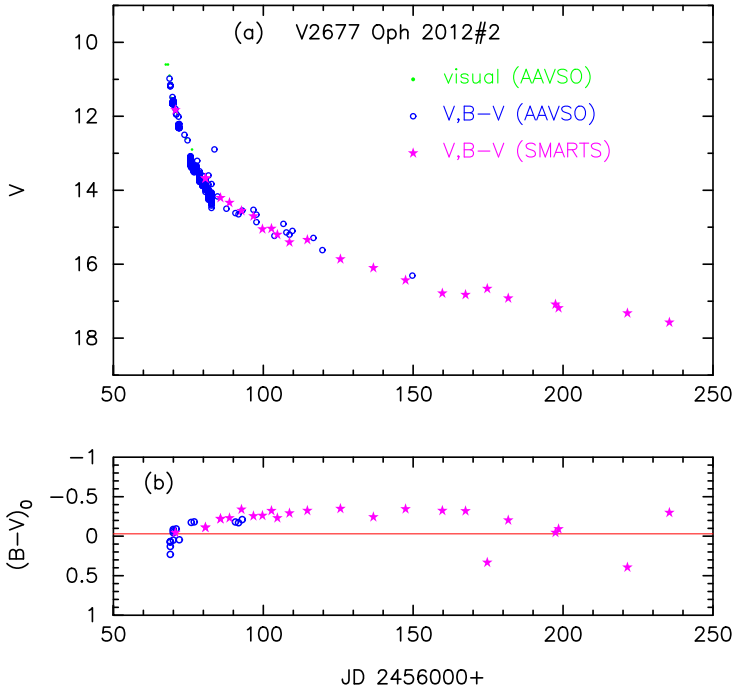

Figure 95. Same as Figure 23, but for V2677 Oph. (a) The visual data (green dots) are taken from AAVSO. The *BV* data are taken from AAVSO (unfilled blue circles) and SMARTS (filled magenta stars). (b) The $(B-V)_0$ are dereddened with $E(B-V)=1.30$.

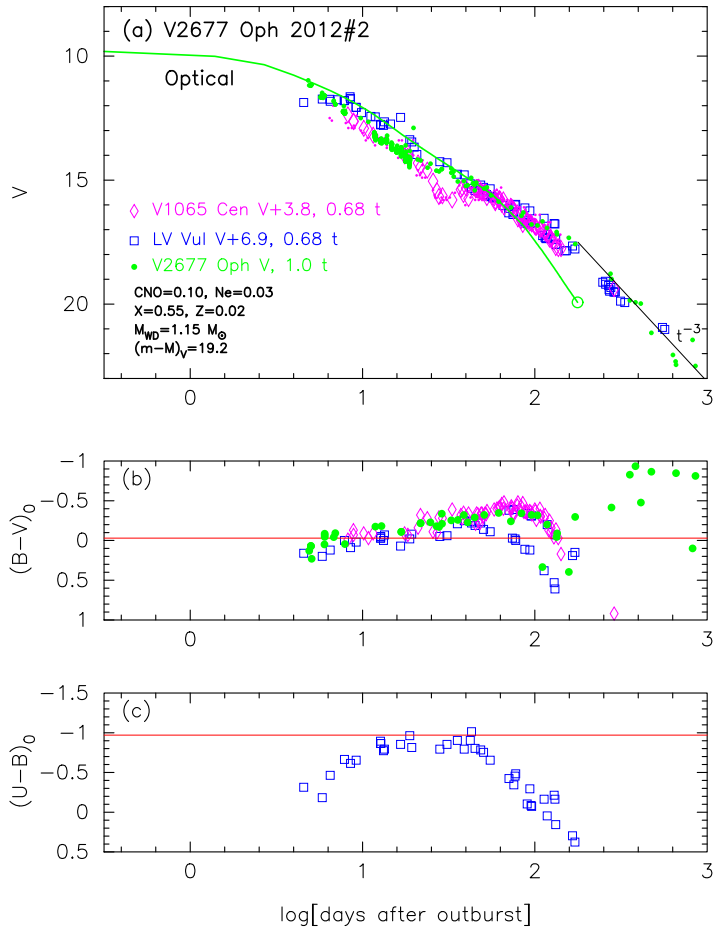

Figure 96. Same as Figure 30, but for V2677 Oph (filled green circles). The data of V2677 Oph are the same as those in Figure 95. The other data are the same as those in Figure 4 of Hachisu & Kato (2018a). Assuming that $(m-M)_V=19.2$, we plot a model light curve of a 1.15 $M_\odot$ WD (solid green line, Ne2; Hachisu & Kato 2010).

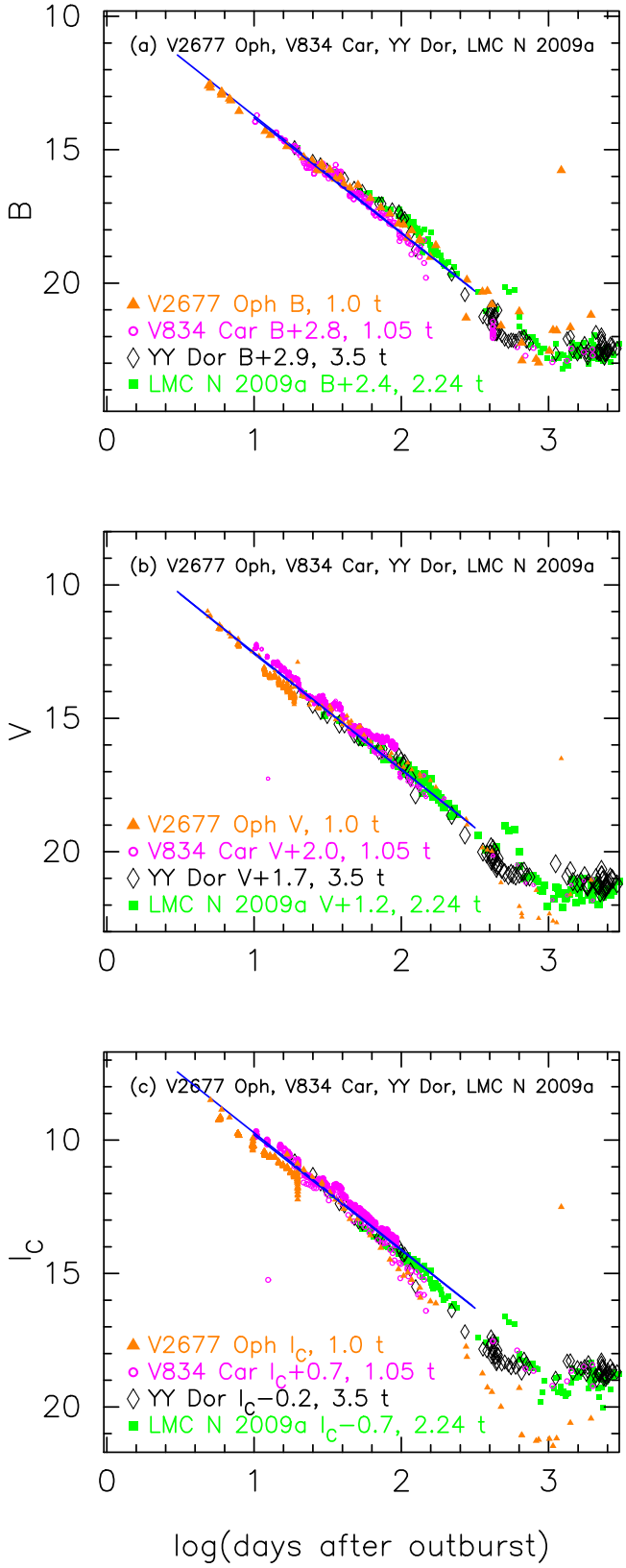

Figure 97. Same as Figure 25, but for V2677 Oph. The *BV* data of V2677 Oph are the same as those in Figure 95. The I_C data of V2677 Oph are taken from AAVSO and SMARTS.

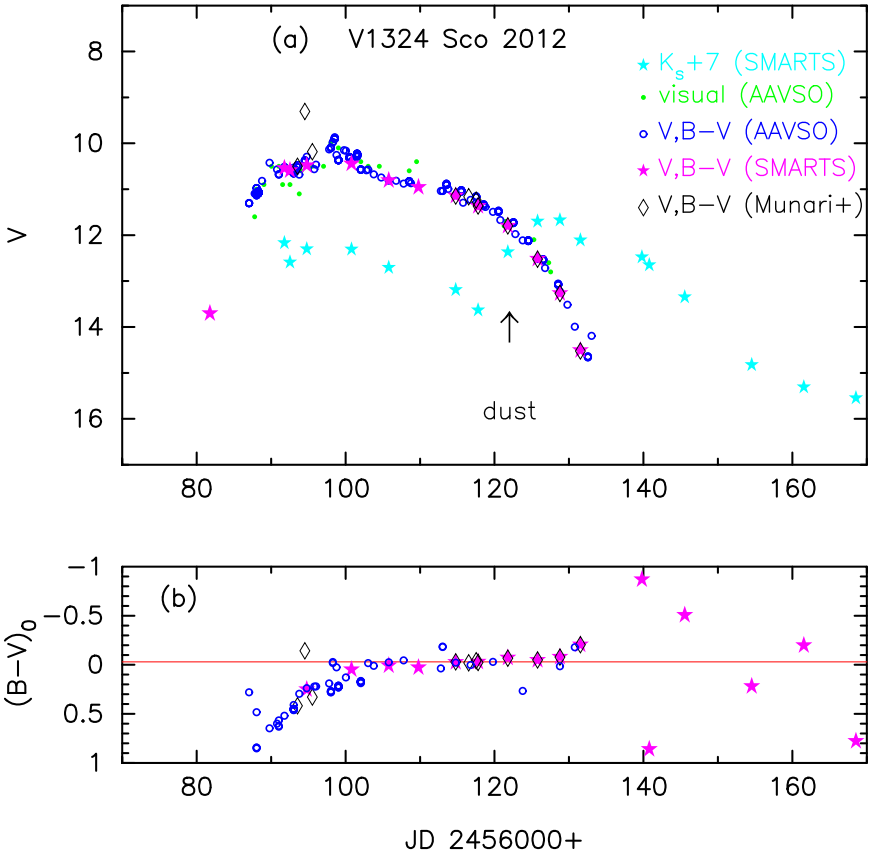

Figure 98. Same as Figure 23, but for V1324 Sco. (a) The visual data (green dots) are taken from AAVSO. The *BV* data are taken from AAVSO (unfilled blue circles), SMARTS (filled magenta stars), and Munari et al. (2015b, unfilled black diamonds). The K_s data are taken from SMARTS (filled cyan stars). The rise of the K_s magnitude indicates the formation of a dust shell as shown by the arrow labeled "dust." (b) The $(B-V)_0$ are dereddened with $E(B-V)=1.32$.

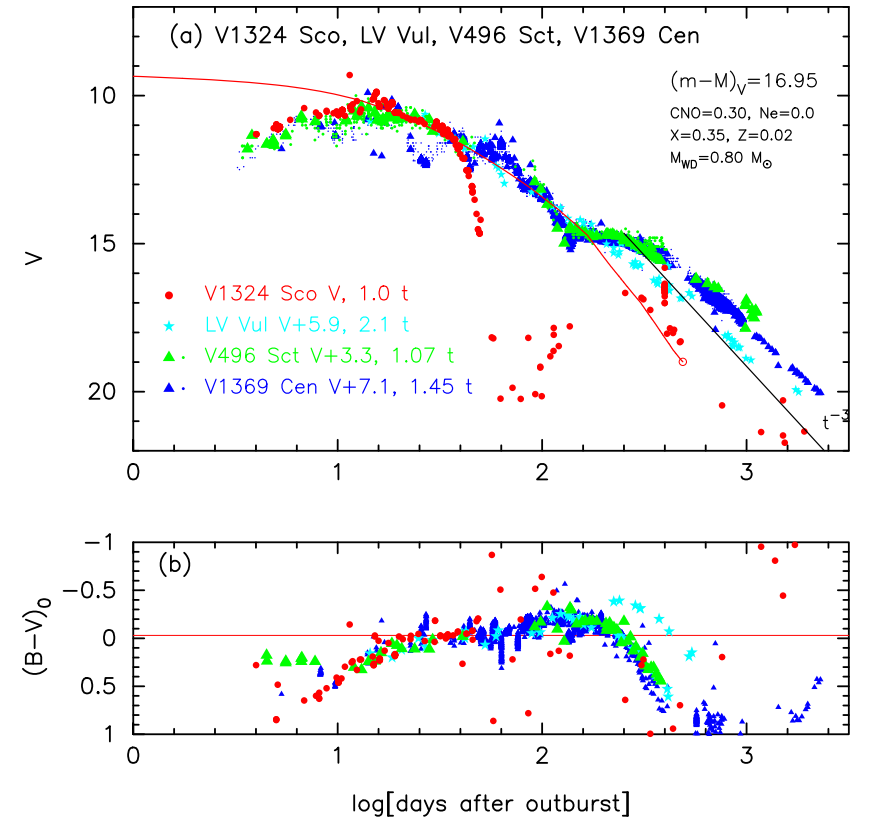

Figure 99. Same as Figure 30, but for V1324 Sco (filled red circles). The data of V1324 Sco are the same as those in Figure 98. We add the model *V* light curve of a 0.80 $M_\odot$ WD (CO2, solid red line; Hachisu & Kato 2010), assuming $(m-M)_V=16.95$ for V1324 Sco.

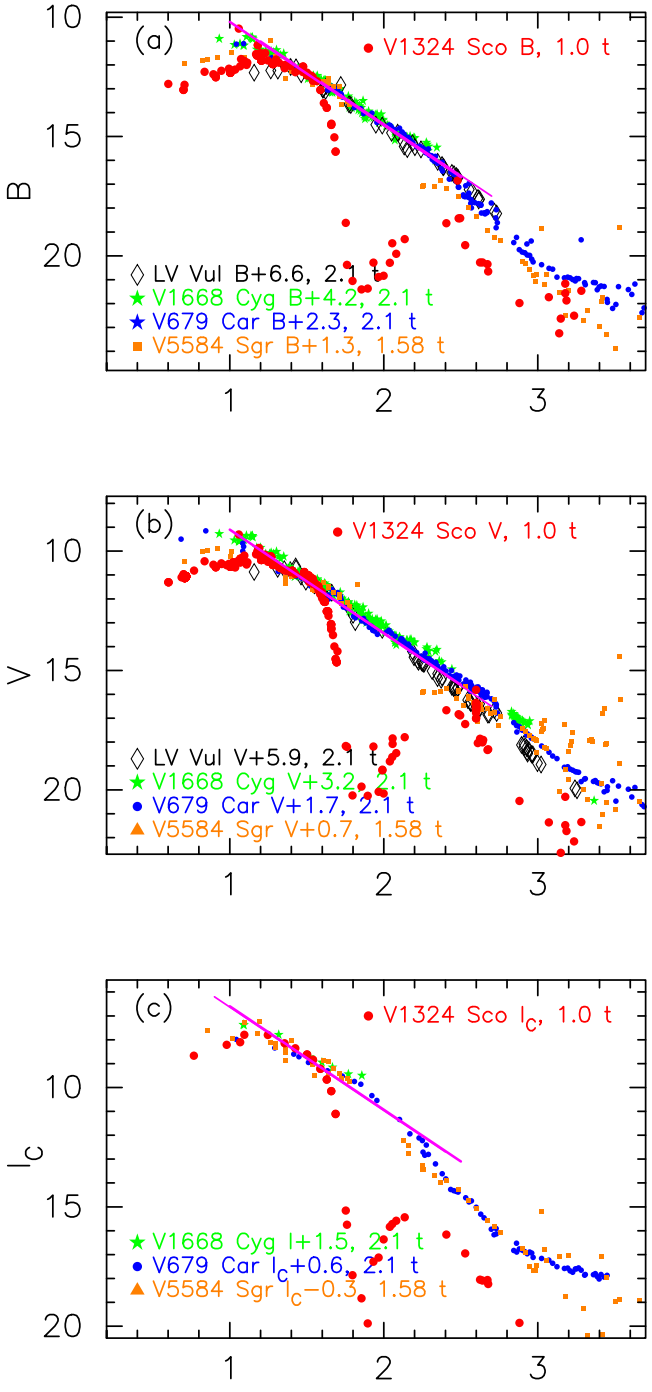

Figure 100. Same as Figure 25, but for V1324 Sco. The (a) *B*, (b) *V*, and (c) I_C light curves of V1324 Sco as well as those of V5584 Sgr, V679 Car, LV Vul, and V1668 Cyg. The *BV* data of V1324 Sco are the same as those in Figure 98. The I_C data of V1324 Sco are taken from Munari et al. (2015b), AAVSO, and SMARTS. No I_C data are available for LV Vul.

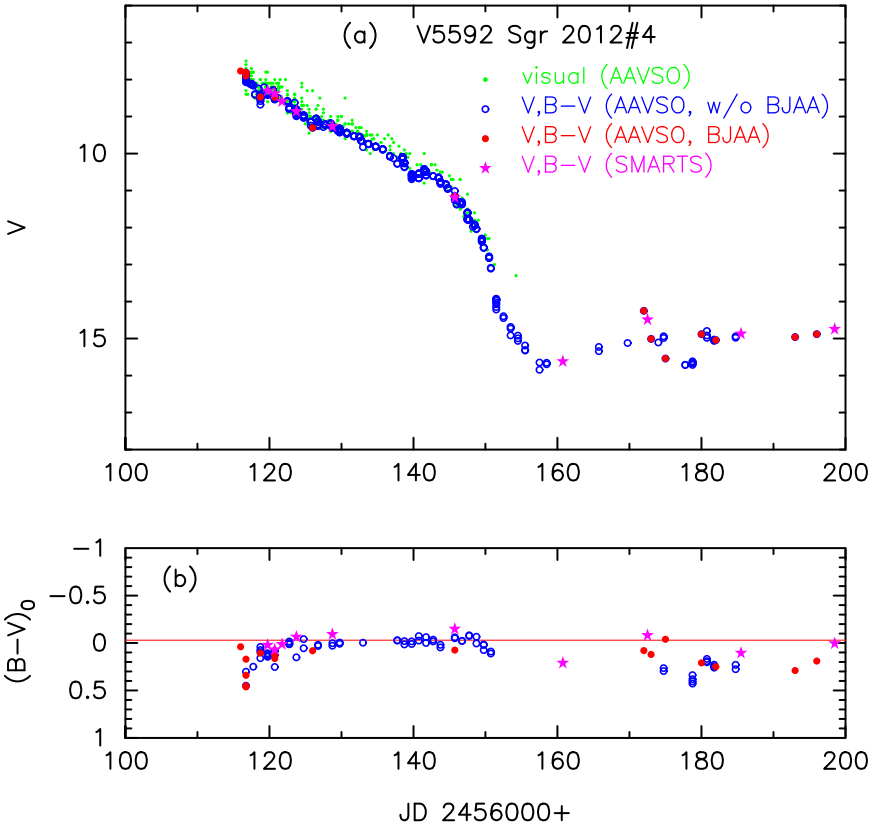

Figure 101. Same as Figure 23, but for V5592 Sgr. (a) The visual data (green dots) are taken from AAVSO. The *BV* data are taken from AAVSO (unfilled blue circles and filled red circles) and SMARTS (filled magenta stars). (b) The $(B-V)_0$ are dereddened with $E(B-V)=0.33$. The $B-V$ of BJAA's data (filled red circles) taken from AAVSO are shifted redward by 0.20 mag. See the text for details.

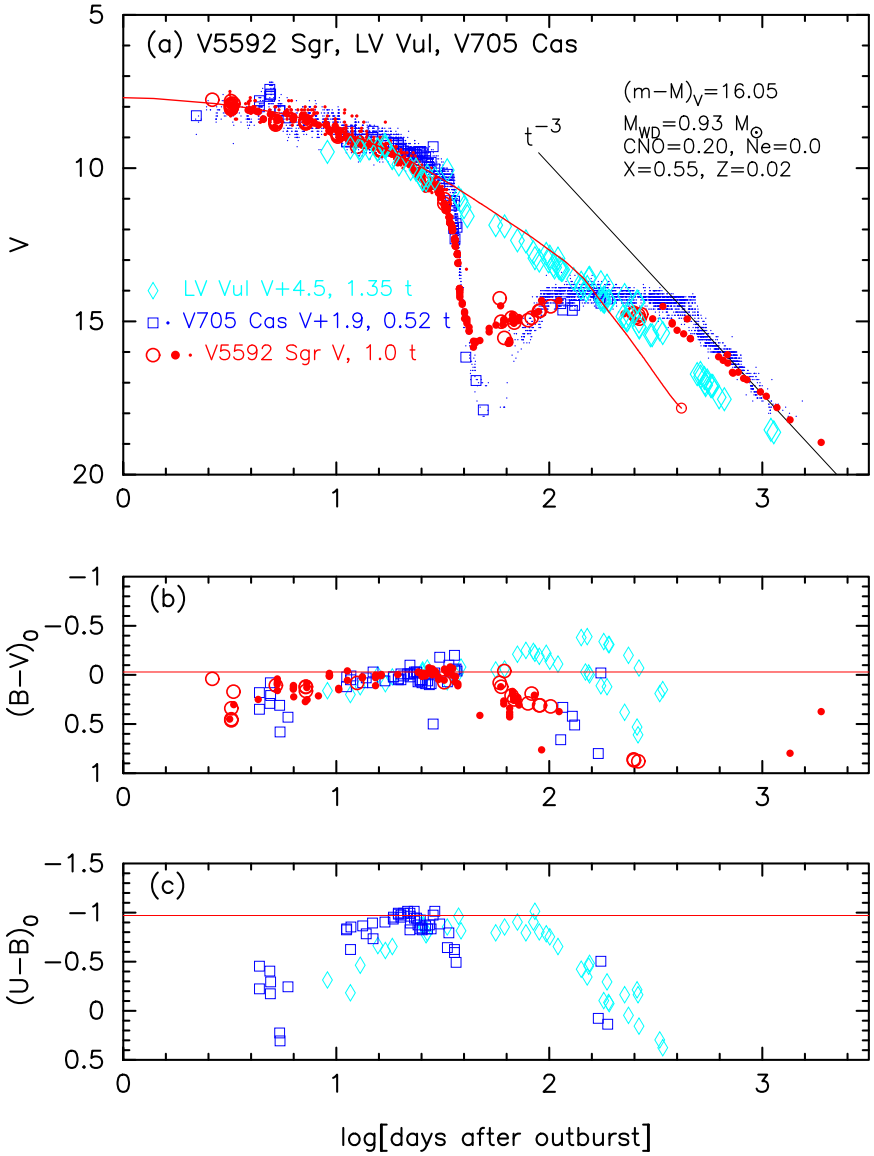

Figure 102. Same as Figure 30, but for V5592 Sgr (red dots for visual, unfilled red circles and filled red squares for V). The data of V5592 Sgr are the same as those in Figure 101. We add the model V light curve of a 0.93 $M_\odot$ WD (CO4, solid red line; Hachisu & Kato 2015), assuming $(m - M)_V = 16.05$ for V5592 Sgr.

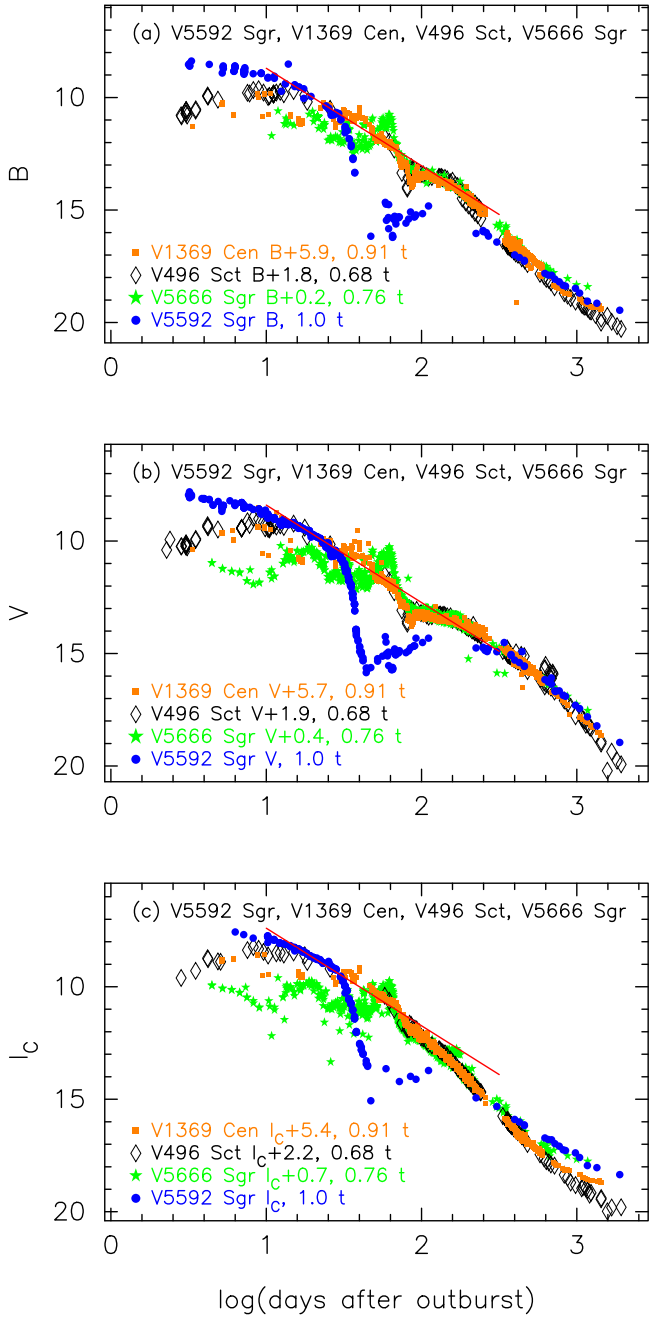

Figure 103. Same as Figure 25, but for V5592 Sgr. We plot the (a) *B*, (b) *V*, and (c) I_C light curves of V5592 Sgr as well as those of V1369 Cen, V496 Sct, and V5666 Sgr. The *BV* data of V5592 Sgr are the same as those in Figure 101. The I_C data of V5592 Sgr are taken from AAVSO and SMARTS.

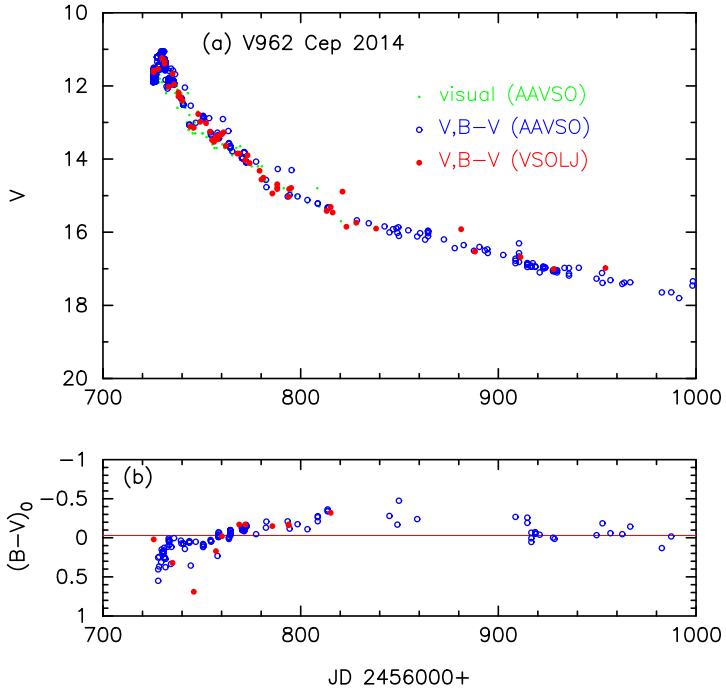

Figure 104. Same as Figure 23, but for V962 Cep. (a) The visual data (green dots) are taken from AAVSO. The *BV* data are taken from AAVSO (unfilled blue circles) and VSOLJ (filled red circles). (b) The $(B-V)_0$ are dereddened with $E(B-V)=1.10$.

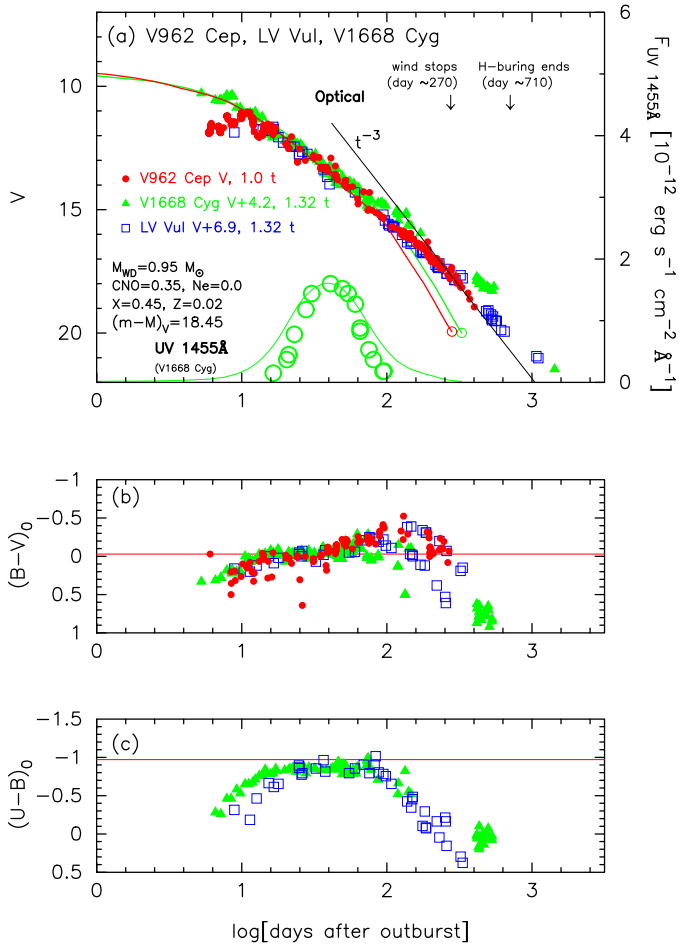

Figure 105. Same as Figure 30, but for V962 Cep (filled red circles). The data of V962 Cep are the same as those in Figure 104. We add the model *V* light curve of a 0.95 $M_\odot$ WD (CO3, solid red line; Hachisu & Kato 2016a), assuming $(m-M)_V=18.45$ for V962 Cep. The solid green lines denote the *V* and UV 1455 Å light curves of a 0.98 $M_\odot$ WD (CO3), assuming $(m-M)_V=14.6$ for V1668 Cyg.

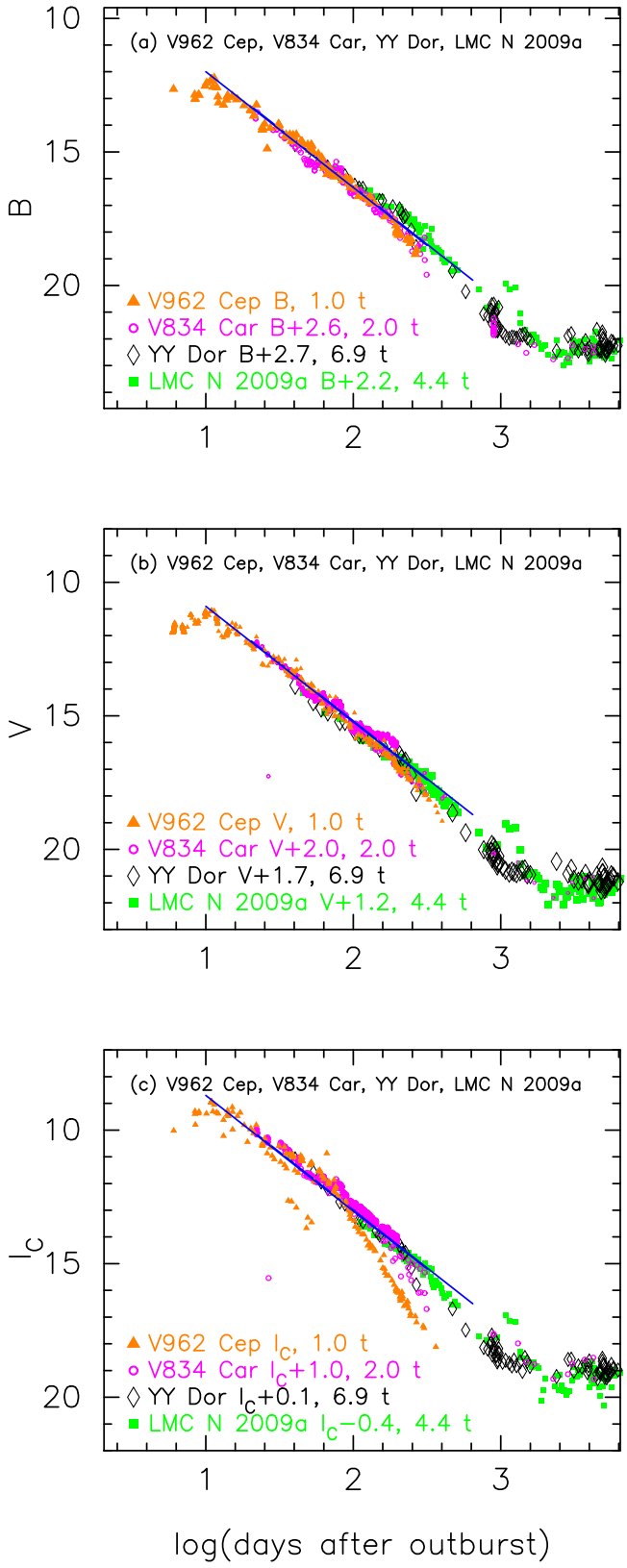

Figure 106. Same as Figure 25, but for V962 Cep. The *BV* data of V962 Cep are the same as those in Figure 104. The I_C data of V962 Cep are taken from AAVSO and VSOLJ.

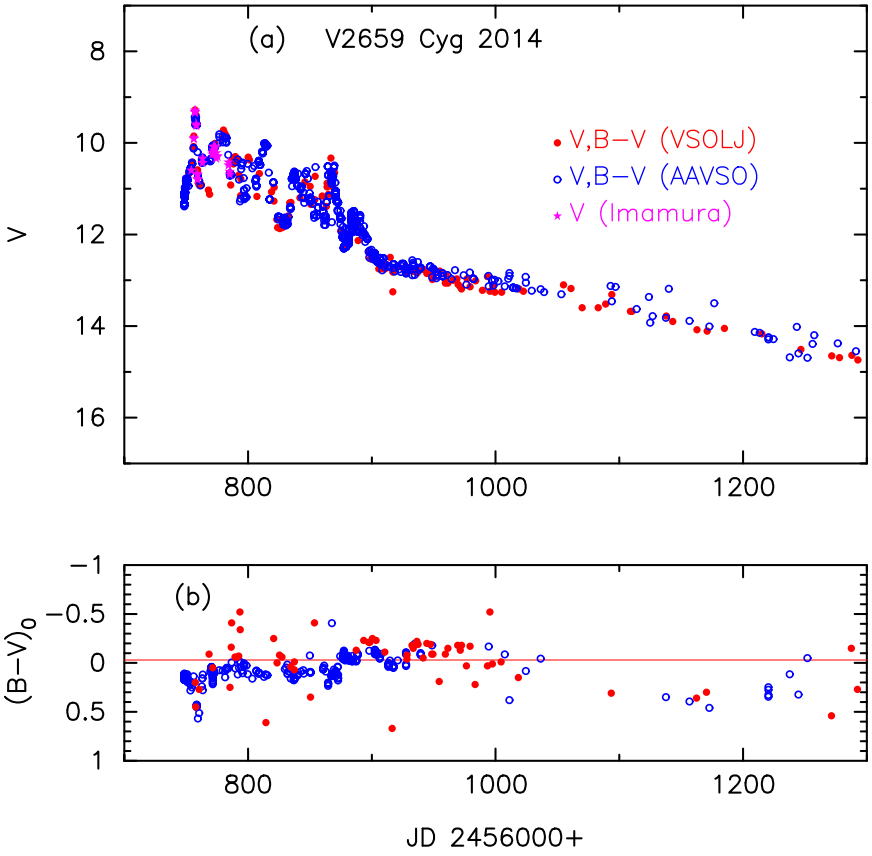

Figure 107. Same as Figure 23, but for V2659 Cyg. (a) The V data (filled magenta stars) are taken from Imamura et al. (2014). The BV data are from AAVSO (unfilled blue circles) and VSOLJ (filled red circles). (b) The $(B-V)_0$ are dereddened with $E(B-V)=0.80$.

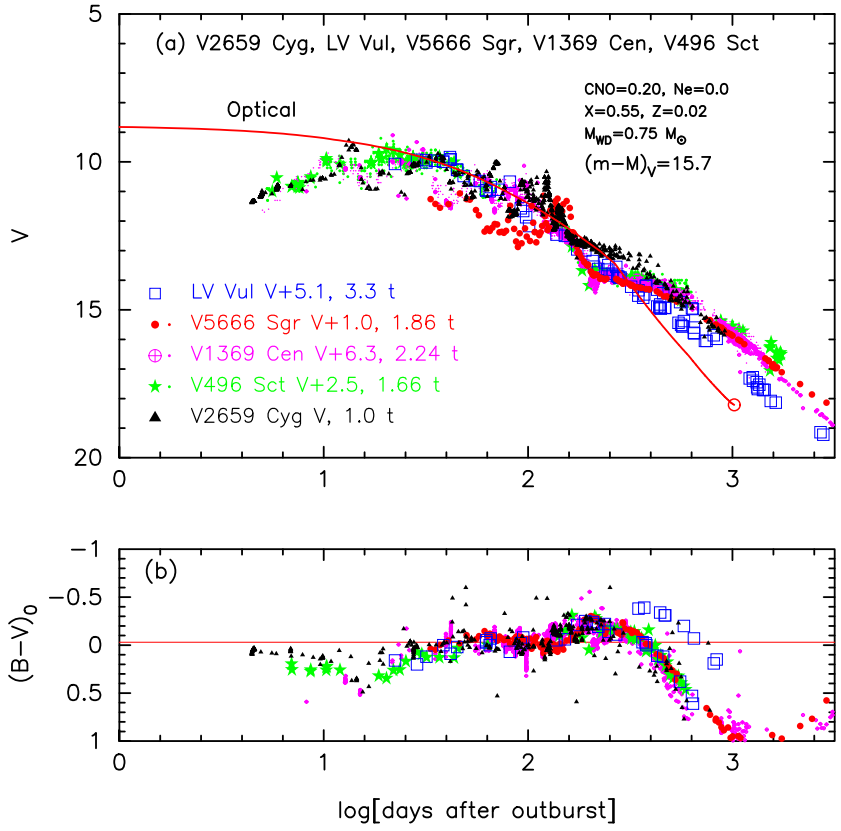

Figure 108. Same as Figure 30, but for V2659 Cyg (filled black triangles). We add the light/color curves of LV Vul, V5666 Sgr, V1369 Cen, and V496 Sct. The data of V2659 Cyg are the same as those in Figure 107. In panel (a), we add the model V light curve of a 0.75 $M_\odot$ WD (CO4, solid red line; Hachisu & Kato 2015), assuming $(m-M)_V=15.7$ for V2659 Cyg.

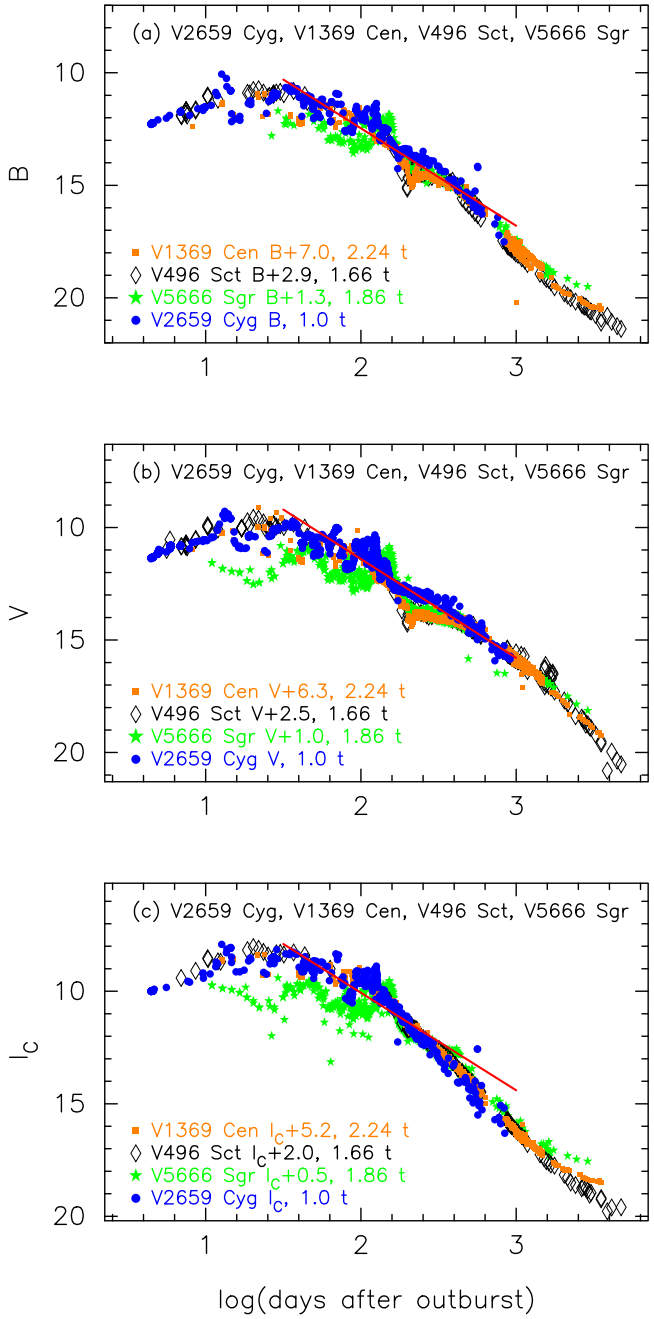

Figure 109. Same as Figure 25, but for V2659 Cyg. We plot the (a) *B*, (b) *V*, and (c) I_C light curves of V2659 Cyg as well as those of V1369 Cen, V496 Sct, and V5666 Sgr. The *BV* data of V2659 Cyg are the same as those in Figure 107. The I_C data of V2659 Cyg are taken from AAVSO and VSOLJ.

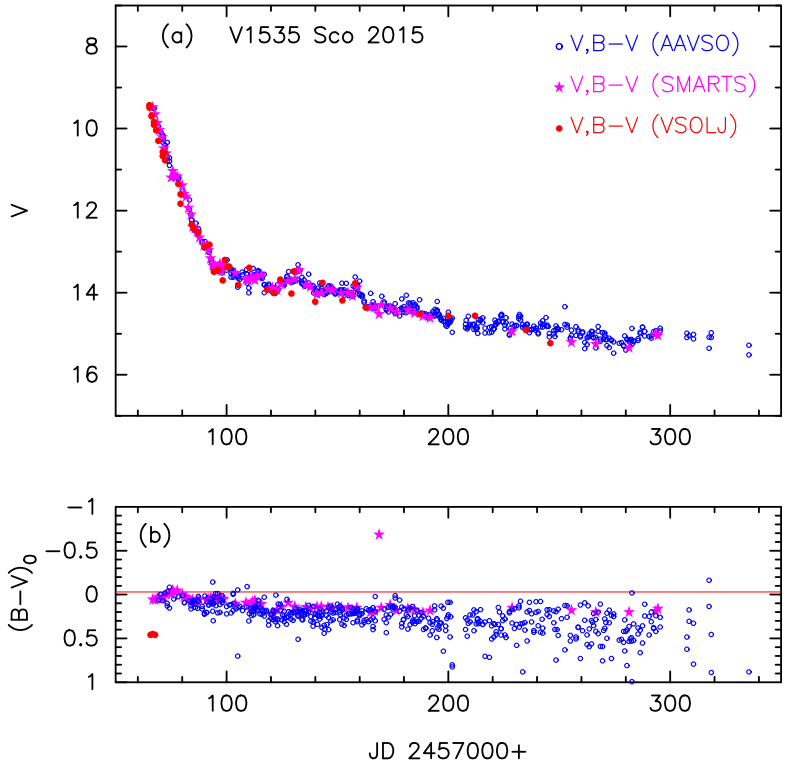

Figure 110. Same as Figure 23, but for V1535 Sco. (a) The BV data are taken from AAVSO (unfilled blue circles), SMARTS (filled magenta stars), and VSOLJ (filled red circles). (b) The $(B-V)_0$ are dereddened with $E(B-V)=0.78$.

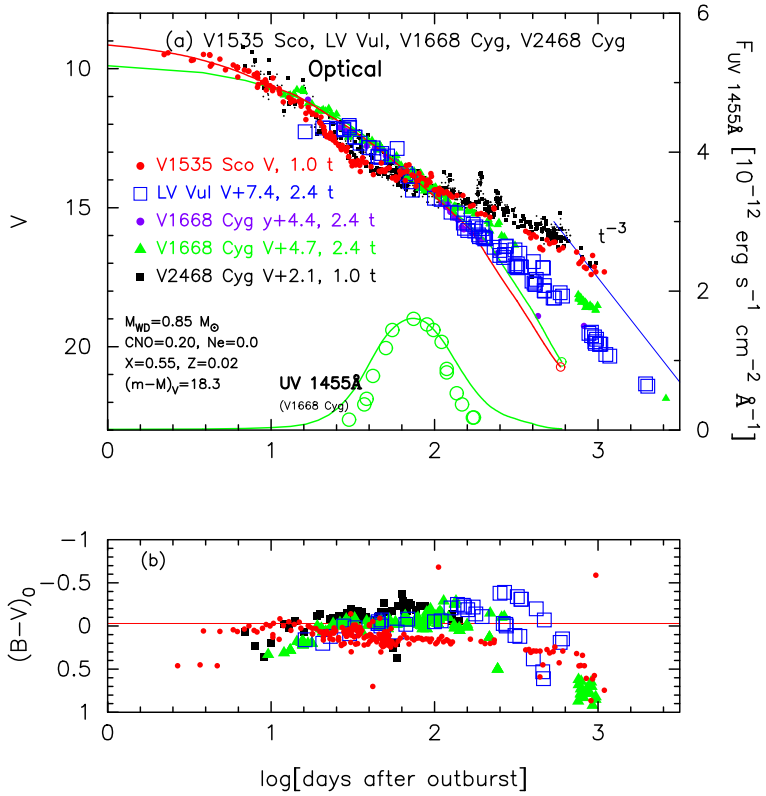

Figure 111. Same as Figure 30, but for V1535 Sco (filled red circles). We plot the (a) V light and (b) $(B-V)_0$ color curves of V1535 Sco as well as those of LV Vul, V1668 Cyg, and V2468 Cyg. In panel (a), we add the model V light curve (solid red line) of a 0.85 $M_\odot$ WD (CO4, Hachisu & Kato 2015), assuming that $(m-M)_V=18.3$ for V1535 Sco. We also add model V and UV 1455 Å light curves of a 0.98 $M_\odot$ WD (CO3, solid green lines; Hachisu & Kato 2016a), assuming that $(m-M)_V=14.6$ for V1668 Cyg.

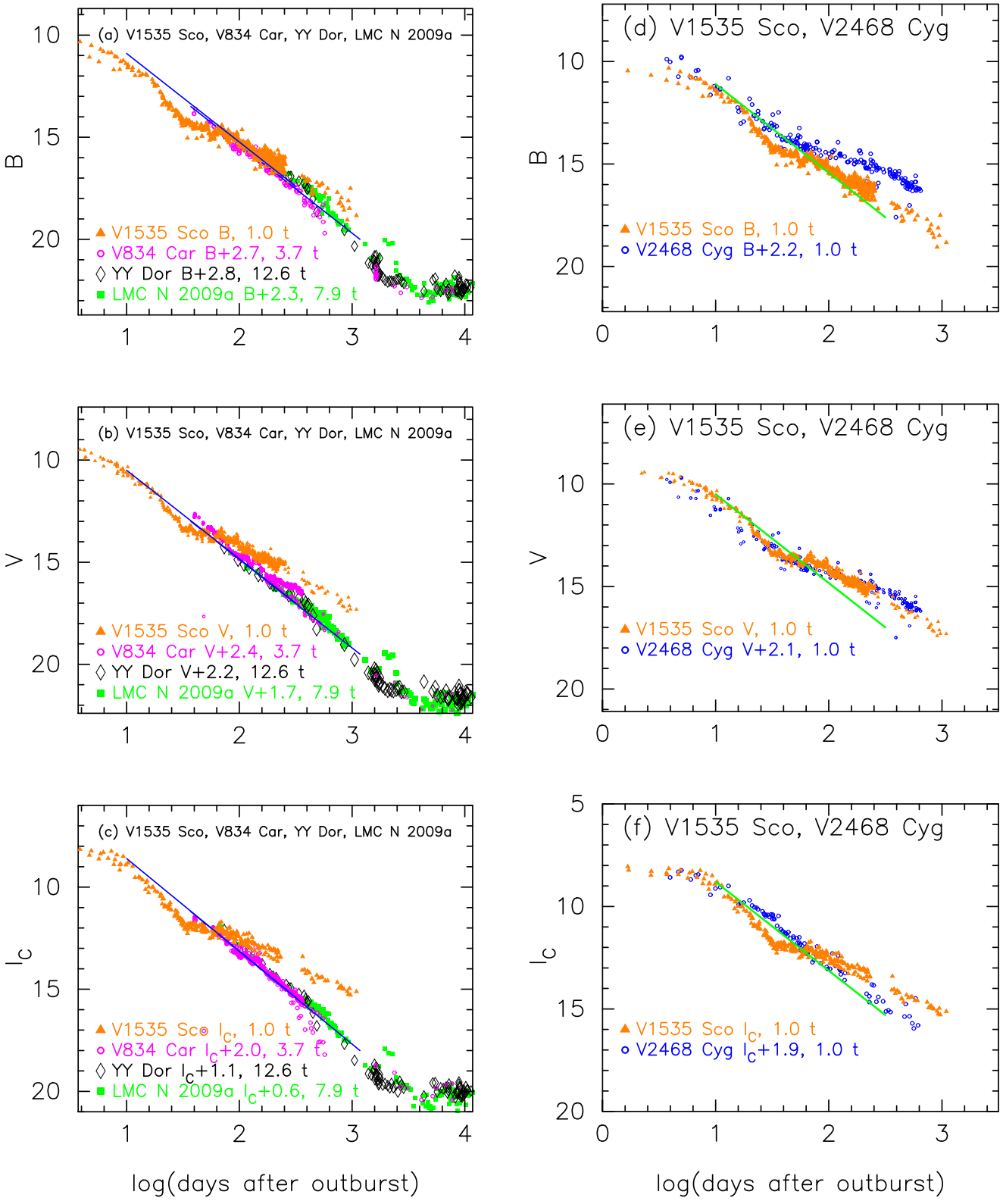

Figure 112. Same as Figure 25, but for V1535 Sco. The *BV* data of V1535 Sco are the same as those in Figure 110. The I_C data of V1535 Sco are taken from AAVSO, VSOLJ, and SMARTS. The BVI_C data of V2468 Cyg are the same as those in Figure 47 of Hachisu & Kato (2019).

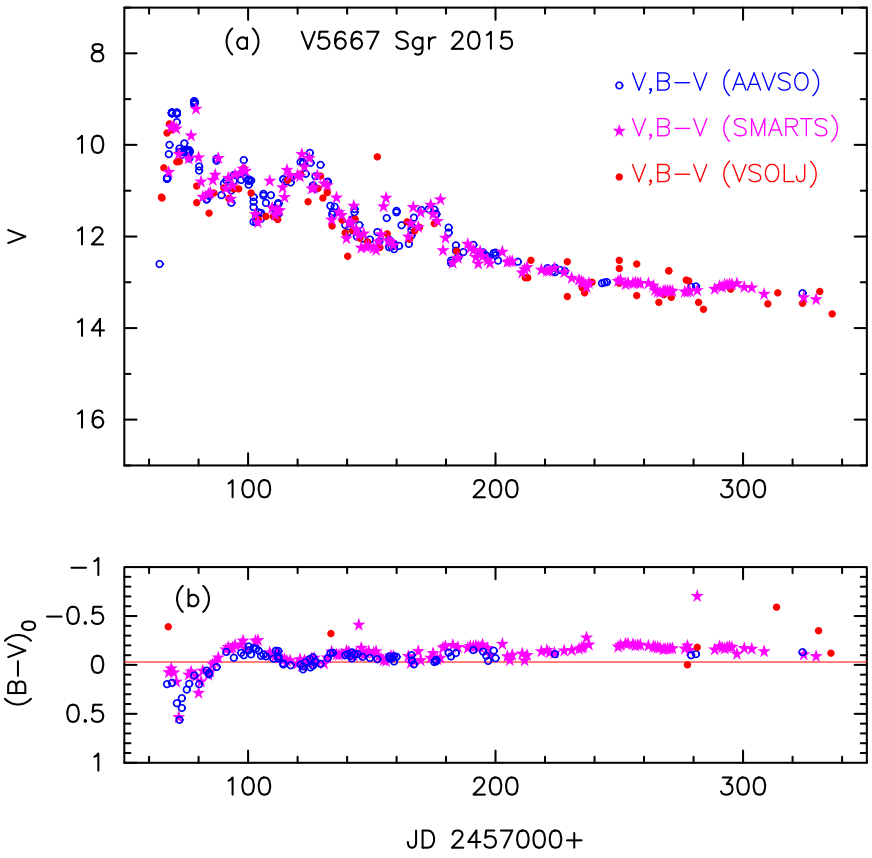

Figure 113. Same as Figure 23, but for V5667 Sgr. (a) The *BV* data are taken from AAVSO (unfilled blue circles), SMARTS (filled magenta stars), and VSOLJ (filled red circles). (b) The $(B-V)_0$ are dereddened with $E(B-V)=0.63$.

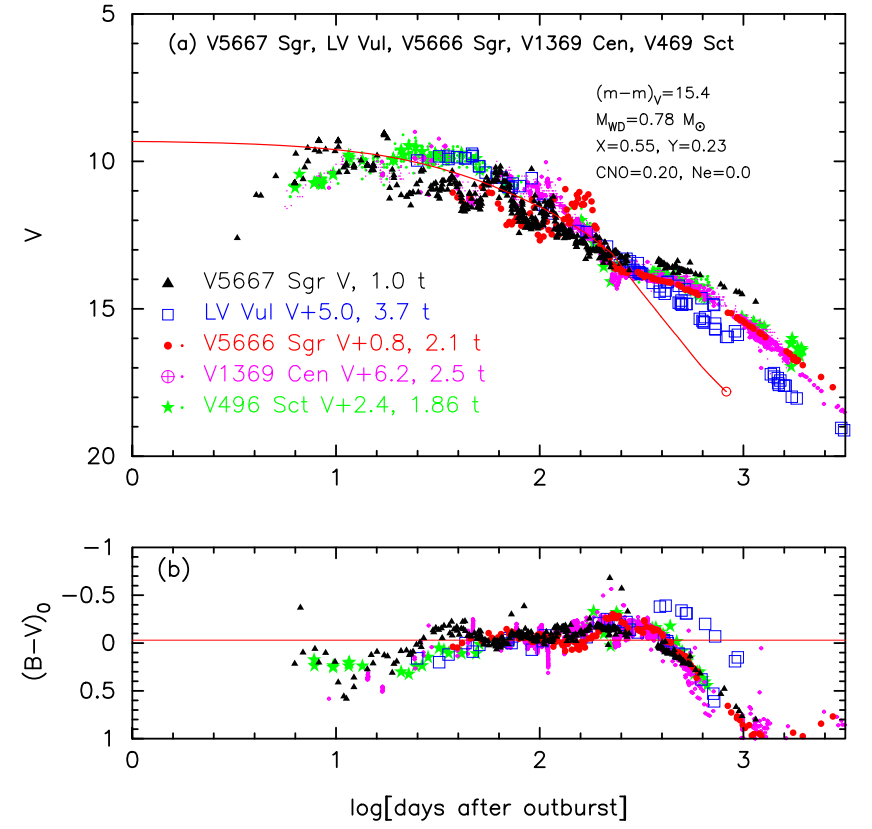

Figure 114. Same as Figure 30, but for V5667 Sgr (filled black triangles). We plot the (a) V light and (b) $(B-V)_0$ color curves of V5667 Sgr as well as those of LV Vul, V5666 Sgr, V1369 Cen, and V496 Sct. In panel (a), we add a model V light curve (solid red line) of a 0.78 $M_\odot$ WD (CO4, Hachisu & Kato 2015), assuming that $(m-M)_V=15.4$ for V5667 Sgr.

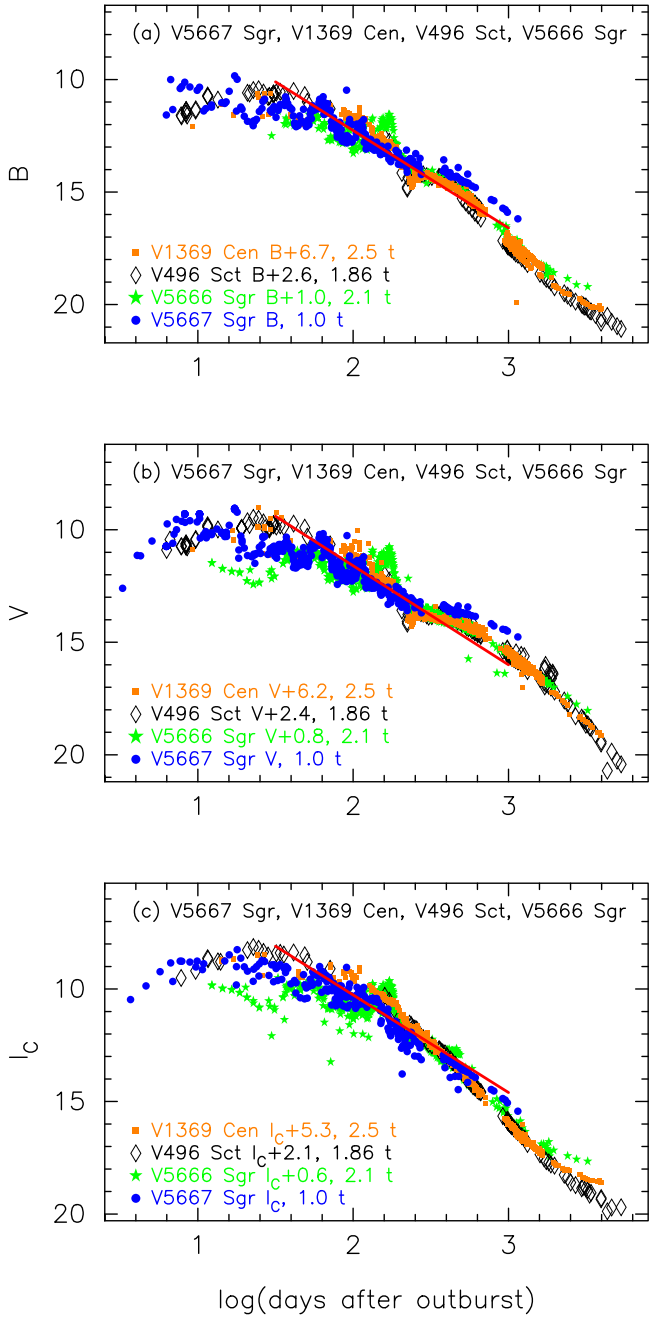

Figure 115. Same as Figure 25, but for V5667 Sgr. The (a) *B*, (b) *V*, and (c) I_C light curves of V5667 Sgr as well as those of V1369 Cen, V496 Sct, and V5666 Sgr. The *BV* data of V5667 Sgr are the same as those in Figure 113. The I_C data of V5667 Sgr are taken from VSOLJ and SMARTS.

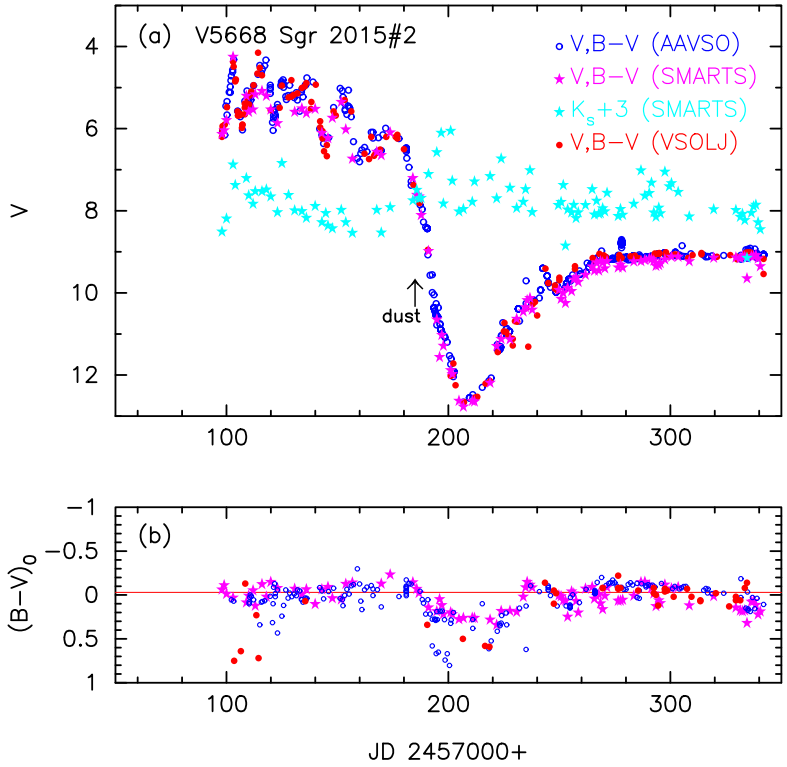

Figure 116. Same as Figure 23, but for V5668 Sgr. (a) The *BV* data are taken from AAVSO (unfilled blue circles), SMARTS (filled magenta stars), and VSOLJ (filled red circles). The K_s data are taken from SMARTS (filled cyan stars). We denote the epoch when a dust shell formed by the arrow labeled dust. (b) The $(B-V)_0$ are dereddened with $E(B-V)=0.20$.

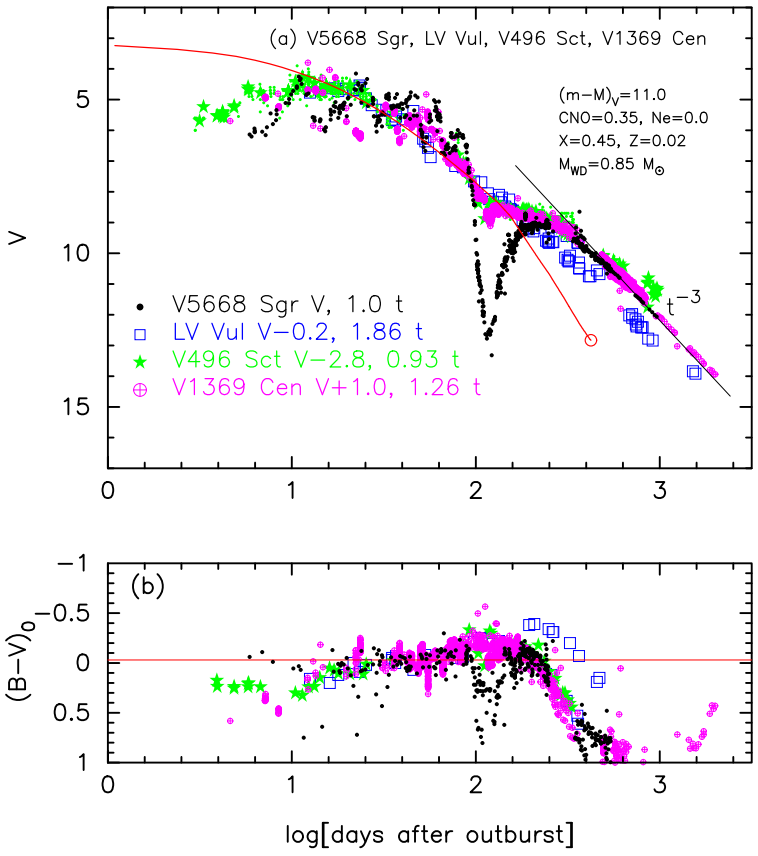

Figure 117. Same as Figure 30, but for V5668 Sgr (filled black circles). We plot the (a) *V* light and (b) $(B-V)_0$ color curves of V5668 Sgr as well as those of LV Vul, V496 Sct, and V1369 Cen. The data of V5668 Sgr are the same as those in Figure 116. In panel (a), we add a model *V* light curve of a 0.85 $M_\odot$ WD (CO3, solid red line; Hachisu & Kato 2016a), assuming that $(m-M)_V=11.0$ for V5668 Sgr.

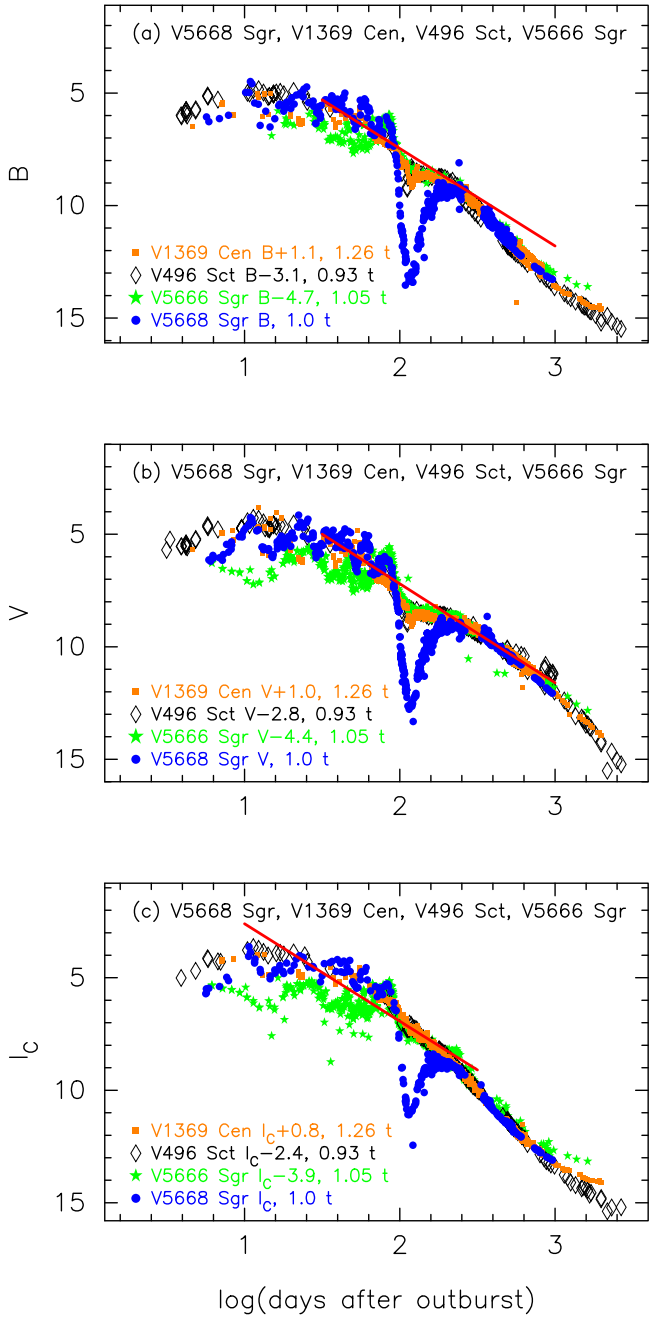

Figure 118. Same as Figure 25, but for V5668 Sgr. The (a) *B*, (b) *V*, and (c) I_C light curves of V5668 Sgr as well as those of V1369 Cen, V496 Sct, and V5666 Sgr. The *BV* data of V5668 Sgr are the same as those in Figure 116. The I_C data of V5668 Sgr are taken from AAVSO, VSOLJ, and SMARTS.

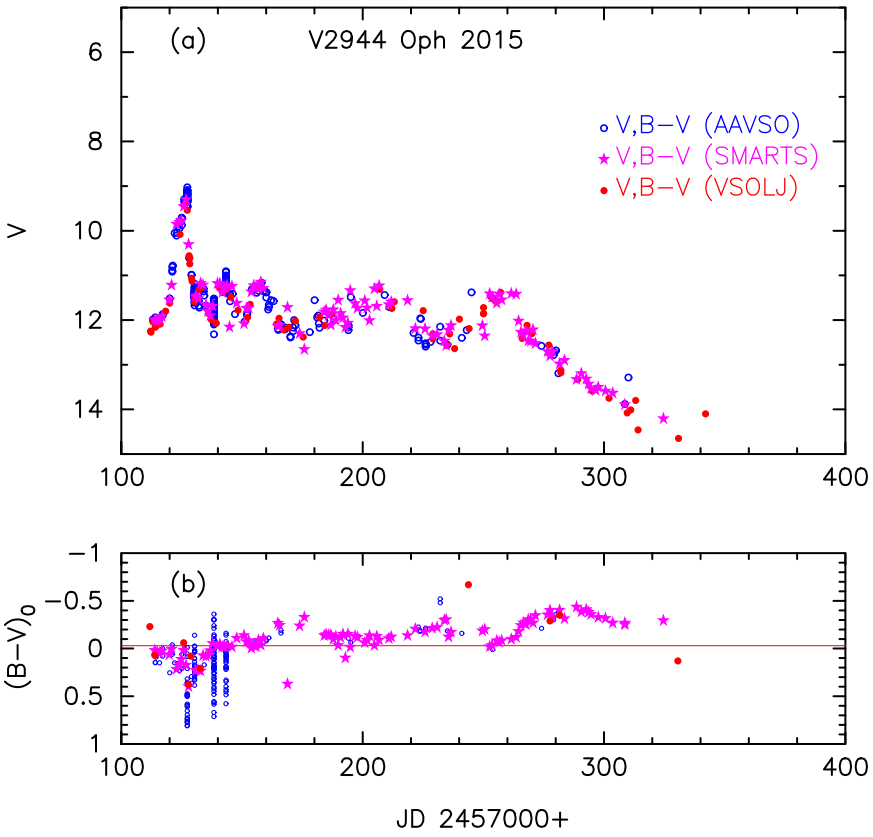

Figure 119. Same as Figure 23, but for V2944 Oph. (a) The V data are taken from AAVSO (unfilled blue circles), SMARTS (filled magenta stars), and VSOLJ (filled red circles). (b) The $(B-V)_0$ are dereddened with $E(B-V)=0.62$.

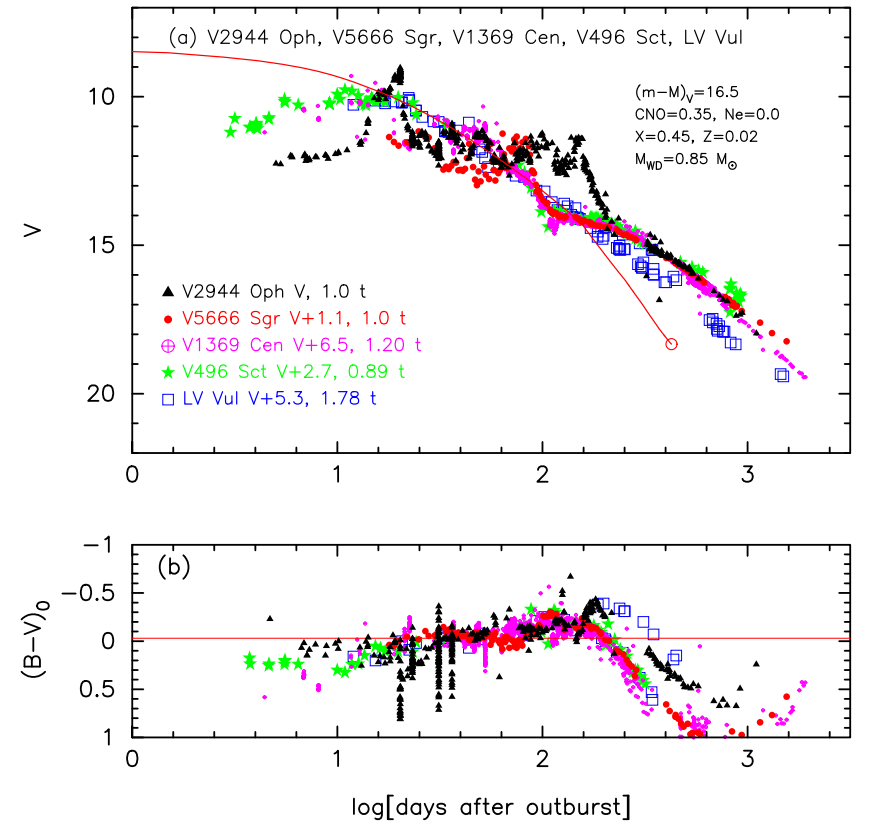

Figure 120. Same as Figure 30, but for V2944 Oph (filled black triangles). We plot the (a) V light and (b) $(B-V)_0$ color curves of V2944 Oph as well as those of V5666 Sgr, V1369 Cen, V496 Sct, and LV Vul. The data of V2944 Oph are the same as those in Figure 119. In panel (a), we add the model V light curve of a 0.85 $M_\odot$ WD (CO3, solid red line; Hachisu & Kato 2016a), assuming that $(m-M)_V=16.5$ for V2944 Oph.

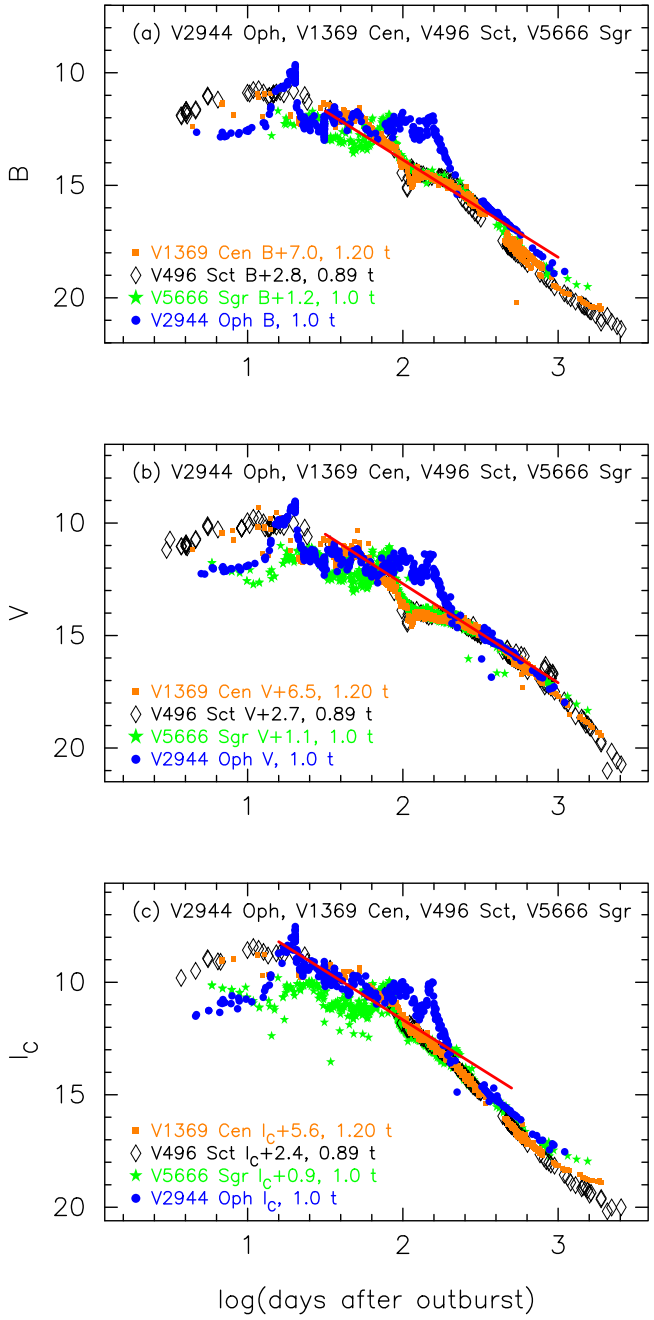

Figure 121. Same as Figure 25, but for V2944 Oph. The (a) B, (b) V, and (c) I_C light curves of V2944 Oph as well as those of V1369 Cen, V496 Sct, and V5666 Sgr. The BV data of V2944 Oph are the same as those in Figure 119. The I_C data of V2944 Oph are taken from AAVSO, VSOLJ, and SMARTS.

From the I_C-band data in Figure 121(c), we obtain

$$\begin{aligned}(m-M)_{I,\mathrm{V2944\ Oph}} &= ((m-M)_I + \Delta I_C)_{\mathrm{V1369\ Cen}} - 2.5\log 1.20 \\ &= 10.07 + 5.6 \pm 0.3 - 0.2 = 15.47 \pm 0.3 \\ &= ((m-M)_I + \Delta I_C)_{\mathrm{V496\ Sct}} - 2.5\log 0.89 \\ &= 12.98 + 2.4 \pm 0.3 + 0.13 = 15.51 \pm 0.3 \\ &= ((m-M)_I + \Delta I_C)_{\mathrm{V5666\ Sgr}} - 2.5\log 1.0 \\ &= 14.6 + 0.9 \pm 0.3 - 0.0 = 15.5 \pm 0.3, \end{aligned} \quad (175)$$

where we adopt $(m-M)_{I,\mathrm{V1369\ Cen}} = 10.07$, $(m-M)_{I,\mathrm{V496\ Sct}} = 12.98$, and $(m-M)_{I,\mathrm{V5666\ Sgr}} = 14.6$ from Appendix A.12. We have $(m-M)_{I,\mathrm{V2944\ Oph}} = 15.5 \pm 0.2$.

We plot $(m-M)_B = 17.11$, $(m-M)_V = 16.5$, and $(m-M)_I = 15.5$ in Figure 19(d). Thus, we obtain $d = 8.2 \pm 1$ kpc and $E(B-V) = 0.62 \pm 0.05$.

Appendix B
Timescaling Law of Free–Free Emission Light Curves

The timescaling law of nova light curves can be explained with optically thick wind solutions on WDs. Kato & Hachisu (1994) calculated the nova evolution for various WD masses from 0.5 $M_\odot$ to 1.38 $M_\odot$ based on the optically thick wind theory. They obtained the wind mass-loss rate $\dot{M}_{\mathrm{wind}}$, photospheric temperature T_{ph}, velocity v_{ph}, and radius R_{ph} for a specific envelope mass M_{env} and WD mass M_{WD}. We plot such results in Figures 122 and 123 for three WD masses of 1.33,

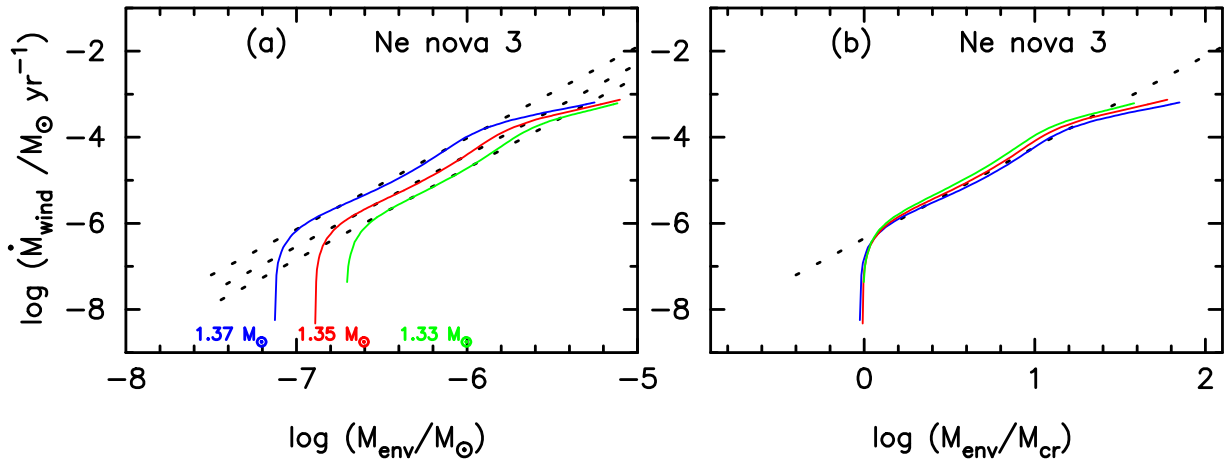

Figure 122. (a) Wind mass-loss rate vs. hydrogen-rich envelope mass of optically thick wind solutions for three WD masses with the chemical composition of Ne nova 3 (Ne3). The solid blue, red, and green lines denote 1.37 $M_\odot$, 1.35 $M_\odot$, and 1.33 $M_\odot$ WD models, respectively. (b) The horizontal axis is scaled by the critical mass of each hydrogen-rich envelope. The critical mass $M_{\rm cr}$ is the minimum mass for wind solutions. The three (blue, red, and green) lines almost overlap.

1.35, and 1.37 $M_\odot$ (Ne3; Hachisu & Kato 2016a). See Figure 6 of Kato & Hachisu (1994) for less massive WDs.

Figure 122 shows (a) the wind mass-loss rate versus hydrogen-rich envelope mass of optically thick wind solutions for three WD masses of 1.37 $M_\odot$ (blue), 1.35 $M_\odot$ (red), and 1.33 $M_\odot$ (green). The wind mass-loss rate decreases with the decreasing envelope mass. The wind stops at the critical envelope mass $M_{\rm cr}$. If we normalize the envelope mass by each critical mass, these three lines almost overlap each other as shown in Figure 122(b). We show only the three WD masses in this figure, but obtained the similar tendency of envelope solutions for other WD masses from 0.5 $M_\odot$ to 1.33 $M_\odot$ with the same or different chemical compositions (see, e.g., Figure 6 of Kato & Hachisu 1994).

Figure 123 shows (a) the wind mass-loss rate versus the photospheric radius, (b) the wind mass-loss rate versus the photospheric temperature, and (c) the wind mass-loss rate versus the photospheric velocity, for the three WD masses of 1.37 $M_\odot$ (Ne3, blue), 1.35 $M_\odot$ (Ne3, red), and 1.33 $M_\odot$ (Ne3, green), which are the same model sequences in Figure 122. It is clearly shown that these three lines almost overlap each other. We obtained a similar tendency of the envelope solutions for other WD masses with the same or different chemical compositions (see, e.g., Figure 7 of Kato & Hachisu 1994).

Our free–free emission flux is approximately calculated from $F_\nu \propto \dot{M}_{\rm wind}^2/v_{\rm ph}^2 R_{\rm ph}$ (Hachisu & Kato 2006). The above overlapping solutions directly means that

$$\left[\frac{\dot{M}_{\rm wind}^2}{v_{\rm ph}^2 R_{\rm ph}}\right]_{(t)}^{\{M_{\rm WD}\}} = \left[\frac{\dot{M}_{\rm wind}^2}{v_{\rm ph}^2 R_{\rm ph}}\right]_{(t')}^{\{1.37\,M_\odot\}} = \left[\frac{\dot{M}_{\rm wind}^2}{v_{\rm ph}^2 R_{\rm ph}}\right]_{(t'')}^{\{1.35\,M_\odot\}} = \left[\frac{\dot{M}_{\rm wind}^2}{v_{\rm ph}^2 R_{\rm ph}}\right]_{(t''')}^{\{1.33\,M_\odot\}}, \quad (176)$$

for the same wind mass-loss rate of $\dot{M}_{\rm wind}$. The only difference is the timescale. The time is calculated from the decreasing rate of the envelope mass, that is,

$$t \approx \int \frac{dM_{\rm env}}{\dot{M}_{\rm wind}} = M_{\rm cr} \int \frac{d(M_{\rm env}/M_{\rm cr})}{\dot{M}_{\rm wind}} = M_{\rm cr}(M_{\rm WD})\tau, \quad (177)$$

where

$$\tau \equiv \int \frac{d(M_{\rm env}/M_{\rm cr})}{\dot{M}_{\rm wind}}. \quad (178)$$

The overlapping of lines in Figure 122(b) guarantees that

$$t' \approx M_{\rm cr}(1.37\,M_\odot)\tau, \quad (179)$$

$$t'' \approx M_{\rm cr}(1.35\,M_\odot)\tau, \quad (180)$$

$$t''' \approx M_{\rm cr}(1.33\,M_\odot)\tau. \quad (181)$$

These relations read

$$\frac{t}{M_{\rm cr}(M_{\rm WD})} \approx \frac{t'}{M_{\rm cr}(1.37\,M_\odot)} \approx \frac{t''}{M_{\rm cr}(1.35\,M_\odot)} \approx \frac{t'''}{M_{\rm cr}(1.33\,M_\odot)}. \quad (182)$$

Thus, the free–free emission light curves obey a timescaling law, and its timescaling factor is approximated by the ratio of the critical envelope masses. From Equation (182), the fluxes in Equation (176) are the time-stretched free–free fluxes. We define these fluxes as

$$F^{\{M_{\rm WD}\}}(t) \equiv \left[\frac{\dot{M}_{\rm wind}^2}{v_{\rm ph}^2 R_{\rm ph}}\right]_{(t)}^{\{M_{\rm WD}\}}, \quad (183)$$

$$F'^{\{1.37\,M_\odot\}}(t') \equiv \left[\frac{\dot{M}_{\rm wind}^2}{v_{\rm ph}^2 R_{\rm ph}}\right]_{(t')}^{\{1.37\,M_\odot\}}, \quad (184)$$

$$F''^{\{1.35\,M_\odot\}}(t'') \equiv \left[\frac{\dot{M}_{\rm wind}^2}{v_{\rm ph}^2 R_{\rm ph}}\right]_{(t'')}^{\{1.35\,M_\odot\}}, \quad (185)$$

and

$$F'''^{\{1.33\,M_\odot\}}(t''') \equiv \left[\frac{\dot{M}_{\rm wind}^2}{v_{\rm ph}^2 R_{\rm ph}}\right]_{(t''')}^{\{1.33\,M_\odot\}}. \quad (186)$$

We formulate the conversion from (t, $F(t)$) to (t', $F'(t')$) by the time stretch of $t' = t/f_{\rm s}$. Applying $t' = t/f_{\rm s}$ to the V fluxes of

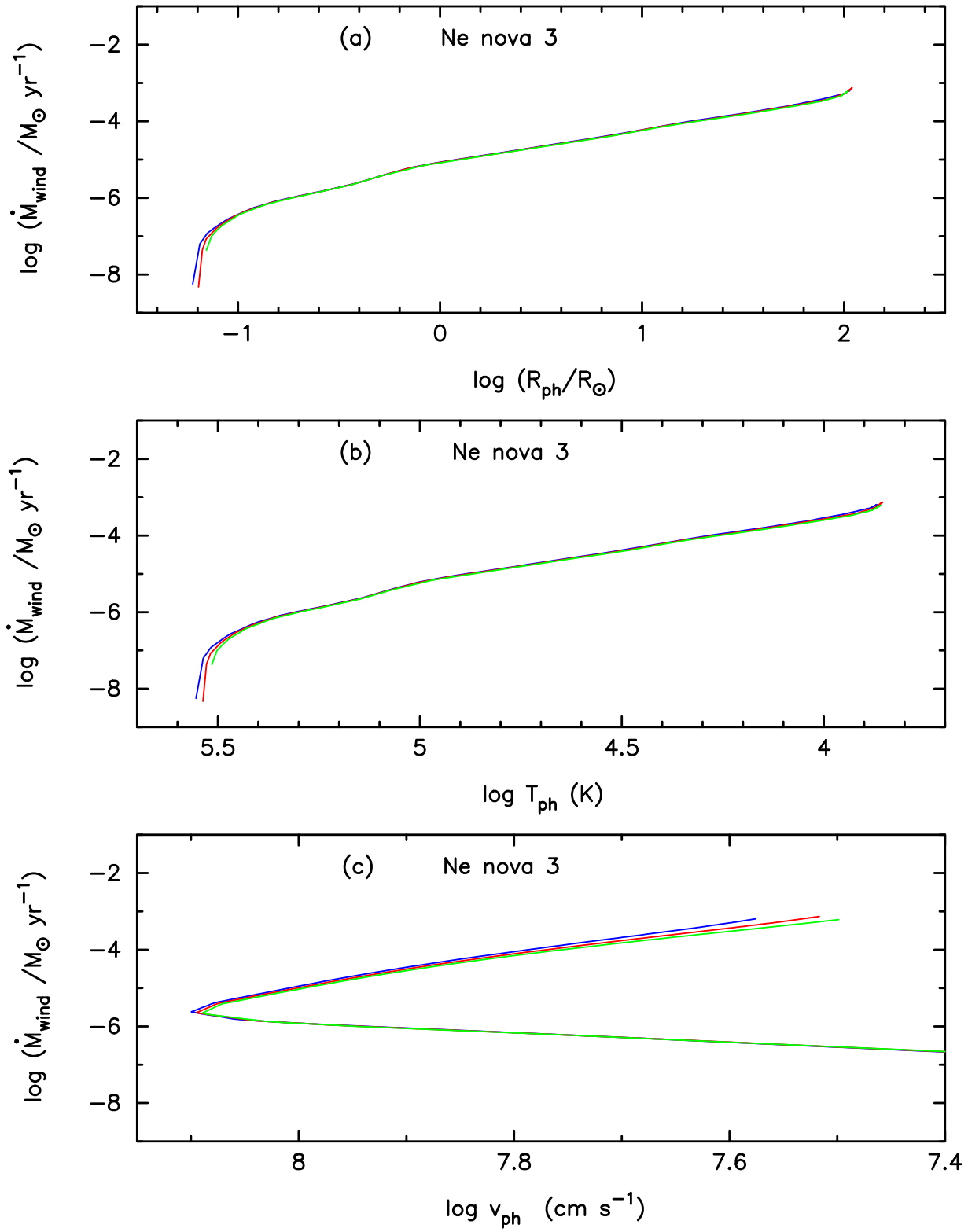

Figure 123. Wind mass-loss rate (a) vs. photospheric radius, (b) vs. photospheric temperature, and (c) vs. photospheric velocity for the three (1.37, 1.35, and 1.33 $M_\odot$) WD mass models in Figure 122. The three (blue, red, and green) lines almost overlap each other.

Equation (184), we take the time derivative of energy E as

$$F'(t') \equiv \frac{dE}{dt'} = f_s \frac{dE}{dt} \equiv f_s F(t/f_s), \quad (187)$$

and obtain

$$F^{\{M_{WD}\}}(t) \equiv \left[\frac{\dot{M}_{wind}^2}{v_{ph}^2 R_{ph}}\right]_{(t)}^{\{M_{WD}\}} = \left[\frac{\dot{M}_{wind}^2}{v_{ph}^2 R_{ph}}\right]_{(t')}^{\{1.37\,M_\odot\}}$$
$$\equiv F'^{\{1.37\,M_\odot\}}(t') = f_s F^{\{1.37\,M_\odot\}}(t/f_s). \quad (188)$$

Then, we take the absolute magnitude of the V flux and obtain

$$M_V^{\{M_{WD}\}}(t) = M_V'^{\{1.37\,M_\odot\}}(t')$$
$$= M_V^{\{1.37\,M_\odot\}}(t/f_s) - 2.5\log f_s, \quad (189)$$

where M_V is the absolute V magnitude of the free–free emission light curve. Here, the conversion from (t, $F(t)$) to (t', $F'(t')$) corresponds to the conversion from (t, $M_V(t)$) to (t', $M_V'(t')$). Thus, we derive Equation (1).

For the UV 1455 Å light curves, we calculate the flux based on blackbody approximation, that is, $F_\nu = 4\pi R_{ph}^2 B_\nu(T_{ph})$, where $B_\nu(T_{ph})$ is Planckian. Using the above overlapping solutions in Figure 123, we obtain

$$[R_{ph}^2 B_\nu(T_{ph})]_{(t)}^{\{M_{WD}\}} = [R_{ph}^2 B_\nu(T_{ph})]_{(t')}^{\{1.37\,M_\odot\}}$$
$$= [R_{ph}^2 B_\nu(T_{ph})]_{(t'')}^{\{1.35\,M_\odot\}} = [R_{ph}^2 B_\nu(T_{ph})]_{(t''')}^{\{1.33\,M_\odot\}}, \quad (190)$$

for the same wind mass-loss rate of $\dot{M}_{wind}$. Therefore, the UV 1455 Å fluxes also follow the same timescaling law as that of the free–free emission light curves from Equation (182). Similarly, we have

$$F_\nu'(t') \equiv \frac{dE_\nu}{dt'} = f_s \frac{dE_\nu}{dt} \equiv f_s F_\nu(t/f_s). \quad (191)$$

This reads

$$F_\nu^{\{M_{WD}\}}(t) \equiv [4\pi R_{ph}^2 B_\nu(T_{ph})]_{(t)}^{\{M_{WD}\}}$$
$$= [4\pi R_{ph}^2 B_\nu(T_{ph})]_{(t')}^{\{1.37\,M_\odot\}} \equiv F_\nu'^{\{1.37\,M_\odot\}}(t')$$
$$= f_s F_\nu^{\{1.37\,M_\odot\}}(t/f_s) \quad (192)$$

for the UV 1455 Å blackbody flux. The UV 1455 Å flux obeys the same scaling law as the free–free emission flux, i.e., Equations (188) and (192). Thus, our free–free and UV 1455 Å fluxes obey the same timescaling law, and their fluxes overlap independently of the WD mass if we properly stretch/squeeze the timescale. Such results are shown in Figure 8 of Hachisu & Kato (2006) for various WD masses and chemical compositions.

It should be noted that the soft X-ray light curves do not obey the same timescaling law. In the supersoft X-ray source (SSS) phase, the optically thick winds had already stopped and the hydrogen-rich envelope mass decreases by hydrogen burning, not by wind mass-loss. Thus, the SSS phase does not follow the same timescaling law of the universal decline law. The model soft X-ray light curves are calculated from a blackbody approximation like the UV 1455 Å light curves (e.g., Hachisu & Kato 2006, 2010), but its flux increases after optically thick winds stop. This means that we do not use the above overlapping solutions in Figure 123 and the relation of Equation (182) because $\dot{M}_{wind} = 0$ after the optically thick winds stop. Therefore, the soft X-ray light curves do not follow the same timescaling law as those of free–free emission and UV 1455 Å light curves. A detailed explanation is given by Hachisu & Kato (2010), and their detailed results are shown in their Figure 6.

Appendix C
Comparison of M31N 2008–12a and V745 Sco with V1500 Cyg and LV Vul

The universal decline law can be applied to many novae as already shown in the main text. Hachisu & Kato (2018b) analyzed fast and recurrent novae and showed that some of them deviate from the universal decline law. As shown in Figure 124, V407 Cyg shows a decay trend of $F_\nu \propto t^{-1.0}$ in the early phase, which is different from the universal decline law of $F_\nu \propto t^{-1.75}$. V745 Sco does not have a substantial slope of $F_\nu \propto t^{-1.75}$, but rather a steeper decline of $F_\nu \propto t^{-3.5}$. Here, we explain the reason why these light curves deviate from the universal decline law and discuss the applicability of the time-stretching method to such novae.

We first explain the reason for $F_\nu \propto t^{-1.0}$, which is much more gradual than the universal decline of $F_\nu \propto t^{-1.75}$, and then the reason for $F_\nu \propto t^{-3.5}$, which is much steeper than the universal decline. The companion star to the WD of V407 Cyg is a Mira (Munari et al. 1990; Kolotilov et al. 1998, 2003). The Mira companion emits massive cool winds and, as a result, CSM accumulates around the binary (e.g., Mohamed & Podsiadlowski 2012). V407 Cyg outbursted in 2010 as a classical nova (Nishiyama et al. 2010). Just after the nova explosion, the nova ejecta plunge into the CSM and create a strong shock (e.g., Orlando & Drake 2012; Pan et al. 2015). Shore et al. (2011) and Iijima (2015) showed clear evidence of a strong shock in their spectra. Such a CSM shock has been observed in many Type IIn supernovae. Moriya et al. (2013) presented a decay trend of $F_\nu \propto t^{-1}$ in SN 2005ip. Thus, we regard the decay trend of $F_\nu \propto t^{-1}$ to be an effect of strong CSM shock. Both the V and I_C light curves show a similar trend as shown in Figure 124. Hachisu & Kato (2018b) explained the decline trend as follows: just after the nova outburst, the nova ejecta created a strong CSM shock. This shock-heating made a significant contribution to the continuum flux (both in the V and I_C bands). The strong shock has broken out of the CSM on day ~45. Because the shock-heating disappears, the continuum flux drops and decays as $F_\nu \propto t^{-1.55}$ like RS Oph (Figure 124).

RS Oph decays as $F_\nu \propto t^{-1.55}$ in the V band (Figure 124). It should be noted that the radio flux of RS Oph also follows $F_\nu \propto t^{-1.55}$ (see Figure 18 of Hachisu & Kato 2018b). The companion star to the WD is not a Mira but a red giant in RS Oph. Cool winds in RS Oph are much less massive than in V407 Cyg. The ejecta created a CSM shock, but the CSM shock is much weaker than in V407 Cyg. We suppose that the CSM shock is not strong enough to increase the continuum flux to $F_\nu \propto t^{-1.0}$ in RS Oph. However, the *SMEI* light curve of RS Oph follows $L_{SMEI} \propto t^{-1.0}$, where L_{SMEI} is the *SMEI* band luminosity (peak quantum efficiency at 7000 Å with an FWHM of 3000 Å). This is because the CSM shock increases the Hα flux, which is included in the *SMEI* band.

V745 Sco, T CrB, and V1534 Sco also have a red-giant companion, but do not show evidence of a CSM shock in their V light curves. Their V light curves almost overlap the V838 Her V light curve (see, e.g., Hachisu & Kato 2018b). This implies that their CSM is extremely less massive because

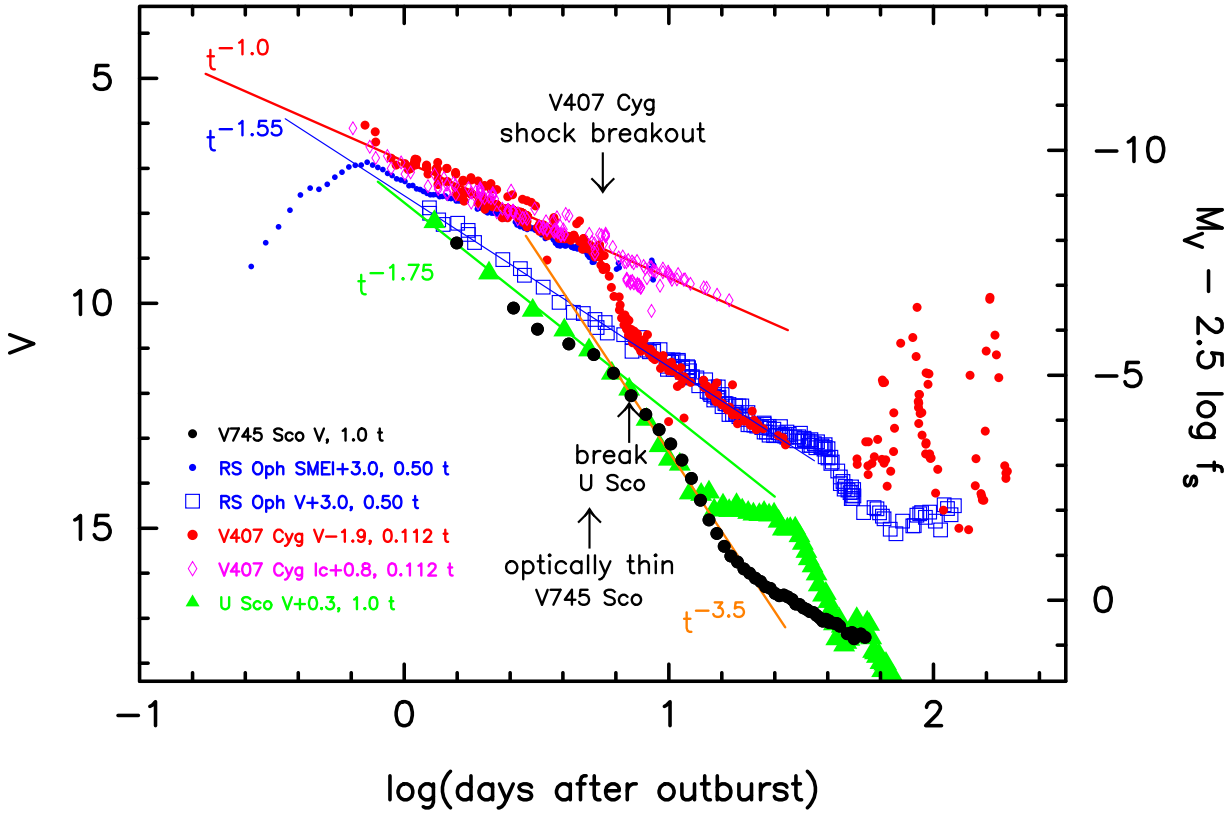

Figure 124. Nova *V* light curves for V745 Sco, U Sco, RS Oph, and V407 Cyg on logarithmic timescales. We add the I_C light curves of V407 Cyg and the *SMEI* magnitudes (Hounsell et al. 2010) of RS Oph for comparison. We also add the time-stretched absolute magnitude, $M_V - 2.5\log f_s$, against V745 Sco ($f_s = 1$ for V745 Sco), in the right ordinate. The *V* light curves of the V745 Sco (2014) and U Sco (2010) outbursts are plotted with the filled black circles and green triangles, respectively. The *V* and I_C light curves of V407 Cyg are represented by the filled red circles and unfilled magenta diamonds, respectively. The *SMEI* and *V* magnitudes of the RS Oph (2006) outburst are depicted by the blue dots and unfilled blue squares, respectively. The sources of the data are all the same as those in Hachisu & Kato (2018b). The solid red, blue, green, and orange lines represent the decline trends of $F_\nu \propto t^{-1.0}$, $t^{-1.55}$, $t^{-1.75}$, and $t^{-3.5}$, respectively.

V838 Her has a main-sequence companion (e.g., Ingram et al. 1992; Leibowitz et al. 1992), and we expect no CSM shock in V838 Her. The X-ray fluxes were observed with *Swift* in V407 Cyg, RS Oph, V745 Sco, and V1534 Sco. The origin of these early phase fluxes is shock-heating. On the other hand, Munari & Banerjee (2018) showed no deceleration of the V1534 Sco ejecta. We suppose that the decay trend of the *V* light curve changes from an extremely strong CSM shock to a relatively weak shock, that is, from the trend of V407 Cyg ($F_\nu \propto t^{-1.0}$) to RS Oph ($F_\nu \propto t^{-1.55}$), and finally to V745 Sco and V1534 Sco (Hachisu & Kato 2018b) as shown in Figure 124.

Next, we explain the steep decline of $F_\nu \propto t^{-3.5}$. The slope of the nova decay trend changes from $F_\nu \propto t^{-1.75}$ (universal decline) to $F_\nu \propto t^{-3.5}$ (rapid decline) on day ∼8 (upward black arrow labeled "break U Sco" in Figure 124). This change in the slope is universal among the model light curves (see Figure 3). Hachisu & Kato (2006) called this change the break. It accompanies the quick drop in the wind mass-loss rate and the rapid shrinking of the photosphere. In the case of V1668 Cyg in Figure 3, this change is almost coincident with the start of the nebular phase on day ∼100. The break in the V745 Sco *V* light curve almost coincides with that of U Sco in Figure 124. This epoch is close to the epoch when the ejecta of V745 Sco became optically thin (upward black arrow labeled "optically thin V745 Sco"). We regard the change from $F_\nu \propto t^{-1.75}$ to $F_\nu \propto t^{-3.5}$ to be the transition of the ejecta from being optically thick to thin.

A nova reaches point A or a brighter point on the model light curves in Figure 2 if the ignition mass is large. Then, the nova declines along the model light curve with decreasing envelope mass, that is, it passes through points B and C, and eventually goes down through the break point. If the initial envelope mass is very small, a nova cannot reach the universal decline segment ($F_\nu \propto t^{-1.75}$). It starts from some place on the rapid decline segment ($F_\nu \propto t^{-3.5}$). Thus, its maximum brightness is much fainter than that of normal-decline-type, novae which start from some place on the universal decline segment. Such novae, having very small ignition masses, like M31N 2008–12a, are located much below the empirical MMRD relations (Figure 4).

Hachisu & Kato (2018b) categorized these novae into three types:

1. Novae that follow the trend of the universal decline law ($F_\nu \propto t^{-1.75}$) in the early phase, as shown in Figure 124, are called normal-decline (or U Sco) types.
2. Novae that start from some place on the rapid decline ($F_\nu \propto t^{-3.5}$) segment after the break, as shown in Figure 124, are called rapid-decline (or V745 Sco) types. The change in the slope from $F_\nu \propto t^{-1.75}$ to $F_\nu \propto t^{-3.5}$ corresponds to the break in the model *V* light curves in Figure 3.
3. Novae that follow a slow decline trend of $F_\nu \propto t^{-1.0}$ in the early phase, as shown in Figure 124, are called CSM-shock (or RS Oph) types. Novae of this type show a

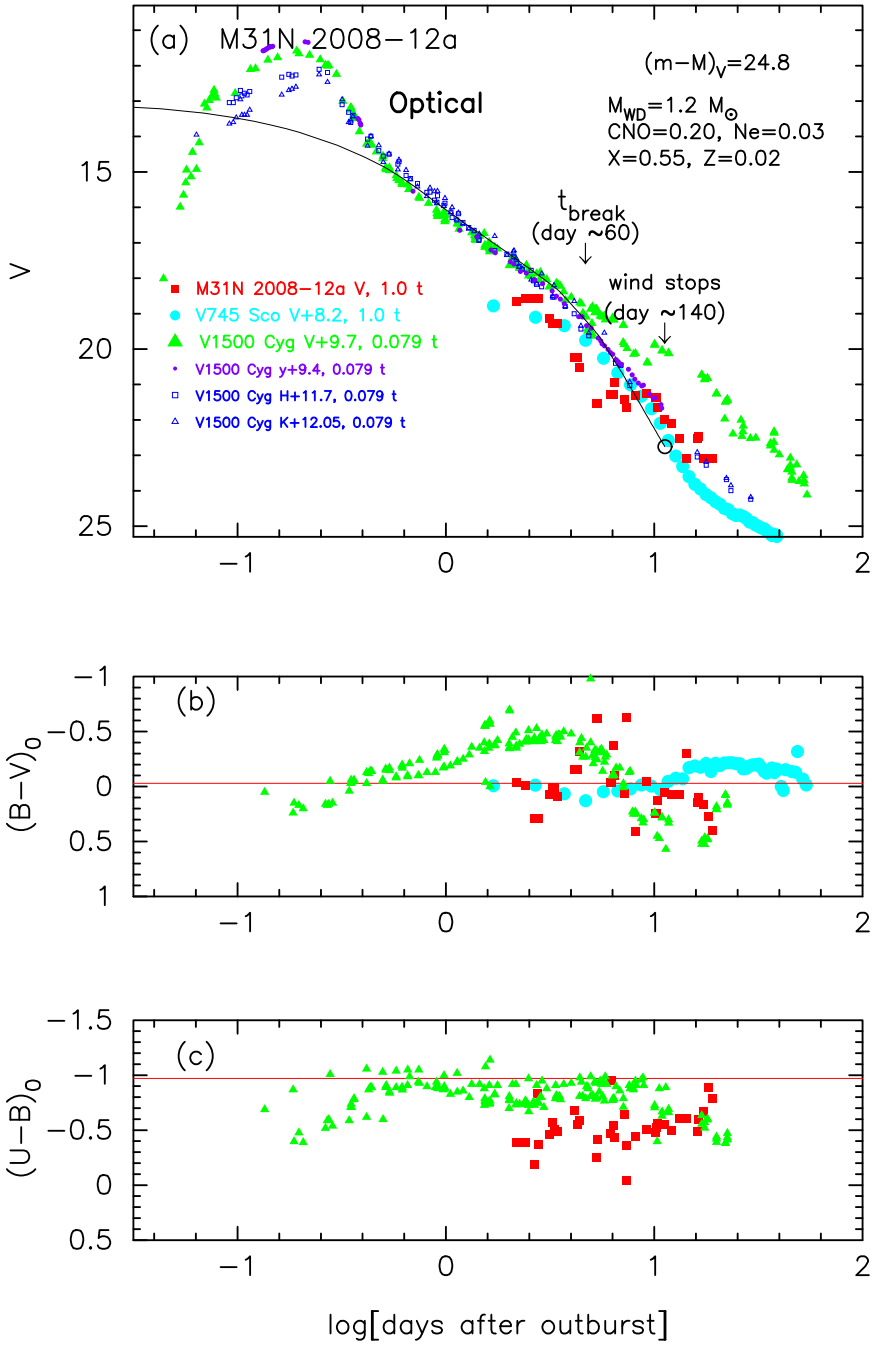

Figure 125. Same as Figure 45, but for M31N 2008-12a. We add the light/color curves of V745 Sco and V1500 Cyg. In panel (a), assuming that $(m - M)_V = 12.3$ for V1500 Cyg, we add the model V light curve of a 1.2 $M_\odot$ WD (Ne2, solid black line; Hachisu & Kato 2010). We also add two epochs of the V1500 Cyg light curves: one is the break (about day ∼60) in the light curves (Hachisu & Kato 2014) and the other is the epoch when the wind stops (about day ∼140) for our 1.2 $M_\odot$ WD model (Hachisu & Kato 2014).

strong CSM shock interaction, which contributes significantly to the F_ν flux.

These three kinds of very fast (or recurrent) novae sometimes do not follow the universal decline law, and we cannot directly apply Equation (6) to them because it is based on the universal decline law. The physical reasons for the deviations are well understood as already explained above. Therefore, Hachisu & Kato (2018b) proposed different template novae instead of V1500 Cyg and LV Vul. For example, CSM-shock-type novae broadly follow the V or I_C light curve of V407 Cyg (or RS Oph) in the early phase. If we properly stretch the timescales of such novae and can overlap their V light curves with one of the template novae V407 Cyg and RS Oph, we apply Equation (6) to them. Such an example is LMC N 2013 as discussed by Hachisu & Kato (2018b). Hachisu & Kato (2018b) also examined the case of rapid-decline-type novae, that is, V745 Sco, T CrB, V838 Her, and V1534 Sco in our Galaxy, LMC N 2012a in the LMC, and M31N 2008-12a in M31. They overlapped the V light curve of T CrB, V838 Her, and V1534 Sco with that of V745 Sco by stretching their timescales and obtained reasonable $(m - M)_V$ for T CrB, V838 Her, and V1534 Sco with Equation (6).

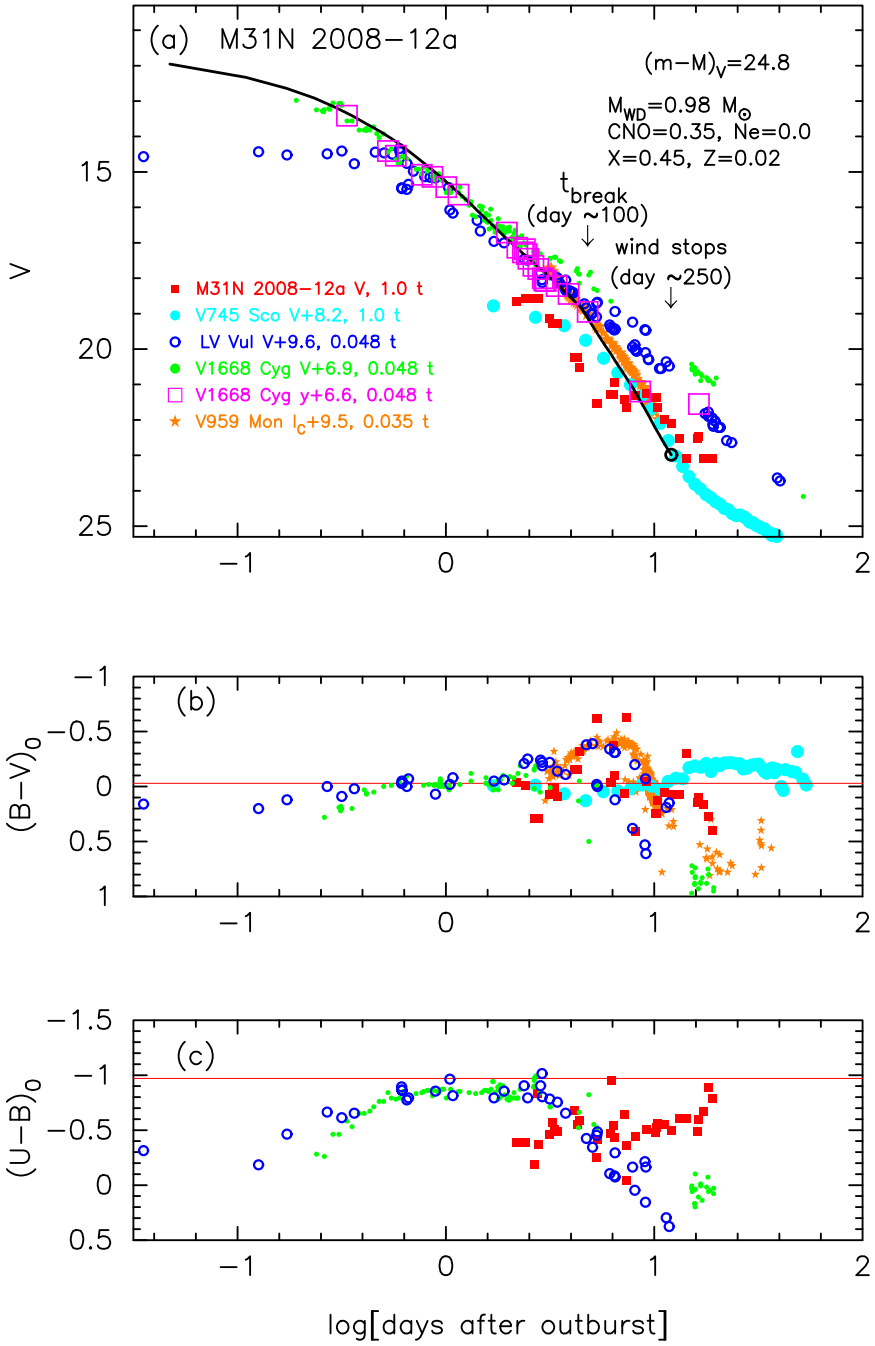

Figure 126. Same as Figure 24, but for M31N 2008-12a. We add the light/color curves of V745 Sco, LV Vul, V1668 Cyg, and V959 Mon. The data of V959 Mon are taken from AAVSO, VSOLJ, SMARTS, and Munari et al. (2013). In panel (a), assuming that $(m - M)_V = 14.6$ for V1668 Cyg, we add the model V light curve of a 0.98 $M_\odot$ WD (CO3, solid black line; Hachisu & Kato 2016a). We also add two epochs of the V1668 Cyg light curves: one is the break (about day ~100) in the y light curve and the other is the epoch when the optically thick wind stops (about day ~250) for our 0.98 $M_\odot$ WD model (Hachisu & Kato 2018a).

Finally, we compare the light curve of M31N 2008-12a with the template novae V1500 Cyg and LV Vul and show that the V light curve of M31N 2008-12a does not overlap with the template nova V1500 Cyg or LV Vul, that is, Equation (6) cannot directly apply to the pair of M31N 2008-12a and V1500 Cyg (or LV Vul). We first depict M31N 2008-12a, V745 Sco, and V1500 Cyg in Figure 125. We next plot M31N 2008-12a, V745 Sco, LV Vul, V1668 Cyg, and V959 Mon in Figure 126. We always include the light/color curves of V745 Sco because V745 Sco is a template nova for rapid-decline-type novae like M31N 2008-12a. Then, we discuss the relation between M31N 2008-12a and V1500 Cyg (or LV Vul), and describe how to apply Equation (6) to the pair of M31N 2008-12a and V1500 Cyg (or LV Vul).

Hachisu & Kato (2018b) discussed that M31N 2008-12a and V745 Sco belong to the rapid-decline type. They determined the timescaling factor f_s mainly from the rapid decline segment of $F_\nu \propto t^{-3.5}$ together with X-ray phase (see also Figures 124, 125, and 126). It should be noted that our light-curve fitting method is not only based on the shape of the V light curve but also includes global evolutionary features that represent the physical properties of novae. In this fitting, we first overlap the V light curve of M31N 2008-12a with that of V745 Sco because V745 Sco is a template nova of the rapid-decline type.

This process was described in detail in Hachisu & Kato (2018b). We consider the pair of M31N 2008-12a and V745 Sco as a whole. We match the starts of the nebular phases both for M31N 2008-12a and V1500 Cyg in Figure 125. The nebular phase of V1500 Cyg started almost 60 days after the outburst. The start of the nebular phase of M31N 2008-12a is not clear, but the SSS phase started at least six days after the peak. This means that we set the phase of day 5 of M31N 2008-12a at the phase of day 60 of V1500 Cyg.

We try to overlap the rapid-decline ($F_\nu \propto t^{-3.5}$) segment of V1500 Cyg with that of M31N 2008-12a and V745 Sco. V1500 Cyg shows no break in the V light curve, so we cannot find the rapid-decline segment. Instead, we find a clear break on the y- and NIR-band light curves as shown in Figure 125. This is because strong [O III] lines cloud the break on the V light curve. Fortunately, y and NIR H- and K-band data are available for V1500 Cyg. Therefore, we use the y-band light curve to detect the break in the light curve. These y band and NIR H and K bands have no strong effect from the emission lines. The V light curves of V745 Sco and M31N 2008-12a also have no strong effect from emission lines because their ejecta are much less massive than the ejecta of V1500 Cyg. Therefore, the V light curves of V745 Sco and M31N 2008-12a broadly follow the rapid-decline part of V1500 Cyg on the y light curve. We add the model V light curve of a 1.2 $M_\odot$ WD (Ne2; Hachisu & Kato 2010). The model V light curve broadly follows the break of the y light curve of V1500 Cyg. Applying Equation (6) to them, we have the relation

$$\begin{aligned}(m-M)_{V,\mathrm{M31N\ 2008-12a}} &= (m-M+\Delta V)_{V,\mathrm{V1500\ Cyg}} - 2.5\log 0.079 \\ &= 12.3 + 9.7 \pm 0.4 + 2.75 = 24.75 \pm 0.4 \\ &= (m-M+\Delta V)_{V,\mathrm{V745\ Sco}} - 2.5\log 1.0 \\ &= 16.6 + 8.2 \pm 0.4 + 0.0 = 24.8 \pm 0.4, \end{aligned} \quad (193)$$

where we adopt $(m-M)_{V,\mathrm{V1500\ Cyg}} = 12.3$ from Hachisu & Kato (2019) and $(m-M)_{V,\mathrm{V745\ Sco}} = 16.6$ from Hachisu & Kato (2018b). Thus, we obtain $(m-M)_V = 24.8 \pm 0.3$ and $f_s = 0.079$ against V1500 Cyg.

We also try to overlap LV Vul (and V1668 Cyg) with M31N 2008-12a and V745 Sco. LV Vul shows no break in the V light curve as shown in Figure 126. V1668 Cyg has no break on the V light curve, too, but does show a break on the y light curve. This is because strong [O III] lines contribute to the broadband V in the nebular phase, but not to the intermediate band y (see, e.g., Figure 1 of Munari et al. 2013). The y band is designed to avoid strong emission lines such as [O III], so it is useful to detect the break. The number of the V1668 Cyg y data points after the break is very few, so we add the I_C-band light curve of V959 Mon, the data of which are taken from SMARTS and Munari et al. (2013). The timescaling factor, reddening, and distance modulus in the V band of V959 Mon are taken from Hachisu & Kato (2018a). The I_C band is also not affected by strong emission lines in the nebular phase so that the I_C light curve of V959 Mon does show a similar shape to the y-band light curve of V1668 Cyg. The V light curves of V745 Sco and M31N 2008-12a have no strong effects of emission lines because their ejecta are much less massive than the ejecta of LV Vul and V1668 Cyg. Therefore, the V light curves of V745 Sco and M31N 2008-12a broadly follow the rapid-decline part of V1668 Cyg on the y-band light curve after the break. We also add a model V light curve of a 0.98 $M_\odot$ WD (CO3; Hachisu & Kato 2016a). The model V light curve broadly follows the break of the y light curve of V1668 Cyg.

We place the phase of day 5 of M31N 2008-12a (start of the nebular phase) at the phase of day 100 (time of the break = start of the nebular phase) of V1668 Cyg to adjust both timescales. This suggests that $f_s \approx 0.05$ against the timescales of LV Vul and V1668 Cyg, because those of LV Vul and V1668 Cyg are the same (see, e.g., Hachisu & Kato 2019). We finally obtain the fitting locations of M31N 2008-12a, V745 Sco, LV Vul, V1668 Cyg, and V959 Mon as shown in Figure 126. Applying Equation (6) to them, we have the relation

$$\begin{aligned}(m-M)_{V,\mathrm{M31N\ 2008-12a}} &= (m-M+\Delta V)_{V,\mathrm{LV\ Vul}} - 2.5\log 0.048 \\ &= 11.85 + 9.6 \pm 0.4 + 3.3 = 24.75 \pm 0.4 \\ &= (m-M+\Delta V)_{V,\mathrm{V1668\ Cyg}} - 2.5\log 0.048 \\ &= 14.6 + 6.9 \pm 0.4 + 3.3 = 24.8 \pm 0.4 \\ &= (m-M+\Delta V)_{V,\mathrm{V745\ Sco}} - 2.5\log 1.0 \\ &= 16.6 + 8.2 \pm 0.4 + 0.0 = 24.8 \pm 0.4, \end{aligned} \quad (194)$$

where we adopt $(m-M)_{V,\mathrm{LV\ Vul}} = 11.85$ and $(m-M)_{V,\mathrm{V1668\ Cyg}} = 14.6$ from Hachisu & Kato (2019). We obtain $(m-M)_V = 24.8 \pm 0.3$ and $f_s = 0.048$ ($\log f_s = -1.32$) against LV Vul.

We summarize this section as follows:

1. There are exceptions, the V light curves of which deviate largely from the universal decline law.
2. We cannot directly apply the template nova V1500 Cyg or LV Vul (or V1668 Cyg) to these exceptional novae in the context of Equation (6), because their V light curves never overlap with the V light curve of V1500 Cyg or LV Vul (or V1668 Cyg).
3. Hachisu & Kato (2018b) examined very fast (or recurrent) novae and proposed different templates depending on the physical reason of deviation. Adopting different template novae, they applied Equation (6) to the exceptions.
4. For the special case of M31N 2008-12a, its V light curve does not overlap that of V1500 Cyg or LV Vul (or V1668 Cyg) in the context of Equation (6). M31N 2008-12a belongs to the rapid-decline type, and the template is V745 Sco (Hachisu & Kato 2018b). Therefore, we consider the pair of M31N 2008-12a and V745 Sco as a whole. If we use the V1500 Cyg y light curve, we can find an overlapping part on the rapid-decline segment and apply Equation (6) to the pair of M31N 2008-12a and V745 Sco. Similarly, if we use the V1668 Cyg y light curve, we are able to find an overlapping part on the rapid-decline segment of V1668 Cyg and apply Equation (6).

ORCID iDs

Izumi Hachisu https://orcid.org/0000-0002-0884-7404
Mariko Kato https://orcid.org/0000-0002-8522-8033

References

Ackermann, M., Ajello, M., Albert, A., et al. 2014, Sci, 345, 554
Arai, A., & Isogai, M. 2012, CBET, 3072, 2
Arai, A., Kajikawa, T., & Naka, C. 2011, CBET, 2813, 4

Banerjee, D. P. K., Srivastava, M. K., Ashok, N. M., & Venkataraman, V. 2016, MNRAS, 455, L109
Bode, M. F., Darnley, M. J., Beardmore, A. P., et al. 2016, ApJ, 818, 145
Boyd, D., & Poyner, G. 2006, JBAA, 116, 320
Brown, N. J., Amorim, A., Liller, W., et al. 2008, IAUC, 8931, 1
Burwitz, V., Starrfield, S., Krautter, J., & Ness, J.-U. 2002, in Classical Nova Explosions, ed. M. Hernanz & J. José (New York: AIP), 377
Cassatella, A., Altamore, A., & González-Riestra, R. 2002, A&A, 384, 1023
Chen, B.-Q., Huang, Y., Liu, X.-W., et al. 2018, MNRAS, 483, 4277
Cheung, C. C., Jean, P., Shore, S. N., et al. 2016, ApJ, 826, 142
Chochol, D., Shugarov, S., Pribulla, T., & Volkov, I. 2014, CoSka, 43, 330
Cohen, J. G. 1988, in ASP Conf. Ser. 4, The Extragalactic Distance Scale, ed. S. van den Bergh & C. J. Pritchet (San Francisco, CA: ASP), 114
Danilet, A. B., Holoien, T. W.-S., Wagner, R. M., et al. 2015, ATel, 7339, 1
Darnley, M. J., Henze, M., Bode, M. F., et al. 2016, ApJ, 833, 149
de Vaucouleurs, G. 1978, ApJ, 223, 351
della Valle, M. 1991, A&A, 252, L9
della Valle, M., & Livio, M. 1995, ApJ, 452, 704
Dennefeld, M., Ricquebourg, F., & Damerdji, Y. 2005, IAUC, 8544, 1
Dobrotka, A., Retter, A., & Liu, A. 2008, A&A, 478, 815
Downes, R. A., & Duerbeck, H. W. 2000, AJ, 120, 2007
Ennis, D., Becklin, E. E., Beckwith, S., et al. 1977, ApJ, 214, 478
Evans, P. A., Beardmore, A. P., Page, K. L., et al. 2009, MNRAS, 397, 1177
Finzell, T., Chomiuk, L., Metzger, B. D., et al. 2018, ApJ, 852, 108
Finzell, T., Chomiuk, L., Munari, U., & Walter, F. M. 2015, ApJ, 809, 160
Gallagher, J. S., & Ney, E. P. 1976, ApJL, 204, L35
Gilmore, A. C., & Kilmartin, P. M. 2005, IAUC, 8559, 2
Green, G. M., Schlafly, E. F., Finkbeiner, D. P., et al. 2015, ApJ, 810, 25
Green, G. M., Schlafly, E. F., Finkbeiner, D. P., et al. 2018, MNRAS, 478, 651
Hachisu, I., & Kato, M. 2006, ApJS, 167, 59
Hachisu, I., & Kato, M. 2007, ApJ, 662, 552
Hachisu, I., & Kato, M. 2010, ApJ, 709, 680
Hachisu, I., & Kato, M. 2014, ApJ, 785, 97
Hachisu, I., & Kato, M. 2015, ApJ, 798, 76
Hachisu, I., & Kato, M. 2016a, ApJ, 816, 26
Hachisu, I., & Kato, M. 2016b, ApJS, 223, 21
Hachisu, I., & Kato, M. 2017, in Proc. Palermo Workshop 2017, The Golden Age of Cataclysmic Variables and Related Objects IV, ed. F. Giovannelli (Trieste: PoS), 47
Hachisu, I., & Kato, M. 2018a, ApJ, 858, 108
Hachisu, I., & Kato, M. 2018b, ApJS, 237, 4
Hachisu, I., & Kato, M. 2019, ApJS, 241, 4
Hachisu, I., Kato, M., Kato, T., & Matsumoto, K. 2000, ApJL, 528, L97
Hachisu, I., Kato, M., Kiyota, S., & Maehara, H. 2009, arXiv:0912.5056
Hauschildt, P. H., Starrfield, S., Shore, S. N., Allard, F., & Baron, E. 1995, ApJ, 447, 829
Helton, L. A., Woodward, C. E., Vanlandingham, K., & Schwarz, G. J. 2008, CBET, 1449, 1
Henden, A., & Munari, U. 2007, IBVS, 5771, 1
Henze, M., Ness, J.-U., Darnley, M., et al. 2015, A&A, 580, A46
Holdsworth, D. L., Rushton, M. T., Bewsher, D., et al. 2014, MNRAS, 438, 3483
Hounsell, R., Bode, M. F., Hick, P. P., et al. 2010, ApJ, 724, 480
Hounsell, R., Darnley, M. J., Bode, M., et al. 2016, ApJ, 820, 104
Iijima, T. 2015, AJ, 150, 20
Imamura, K., Akazawa, H., & Maehara, H. 2014, ATel, 6128, 1
Imara, N., & Blitz, L. 2007, ApJ, 662, 969
Ingram, D., Garnavich, P., Green, P., & Szkody, P. 1992, PASP, 104, 402
Kasliwal, M. M., Cenko, S. B., Kulkarni, S. R., et al. 2011, ApJ, 735, 94
Kato, M., & Hachisu, I. 1994, ApJ, 437, 802
Kato, M., Saio, H., & Hachisu, I. 2015, ApJ, 808, 52
Kato, M., Saio, H., & Hachisu, I. 2017a, ApJ, 838, 153
Kato, M., Saio, H., & Hachisu, I. 2017b, ApJ, 844, 143
Kato, M., Saio, H., Hachisu, I., & Nomoto, K. 2014, ApJ, 793, 136
Kawakita, H., Arai, A., & Fujii, M. 2016, PASJ, 68, 87
Kawakita, H., Fujii, M., Nagashima, M., et al. 2015, PASJ, 67, 17
Kawakita, H., Ootsubo, T., Arai, A., Shinnaka, Y., & Nagashima, M. 2017, AJ, 153, 74
Kolotilov, E. A., Munari, U., Popova, A. A., et al. 1998, AstL, 24, 451
Kolotilov, E. A., Shenavrin, V. I., Shugarov, S. Yu., & Yudin, B. F. 2003, ARep, 47, 777
Kos, J., & Zwitter, T. 2013, ApJ, 774, 72
Lane, B. F., Retter, A., Eisner, J. A., et al. 2007, ApJ, 669, 1150
Leibowitz, E., Mendelson, H., Mashal, E., Prialnik, D., & Seitter, W. C. 1992, ApJL, 385, L49
Liller, W. 2005, IAUC, 8559, 1
Liller, W., Bolt, G., Santallo, R., et al. 2007, IAUC, 8850, 1
Liller, W., & Walter, F. M. 2009, IAUC, 9012, 2
Linford, J. D., Chomiuk, L., Nelson, T., et al. 2017, ApJ, 842, 73
Liszt, H. S. 2014, ApJ, 780, 10
Lynch, D. K., Rudy, R. J., Venturini, C. C., et al. 2006a, IAUC, 8730, 5
Lynch, D. K., Russell, R. W., Rudy, R. J., Prater, T., & Woodward, C. E. 2007, IAUC, 8851, 1
Lynch, D. K., Russell, R. W., Rudy, R. J., & Woodward, C. E. 2006b, IAUC, 8706, 2
Maehara, H. 2009, CBET, 2142, 1
Malasan, H. L., Suherli, J., Wiyando, E., et al. 2011, CBET, 2796, 4
Marshall, D. J., Robin, A. C., Reylé, C., Schultheis, M., & Picaud, S. 2006, A&A, 453, 635
Mohamed, S., & Podsiadlowski, Ph. 2012, BaltA, 21, 88
Moriya, T. J., Maeda, K., Taddia, F., et al. 2013, MNRAS, 435, 1520
Mróz, P., Udalski, A., Poleski, R., et al. 2015, ApJS, 219, 26
Munari, U. 2014, in ASP Conf. Ser. 490, Stella Novae: Past and Future Decades, ed. P. A. Woudt & V. A. R. M. Ribeiro (San Francisco, CA: ASP), 183
Munari, U., & Banerjee, D. P. K. 2018, MNRAS, 475, 508
Munari, U., Dallaporta, S., Castellani, F., et al. 2013, MNRAS, 435, 771
Munari, U., Hambsch, F.-J., & Frigo, A. 2017, MNRAS, 469, 4341
Munari, U., Henden, A., Banerjee, D. P. K., et al. 2015a, MNRAS, 447, 1661
Munari, U., Joshi, V. H., Ashok, N. M., et al. 2011, MNRAS, 410, L52
Munari, U., Margoni, R., & Stagni, R. 1990, MNRAS, 242, 653
Munari, U., Saguner, T., Siviero, A., et al. 2009, CBET, 1999, 1
Munari, U., Siviero, A., Moretti, S., et al. 2008, CBET, 1352, 1
Munari, U., Siviero, A., Valisa, P., et al. 2007, CBET, 1183, 1
Munari, U., & Walter, F. M. 2015, MNRAS, 455, L57
Munari, U., Walter, F. M., Henden, A., et al. 2015b, IBVS, 6139, 1
Nagashima, M., Arai, A., Kajikawa, T., et al. 2014, ApJL, 780, L26
Nagashima, M., Arai, A., Kajikawa, T., et al. 2015, AcPPP, 2, 212
Naik, S., Banerjee, D. P. K., & Ashok, N. M. 2009, MNRAS, 394, 1551
Naito, H., & Tokimasa, N. 2007, IAUC, 8896, 2
Nelson, T., Linford, J., Chomiuk, L., et al. 2015, ATel, 7085, 1
Ness, J.-U., Starrfield, S., Schwarz, G., Page, K. L., & Osborne, J. P. 2007, CBET, 1030, 1
Ness, J.-U., Starrfield, S., Schwarz, G. J., et al. 2008, IAUC, 8911, 2
Nishiyama, K., Kabashima, F., Kojima, T., et al. 2010, IAUC, 9130, 1
Nishiyama, K., Kabashima, F., Kojima, T., & Walter, F. M. 2015, IAUC, 9274, 3
Nishiyama, K., Kabashima, F., Masi, G., et al. 2014, CBET, 3842, 1
Nishiyama, K., & Nakano, S. 2012, CBET, 3166, 1
Nishiyama, S., Tamura, M., Hatano, H., et al. 2009, ApJ, 696, 1407
Orio, M., Ciroi, S., Aydi, E., & Buckley, D. 2019, ATel, 12385, 1
Orio, M., Parmar, A. N., Greiner, J., et al. 2002, MNRAS, 333, L11
Orlando, S., & Drake, J. J. 2012, MNRAS, 419, 2329
Özdörmez, A., Ege, E., Güver, T., & Ak, T. 2018, MNRAS, 476, 4162
Özdörmez, A., Güver, T., Cabrera-Lavers, A., & Ak, T. 2016, MNRAS, 461, 1177
Page, K. L., Osborne, J. P., Kuin, N. P. M., et al. 2015, MNRAS, 454, 3108
Pan, K.-C., Ricker, P. M., & Taam, R. E. 2015, ApJ, 806, 27
Payne-Gaposchkin, C. 1957, The Galactic Novae (Amsterdam: North-Holland)
Pfau, W. 1976, IBVS, 1106, 1
Pietrzyński, G., Graczyk, D., Gieren, W., et al. 2011, Natur, 495, 76
Poggiani, R. 2006, AN, 327, 895
Poggiani, R. 2008, Ap&SS, 323, 319
Poggiani, R. 2010, NewA, 15, 170
Poggiani, R. 2011, Ap&SS, 333, 115
Pojmanski, G., & Oksanen, A. 2005, IAUC, 8540, 1
Pojmanski, G., Szczygiel, D., Pilecki, B., et al. 2009, IAUC, 9043, 1
Pojmanski, G., Yamaoka, H., Kiyota, S., et al. 2006, IAUC, 8671, 1
Puetter, R. C., Rudy, R. J., & Lynch, D. K. 2005, IAUC, 8640, 2
Raj, A., Ashok, N. M., & Banerjee, D. P. K. 2011, MNRAS, 415, 3455
Raj, A., Das, R. K., & Walter, F. M. 2017, ApJ, 835, 274
Raj, A., Munari, U., Lee, B.-C., et al. 2014, ATel, 6181
Rieke, G. H., & Lebofsky, M. J. 1985, ApJ, 288, 618
Rudy, R. J., Ardila, D. R., Crawford, K. B., et al. 2015, IAUC, 9275, 2
Rudy, R. J., Lynch, D. K., Venturini, C. C., et al. 2006, IAUC, 8728, 1
Rudy, R. J., Russell, R. W., Sitko, M. L., et al. 2012, CBET, 3103, 1
Russell, R. W., Laag, E. A., Rudy, R. J., Skinner, M. A., & Gregory, S. A. 2010, IAUC, 9118, 2
Russell, R. W., Lynch, D. K., Rudy, R. J., & Woodward, C. E. 2008a, IAUC, 8936, 3
Russell, R. W., Rudy, R. J., Lynch, D. K., et al. 2007, IAUC, 8846, 1
Russell, R. W., Rudy, R. J., Lynch, D. K., et al. 2008b, IAUC, 8948, 1

Russell, R. W., Rudy, R. J., Lynch, D. K., et al. 2008c, IAUC, 8956, 1
Russell, R. W., Rudy, R. J., Lynch, D. K., & Woodward, C. E. 2006, IAUC, 8710, 2
Saito, R. K., Minniti, D., Angeloni, R., et al. 2013, A&A, 554, A123
Sala, G., Hernanz, M., Ferri, C., & Greiner, J. 2008, ApJL, 675, L93
Sala, G., Ness, J. U., Hernanz, M., & Greiner, J. 2017, A&A, 601, A93
Sale, S. E., Drew, J. E., Barentsen, G., et al. 2014, MNRAS, 443, 2907
Schaefer, B. E. 2011, ApJ, 742, 112
Schaefer, B. E. 2018, MNRAS, 481, 3033
Schlafly, E. F., & Finkbeiner, D. P. 2011, ApJ, 737, 103
Schmidt, Th. 1957, ZA, 41, 181
Schultheis, M., Chen, B. Q., Jiang, B. W., et al. 2014, A&A, 566, A120
Schwarz, G. J., Ness, J.-U., Osborne, J. P., et al. 2011, ApJS, 197, 31
Schwarz, G. J., Osborne, J. P., Page, K. L., et al. 2010, ATel, 2904, 1
Seach, J. 2010, CBET, 2140, 1
Shore, S. N., Wahlgren, G. M., Augusteijn, T., et al. 2011, A&A, 527, A98
Sitko, M., Lynch, D. K., Russell, R. W., Rudy, R. J., & Woodward, C. E. 2008, IAUC, 8998, 3
Srivastava, M. K., Ashok, N. M., Banerjee, D. P. K., & Sand, D. 2015, MNRAS, 454, 1297
Srivastava, M. K., Banerjee, D. P. K., Ashok, N. M., et al. 2016, MNRAS, 462, 2074
Tajitsu, A., Sadakane, K., Naito, H., et al. 2015, ApJ, 818, 191
Tanaka, J., Nogami, D., Fujii, M., Ayani, K., & Kato, T. 2011, PASJ, 63, 159
Thompson, W. T. 2017, MNRAS, 470, 4061
van den Bergh, S., & Younger, P. F. 1987, A&AS, 70, 125
Waagen, E., & Noguchi, T. 2011, CBET, 2813, 2
Waagen, E. O., Amorim, A., Pearce, A., et al. 2015, CBET, 4018, 4
Wagner, R. M., Dong, S., Bensby, T., et al. 2012, CBET, 3136, 1
Walter, F. M. 2011, CBET, 2796, 3
Walter, F. M. 2015a, ATel, 7060, 1
Walter, F. M. 2015b, in ASP Conf. Ser. 493, XIX European Workshop on White Dwarfs, ed. P. Dufour, P. Bergeron, & G. Fontaine (San Francisco, CA: ASP), 507
Walter, F. M., Battisti, A., Towers, S. E., Bond, H. E., & Stringfellow, G. S. 2012, PASP, 124, 1057
Warner, B., & Woudt, P. A. 2009, MNRAS, 397, 979
Weston, J. H. S., Sokoloski, J. L., Chomiuk, L., et al. 2016, MNRAS, 460, 2687
Woodward, C. E., Gehrz, R. D., Jones, T. J., Lawrence, G. F., & Skrutskie, M. F. 1997, ApJ, 477, 817
Yamaoka, H., Ayani, K., Murakami, N., et al. 2007, CBET, 1181, 2
Yamaoka, H., Nakamura, Y., Itagaki, K., Nakano, S., & Nishimura, H. 2007, IAUC, 8810, 1